OAK RIDGE NATIONAL LABORATORY LIBRARIES
3 4456 0548160 8

CENTRAL RESEARCH LIBRARY
DOCUMENT COLLECTION

2

ORNL-3994
UC-4 – Chemistry

CHEMISTRY DIVISION
ANNUAL PROGRESS REPORT
FOR PERIOD ENDING MAY 20, 1966

OAK RIDGE NATIONAL LABORATORY
operated by
UNION CARBIDE CORPORATION
for the
U.S. ATOMIC ENERGY COMMISSION

CENTRAL RESEARCH LIBRARY
DOCUMENT COLLECTION
LIBRARY LOAN COPY
DO NOT TRANSFER TO ANOTHER PERSON
If you wish someone else to see this document, send in name with document and the library will arrange a loan.

Printed in USA. Price $5.00 . Available from the Clearinghouse for Federal Scientific and Technical Information, National Bureau of Standards, U.S. Department of Commerce, Springfield, Virginia 22151

LEGAL NOTICE

This report was prepared as an account of Government sponsored work. Neither the United States, nor the Commission, nor any person acting on behalf of the Commission:

A. Makes any warranty or representation, expressed or implied, with respect to the accuracy, completeness, or usefulness of the information contained in this report, or that the use of any information, apparatus, method, or process disclosed in this report may not infringe privately owned rights; or

B. Assumes any liabilities with respect to the use of, or for damages resulting from the use of any information, apparatus, method, or process disclosed in this report.

As used in the above, "person acting on behalf of the Commission" includes any employee or contractor of the Commission, or employee of such contractor, to the extent that such employee or contractor of the Commission, or employee of such contractor prepares, disseminates, or provides access to, any information pursuant to his employment or contract with the Commission, or his employment with such contractor.

ORNL-3994

Contract No. W-7405-eng-26

CHEMISTRY DIVISION ANNUAL PROGRESS REPORT

for Period Ending May 20, 1966

E. H. Taylor, Director
M. A. Bredig, Associate Director
Ralph Livingston, Associate Director
B. H. Ketelle, Assistant Director

SEPTEMBER 1966

OAK RIDGE NATIONAL LABORATORY
Oak Ridge, Tennessee
operated by
UNION CARBIDE CORPORATION
for the
U. S. ATOMIC ENERGY COMMISSION

OAK RIDGE NATIONAL LABORATORY LIBRARIES
3 4456 0548160 8

Contents

SUMMARY vii

1. NUCLEAR CHEMISTRY 1

Neutron Capture Cross Section of the 6.75-Day Uranium-237 1

Reactor Neutron Cross Sections for the Cadmium Isotopes 110, 111, and 112 1

Thermal Neutron Cross Section and Resonance Integral of 36-hr Rhodium-105 2

Thermal Neutron Cross Sections and Resonance Integrals of Lanthanum-139 and -140 4

Thermal Neutron Cross Section and Resonance Integral of 7.5-Day Silver-111 7

Nuclear Charge Distribution in Fission: Yield of Palladium-115 from Thermal-Neutron Fission of Uranium-235 7

Nuclear Charge Distribution in Fission: Yields of Barium-143 and -144 from Thermal-Neutron Fission of Uranium-235 8

Nuclear Charge Distribution in Fission: Yields of Molybdenum-103, -105, and -106 from Thermal-Neutron Fission of Uranium-235 11

Compound-Nucleus Excitation of Medium-Weight Nuclei 11

Level Structure of Zirconium-94 13

Level Structure of Molybdenum-92 15

Decay of Technetium-94 Isomers to Levels in Molybdenum-94 17

The Decay of 12.8-hr Iodine-130*g* and 8.8-min Iodine-130*m* 17

Energy Levels of Tungsten-184 Populated in the Decay of Tantalum-184 19

Decay Properties of Europium-152 22

Studies of the Decay of Bromine-80*m* 23

Gamma-Ray Intensities in the Decay of Europium-154 23

Decay Schemes of Praseodymium-136 and -137 23

2. ISOTOPE CHEMISTRY 27

Nonaqueous Microtitration of Dibenzoylmethane and Other Weak Acids 27

Separation of Boron Isotopes 27

Carbon Isotope Effect in the Depolymerization of Paraldehyde 28

Attempt to React Boron Halides with CO 28

Isotope Effects in the Alkaline Reduction of NO_3^-, NO_2^-, and NH_2OH by Fe(II) 28

Oxygen Isotope Enrichment 29

Raman and Infrared Spectroscopy 29

Computed Carbon and Boron Isotopic Fractionation Factors for Exchange Reactions Involving Borine Carbonyl 29

Raman and Infrared Spectra of the BF_3 Complex with Dimethyl Sulfide and the Isotopic Exchange of the Complex with BF_3 32

Infrared and Raman Spectra of the Hexafluoride Ions of Silicon, Germanium, and Tin 36

Nuclear Magnetic Resonance Spectroscopy 36

Low-Temperature NMR Study of the Species $(C_2H_5)_2O{\cdot}(BF_3)n$ 36

NMR Observations on BrF_3 37

NMR Study of Complexes Between Sn(IV) and F^- 37
NMR Study of SbF_5 and AsF_5 37
Isotopic Mass Spectra 38
Molecular Force Constants 38

3. RADIATION CHEMISTRY 40
Pulse Radiolysis and Flash Photolysis 40
Equipment Development 40
Preliminary Studies 41
Radiolysis of Nitrous-Oxide-Saturated Solutions 42
2-Propanol and Sodium Formate Solutions 42
Sodium Nitrate Solutions 43
Postirradiation Reduction of Cerium(IV) in the ^{60}Co Gamma Radiolysis of Concentrated Nitrate Solutions. I. Dependence of G_{HNO_2} on Sodium Nitrate Concentration 44
Postirradiation Reduction of Cerium(IV) in the ^{60}Co Gamma Radiolysis of Concentrated Nitrate Solutions. II. Effect of 2-Propanol on $G(Ce^{III})$ and G_{HNO_2} 46
Radiolysis of Carbon Dioxide 48
Radiation-Induced Surface Reactions 49
Hydrogen Atoms 49
Nitrous Oxide Decomposition 50
Decomposition of Formic Acid 51
Decomposition of Isopropanol 51
Radiation and Hot-Atom Chemistry of Inorganic Crystalline Solids 52
Radiolysis of $LiNO_3$: Dose Rate Effects in the Molten State 52
Radiolysis of $LiNO_3$: LET and the Effect of the Solid-Liquid Phase Change 52

4. ORGANIC CHEMISTRY 53
A Method for Relating Rates of Interconversion and Destruction of Classical Carbonium Ions 53
Concerning the Effect of a Competing Equilibrium on a Kinetically Controlled Process 54
Consecutive Hydride Shifts During Norbornyl Rearrangements 56
The Acetolysis of 2-*exo*-Hydroxy-2-Phenyl-3-*exo*-Norbornyl-5,6-*exo*-d_2 Tosylate 58
Stereospecific 6,1 Migration of Deuterium During Rearrangement of 2-Phenylnorbornane-2,3-*cis*-*exo*-Diol-5,6-d_2 59
The Deamination of 3-*endo*-Amino-2-*exo*-Phenylnorbornanol-2 61
Stereospecific Elimination and Migration of Deuterium During Hydrolysis of a Substituted Norbornyl Tosylate 62
Organic Compounds in Nuclear Technology. Extraction with 2-Ethyl-Hexanohydroxamic Acid 63

5. CHEMISTRY OF AQUEOUS SYSTEMS 65
The Thermodynamic Properties of HCl-$BaCl_2$ Mixtures 65
Expressions for $\gamma \pm$ of HCl and $BaCl_2$ in the Mixtures 65
The Solubility of Ag_2SO_4 in $AgNO_3$ Solutions 68
The Solubility of Lanthanum Sulfate in Sulfuric Acid Solutions at Elevated Temperatures 70
The Apparent Molal Volumes in Aqueous Solution of LiCl and NaCl at 5 and 35° 73

Hydrolysis of Thorium(IV) 75

Ion Exchange Separations 76
Cation Exchange of the Elements in HBr Solutions 76
Comparison of Adsorbabilities in HCl, HBr, and $HClO_4$ Solutions 77
Separation of Alkali-Metal Ions 77

Physical Chemistry of Polyelectrolyte Systems 77
Structural Effects on the Enthalpy and Entropy of Dilution of Aqueous Solutions of the Quaternary Ammonium Halides at 25°C 77
Structural Effects on the Osmotic and Activity Coefficients of the Quaternary Ammonium Halides in Aqueous Solutions at 25° 80
Thermodynamics of Aqueous Solutions of Tetra-*n*-alkylammonium Halides. Enthalpy and Entropy of Dilution 80
Thermodynamic Quantities in the Exchange of Lithium with Cesium Ion on Cross-Linked Phosphonic Acid Cation Exchangers 80

Water Research Program 81
Hyperfiltration Studies 81
Osmotic Coefficients of Sea Salt Solutions 83
Thermodynamic Properties of Sea Salt Solutions 84
Use of Cationic Glass Electrodes to Measure the Activity of KCl Solutions 86

6. ELECTROCHEMICAL KINETICS AND ITS APPLICATION TO CORROSION 88

Studies on the Inhibition of Corrosion 88

Mechanism of Corrosion Inhibition 88

Electrochemistry of Zirconium 90
Dissolution by HF 90
Effects of Chloride Ions 90
Diffusion Coefficient of HF 91

Rotating Disk Studies on the Dissolution of Aluminum in Chloride Solutions 91

Kinetics of Pitting Attack of Titanium in Chloride Solutions 92

Effect of Temperature on Pitting Corrosion of Titanium in Chloride Solutions 93

Corrosion of Aluminum in Saline Waters at Elevated Temperature 94

7. NONAQUEOUS SYSTEMS AT HIGH TEMPERATURES 95

Condensed-Phase Behavior of the Aluminum Chloride–Zirconium Chloride System 95

Pretransition Behavior of Solid Potassium and Thallium Sulfates from Heat Content and Thermal Expansion 95

Molten-Salt–Metal Solutions 98
EMF Measurements in Molten Rare-Earth-Metal–Metal Halide Solutions 98
Strontium Metal–Strontium Halide Systems 102
Metal–Metal Fluoride Miscibility in Liquid and Solid Phase 104

8. CHEMICAL PHYSICS 106

The Absorption Spectrum of Ammonia in the Near-Infrared Region as a Function of Temperature from Below the Freezing Point to Above the Critical Point 106

The Absorption Spectrum of Normal Hexane and Cyclohexane in the Near-Infrared Region as a Function of Temperature from Below the Freezing Point to Above the Critical Point 106

Calorimetry 107
The Heat Capacity of Potassium Hexaiodorhenate(IV) from 6 to 320°K 107
High-Temperature Enthalpy of Potassium Pertechnetate. Second-Order Transition with a Heat Capacity Maximum at 750°K 110
Enthalpy and Free Energy of Formation of the Hexachlororhenate(IV) Ion and Its Enthalpy of Hydrolysis 111

Microwave and Radio-Frequency Spectroscopy 113
Paramagnetic Resonance Studies of Single Crystals 113
Paramagnetic Resonance Study of Free Radicals Formed in Liquids During Ultraviolet Photolysis 113

Neutron and X-Ray Crystallography 114
X-Ray Determination of the Crystal Structure, Molecular Structure, and Absolute Configuration of Leucoxine Hydrobromide 114
The Structure of Copper Ammonium Sulfate Hexahydrate from Neutron-Diffraction Data 117
A Model for Torsional Oscillators in Least-Squares Refinement of Crystal Structures: Application to the Methyl Groups in $Cu_2(CH_3COO)_4 \cdot 2H_2O$ 119
A Neutron Diffraction Study of the Cubic Phase of Xenon Hexafluoride 121
The Oak Ridge Computer-Controlled X-Ray Diffractometer 121
Stereoscopic Drawings Showing the Symmetry Elements of the Crystallographic and Shubnikov Space Groups 122
The Structure of $MnCl_2 \cdot 4H_2O$: A Neutron-Diffraction Study 123
X-Ray Reflection Data for Analysis of the Crystal Structure of Sedoheptulosan Monohydrate 125
Citric Acid Monohydrate: A Crystal-Structure Determination by Neutron Diffraction Using Deuterium for Isomorphous Replacement 125
The Crystal Structure of Sodium Zirconium Fluoride, $Na_7Zr_6F_{31}$ 127
X-Ray Diffraction Studies of Liquids 128

Molecular Beam Studies 130
Elastic Scattering in Hydrogen-Helium Systems 130
Alkali-Atom–Halogen-Molecule Reactions 130
A Molecular Beam Study of the Reaction of Ozone with Atomic Hydrogen 131
Collisional Excitation of Vibrational Levels in Hydrogen 131
A Program to Compute the Classical Deflection Function 132

Mass Spectrometry and Related Techniques 134
Mass Spectrometric Evidence for H_3O, HD_2O, and D_3O 134
Transient Species Produced by the Heterogeneous Decomposition of Acetone in a Mass Spectrometer 135
Experimental and Theoretical Considerations for Ionization of Simple Hydrocarbons, H_2, D_2, O_2, H_2O, and the Rare Gases by 2.2-Mev Alpha Particles and by Electrons in a Mass Spectrometer 137
High-Transmission and Dual-Electron-Beam Ion Sources for Mass Spectrometry 139
Two-Stage Mass Spectrometer 141
Measurement of the Relative Abundances and Recoil Energy Spectra of Fragment Ions Produced as the Initial Consequences of X-Ray Interaction with C_2H_5I, $C_2H_3D_2I$, and $Pb(CH_3)_4$ 142

PUBLICATIONS 145

PAPERS PRESENTED AT SCIENTIFIC MEETINGS 151

LECTURES 155

Summary

1. NUCLEAR CHEMISTRY

The irradiation of a particularly pure sample of ^{236}U in the high-flux reactor at Savannah River and a mass analysis of the ^{238}U formed permitted a preliminary estimate of approximately 100 barns to be made for the reactor neutron capture cross section of ^{237}U.

The reactor cross sections of ^{110}Cd, ^{111}Cd, and ^{112}Cd were measured as 11 ± 2, 24 ± 3, and 2.2 ± 0.5 barns respectively.

The irradiation of ^{104}Ru and the mass analysis of the palladium produced permitted the calculation of a thermal cross section σ_{th} = 14.4 ± 1.5 kilobarns and a resonance integral of 17 ± 3 kilobarns for the 36-hr ^{105}Rh.

The thermal neutron capture cross sections and resonance integrals of ^{139}La and ^{140}La were measured by determining the ^{140}La and ^{141}Ce produced in high-flux irradiations.

The neutron cross section and resonance integral of 7.5-day ^{111}Ag were determined from measurements of the 3.2-hr ^{112}Ag formed in reactor irradiations and are reported as 3.2 ± 2 and 105 ± 20 barns respectively.

The fractional cumulative yield of ^{115}Pd from ^{235}U thermal-neutron fission was measured to be 0.883 ± 0.020.

The fractional cumulative fission yields for ^{143}Ba and ^{144}Ba from ^{235}U thermal-neutron fission indicate that the nuclear charge distributions for these masses continue the trends observed for lighter fission products in the heavy-mass peak.

Cumulative yields of ^{103}Mo, ^{105}Mo, and ^{106}Mo fission products were shown to include large fractions of their respective chain yields. Thus, from uranium fission, fragments with $Z > 42$ seem to be formed with small probability. One may infer that this is due to the difficulty of forming the complementary fission fragments with $Z < 50$, where the strong 50-proton shell may affect fragment yields.

Gamma rays accompanying compound-nucleus reactions produced by bombarding ^{93}Nb, ^{94}Zr, and ^{114}Cd with 40- to 60-Mev alpha particles were measured with Ge(Li) detectors.

Levels in ^{94}Zr were studied by inelastic scattering of 12.7-Mev protons.

Energies for 34 excited states in ^{92}Mo were determined by analyzing data from inelastic scattering of 10-Mev protons and from the associated gamma-ray spectrum.

From the decay of the 53-min and 5-hr isomers of ^{94}Tc, measured with Ge(Li) and NaI detectors, a level scheme was constructed which was compared with shell-model predictions.

The decay of the isomers of ^{130}I was investigated with Ge(Li) and NaI(Tl) detectors, with a single-gap toroidal field spectrometer, and with coincidence techniques. The upper isomer, in addition to independent beta decay, decays to the ground state via a 48.2-kev $M3$ transition.

A detailed study was made on the levels in ^{184}W populated in the decay of 8.7-hr ^{184}Ta. The level scheme proposed as a result of these measurements includes at least 17 states in ^{184}W and 27 associated gamma-ray transitions. Among the levels observed are members of the ground-state rotational band up through the 6^+ state, the 2^+, 3^+, and 4^+ members of the γ-vibrational band, and a group of levels above 1285 kev which appear to belong to an intrinsic two-quasi-particle excitation.

The gamma rays from the decay of 12.4-year ^{152}Eu were studied with high-resolution germanium detectors as well as by gamma-gamma coincidence experiments which utilize a multiparameter analyzer. These studies disclosed several new

features of the level schemes of ^{152}Gd and ^{152}Sm, including the population of an additional member of the β-vibrational band in the latter.

The gamma-ray spectrum of ^{80m}Br was studied by means of a lithium-drifted germanium detector and NaI coincidence spectrometers in conjunction with a three-dimensional multichannel analyzer. From these measurements, level schemes in ^{80}Se and ^{80}Kr populated from the decay of ^{80m}Br are proposed.

High-resolution measurements of the gamma-ray spectrum of ^{154}Eu revealed several new features of the excited levels in ^{154}Gd.

The energy levels populated by the decay of ^{136}Pr and ^{137}Pr in the respective cerium isotopes were deduced from observed gamma-ray energies, intensities, and coincidences. A total decay energy of 5.07 ± 0.05 Mev was derived for 13.5-min ^{136}Pr from quadruple coincidence measurements using one anthracene and three sodium iodide detectors.

2. ISOTOPE CHEMISTRY

A micromethod was developed for the quantitative determination of dibenzoylmethane and other weak acids by titration in anhydrous ethylenediamine or pyridine. A bimetallic electrode system consisting of anodized platinum and cathodized antimony was used to determine the end point potentiometrically. The titrant was tetrabutylammonium methylate in 90% benzene–10% methanol.

A new determination was made of the temperature dependence of the isotopic equilibrium constants for the reaction

$$\text{donor}\cdot{}^{11}BF_3 + {}^{10}BF_3 = \text{donor}\cdot{}^{10}BF_3 + {}^{11}BF_3 ,$$

where the donors were Me_2S and Bu_2S. The new equilibrium constants are given by

$$\log K_{eq}(Me_2S) = \frac{10.72}{T} - 0.01976 ,$$

$$\log K_{eq}(Bu_2S) = \frac{9.639}{T} - 0.01816 .$$

The fractionation of boron isotopes,

$$({}^{10}B/{}^{11}B)\text{complex}/({}^{10}B/{}^{11}B)\text{gas} ,$$

in the reaction

$$C_6H_5OCH_3\cdot BF_3 \xrightarrow{50\%} C_6H_5OCH_3 + BF_3$$

was 1.04 at 25°C, a value only slightly larger than that for the equilibrium isotopic exchange reaction.

Experimental values of k^{12}/k^{13} for the carbon kinetic isotope effect in the depolymerization of paraldehyde are 1.006 at 64° and 1.012 at 69°C.

No addition compound was formed between CO and BF_3, BCl_3, or BBr_3.

The nitrogen kinetic isotope effect, k^{14}/k^{15}, for the alkaline reduction by Fe(II) of NO_3^- to NH_3 was 1.075 ± 0.004 at 25°C. The corresponding value for the reduction of NO_2^- and NH_2OH to NH_3 was 1.032 ± 0.002. Isotope effects in good agreement with these values were computed on theoretical grounds, assuming cleavage of an N–O bond as the significant kinetic step in the reduction of each species. The inverse isotope effect previously observed in the reduction of NO_2^- to NH_3 by Fe(II) in the presence of MgO was explained in terms of competing reactions which produced N_2O instead of NH_3.

The Oxygen-17 Facility operated continuously during the year except for one interruption on November 28 when an electrical transformer ignited. The peak concentrations of ^{17}O and ^{18}O in the system reached 24.0 and 99.8% respectively. Several hundred grams of isotopically enriched H_2O and O_2 were made available for distribution to prospective users.

Raman spectra were obtained for a number of interhalogen ions. Raman and infrared spectra were observed for $^{10}BF_3\cdot(CH_3)_2S$ and $^{11}BF_3\cdot(CH_3)_2S$ in the liquid state. The equilibrium constant for the exchange of boron isotopes between BF_3 and BF_3–dimethyl sulfide complex was calculated and compared with experiment. The isotopic separation factors for carbon, oxygen, and boron isotopes were computed using spectral data for several systems involving borine carbonyl.

Five fundamental vibrational frequencies associated with regular octahedral symmetry (point group O_h) were observed in the infrared and Raman spectra of crystals containing SiF_6^{2-}, GeF_6^{2-}, and SnF_6^{2-} ions.

Evidence was obtained from nuclear magnetic resonance spectra for a second addition compound between BF_3 and $(C_2H_5)_2O$ existing at temperatures

below $-30°C$. Only a single peak was observed in the NMR spectrum of BrF_3.

NMR measurements on acid solutions containing Sn(IV) and F^- indicate that a large number of fluorine-containing species are present which exchange slowly enough for their ^{19}F resonance to be observed.

The ^{19}F NMR spectra of SbF_5 and AsF_5 were observed at several temperatures. Chemical shifts and a spin-spin coupling constant were measured for an addition compound between SbF_5 and CF_3COOH.

Studies were made of the uses and effects of Coriolis coupling and centrifugal distortion constants in force-constant determinations. Similar studies were made of the use of mean square amplitudes of vibration from electron diffraction studies of gases. Several existing computer programs were modified to permit the extraction of Coriolis coupling and anharmonic constants from the experimental data by the method of least squares.

More than 900 samples of O_2, N_2, CO_2, and BF_3 were analyzed for isotopic composition during this report period.

3. RADIATION CHEMISTRY

A program of pulse radiolysis was started in which a field emission electron accelerator will be used. The fast-recording spectrographic-spectrophotometric detection equipment was assembled and tested. A new flash lamp which provides a 3-μsec flash (5 to 95% light emission) was developed. The detection equipment allows measurement of intermediates during the flash with a time resolution of 0.1 μsec. A program of flash photolysis of aqueous solutions was initiated. The spectrum of the OH radical was determined.

Hydrogen yields observed in the ^{60}Co gamma radiolysis of aqueous N_2O-saturated 2-propanol solutions are interpreted as arising from (1) the radiolysis of N_2O-saturated water ($G_{H_2} = 0.34$), (2) the H atom abstraction of hydrogen from the organic solute ($G_H = 0.61$), and (3) a "direct effect" equal to 0.54[2-propanol]. Similar treatment of the sodium formate data yields $G_H = 0.57$ and a "direct effect" of 0.16[sodium formate]. The simultaneously measured nitrogen yields are constant, indicating that H atoms are not reducing N_2O to N_2.

Radiolysis of N_2O-saturated $NaNO_3$ solutions has given $k(NO_3^- + \text{Red})/k(N_2O + \text{Red})$ as 1.44 and the yield of reducing radicals not producing molecular hydrogen as 2.95.

A program SLOPULSE was written for the CDC 1604-A computer to determine G_{HNO_2} in the radiolysis of concentrated sodium nitrate solutions in 0.4 *M* sulfuric acid containing 10^{-4} *M* cerium(IV). The dependence of $G(Ce^{III})$ and G_{HNO_2} on sodium nitrate concentration is very striking: an increase in $G(Ce^{III})$ with increase in sodium nitrate concentration is accompanied by an equal increase in $2G_{HNO_2}$. Two processes are required to denote the formation of earliest detectable intermediates in the radiolysis of concentrated sodium nitrate solutions in 0.4 *M* sulfuric acid:

$$H_2O \rightsquigarrow H_2, H_2O_2, H, OH \ ,$$

$$NO_3^- \rightsquigarrow NO_2^-, O_2 \ .$$

Addition of 2-propanol to concentrated sodium nitrate solutions in air-saturated 0.4 *M* sulfuric acid containing cerium(IV) increases $G(Ce^{III})$ by $2G_{OH}$ and G_{HNO_2} by $0.5G_{OH}$. This is consistent with a reaction mechanism in which (1) NO_2 radicals disproportionate to yield nitrous acid and (2) oxidation of nitrous acid by OH or HSO_4 is inhibited by reaction of 2-propanol with OH or HSO_4 to yield $CH_3\dot{C}OHCH_3$, which reduces cerium(IV).

Gaseous carbon dioxide shows a high radiation stability because of an efficient back-reaction of products. Additives intercept the species responsible for back-reaction and permit a net production of carbon monoxide. Judging from the CO yield, hydrogen, methane, and ethylene show increasing efficiency of interception. The CH_4, C_2H_4, and possibly H_2 are consumed in interception but at a lower rate than that at which CO is produced. An oxygen material balance was not attained, but CH_3OH and HCHO do not appear to be important products. Considerable energy transfer occurs in the radiolysis of CH_4-CO_2 mixtures, and almost as much C_2H_6 is produced as would be in the irradiation of CH_4 alone.

Relative radiolytic yields for hydrogen atom formation on several adsorbents and absolute yields

for three other radiolyses on adsorbents (decomposition of nitrous oxide, of isopropanol, and of formic acid) were measured.

A clear dose rate effect was observed in the radiolysis of molten $LiNO_3$ to oxygen gas and nitrite ion by ^{60}Co gamma rays. A kinetic mechanism capable of giving a quantitative description of the experimental results was developed.

4. ORGANIC CHEMISTRY

A study was made of the rate at which carbonium ions interconvert as compared with the rates at which they react with entering groups or eject protons to form products in a system known to proceed through classical ionic intermediates. Carbon-14 labeling and NMR spectroscopy were used to circumvent the need for extraordinary experimental precision.

The concept that "internal return in carbonium ion processes necessarily alters the product ratios" was studied both mathematically and chemically and shown to be incorrect.

The mechanism by which hydrogens migrate during solvolysis reactions of the norbornyl system was partially elucidated.

Three rearranged products were formed when 2-*exo*-hydroxy-2-phenyl-3-*exo*-norbornyl-5, 6-*exo*-d_2 tosylate was treated with boiling acetic acid. The deuterium distribution in these products was determined, and the relation of the acetolysis and hydrolysis reactions was studied.

Data are presented showing how 2-phenylnorbornane-2,3-*cis*-*exo*-diol-5,6-d_2 reacts, when treated with concentrated sulfuric acid, to give 3-*endo*-phenylnorbornanone-*exo*-5-*anti*-7-d_2, a result of intramolecular rearrangement involving a stereospecific migration of deuterium.

The deamination of 3-*endo*-amino-2-*exo*-phenylnorbornanol-2 in glacial acetic acid led to the production and isolation of six compounds in approximately 85% yield. These products were identified either completely or partially by interpretation of their NMR spectra and by independent syntheses. The mechanistic significance of these data is discussed briefly.

It was shown that during the hydrolysis of 2-*exo*-hydroxy-2-phenyl-3-*exo*-norbornyl tosylate, one of the products, 2-*exo*-phenylnorbornane-2-*endo*-5-*exo*-diol, is formed as a result of two consecutive 1,2 hydride shifts.

2-Ethyl-hexanohydroxamic acid was prepared and tested as a solvent for cations in equilibrium distribution studies. With this hydroxamic acid, a selectivity for zirconium, niobium, and hafnium over cobalt, uranyl, thorium, and ferric iron was found.

5. CHEMISTRY OF AQUEOUS SYSTEMS

The activity coefficient of HCl in HCl-$BaCl_2$ mixtures was studied to 175°. At constant temperature and ionic strength the logarithm of the activity coefficient of HCl in the mixtures varies linearly with the ionic strength fraction of $BaCl_2$, in conformity with Harned's rule. The activity coefficient of $BaCl_2$ in the mixtures was calculated using the parameters describing this variation and those for the variation of the activity coefficient of $BaCl_2$ with ionic strength in pure $BaCl_2$ solutions.

The solubility of Ag_2SO_4 was measured in 0.056, 0.109, and 0.242 *m* $AgNO_3$ solutions in the temperature range 25 to 150°. It was found that the variation of the molality solubility product with ionic strength could be expressed by a single-parameter expression of the Debye-Hückel type even though, in contrast to other systems studied, the solubility of the Ag_2SO_4 in the supporting electrolyte was at all temperatures and ionic strengths lower than the solubility in pure water.

The solubility of $La_2(SO_4)_3$ was measured in 0.234, 0.471, and 0.714 *m* H_2SO_4 solutions in the temperature range 120 to 175°C. It was found that even in this case of a 3-2 valent salt the variation of the molality solubility product with ionic strength could be expressed by a single-parameter expression of the Debye-Hückel type, as was found in previous studies of the solubility of Ag_2SO_4 in H_2SO_4. In addition to this parameter, the solubility of $La_2(SO_4)_3$ in water, which could not be measured in this temperature range due to hydrolysis, was calculated from the least-squares fit of the data.

Accurate density measurements were made of aqueous solutions of NaCl and LiCl at 5° and of LiCl at 35°. The results at very low concentrations, obtained for the first time with high accuracy at temperatures other than 25°C, are not inconsistent with the Debye-Hückel limiting law.

Further evidence is presented for the existence of salt-induced structure transitions in solution.

The hydrolytic polymerization of Th(IV) in perchlorate media was investigated by equilibrium ultracentrifugation from 0 to 3 hydroxyls bound per thorium, n; up to n = 2.5 aggregated species were of low molecular weight and appeared to be in chemical equilibrium with one another.

A systematic study of the cation exchange behavior of elements in dilute to concentrated HBr solutions was carried out with a sulfonic acid resin. Many useful column separations may be designed from the data.

The adsorption of alkali-metal ions, Li^+ to Fr^+, in HCl-water-methanol solutions was investigated with sulfonic acid cation exchangers of the polystyrene-divinylbenzene and phenol-formaldehyde types. Procedures for separating alkali elements from each other were devised from the results.

The effect of the structure of quaternary ammonium cations on their thermodynamic properties in aqueous solutions was investigated by measurements of osmotic coefficients and enthalpies of dilution with solutions of several quaternary ammonium halides at 25°C. The relative partial molal entropy of the solvent, $\overline{S}_1 - S_1^\circ$, derived from these measurements was employed to interpret the effect of the cation on the water structure. Similar measurements on the tetra-*n*-alkylammonium halides were employed to obtain excess apparent molal entropies, which showed a pronounced dependence on the cation size.

Calorimetric measurements of the heat of exchange of Li^+ with Cs^+ ion in several phosphonic acid–type cation exchangers indicated that "site binding" was probably the cause for the preference of the exchanger for the former over the latter ion.

Water Research Program

Salt filtration was observed when solution was forced by pressure through a porous glass (50 A average pore diameter), and rejection was enhanced by increasing the ion exchange capacity of the glass. Membranes were created dynamically by exposing bodies having pores of diameters in the range 0.1 to 5 μ to pressurized feeds containing suitable additives; these membranes frequently combine substantial salt rejections with high permeation rates, sometimes of several hundred gallons per square foot per day.

Measurements of isopiestic ratios of solutions having the solute composition of seawater to NaCl solutions indicate that osmotic coefficients of seawater and its concentrates, ϕ_{sw}, can be computed from empirical equations for ϕ_{NaCl} by insertion of seawater concentration in terms of ionic strength.

Recent work at 25°C showed that the osmotic coefficient of sea salt solutions to saturation could be expressed very well by a Debye-Hückel term plus a power series in ionic strength, where the coefficients of the series were evaluated from measurements on pure NaCl solutions. The power series parameters for NaCl solutions to 260°C were reevaluated using the most recent data available. By the use of the new values of the parameters, values of boiling-point elevations (BPE), minimum energies of recovery, and osmotic pressure were recalculated. The largest change was a 12% increase in BPE at 25° and 28 wt % solids.

The Beckman 39137 cationic glass electrode was used in the temperature range 15 to 55° to measure the activity of KCl solutions in the concentration range 0.01 to 2.5 *m*. It was found that except at high salt concentrations at 15° the agreement between the activities measured with the glass electrode and those reported from vapor pressure measurements was satisfactory.

6. ELECTROCHEMICAL KINETICS AND ITS APPLICATION TO CORROSION

Further studies on the inhibition of corrosion of iron and steel showed that inorganic substances of the general formula XO_4^{n-} exert a noncathodic effect which greatly facilitates the passivation process.

A mechanism is proposed which accounts for the complex electrochemical behavior of iron in the presence of adsorbed anionic inhibitors.

Studies with a rotating disk electrode assembly on the dissolution of zirconium in HF-HCl and HF-HNO_3 mixtures showed that at potentials below the pitting potential in chloride media the rates of dissolution in the two solutions are identical. This result suggests that neither Cl^- nor NO_3^- ions exert a specific effect on the dissolution of

the passive oxide layer by HF. Other experiments in HF-H_3PO_4 solutions disclosed a reduction in dissolution rate by several orders of magnitude; PO_4^{3-} ion inhibits the dissolution reaction by HF in a manner similar to the SO_4^{2-} ion. The diffusion coefficient of HF in certain solutions of interest was determined by the open-ended capillary method.

The rate of the anodic dissolution reaction of aluminum in alkaline NaCl solutions was measured as a function of pH, electrode potential, and time by use of a rotating disk electrode assembly. Observed changes in the rate of the dissolution reaction with time may be interpreted in terms of the kinetics of formation and dissolution of a porous aluminum oxide layer on the metal surface. This hypothesis was verified by electron micrographs of the oxide layers.

Experiments were initiated on electrochemical aspects of the formation and growth of pits on titanium in chloride solutions. No significant effect of solution velocity on the initiation and growth processes was observed up to approx 3500 rpm. Breakdown potentials observed on application of constant current were found to depend to some extent on the initial thickness of the passive oxide layer, although the final pitting potential was relatively unaffected. Addition of sulfate ions increases the breakdown potentials but hardly affects the pitting potential. Growth kinetics of single pits were investigated potentiostatically.

Polarization curves of titanium and some of its alloys were measured in chloride solutions at temperatures up to 200°C by use of a titanium loop facility equipped for electrochemical studies. In the presence of a sufficient quantity of chloride ions, titanium alloys exhibit a pitting potential which in some cases is low enough to allow pitting attack to proceed spontaneously. Increase of temperature profoundly affects the value of the pitting potential; plots of pitting potential as a function of temperature are reproducible and show clearly which alloys are superior in tendency towards pitting attack.

Electrochemical aspects of the corrosion of types 5454 and 6061 aluminum alloys were studied in 1 *M* NaCl at 150°C in titanium loop facilities. Changes in the polarization curves of anodic and cathodic processes occurring at the aluminum-electrolyte interface with pH provided a kinetic explanation for the existence of a minimum corrosion rate in chloride media. An enhanced rate of the cathodic process on the 6061 alloy accounts for its greater corrosion rate at any pH and for its susceptibility to pitting attack; this catalysis may be attributable to the copper content of the 6061 alloy.

7. NONAQUEOUS SYSTEMS AT HIGH TEMPERATURES

In contrast to earlier suggestions it was shown that aluminum chloride and zirconium tetrachloride form a simple eutectic system without a miscibility gap in the liquid state.

In agreement with x-ray diffraction data for thermal expansion, drop-calorimetric measurements of the heat contents of potassium and thallium sulfates showed these diisomorphous salts to differ significantly with respect to the transition from an orthorhombic (pseudohexagonal) to a hexagonal crystal structure. While in potassium sulfate most of this change occurs isothermally at 584°C, the corresponding change in thallium sulfate has a very small isothermal part and is predominantly a gradual pretransitional process. The difference is attributable to the high polarizability of the Tl^+ ion.

With the recently developed technique which allows emf measurements in molten metal–salt systems corrosive to ceramics, a study of the Ce-$CeCl_3$ and Nd-$NdCl_3$ systems was made. A rather surprising similarity in the emf results was found in contrast to the quite distinct differences in the two systems as shown by phase equilibria and electrical conductivity studies. An explanation correlating the various observations with the extent of the dissociation $M^{2+} \rightarrow M^{3+} + e^-$ is presented.

The study of metal-salt miscibility in systems of divalent metals such as the alkaline earths was continued with a determination of the phase equilibria between strontium metal and its halides. As expected, the behavior of strontium was found to be intermediate between that of calcium and barium, though closer to the latter. Critical solution temperatures ranged from 1056 to 1106°C.

The study of the miscibility of metals with their fluorides showed solid barium fluoride to be as much as four times as soluble in liquid barium metal as solid calcium fluoride in liquid calcium. Separation into two liquids does not occur in

either system. Following the trend in miscibility, the solubility of magnesium metal in molten magnesium fluoride was found to be as low as 0.5 mole % at 1256°, the melting point of the salt.

8. CHEMICAL PHYSICS

Studies of the effect of temperature on the near-infrared spectra of CO_2 and simple hydrogen-containing solvents (H_2O and D_2O) were extended to include NH_3 (–80 to 146°), *n*-hexane (–100 to 250°), and cyclohexane (0° to 250°). The temperature sensitivities of the five complex bands of NH_3, centered near 1.04, 0.93, 0.89, 0.80, and 0.65 μ, are intermediate between those of the relatively sharp bands of CO_2 and those of the extremely broad bands of water in this spectral region. The spectra of *n*-hexane and cyclohexane, consisting of closely similar complex bands centered at 1.4, 1.2, 1.02, 0.92, and 0.75 μ, are even less sensitive to changes of temperature and state than that of CO_2. These observations agree with the behavior to be expected on the basis of bond polarity, namely,

$$C-H < C-O < N-H < O-H \ .$$

The heat capacity of potassium hexaiodorhenate(IV), K_2ReI_6, was determined from 6 to 320°K. The Néel temperature of the magnetic system ($5d^3$ electronic configuration) was observed to be 23.7°K. Anomalous heat capacities occur between 190 and 240°K. The entropy of K_2ReI_6 at 25°C is 118.16 cal deg^{-1} $mole^{-1}$.

Precise high-temperature relative enthalpy measurements on $KTcO_4$ revealed a lambda-type anomaly in the derived heat capacity curve. The anomaly occurs at 750°K, only 50° below the melting point.

The standard enthalpy of oxidation of $K_2ReCl_6(c)$ by alkaline hypochlorite solution was measured to be –152.7 ± 0.6 kcal/mole. This result when combined with other available thermodynamic data gives –183.0 and –141.6 kcal/mole for the enthalpy and free energy of formation of $ReCl_6^{2-}(aq)$ respectively. The enthalpy of hydrolysis observed, –63.6 kcal/mole, was found to be inconsistent with the thermodynamic properties of $ReO_2 \cdot 2H_2O$ derived from the potential of the $ReO_2 \cdot 2H_2O$-ReO_4^- couple given in the literature. It is suggested that the thermodynamic properties of freshly precipitated $ReO_2 \cdot 2H_2O$, as obtained in the hydrolysis measurements, differ significantly from those of the aged dioxide present in the potential measurements.

A paramagnetic resonance spectrometer was designed and constructed so that samples can be gamma irradiated at 4°K and spectra observed without warming. Spectra were studied for single crystals of calcium hydroxide after irradiation with gamma rays. Two species were found in addition to the previously studied species, which was thought to be O^-. One of these species is a precursor of O^-, is stable at 4°K but disappears on warming, and is probably the OH radical. The other species is O_2^-, which forms when crystals containing O^- are warmed to room temperature, but the spectrum can only be observed at very low temperatures.

Paramagnetic resonance spectra were obtained during photolysis of liquid acetone and acetone solutions. Photolyzed acetone abstracts hydrogen from suitable donors. The radicals $(CH_3)_2\dot{C}OH$, $\dot{C}H_2COCH_3$, and a small amount of $\dot{C}H_3$ were obtained from pure acetone. With suitable alcohols in acetone solution the radicals $(CH_3)_2\dot{C}OH$, $\dot{C}H_2OH$, and $CH_3\dot{C}HOH$ were obtained. Similarly, radicals were formed from ether and from dioxane. The temperature dependence of the hydroxyl proton hyperfine interaction of $CH_3\dot{C}HOH$ was studied. A study was also made of the acid-catalyzed exchange of hydroxyl protons of $\dot{C}H_2OH$ and of $(CH_3)_2\dot{C}OH$. Also studied were the effects of water and acid on the radical yields from photolyzed solutions containing alcohols and hydrogen peroxide.

The crystal structure of the hydrobromide of the alkaloid leucoxine was determined by precise x-ray analysis. All of the hydrogen atoms were located. The structure of the leucoxine ion, $C_{20}H_{22}O_5N^+$, which was previously only partly known from a preliminary characterization, was elucidated in complete detail. The absolute configuration is the same as that found by others in the related aporphine alkaloid bulbocapnine, but the twist about the central bond of the biphenyl system embedded in the molecule is 14° instead of 30°.

A refinement of the crystal structure of copper ammonium sulfate hexahydrate based on neutron diffraction data confirmed the structure derived by others from x-ray analysis and yielded precise

hydrogen-atom coordinates, from which the structural parameters of the water molecules, the ammonium ion, and the hydrogen bonds were derived. The bond length N – H appears to be about 1.06 *A*, somewhat higher than values from previous less precise neutron determinations of crystals containing ammonium ions. The O – H bonds are of normal length; the H – O – H angles are 109.3, 105.9, and 105.7°.

A mathematical model for including explicitly the motion of torsional oscillators in least-squares refinement of crystal structures was developed and applied to the methyl groups in refinement of the $Cu_2(CH_3COO)_4 \cdot 2H_2O$ structure.

A second crystal modification of XeF_6 was grown, and neutron diffraction data were obtained. The measurements disclose that this phase is face-centered cubic with probable space group $P\bar{4}3c$ or $Fm3c$.

The Oak Ridge computer-controlled x-ray diffractometer has been in operation for about ten months. It has been programmed to perform all the basic operations required to collect data for crystal structure studies.

A computer program to plot stereoscopic illustrations showing the symmetry elements of crystallographic and Shubnikov space groups is under development. The Shubnikov groups can often be used to describe the symmetry of the distribution of spin magnetic moments.

The hydrogen atoms in $MnCl_2 \cdot 4H_2O$ were located precisely by neutron diffraction analysis. The resulting data have been useful to other workers studying antiferromagnetism of this substance at low temperature and have provided independent confirmation and refinement of the hydrogen-bonding pattern deduced from a previous x-ray analysis and electrostatic calculations. Some of the O – H bonds appear rather short because of the effects of thermal motion. The four different H – O – H angles found vary from 104.3 to 112.4°.

A three-dimensional set of x-ray diffraction intensity data were collected from a crystal of sedoheptulosan monohydrate for a projected determination of the crystal structure.

The crystal structure of citric acid monohydrate was determined with neutron diffraction by using hydrogen-deuterium isomorphous replacement. A crystal of a stereospecifically deuterated isomer was found to have enantiomorphous domains.

The crystal structure of $Na_7Zr_6F_{31}$ was shown to consist of ZrF_8 antiprisms joined in a network. Cuboctahedral cavities between antiprisms contain F and Na atoms.

The x-ray diffraction study of liquid water as a function of temperature between 4 and 200°C was completed. Good agreement was obtained between calculated and observed x-ray intensity and radial distribution functions for a model based on an anisotropically expanded ice I structure. X-ray measurements on liquid carbon tetrachloride are quantitatively explained by a perturbed close packing of the chlorine atoms, which are tetrahedrally arranged around the carbon atoms.

Total elastic scattering cross sections were measured in hydrogen-helium systems (H_2 in ^3He, D_2 in ^3He, and H_2 in ^4He). The cross sections were all 42 ± 1 A^2 and were independent of temperature at relative velocities above *ca.* 1.2×10^5 cm/sec.

A theoretical mechanism called "spectator stripping" was developed to treat the results of the molecular beam studies of alkali-atom–halogen-molecule reactions and was able to predict successfully the gross features observed. An experimental test of the model involving the scattering of Na from Br_2 was undertaken.

The new permanent-gas crossed-beam apparatus was used to survey the feasibility of studying some new reaction types. Preliminary experiments on the reactions of ozone with nitrous oxide and with atomic hydrogen were carried out.

A new method involving the use of time-of-flight techniques was developed for the study of collision-induced vibrational excitation and other inelastic molecular processes.

A computer program was written which may be useful in the intepretation, in terms of classical mechanics, of angular distributions measured in experiments on molecular beam scattering. The program is written in two parts: the first part is used to adjust the minimum value of the interatomic potential to any desired equilibrium internuclear distance by adjusting the strength of the repulsive portion of the potential, while the second part computes the classical deflection function, the corresponding phase shift, and the angular spacing between the principal rainbow and the second-order rainbow.

The ions H_3O^+, HD_2O^+, and D_3O^+ were observed in a mass spectrometer. The evidence strongly suggests these are due to the ionization of the

corresponding neutral species, which are formed by a surface reaction.

A study of the heterogeneous decomposition of acetone over platinum showed that two negative ions, CH_3^- and $CH_3COCH_2^-$, and two free radicals, CH_3 and CH_3COCH_2, were present in the gas phase during the course of the decomposition reaction. Results from this study indicated that the first two steps in the decomposition are $CH_3COCH_3 \rightarrow 2CH_3 + CO$ and $CH_3 + CH_3COCH_3 \rightarrow CH_4 + CH_3COCH_2$.

The measured ionization cross sections produced by 2.2-Mev alpha particles were found to conform well with predictions of the Born-Bethe and classical approximations for the removal of one electron from the outer shell of H_2, He, and Ar. However, the mass spectra of simple molecules produced by the heavy ions show considerably less fragmentation than the mass spectra produced by electrons of equivalent velocity. In the rare gases the electrons produce more multiple ionization than the alpha particles. These differences are contrary to expectations on the basis of the Born-Bethe approximation.

Two high (>85%) transmission electron-bombardment ion sources capable of measuring partial pressures as low as 10^{-17} atm were designed and constructed. One ion source was designed for general use with experiments in which high sensitivity is required, while the second, a dual-electron-beam source, was designed for the study of unstable species such as excited neutral molecules, products of ion-molecule reactions, and free radicals.

The electrodeposition of isotopic samples on small wires (~6 mils in diameter) was developed to circumvent two types of sample preparation problems encountered in most spectroscopy.

Investigation of fragment ions that result from the formation of a vacancy in one of the inner shells of a heavy atom was extended to large molecules, namely, C_2H_5I and $Pb(CH_3)_4$. The studies show that extensive ionization occurs followed by a Coulombic explosion of the aggregate ions. Even for these large molecules, decomposition into the constituent elements is essentially complete.

1. Nuclear Chemistry

NEUTRON CAPTURE CROSS SECTION OF THE 6.75-DAY URANIUM-237

J. Halperin J. J. Pinajian[1]
C. R. Baldock J. H. Oliver
R. W. Stoughton

The irradiation of a particularly pure sample of ^{236}U in the high-flux reactor at Savannah River has permitted an estimate to be made of the reactor capture cross section of ^{237}U by analysis of the ^{238}U produced; see Eq. (1):

$$^{236}U(n,\gamma)^{237}U \xrightarrow[\beta^-]{6.75\text{ days}} {}^{238}U \qquad (1)$$

The calutron-separated samples of ^{236}U containing $\sim$45 ppm ^{238}U were irradiated at an average flux of $\sim 8 \times 10^{14}$ neutrons cm^{-2} sec^{-1} for an integrated flux-time of $\sim 0.6 \times 10^{21}$ neutrons/cm^2. The ^{238}U content of the sample was found to be $\sim$120 ppm following the irradiation. The uranium samples were assayed using a two-stage mass spectrometer. Singly charged uranium metal ions were produced by surface ionization from rhenium filaments and measured with a 14-stage electron multiplier. A preliminary value of the reactor capture cross section of the order of 100 barns can be reported for ^{237}U. A more thorough analysis awaits the obtaining of a more complete description of the complex flux history of the sample from Savannah River.

It may be noted that the ^{237}U capture cross section of $\sim$100 barns is comparable to the value of 100 barns for ^{235}U and greater than the value of 22 barns reported for ^{239}U. The fission cross section of ^{237}U can be estimated to be less than $\sim$50 barns using the method of Huizenga[2] to estimate the value of $\alpha = (\sigma_{capture}/\sigma_{fission})$ from neutron binding energies.

[1]Isotopes Division.

REACTOR NEUTRON CROSS SECTIONS FOR THE CADMIUM ISOTOPES 110, 111, AND 112

C. R. Baldock L. E. Idom
J. Halperin J. H. Oliver

Calutron-enriched isotopes of ^{110}Cd, ^{111}Cd, and ^{112}Cd have been irradiated in the ORR to an integrated flux-time of $\sim 3 \times 10^{20}$ neutrons/cm^2. The irradiated samples as well as the original samples were examined mass spectrographically to measure the enhancement of the product isotope (i.e., the next higher mass number of the sample irradiated). The cadmium was deposited on a rhenium filament with boric acid to enhance ion production by thermal ionization in the two-stage mass spectrometer. The ions were detected with a 14-stage electron multiplier.

The flux during the irradiation was monitored with dilute cobalt alloys and included the use of cadmium filters so as to measure both the thermal and the resonance flux. The ratio of thermal to resonance flux in this irradiation was $\sim$8.6, a relatively hard spectrum, and the thermal flux was measured as $\sim 1.5 \times 10^{14}$ neutrons cm^{-2} sec^{-1}.

The experimental data are summarized in Table 1.1. The pertinent mass data are shown in columns 2, 3, and 4, and the computed reactor neutron cross sections based on the thermal flux are shown in

[2]J. R. Huizenga, *Proc. Intern. Conf. Peaceful Uses At. Energy, Geneva, 1955* **2**, 208 (1956).

Table 1.1. Neutron Capture Cross Sections of $^{110,111,112}Cd$

Enriched Nuclide	Mass Analysis: Nuclide Ratio	Mass Analysis: Initial	Mass Analysis: Final	σ_{eff} (barns)
^{110}Cd	111/110	0.01048 ±0.00007	0.01392 ±0.00006	11.0 ± 1
^{111}Cd	112/111	0.01763 ±0.00008	0.02423 ±0.00008	24.3 ± 3
^{112}Cd	(113 + 114)/112	0.00923 ±0.00006	0.00990 ±0.00006	2.2 ± 0.5

the last column. The mass data are most conveniently interpreted in terms of Eq. (1), where the subscripts f and o refer to the ratios following irradiation and before irradiation respectively:

$$\sigma_i = \frac{(N_{i+1}/N_i)_f - (N_{i+1}/N_i)_o}{\phi t[1 - 0.5\phi t(\sigma_{i+1} - \sigma_c)][1 + (N_{i+1}/N_i)_o]} + \frac{(N_{i+1}/N_i)_o\,\sigma_{i+1}}{1 + (N_{i+1}/N_i)_o} . \quad (1)$$

It is not possible to measure the resonance integral of the cadmium isotopes using a cadmium filter technique, because of the self-shielding of the cadmium resonances. A samarium or gadolinium neutron filter could be used in this instance for such a measurement.

The mass chains 110, 111, and 112 lie in the valley of the fission yield curve for ^{235}U and ^{233}U and thus would negligibly affect neutron losses in reactors fueled with those nuclides. They are somewhat more important in a thermal ^{239}Pu reactor, where the fission yields are one to two orders of magnitude higher.

THERMAL NEUTRON CROSS SECTION AND RESONANCE INTEGRAL OF 36-hr RHODIUM-105

J. Halperin L. E. Idom
C. R. Baldock J. H. Oliver
R. W. Stoughton

The high neutron cross section of ^{105}Rh and its implications for reactor operations have prompted a reevaluation of both the thermal cross section and resonance integral of this nuclide. Glendenin and co-workers,[3-5] who first observed this unusually high thermal cross section, also noted only minor epicadmium capture. This is consistent with a large resonance in the thermal region below 0.5 ev.

In the present experiment we have examined mass spectrographically the palladium product formed following irradiation of ^{104}Ru, to deduce the capture cross section of ^{105}Rh; see Eq. (1):

$$\begin{array}{ccc} ^{105}Pd & (n,\gamma)^{106}Pd & \\ \uparrow \beta^- \; 36\text{ hr}/30\text{ sec} & \uparrow \beta^- \; 2.2\text{ hr}/30\text{ sec} & \\ ^{105}Rh & (n,\gamma)^{106}Rh & \\ \uparrow \beta^- \; 4.4\text{ hr} & & \\ ^{104}Ru(n,\gamma)^{105}Ru & & \end{array} \quad (1)$$

The measurement of the palladium product has the advantage of yielding a measure of the *total* capture cross section of ^{105}Rh. If an unidentified short-lived isomer of ^{106}Rh were formed during irradiation, then the identification of partial cross sections, that is, to the 2.2-hr and 30-sec states, would yield an incomplete and low value of the cross section for ^{105}Rh.

[3] J. G. Cuninghame, L. E. Glendenin, and A. L. Harkness, *J. Inorg. Nucl. Chem.* **24**, 1009 (1962).

[4] L. E. Glendenin and R. A. Schmitt, *Nucl. Sci. Eng.* **20**, 298 (1964).

[5] L. E. Glendenin, H. C. Griffin, and R. A. Schmitt, ANL-6797, p. 388 (1965).

Samples of metallic calutron-enriched ^{104}Ru were irradiated in the hydraulic tube facility of the ORR at a flux of about 2×10^{14} neutrons cm^{-2} sec^{-1} for an integrated flux-time of $\sim 6 \times 10^{20}$ neutrons/cm^2. In addition to bare samples, irradiations were made with neutron filters of 880 mg/cm^2 of cadmium, 44 mg/cm^2 of ^{10}B, and 101 mg/cm^2 of ^{10}B. The filters were in the form of 11×11 mm cylinders of 40-mil wall thickness in the case of cadmium and 100-mil thickness in the ^{10}B cases. The boron was dispersed in an aluminum matrix as a cermet. Elemental ^{10}B and aluminum powders had been compressed at pressures of $\sim$20,000 lb/in.^{2} to form cylinders that were sufficiently sturdy to be machined to the required sizes.

Following the irradiations, the ruthenium samples were dissolved in an $NaNO_3$-Na_2O_2 fused salt mixture and taken up in HCl. At this point a calutron-separated sample of ^{110}Pd was added as a carrier. The palladium was plated from the ruthenium solution onto a nickel foil, removed with HNO_3, and passed through a Dowex 50 cation exchange resin column in 9 *M* HBr. This was followed by sorption onto a second Dowex 50 cation column from 0.5 *M* $HClO_4$ and eluted with 0.1 *M* HCl. The palladium was then electroplated onto a rhenium filament suitable as a source for the mass spectrometer. Palladium metal ions were produced from the filament by thermal ionization and detected in the two-stage mass spectrometer with an electron multiplier.

The experimental data have been summarized in Table 1.2. The calculated effective cutoffs for the neutron filters[6] are listed in column 3. The thermal flux and the resonance flux per unit lethargy are listed in columns 4 and 5 respectively. The fluxes were measured with dilute cobalt monitors and were based upon $\sigma_0 = 37$ barns and $I = 75$ barns for the ^{59}Co cross-section values. The thermal flux is taken as the Maxwellian component of the flux spectrum and is represented as the equivalent 2200-m/sec flux. Selected mass ratio determinations are shown in columns 7, 8, and 9. All mass assays included a measurement at the 108 mass position. This served as a sensitive indicator of possible sample contamination by natural palladium. One such sample which showed a $^{108}Pd/^{110}Pd$ ratio greater than that of the added standard was discarded. The $^{106}Pd/^{105}Pd$ ratio listed in column 7 has been corrected for the ^{110}Pd carrier added to the irradiated sample. Thus this ratio is a direct measure of the competition between beta decay and neutron capture in the ^{105}Rh produced during the irradiations,

$$\frac{^{106}Pd}{^{105}Pd} = \frac{\bar{\phi}\sigma(^{105}Rh)}{\lambda(^{105}Rh)} , \qquad (2)$$

[6]R. W. Stoughton and J. Halperin, *Effective Cutoff Energies for B, Cd, Gd, and Sm Filters*, ORNL-TM-236 (1962).

Table 1.2. Data for ^{105}Rh Cross-Section Measurement

Irradiation No.	Type of Irradiation	E_c (ev)	ϕ_{th} (neutrons cm^{-2} sec^{-1})	ϕ_r (neutrons cm^{-2} sec^{-1})	$^{106}Pd/^{110}Pd$	$^{105}Pd/^{110}Pd$	$^{106}Pd^a/^{105}Pd$	σ_{eff} (kilobarns)	I (kilobarns)	σ_{th} (kilobarns)
			$\times 10^{14}$	$\times 10^{13}$						
1*a*	Bare		1.89		0.02552	0.03191	0.5574	16.4 ± 1.5		15.0
1*b*					0.01900	0.02011	0.5546			
2	Bare		1.81		0.01757	0.01912	0.4865	15.1 ± 1.5		13.8
3	40-mil Cd filter	0.54		1.50	0.01142	0.03157	0.0450		$16._7 \pm 3$	
4	44-mg/cm^2 ^{10}B filter	2		1.54	0.01068	0.03365	0.0156		$5._6 \pm 2$	
5	101-mg/cm^2 ^{10}B filter	15		1.50	0.01089	0.06059	0.0114		$4._2 \pm 2$	

[a]Corrected for ^{110}Pd spike ($^{106}Pd/^{110}Pd = 0.01020$, $^{105}Pd/^{110}Pd = 0.00397$), the contribution of ^{105}Pd capture, and ^{105}Rh decay following irradiation.

where $\bar{\phi}$ is the average thermal or resonance flux and σ is the effective cross section or resonance integral respectively. In this experiment, since the reactor was at full power some 96.38% of the 978.3 hr that the sample was irradiated, the distinction between average flux $\bar{\phi}$ and full-power flux represents only a small difference.

The observed mass ratios of $^{106}Pd/^{105}Pd$ need to be corrected for ^{105}Pd and ^{106}Pd neutron capture during the course of the irradiation. The thermal cross section and resonance integral of ^{106}Pd are known[7] and the effect is too small to influence this measurement. However, the cross section and resonance integral of ^{105}Pd have not been directly measured, but they may be estimated to be large enough to influence the present results. Palladium-105 is the only odd-neutron nuclide among the stable palladiums and very likely has the largest cross section. If the difference between the elemental thermal cross section and that due to ^{102}Pd, ^{106}Pd, ^{108}Pd, and ^{110}Pd is assigned entirely to ^{105}Pd (neglecting the unknown ^{104}Pd cross section), this implies σ_{th} (^{105}Pd) $\cong$ 20 barns. From the reported[8] resonances of palladium and the elemental resonance integral[9] of 23 barns, we estimate $I(^{105}Pd) \cong 60$ barns. These estimated values of the ^{105}Pd cross sections imply a 1.7 and 3.2% correction to the effective cross section and resonance integral of ^{105}Rh respectively. A further diminution of 3.6 and 5.1% in the ^{105}Pd content is required to correct for the ^{105}Pd produced in the sample following removal from the reactor in the bare and filtered samples respectively.

An effective cross section σ_{eff} of 15.8 ± 1.5 kilobarns and a resonance integral of 17 ± 3 kilobarns for ^{105}Rh have been measured in this experiment. Since the flux ratio $(\phi_{th}/\phi_r) = 12.2$, a thermal or subcadmium cross section $\sigma_{th} = 14.4 \pm 1.5$ kilobarns can be reported. This reactor cross section appears to be some 20% lower than that reported by Glendenin, and the resonance integral found here is approximately at the upper limit set in their experiment.

[7]P. M. Lantz, C. R. Baldock, and L. E. Idom, *Thermal Neutron Cross Section and Resonance Integral of ^{106}Pd*, ORNL-3679, p. 10 (1964).

[8]D. J. Hughes, B. A. Magurno, and M. K. Brussel, *Neutron Cross Sections*, BNL-325, 2d ed., suppl. 1 (1960).

[9]R. L. Macklin and H. S. Pomerance, "Resonance Capture Integrals," *Proc. Intern. Conf. Peaceful Uses At. Energy, Geneva, 1955*, 5, 96 (1956).

The cobalt samples irradiated in the boron filters were found to have been activated to the predicted extent within the limits of experimental error. The ratio of the cobalt activation in the 44-mg/cm^2 ^{10}B filter to the activation in the cadmium filter was calculated[6] to be 0.77 and actually measured as 0.75 ± 0.02. This same ratio in the ^{105}Rh experiment was observed as 0.33 ± 0.1. Similarly, the ratio for the cobalt activation in the 101-mg/cm^2 ^{10}B filter to the activation in the cadmium filter was calculated to be 0.58 and actually found to be 0.59 ± 0.02. This same ratio in the ^{105}Rh experiment was observed to be 0.24 ± 0.1. The significance of the lower values of this ratio for ^{105}Rh compared to ^{59}Co indicates that a much larger fraction of the resonance absorption in ^{105}Rh occurs at energies below the 132-ev resonance in ^{59}Co. At these lower energies, ^{10}B is a much more effective filter for neutrons than it is at 132 ev. In view of the average level spacing of ~25 ev observed in ^{103}Rh and this parallel expectation in ^{105}Rh, the largest portion of the resonance integral lies well below 100 ev in ^{105}Rh.

The implication to reactor technology is such that for reactors operating on ^{235}U thermal fission, where the 105 chain yield is 1.8%, a 0.9% neutron loss per fission will be experienced at a flux level of $\sim 3 \times 10^{14}$ neutrons cm^{-2} sec^{-1}. In reactors operating on ^{239}Pu thermal fission the loss would rise to ~2% neutron loss per fission at the same flux level, increasing asymptotically at higher flux levels to the value of the fission yield.

The authors would like to acknowledge the help of Fred Nelson in developing the chemical procedure necessary to produce the very pure samples demanded for the mass spectrographic analyses. We are particularly indebted to P. M. Lantz for many discussions on design of the present experiment and help in avoiding the numerous pitfalls in the measurements.

THERMAL NEUTRON CROSS SECTIONS AND RESONANCE INTEGRALS OF LANTHANUM-139 AND -140

H. A. O'Brien[1] R. E. Druschel
J. S. Eldridge[10] J. Halperin

Both ^{139}La and ^{140}La are produced in fission with high yield in a nuclear reactor. Their cross

[10]Analytical Chemistry Division.

sections are thus of interest to the neutron economy of the reactor system. Further, relatively intense sources of ^{141}Ce which are essentially carrier free can be prepared by irradiating ^{139}La in a high-flux reactor so as to take advantage of neutron capture in ^{140}La. We have measured the thermal cross section and resonance integral of ^{140}La, and in doing so we have remeasured the thermal cross section and resonance integral of ^{139}La.

Upon irradiation of ^{139}La, both ^{140}La and ^{141}Ce are formed; see Eq. (1):

$$\begin{array}{ccc} & & \beta^- \uparrow 32.5 \text{ days} \\ & {}^{140}\text{Ce}\ (n,\gamma) & {}^{141}\text{Ce} \\ \beta^- \uparrow 40.2 \text{ hr} & & \beta^- \uparrow 3.9 \text{ hr} \\ {}^{139}\text{La}(n,\gamma) & {}^{140}\text{La}\ (n,\gamma) & {}^{141}\text{La}\ , \end{array} \qquad (1)$$

In the present experiment weighed samples of La_2O_3 were irradiated in a capsule in a configuration containing two cadmium-wrapped and one unwrapped sample. Dilute alloys of cobalt in aluminum were used to monitor the irradiations. Two capsules were irradiated, for three days and five days, respectively, in the hydraulic tube facility of the ORR.

Following the irradiation and about a one-week cooling period, the lanthanum samples were dissolved and assayed for ^{140}La using NaI gamma-ray spectroscopy and measuring the characteristic 1.60-Mev photopeak. Since the ^{141}Ce was produced in amounts some five orders of magnitude less than the ^{140}La, a chemical separation was required. Following the addition of Ce, La, and Zr carriers, a fluoride precipitation was carried out, followed by redissolution and bromate oxidation. A series of cerium iodate precipitations followed by peroxide dissolutions served to effect the large lanthanum decontamination factor required here.[11] After a hydroxide precipitation the final cerium fraction was precipitated as the oxalate and weighed as $Ce_2(C_2O_4)_3 \cdot 9H_2O$. Chemical yields of the cerium were somewhat in excess of 80%. The 142-kev gamma ray in ^{141}Ce was then assayed for the analysis. Spectral and decay data showed the sample to be radiochemically pure. The ^{139}La concentration was checked in several instances following the irradiation using an ethylenediaminetetraacetic acid (EDTA) titrimetric procedure, which in general corroborated the original weights to within 1%.

The irradiation history for both samples was such that the capsules were exposed to essentially a constant flux. No downtimes were experienced in the three-day irradiation, and a brief excursion to a level of two-thirds full power in the five-day irradiation amounted to less than a 0.1% perturbation in the integrated flux-time. It was thus possible to describe the ^{140}La and ^{141}Ce produced at the end of the irradiation by the ^{140}La neutron capture path by Eqs. (2) and (3) respectively:

$$\frac{{}^{140}A}{{}^{139}N} = \phi\sigma_{139}(1 - e^{-\lambda_{140}t}) , \qquad (2)$$

$$\frac{{}^{141}A}{{}^{140}A} = \frac{\phi\sigma_{140}}{(\lambda_{140} - \lambda_{141})} \times \left[\frac{(1 - e^{-\lambda_{141}t})}{(1 - e^{-\lambda_{140}t})} - \frac{\lambda_{141}}{\lambda_{140}}\right] . \qquad (3)$$

In Eqs. (2) and (3) the terms A and N are activity (disintegrations per second) and atoms respectively. The terms ϕ and σ are to be taken as the appropriate pairs, that is, the resonance flux ϕ_r and the resonance integral I, or as the thermal flux ϕ_{th} and the effective cross section σ_{eff} respectively.[12] The effective cross section, σ_{eff}, can be related to the thermal or sub-cadmium cross section, σ_{th}, through Eq. (4); and to σ_0, the 2200-m/sec cross section (assuming the usual "1/v" dependence in the near-thermal region) through Eq. (5):[12]

$$\sigma_{eff} = \sigma_{th} + \frac{\phi_r}{\phi_{th}} I , \qquad (4)$$

$$\sigma_{th} = g\sigma_0 + \frac{\phi_r}{\phi_{th}} \int_{5E_m}^{E_c} \sigma\, d(\ln E) . \qquad (5)$$

[11] P. C. Stevenson and W. E. Nervick, *The Radiochemistry of the Rare Earths, Scandium, Yttrium, and Actinium*, Nuclear Science Series, National Academy of Sciences, National Research Council, available from the Office of Technical Services, Department of Commerce, Washington 25, D.C., p. 224 (1961).

[12] R. W. Stoughton and J. Halperin, *Nucl. Sci. Eng.* 6, 100 (1959).

The data have been summarized in Table 1.3. The results of two irradiations are shown. The fluxes have been measured with 0.151% cobalt alloys using a 2200-m/sec value of 37 barns and a resonance integral of 75 barns for cobalt. The thermal flux, ϕ_{th}, is taken to represent the Maxwellian component of the spectrum, and the resonance flux, ϕ_r, the epithermal flux per unit lethargy. Cadmium containers of 40-mil wall thickness, 11 mm in diameter and 11 mm high, were used as neutron filters, giving rise to an effective cutoff of 0.54 ev. The activities of ^{140}La and ^{141}Ce are shown in columns 6 and 7. A loss of sample in irradiation No. 1*a* resulted in the omission of the calculated cross section for that case. The cross sections quoted for ^{140}La include a correction for the contribution to the observed ^{141}Ce due to product formed from capture in ^{140}Ce during the irradiation as large as 5% and a 2% correction for the burnout of ^{141}Ce.

The thermal cross section of 2.7 ± 0.3 barns and resonance integral of 69 ± 4 barns reported here may be compared to the measurement of Katcoff and co-workers[13] carried out in the early days of the Plutonium Project. Correcting their reported value of the pile cross section with modern values of the fission cross section of ^{235}U and the yield of ^{140}Ba (which was used as a flux monitor in their experiment), as well as the half-life of ^{141}Ce, which had been taken as 28 days in their work, we calculate their cross section to be ~3.7 barns. Since a 1- to 2-barn contribution to the effective cross section was experienced due to resonance neutrons, it is possible to estimate that a pile cross section of some 4 to 5 barns should have been observed. Since their estimated uncertainty in the value they reported was some 33%, their result actually lies well within their estimated error.

The values of the 2200-m/sec cross section and resonance integral for ^{139}La calculated from the data of Table 1.3 are $\sigma_0 = 9.2 \pm 0.5$ barns and $I = 11.2 \pm 0.6$ barns. They are essentially consistent with the 8.9-barn absorption cross section shown[14] in BNL-325 and with the 11-barn resonance integral quoted by Macklin and Pomerance.[15]

The authors are particularly grateful to C. F. Goeking of the Analytical Chemistry Division for carrying out cerium analyses and to W. R. Laing of the same division for titrimetric analyses of the lanthanum.

[13] S. Katcoff, J. A. Leroy, K. A. Walsh, R. A. Elmer, S. S. Goldsmith, L. D. Hall, E. G. Newbury, J. J. Povelites, and J. S. Waddell, *J. Chem. Phys.* **17**, 421 (1949).

[14] D. J. Hughes, B. A. Magarno, and M. K. Brussel, *Neutron Cross Sections*, BNL-325, 2d ed., suppl. 1 (1960).

[15] R. L. Macklin and H. S. Pomerance, *Proc. Intern. Conf. Peaceful Uses At. Energy, Geneva, 1955*, **5**, 96 (1956).

Table 1.3. Cross-Section Data for ^{139}La and ^{140}La

Irradiation No.	Type of Irradiation	Length of Irradiation (min)	Flux (neutrons cm^{-2} sec^{-1}) Thermal	Flux Resonance	$^{140}A/^{139}N$ (dis sec^{-1} atom^{-1})	$^{140}A/^{141}A$	^{139}La σ_{eff} (barns)	^{139}La I (barns)	^{139}La σ_{th} (barns)	^{140}La σ_{eff}[a] (barns)	^{140}La I (barns)	^{140}La σ_{th}[a] (barns)
			$\times 10^{13}$	$\times 10^{13}$	$\times 10^{-10}$	$\times 10^{-6}$						
1*a*	Neutron filter	4320		1.63	*b*	9.07		*b*			$70._3$	
1*b*	Bare	4320	15.6		12.1	13.1_6	10.9		9.7	10.2		2.7_4
1c	Neutron filter	4320		1.80	1.45_2	9.4_2		11.4			$66._2$	
2*a*	Neutron filter	7196		1.84	1.76_3	17.9_9		10.9			$68._3$	
2*b*	Bare	7196	15.9_6		15.2_5	25.8_3	11.0		9.66	10.7		2.7_0
2c	Neutron filter	7196		1.87	1.86_2	18.6_0		11.4			$69._4$	
												Av = 2.7_2

[a] Corrected for contribution of ^{141}Ce from ^{140}Ce capture.

[b] Not included because of partial sample loss.

THERMAL NEUTRON CROSS SECTION AND RESONANCE INTEGRAL OF 7.5-DAY SILVER-111

R. E. Druschel J. Halperin

Samples of ^{111}Ag have been irradiated at a high flux in the hydraulic tube of the ORR and examined for the 3.2-hr ^{112}Ag formed, in order to evaluate its thermal cross section and resonance integral. The measurement of the ^{112}Ag in the presence of the much larger quantity of ^{111}Ag was carried out by counting the much harder betas of ^{112}Ag (up to 4.1 Mev) with a proportional counter through 410 mg/cm^2 of aluminum, which absorbed the relatively softer betas of ^{111}Ag (up to 1.04 Mev). A least-squares analysis of the decay curve served to resolve the 3.2-hr period from the 7.5-day period.

The efficiency of the counter for ^{111}Ag was determined from a source of ^{111}Ag prepared by an irradiation of ^{110}Pd and measured using a 4π beta-gamma coincidence technique. The purity of the source was verified by a decay measurement as well as by NaI gamma-ray spectrometry. The efficiency of the counter for ^{112}Ag was similarly determined from a source produced by ^{239}Pu fission. The 21-hr ^{112}Pd was isolated by sorption on an anion column from 3 *M* HCl and reduction to metallic palladium followed by a dimethylglyoxime precipitation. The palladium was again adsorbed on an anion exchanger, and periodic elutions of silver with 8 *M* HCl were made so as to maximize the ^{112}Ag eluted with respect to other silver activities present. It was thus possible to prepare a sample with less than 1% impurity as judged from its decay curve.

Two irradiations of ^{111}Pd were carried out using 40-mil cadmium neutron filters together with bare samples. The flux was measured in the usual way with dilute cobalt monitors. The thermal flux was $\sim 1.5 \times 10^{14}$ neutrons cm^{-2} sec^{-1} and the ratio of thermal to resonance flux was found to be $\phi_{th}/\phi_r = 8.95$ in this experiment. The results of the measurement are shown in Table 1.4. In general the effective cross section and resonance integral reflect the large uncertainty ($\sim$20%) introduced due to the relatively small amount of ^{112}Ag produced in the samples. Because of the large ratio of I/σ_{th} for ^{111}Ag, the uncertainty in the value of σ_{th} is relatively large. A value of $\sigma_{th} = 3.2 \pm 2$ barns and $I = 105 \pm 20$ barns is reported for the thermal cross section and resonance integral of ^{111}Ag respectively.

NUCLEAR CHARGE DISTRIBUTION IN FISSION: YIELD OF PALLADIUM-115 FROM THERMAL-NEUTRON FISSION OF URANIUM-235

M. F. Roche[16] R. L. Ferguson
D. E. Troutner[17]

Experimental data concerning the division of nuclear charge in fission events leading to fragments of nearly equal mass is practically nonexistent. To measure the yield of ^{115}Pd, experiments similar to those reported elsewhere[18] have been performed in which palladium dimethylglyox-

[16]ORINS Predoctoral Fellow, University of Missouri.

[17]Department of Chemistry, University of Missouri, Columbia.

[18]N. G. Runnalls, D. E. Troutner, and R. L. Ferguson, "Nuclear Charge Distribution in Fission: Yields of Barium-143 and -144 from Thermal-Neutron Fission of Uranium-235," this report.

Table 1.4. Summary of Cross-Section Measurements of ^{111}Ag

Length of Irradiation (min)	ϕ_{th} (neutrons cm^{-2} sec^{-1})	ϕ_{th}/ϕ_r	σ_{eff} (barns)	I (barns)	σ_{th} (barns)
	$\times 10^{14}$				
1018	1.64	8.95	13.5 ± 2.5	100 ± 20	2.5
620	1.51	8.95	16.2 ± 3	110 ± 20	3.9
				Av = 105 ± 20	Av = 3.2 ± 2

ime was precipitated, filtered, and washed to separate the palladium from other chain members. Precipitation time was measured to about 0.1 sec with slow-motion photography. Half the solution, from which the palladium was not separated, was used for point-by-point normalization of the yield data. Radioactivity of both isomers of ^{115}Cd resulting from the decay of chain members in a series of such samples was measured and used to calculate the fraction of the mass 115 chain present as ^{115}Pd at the time of separation. The ratio of cadmium impurity to ^{235}U in the irradiated solution was about 10^{-6}, so essentially all the cadmium activity seen was produced in fission. A preliminary analysis of the results is shown in Fig. 1.1.

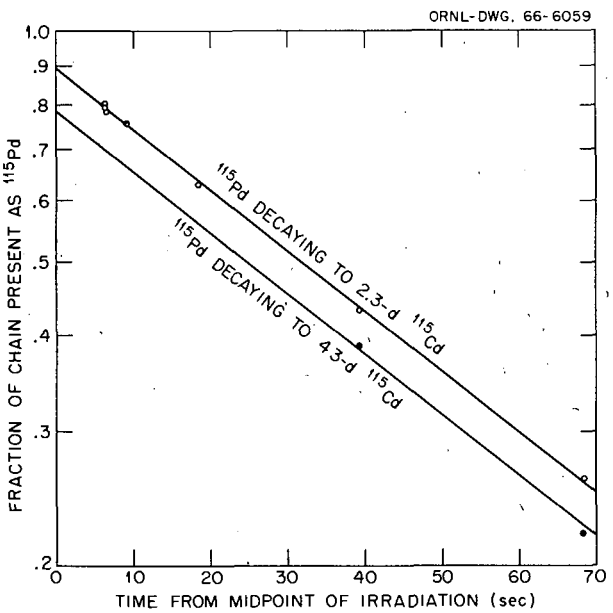

Fig. 1.1. Decay of ^{115}Pd to ^{115}Cd Isomers.

The absence of growth of ^{115}Pd places an upper limit of about 2 sec on the half-life of its precursors. The ^{115}Pd half-life is measured to be 38.0 ± 0.5 sec. The zero time intercepts give the fractions of the 2.3- and 43-day isomers arising from the decay of palladium (zero time on the plot corresponds to the mean irradiation time for 1- to 4-sec irradiations). The fractional cumulative yield for ^{115}Pd computed from these intercepts, normalized by the cumulative chain yields reported for the ^{115}Cd isomers,[19] is 0.883 ± 0.020, in agreement with the measurement reported by Weiss and Reichert[20] of 0.905 ± 0.072. If the ^{115}Cd isomer independent yields are small, the sum of the fractional independent yields of the silver isomers is 0.117 ± 0.020.

NUCLEAR CHARGE DISTRIBUTION IN FISSION: YIELDS OF BARIUM-143 AND -144 FROM THERMAL-NEUTRON FISSION OF URANIUM-235

N. G. Runnalls[17] D. E. Troutner[17]
R. L. Ferguson

The fractional cumulative fission yields of ^{143}Ba and ^{144}Ba from thermal-neutron fission of ^{235}U, and the half-lives of these barium isotopes, have been determined. These results provide information concerning the division of nuclear charge in fission and, in particular, help to define the nuclear charge dispersion (in terms of the normal Gaussian width parameter σ) about the most probable charge Z_p for these fission product masses.

Experiments were performed in which a solution of ^{235}U and lanthanum carrier was irradiated for 2 sec in the pneumatic tube facility of the Oak Ridge Research Reactor. After irradiation, this solution was transferred to a filter funnel which contained barium carrier and ammonium hydroxide; the resulting precipitate of lanthanum hydroxide was filtered and washed quickly. This afforded a rapid, efficient separation of fission product barium from lanthanum. Cerium carrier was later added to the filtrate and to a solution resulting from dissolution of the lanthanum hydroxide. Cerium from each of these samples was purified, and both ^{143}Ce-^{143}Pr and ^{144}Ce-^{144}Pr radioactivities resulting from fission were measured. The ratio of cerium-praseodymium activity from the filtrate sample to the total cerium-praseodymium activity from both samples represents the fraction of each mass chain that was present as barium at the time of the barium-lanthanum separation. In a series of experiments, separation times were varied from 12 to 136 sec after irradiation, and the results obtained are presented in Fig. 1.2. Half-lives of the barium isotopes were obtained from the slopes of these

[19] A. C. Wahl and N. A. Bonner, *Phys. Rev.* **85**, 570 (1952).

[20] H. V. Weiss and W. L. Reichert, USNRDL-TR-943 (1965).

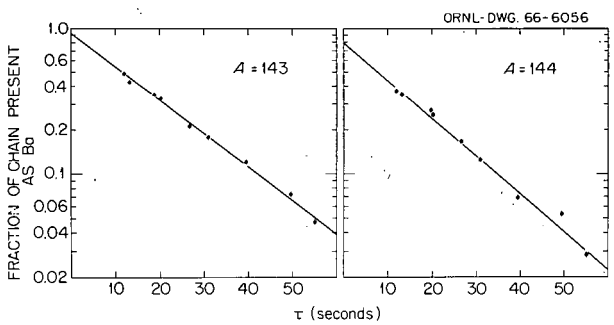

Fig. 1.2. Fractions of Mass 143 and Mass 144 Fission Product Chains Present as Ba as a Function of Time After Irradiation.

"decay" curves, and the fractional cumulative yields were computed from the intercepts at zero separation time.

Figure 1.3 shows "probability" graphs of the ^{143}Ba and ^{144}Ba fractional cumulative yields obtained in this work, along with previously measured yields[21] in these mass chains, plotted as a function of the nuclear charge Z. A Gaussian distribution is represented on these plots by a straight line which has a Z value at 0.50 fractional yield equal to $(Z_p - 0.5)$ and a slope proportional to σ. Summarized in Table 1.5 are the findings of this work; for mass 143 the values of Z_p, σ, and half-life are in agreement with earlier, less-certain values.[21]

Last year[22,23] it was suggested that, contrary to previous assumptions,[21] there may be a small

[21] A. C. Wahl, R. L. Ferguson, D. R. Nethaway, D. E. Troutner, and K. Wolfsberg, *Phys. Rev.* **126**, 1112 (1962).

[22] L. H. Niece, D. E. Troutner, and R. L. Ferguson, *Chem. Div. Ann. Progr. Rept. June 20, 1965*, ORNL-3832, p. 26.

[23] L. H. Niece, *Independent Yields of ^{95}Zr from Thermal Neutron Fission of ^{235}U and ^{233}U*, ORNL-TM-1333 (December 1965).

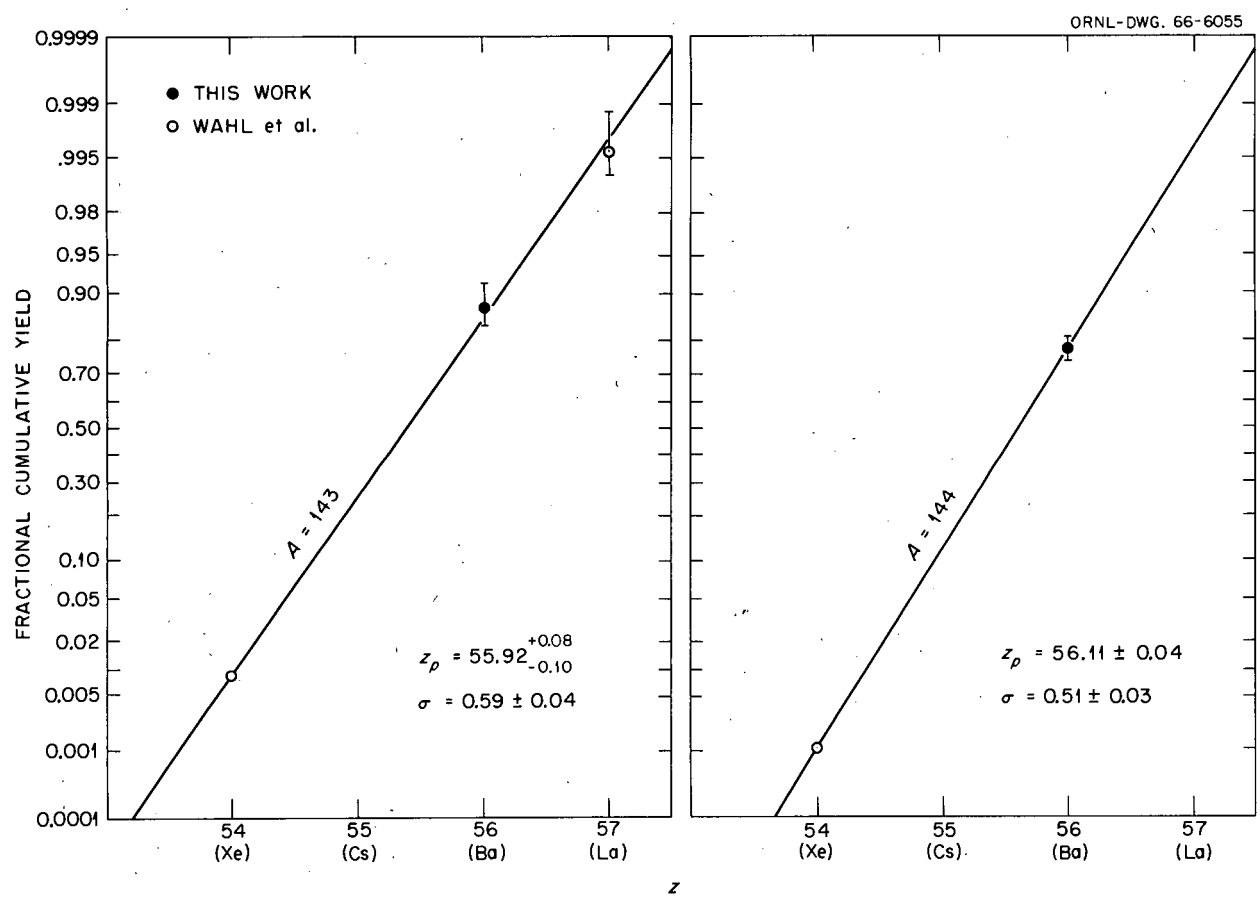

Fig. 1.3. Charge Distributian Probability Graphs for Mass 143 and Mass 144.

Table 1.5. Summary of Results

Fission Product	Fractional Cumulative Yield	Z_p	σ	Half-Life (sec)
^{143}Ba	0.875 ± 0.040	$55.92^{+0.08}_{-0.10}$	0.59 ± 0.04	13.2 ± 0.3
^{144}Ba	0.773 ± 0.035	56.11 ± 0.04	0.51 ± 0.03	11.9 ± 0.25

but sensible variation in the value of σ as a function of fission product mass, at least in the limited mass regions for which appropriate data exist. Evidence has since been obtained at other laboratories[24,25] in support of this contention, and the present results, plotted in Fig. 1.4 along with values obtained previously for adjacent masses,[21] appear to continue the trend described earlier.[22] In addition, the cumulative yield of ^{143}Ba provides a third datum on the charge dispersion of mass 143, which, by the linearity of the probability plot (Fig. 1.3), is shown to be consistent with a Gaussian distribution. The shapes of the charge dispersion curves have been determined radiochemically for only seven other mass chains,[21,24,26] which also were found to be consistent with a Gaussian distribution. However, physical measurements in other mass regions[25] may cast some doubt on the assumption that the dispersion is Gaussian at all fission product masses. Finally, it can be seen from Fig. 1.5 that the decreased charge density, as compared to the fissioning compound nucleus, observed for other heavy-mass chains, is also found at mass 144. The ordinate values of this figure show the

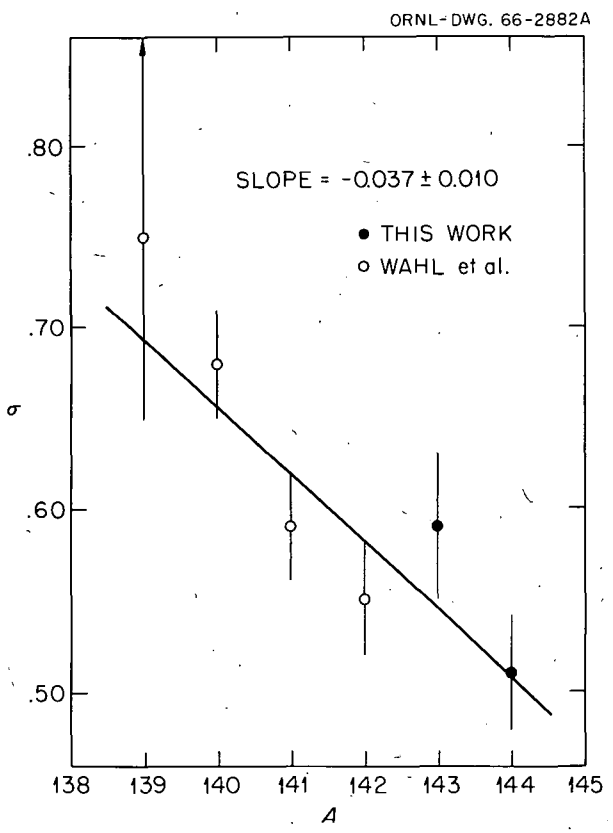

Fig. 1.4. Variation of Nuclear Charge Dispersion with Fission Product Mass.

[24] P. O. Strom, D. L. Love, A. E. Greendale, A. A. Delucchi, D. Sam, and N. E. Ballou, *Phys. Rev.* **144**, 984 (1965).

[25] E. Konecny, H. Opower, H. Günther, and H. Göbel, *Phys. Chem. Fission, Proc. Symp., Salzburg, 1965*, p. 401, Vienna, IAEA, 1965.

[26] A. E. Norris, A. C. Wahl, and R. L. Ferguson, *Phys. Rev.*, in press.

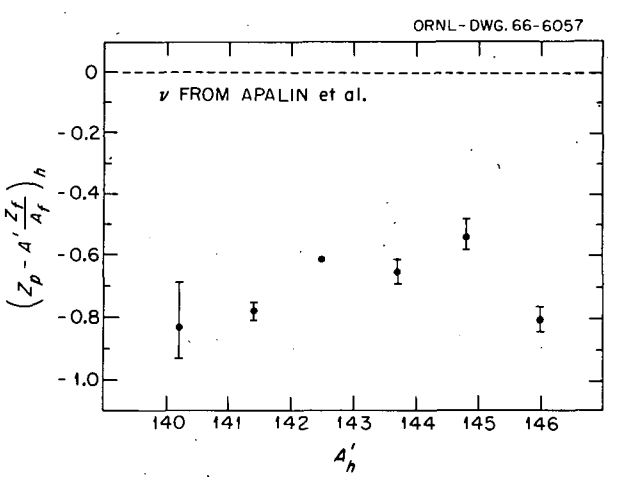

Fig. 1.5. Charge Distribution for ^{235}U Thermal-Neutron Fission. Deviation of Z_p from unchanged charge distribution vs prompt fission fragment mass.

deviations of Z_p, for mass chains in which two or more fractional yields have been measured, from the values that would be found if the fission fragments had the same proton to neutron ratio as the compound nucleus ($^{235}U + n$). The abscissa gives the masses of the prompt fission fragments, that is, the mass numbers of the products actually observed corrected for the emission of prompt neutrons.

NUCLEAR CHARGE DISTRIBUTION IN FISSION: YIELDS OF MOLYBDENUM-103, -105, AND -106 FROM THERMAL-NEUTRON FISSION OF URANIUM-235

J. D. Hastings[17] D. E. Troutner[17]
R. L. Ferguson

It has frequently been suggested that nuclear shell effects may be significant in the mechanism of fission. There is some evidence to indicate that a 50-proton structure is favored and that $_{50}Sn$ nuclides may be preferentially formed in fission;[27] however, more data are needed on this question.

If yields of $_{50}Sn$ isotopes are enhanced, then it follows that, from $_{92}U$ fission, $_{42}Mo$ isotopes (complementary to $_{50}Sn$) must also have high yields. Therefore, experiments analogous to those described for $^{143,144}Ba$[28] were performed to measure the fractional cumulative yields of ^{103}Mo, ^{105}Mo, and ^{106}Mo from thermal-neutron fission of ^{235}U. In this case rapid separations of molybdenum and technetium were achieved by precipitation of the 8-hydroxyquinolinate of molybdenum in one series of experiments and by precipitation of tetraphenylarsonium perrhenate (which carried technetium) in another. The radioactivities measured were ^{103}Ru, ^{105}Rh, and ^{106}Ru.

Preliminary analysis of the results, based on averaged values of published molybdenum half-lives,[29–31] indicates that the fractional cumulative yields of ^{103}Mo and ^{105}Mo are 1.002 ± 0.010 and 0.998 ± 0.020 respectively. Uncertainties in the mass 106 results are quite large, but, based on current counting data, the yield probably lies within the range 0.75 to 1.00 and the ^{106}Mo half-life in the range 8 to 14 sec.

Values of the ^{103}Mo, ^{105}Mo, and ^{106}Mo fractional cumulative yields that are predicted by an empirical charge distribution curve[27] are 1.00, 0.85, and 0.50 respectively. This prediction is based on the assumption that a single charge-dispersion parameter σ is appropriate for all fission product mass chains and on the measured values of fractional yields in neighboring and in nearly complementary chains. The observation in this work that yields for ^{105}Mo and ^{106}Mo appear to be significantly greater than the predicted values indicates that some feature of fission may be operating to enhance the yields of 42-proton nuclides. It is possible that this reflects a preference for forming complementary $_{50}Sn$ nuclides due to the extra stability afforded these nuclei by the strong 50-proton shell.

COMPOUND-NUCLEUS EXCITATION OF MEDIUM-WEIGHT NUCLEI

E. Eichler R. J. Silva
I. R. Williams

The compound system generated by the fusion of a charged particle, such as an alpha particle, with ~50 Mev kinetic energy with a medium-weight target nucleus ($A \sim 100$) will possess 20 to 30 units of angular momentum. Since the neutrons and protons which are evaporated can remove only 2 or 3 $\hbar\omega$ each, the residual nucleus will still retain considerable angular momentum. Hence, gamma-ray transitions are required to deexcite the nucleus. A number of authors have considered the effect of this phenomenon on the compound nucleus mechanism.[32] Others have used these reactions to excite spectroscopically interesting high-spin states.[33] Most of the efforts have fo-

---

[27] A. C. Wahl, R. L. Ferguson, D. R. Nethaway, D. E. Troutner, and K. Wolfsberg, *Phys. Rev.* **126**, 1112 (1962).

[28] N. G. Runnalls, D. E. Troutner, and R. L. Ferguson, "Nuclear Charge Distribution in Fission: Yields of Barium-143 and -144 from Thermal-Neutron Fission of Uranium-235," this report.

[29] A. Baeckmann and E. H. Feuerstein, *Radiochim. Acta* **4**, 111 (1965).

[30] P. Kienle, F. Baumgärtner, B. Weckermann, and U. Zahn, *Radiochim. Acta* **1**, 84 (1963).

[31] P. Kienle and B. Weckermann, *Naturwissenschaften* **49**, 295 (1962).

[32] J. R. Grover, *Phys. Rev.* **127**, 2142 (1962); J. R. Grover, *Phys. Rev.* **123**, 267 (1961); D. G. Sarantites and B. D. Pate, *Nucl. Phys.*, to be published; D. G. Sarantites, *Nucl. Phys.*, to be published.

[33] H. Morinaga and P. C. Gugelot, *Nucl. Phys.* **46**, 210 (1963); F. S. Stephens, N. L. Lark, and R. M. Diamond, *Nucl. Phys.* **63**, 82 (1965); N. L. Lark and H. Morinaga, *Nucl. Phys.* **63**, 466 (1965); J. E. Clarkson, UCRL-16040 (May 1965).

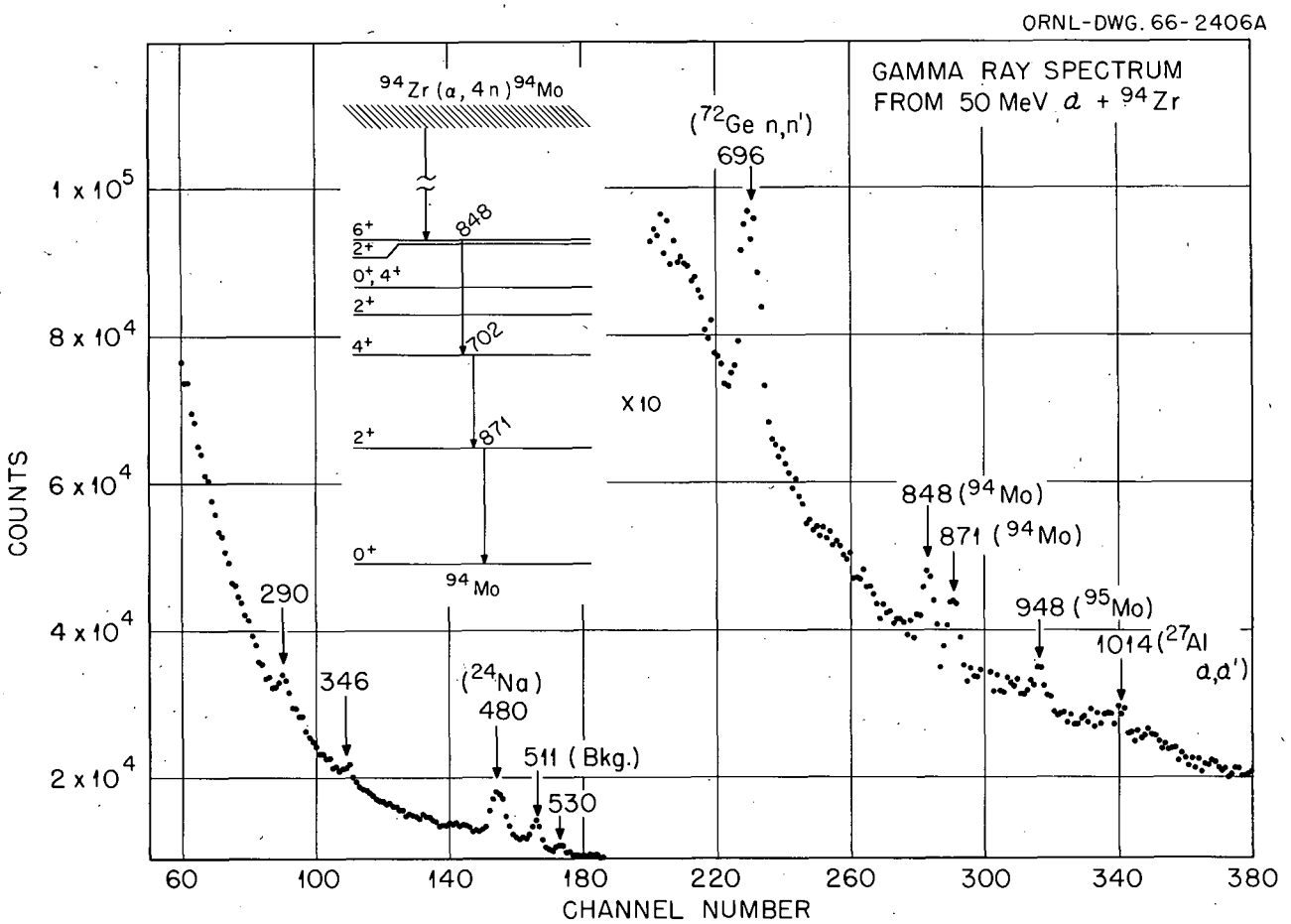

Fig. 1.6. Ge(Li) Gamma-Ray Spectrum from a ^{94}Zr Target Bombarded with 50-Mev Alpha Particles. Inset: relevant portion of the ^{94}Mo level scheme with observed transitions indicated by vertical arrows.

cused on the deformed nuclei in which almost interminable cascades down ground-state rotational bands have been seen.

We have performed preliminary experiments to test the value of the "compound nucleus excitation" technique in the region of $A = 90$ to 100. Targets of ^{93}Nb, ^{94}Zr, and ^{114}Cd were bombarded with alpha particles of energies 40 to 60 Mev from the Oak Ridge Isochronous Cyclotron. Figure 1.6 shows the gamma-ray spectrum from the reaction ^{94}Zr(α,4n)^{94}Mo measured with a 1.5-cm^3 Ge(Li) detector. The 848- and 871-kev gamma rays are members of a $6^+ \rightarrow 4^+ \rightarrow 2^+ \rightarrow 0^+$ cascade indicated in the partial ^{94}Mo level scheme.[34] The 702-kev transition is buried under the intense 690-kev peak which arises from the ^{72}Ge(n,n'). Note that the 2^+ excited states (other than the first) do not seem to be involved in the principal deexciting cascades. In addition, the intensities of the 871- and 848-kev gamma rays are approximately equal, indicating only a small probability for direct population of even the first 2^+ state.

This favoring of cascades from high-spin states resembles the behavior in the deformed nuclei. However, in our case the states in ^{94}Mo are probably shell model in character, members of a $(g_{9/2})^2$ multiplet, as contrasted to the collective rotational states seen in deformed nuclei.

[34] N. K. Aras and E. Eichler, "Decay of Technetium-94 Isomers to Levels in Molybdenum-94," this report.

LEVEL STRUCTURE OF ZIRCONIUM-94

J. K. Dickens[35] R. J. Silva
E. Eichler G. Chilosi[36]

We have measured elastic and inelastic scattering of 12.7-Mev protons from ^{94}Zr, using proton beams from the ORNL Tandem Van de Graaff. The data have been analyzed to obtain excitation energies for levels in ^{94}Zr which are excited by proton scattering. The analysis reported here used eight pulse-height spectra for laboratory angles between 40 and 80°.

Figure 1.7 shows the spectrum obtained at an angle of 50°. Groups of protons scattered by the zirconium target can definitely be distinguished from those scattered by the target contaminants by utilizing the kinematics of the scattering as well as the expected magnitudes of the inelastic scattering. The proton groups can be distinguished from alpha groups because the latter are much broader. Since the isotopic composition of the target was 97% ^{94}Zr, it is unlikely that any numbered proton group in Fig. 1.7 could result from proton scattering by nuclei other than ^{94}Zr.

[35]Neutron Physics Division.
[36]Guest scientist from Italy.

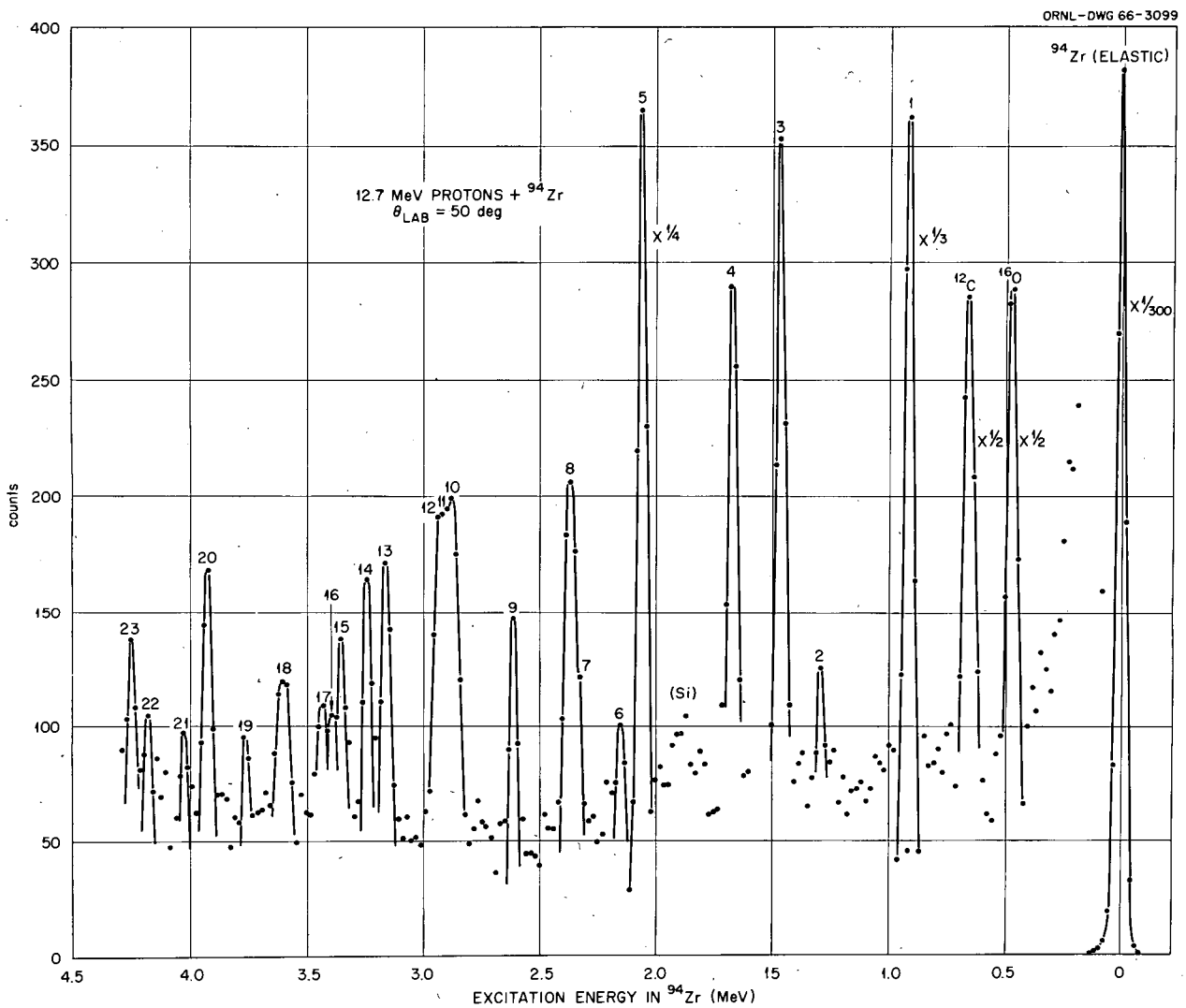

Fig. 1.7. The Spectrum of 12.7-Mev Protons Scattered from ^{94}Zr at a Laboratory Angle of 50°.

Table 1.6. ^{94}Zr Excited States and Suggested Spin and Parity Assignments J^{π}

Peak No.[a]	12.7-Mev Protons (Present Work)		19.4-Mev Protons[b]		15-Mev Deuterons[c]	
	E_{ex} (Mev)	J^{π}	E_{ex} (Mev)	J^{π}	E_{ex} (Mev)	J^{π}
1	0.916	2^+	0.92	2^+	0.92	+
2	1.30	0^+			1.31	+
3	1.47		1.47	(4^+)	1.47	−
4	1.66	2^+	1.66	2^+	1.68	+
5	2.06	3^-	2.05	3^-	2.06	3^-
6	2.16					
7	(2.32)		2.34	2^+	2.35	+
8	2.36	(2^+)				
9	2.61	(−)	2.60	(5^-)	2.60	+
10	(2.85)		2.84			
11	(2.89)		2.92		2.89	
12	(2.94)					
13	3.16	(+)	3.14			
14	3.24		3.22			
15	3.35		3.33	(3,4)	3.28	
16	3.39					
17	3.46					
18	3.60[d]		3.57	(4,5)	3.61	−
19	3.76		3.71			
20	3.92	(−)	3.87		3.92	−
21	4.02					
22	4.18					
23	4.25		4.21			

[a]Corresponding to numbering in Fig. 1.7.

[b]M. M. Stautberg and J. J. Kraushaar, *Bull. Am. Phys. Soc., Ser. II*, **10**, 527 (1965).

[c]R. K. Jolly, E. K. Lin, and B. L. Cohen, *Phys. Rev.* **128**, 2292 (1962).

[d]The proton group associated with this level has a width larger than expected for a single level and may include scattering by more than one excited state of ^{94}Zr.

Table 1.6 presents the excitation energies and suggested spin and parity assignments, and compares our results with previous work.[37,38] We suggest an error of ±30 kev for excitation energies of ~4 Mev, with the error decreasing with decreasing E_{ex}. Several proton peaks had widths larger than our resolution (~40 kev full width at half maximum), suggesting proton scattering by more than one level in ^{94}Zr. Peak-fitting techniques were used to separate the levels; the resulting less-certain excitation energies are given in parentheses in Table 1.6. The broad proton peak at $E_{ex} \cong 2.9$ Mev was studied carefully in all eight spectra. We obtained a good fit to the broad peak at ~2.9 Mev with three peaks (Nos. 10, 11, and 12), but we cannot exclude the possibility of additional levels in this group.

We have also observed the inelastic scattering of 12.7-Mev protons on ^{90}Zr and ^{92}Zr and the (d,p) reaction on ^{91}Zr. These data are being analyzed for ^{90}Zr and ^{92}Zr level information. In addition, the angular distributions of the proton

[37]M. M. Stautberg and J. J. Kraushaar, *Bull. Am. Phys. Soc.* **10**, 527 (1965).

[38]R. K. Jolly, E. K. Lin, and B. L. Cohen, *Phys. Rev.* **128**, 2292 (1962).

groups[39] will be compared to theoretical predictions in order to obtain nuclear reaction and structure information.

LEVEL STRUCTURE OF MOLYBDENUM-92

J. K. Dickens[35] R. J. Silva
E. Eichler I. R. Williams

The nucleus ^{92}Mo consists of two protons plus the rather rigid ^{90}Zr closed core. The level structure, at least for the low-lying levels, may be described by proton configurations involving only $2p_{1/2}$ and $1g_{9/2}$ orbitals. We have studied the excited states of ^{92}Mo by measuring the inelastic scattering of protons and by observing gamma rays emitted following excitation of these levels. The target was a self-supporting metal foil, $\sim$1 mg/cm^2 thick, enriched to 97.6% in ^{92}Mo. Proton beams from the ORNL Tandem Van de Graaff were utilized, and the scattered protons were detected with a surface-barrier silicon detector with an overall energy resolution of $\sim$27 kev (full width at half maximum). Figure 1.8 shows the proton spectrum at 65°. The numbered peaks are due to inelastic scattering of protons from ^{92}Mo and correspond to the energies listed in Table 1.7.

In all spectra several of the peaks have widths larger than our resolution, suggesting excitation of two or more closely spaced levels in ^{92}Mo. Assuming this explanation, peak-fitting methods were used to obtain the excitation energies for the unresolved levels; these results are given in parentheses in Table 1.7. Although the data are reasonably well fitted by this approach, we cannot exclude the possibility of additional levels in this energy region.

Van Lieshout *et al.*[40] observed the NaI gamma-ray spectrum following the decay of 4-min ^{92}Tc to levels in ^{92}Mo. Their results were consistent with a level sequence with $J^\pi = 0^+, 2^+, 4^+, 5^-, 6^+$, and 8^+ expected from the $(g_{9/2})^2$ and $(p_{1/2}\, g_{9/2})$ proton configurations. The dashed peak in Fig. 1.8, located at $E_{ex} \cong 2750$ kev, indicates the expected position of the 8^+ member of the $(g_{9/2})^2$ multiplet. The levels at E_{ex} = 1580, 2281, and 2609 kev are presumably the 2^+, 4^+, and 6^+ members of this configuration. The failure to observe the 8^+ state, due in large part to the centrifugal barrier, suggests that none of the numbered levels in Table 1.7 will have $J > 7$.

Table 1.7. ^{92}Mo Excited States

Peak[a] No.	E_{ex} (kev)[b]	J^π (cf. ref. 36)	Peak[a] No.	E_{ex} (kev)[b]
1	1508	2^+	18	(3922)
2	2281	4^+	19	(3951)
3	2523	5^-	20	4008
4	2609	6^+	21	(4114)
	2754	8^+	22	4149
5	2846	(3^-)[c]	23	(4184)
6	3005		24	(4272)
7	3062		25	4300
8	3089	(2^+)[d]	26	(4339)
9	3367		27	4424
10	3543		28	4481
11	3576		29	4537
12	3618		30	4588
13	3684		31	4636
14	3765		32	4688
15	3810		33	4712
16	(3836)		34	4768
17	3870			

[a]Corresponds to the numbering in Fig. 1.8.

[b]An error of 2 kev is assigned to levels 1 through 4, of 5 kev for levels 5 through 17, and of 10 kev for the remaining levels.

[c]Y. S. Kim and B. L. Cohen, *Phys. Rev.* **142**, 788 (1966).

[d]Suggested by the intensity in Fig. 1.8.

The gamma-ray spectrum following level excitation by 10-Mev protons was measured with a lithium-drifted germanium detector. For these studies the Oak Ridge Isochronous Cyclotron was used as well as the Tandem Van de Graaff. The strongest gamma rays associated with deexcitation of ^{92}Mo levels had energies of 145, 242, 328, 773, and 1508 kev and can be fitted into the level scheme as indicated in Fig. 1.9. The ^{92}Mo energy levels

[39]J. K. Dickens *et al.*, *Elastic and Inelastic Scattering of 12.7-MeV Protons from ^{90}Zr, ^{92}Zr, and ^{94}Zr: Tabulated Differential Cross Sections*, ORNL-3934 (March 1966).

[40]R. van Lieshout, S. Monaro, G. B. Vingiani, and H. Morinaga, *Phys. Letters* **9**, 164 (1964).

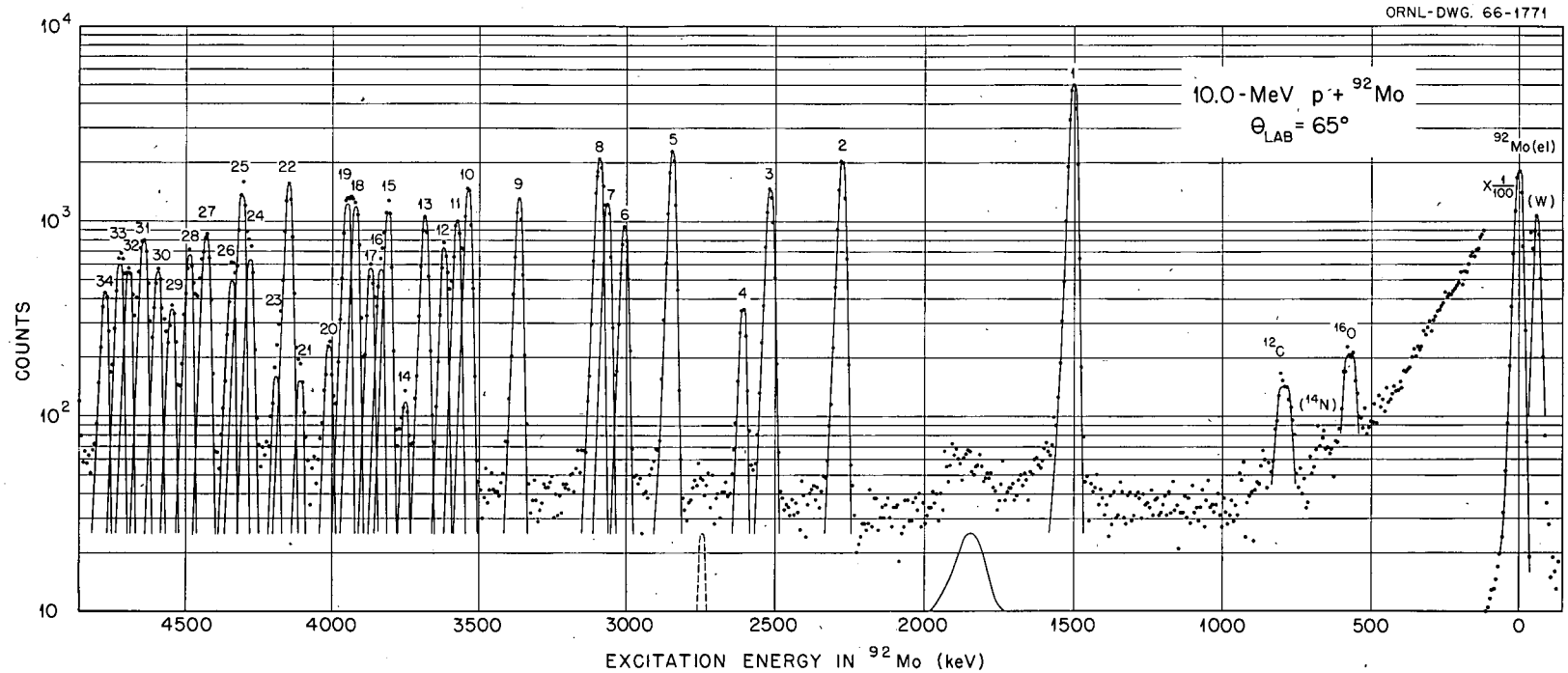

Fig. 1.8. Pulse-Height Spectrum of 10-Mev Protons Scattered from ^{92}Mo at 65°. Peaks corresponding to ^{92}Mo excited states are numbered and are identified in Table 1.7. Peaks corresponding to protons scattered by a target impurity nucleus are marked with the symbol for this nucleus.

ORNL-DWG. 66-4705

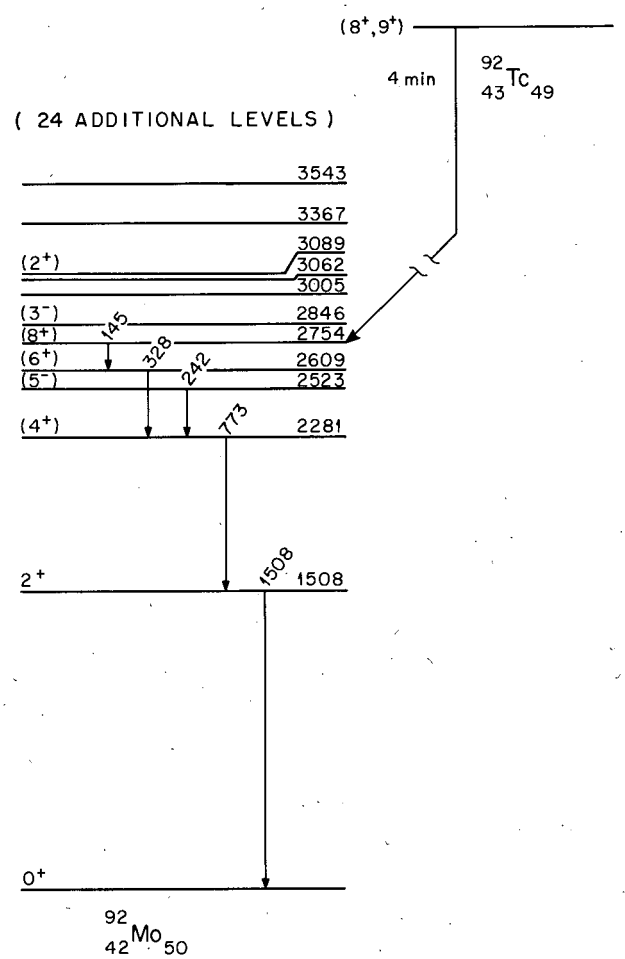

Fig. 1.9. Excited States in ^{92}Mo. Gamma-ray transitions, including those following the β^+ decay of ^{92}Tc, indicated in this figure, account for the strong gamma rays seen in this experiment.

involved were excited not only by the inelastic scattering of protons, but also by the β^+ decay of ^{92}Tc made by the ^{92}Mo(p,n) reaction.[40] Thus, deexcitation gamma rays from the 8^+ state were seen even though this state was not excited by the 10-Mev protons.

We have measured the angular distributions of 12.0-Mev protons inelastically scattered from ^{92}Mo at 27 angles from 30 to 160°. Analysis of these data should lead to spin-parity assignments.

DECAY OF TECHNETIUM-94 ISOMERS TO LEVELS IN MOLYBDENUM-94

N. K. Aras[41] E. Eichler

We have studied the decay of ^{94}Tc isomers using lithium-drifted germanium and NaI detectors for single-crystal and multiparameter coincidence experiments. The 53-min ^{94m}Tc was milked from ^{94}Ru, which was produced by the ^{92}Mo$(\alpha,2n)^{94}$Ru reaction. In this way ^{94m}Tc was obtained free from 5-hr ^{94g}Tc. The ^{94g}Tc was produced by the ^{93}Nb$(\alpha,3n)^{94}$Tc reaction followed by chemical purification. We combined the results of all the experiments to yield the decay scheme shown in Fig. 1.10. The 2^+ assignments for the 1863.3- and 2392.7-kev levels were indicated by the measurements of the angular correlation of the 871-993 and 871-1520 kev cascades. In Fig. 1.11 we give a comparison between the experimental level spectrum and the effective potential shell-model predictions of Bhatt and Ball[42] and Vervier.[43] Note the good agreement below approximately 2300 kev.

THE DECAY OF 12.8-hr IODINE-130*g* AND 8.8-min IODINE-130*m*

C. E. Bemis, Jr. J. F. Emery[44]
N. K. Aras[41]

Recently the existence of a 9-min isomeric state in ^{130}I, formed in the ^{129}I(n,γ) reaction, has been reported.[45] We have investigated the decay properties of this isomer as well as performed additional studies on the decay properties of the well-established ground-state isomer.

Using an iron-cored single-gap electron spectrometer, we have observed the decay modes of the short-lived upper isomer. The decay of this isomer to the ground state of ^{130}I proceeds via a 48.2 ± 0.3 kev transition consistent with an $M3$ multipolarity assignment as determined from the $\Sigma L/\Sigma M$ internal conversion ratio. Gamma-ray transitions resulting from independent beta decay of

[41] Visiting Scientific Staff Member from Turkey.

[42] K. H. Bhatt and J. B. Ball, *Nucl. Phys.* **63**, 286 (1965).

[43] J. Vervier, *Nucl. Phys.* **75**, 17 (1966).

[44] Analytical Chemistry Division.

[45] D. D. Wilkey and J. E. Willard, *J. Chem. Phys.* **44**, 970 (1966).

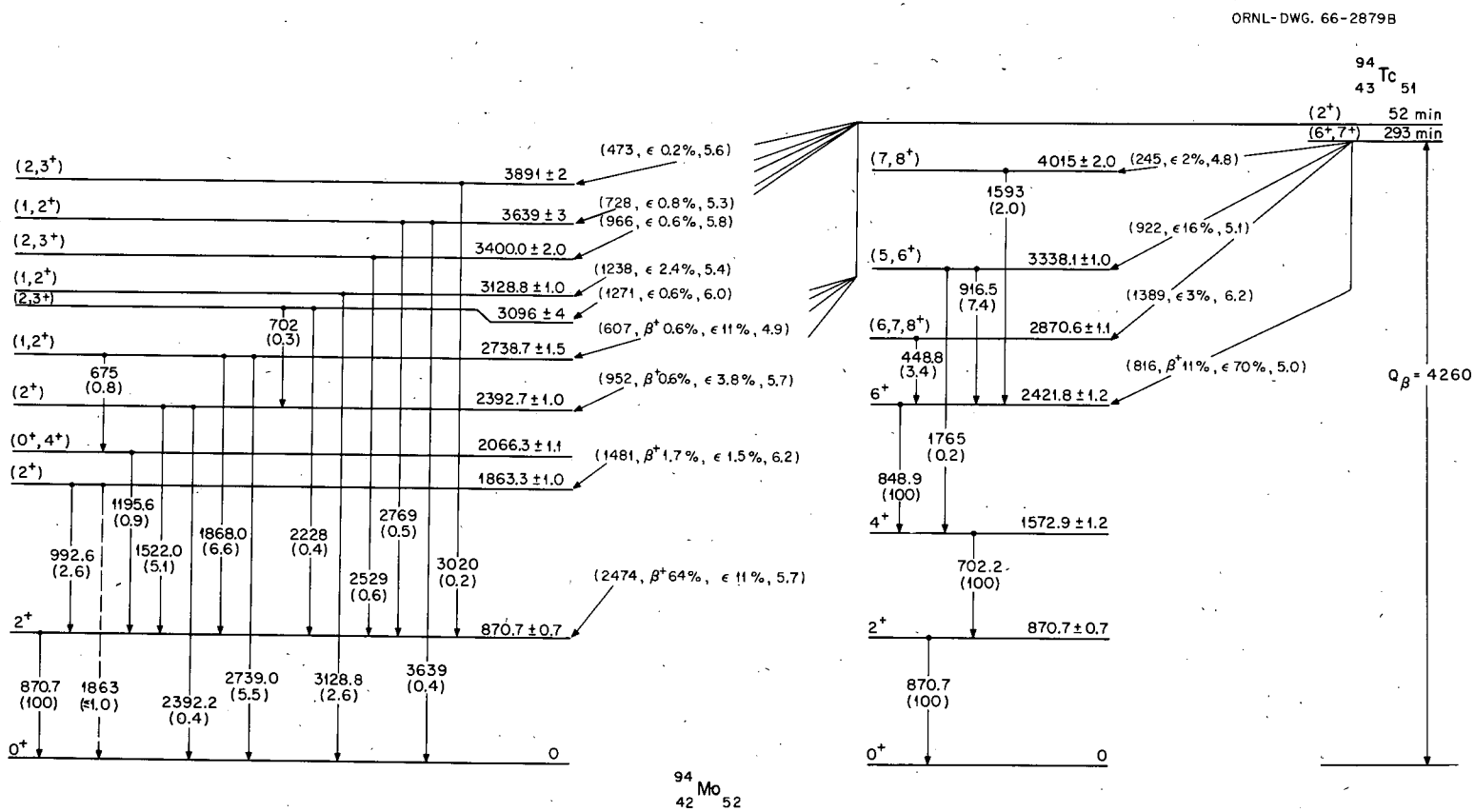

Fig. 1.10. Decay Scheme of the ^{94}Tc Isomers.

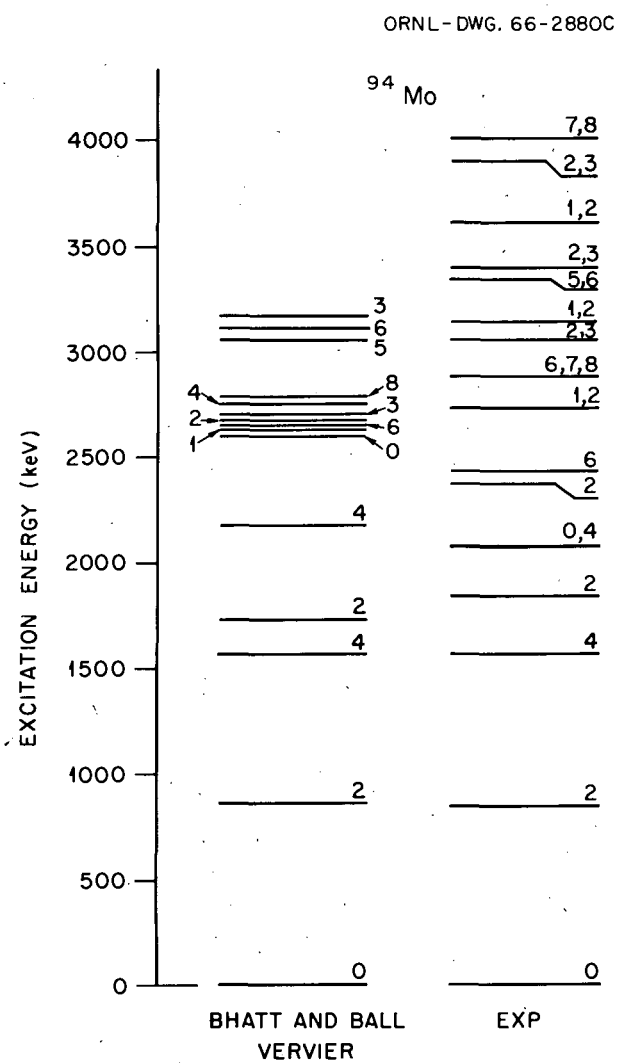

Fig. 1.11. Comparison Between the Experimental Levels of ^{94}Mo and Those Predicted by Bhatt and Ball[42] and Vervier[43].

the upper isomer have been investigated with high-resolution Ge(Li) semiconductor detectors. Transitions of the following energies in kev (and relative intensities) are attributed to the decay of the upper isomer: 536 (100), 1120 (1.31), 1177 (0.32), 1459 (0.54), 1610 (3.14), and 1969 (0.45). Additional gamma-ray transitions in the decay of the ground-state isomer have also been identified by means of Ge(Li) detectors. The following transitions in kev (relative intensity) have been observed: 418 (34.5), 536 (100), 602 (0.5), 609 (<0.4), 666 (100), 686 (1.1), 739 (94.0), 757 (<0.09), 842 (<0.1), 965 (1.1), 1093 (0.4), 1120 (0.2), 1157 (11.5), 1177 (0.05), 1223 (0.2), 1272 (0.7), 1328 (0.04), 1355 (0.03), 1403 (0.4), 1428 (0.04), 1459 (0.02), 1504 (0.03), 1548 (0.04), 1610 (0.05), 1675 (0.02), 1728 (0.02), and ~2350 (<1.0).

Gamma-gamma coincidence experiments with NaI(Tl) detectors have been performed for both isomers. The results of these experiments are currently being analyzed.

ENERGY LEVELS OF TUNGSTEN-184 POPULATED IN THE DECAY OF TANTALUM-184

N. R. Johnson N. K. Aras[41]

In a previous study[46] at this laboratory, the level scheme in ^{184}W populated from the decay of ^{184}Re was determined. In this work it was found that the ^{184}Re ground state has a half-life of 33 ± 3 days and probably a spin of 3^-. Also observed was an isomeric state in ^{184}Re which probably has a high spin of 7^+ or 8^+ and a half-life of 169 ± 8 days. The isomer, which was present in very low abundance, decays primarily to the ground state of ^{184}Re and hence gives rise to only a very small direct population of high-spin (e.g., spins of 5 or 6) intrinsic states in ^{184}W. Such high-spin two-quasi-particle states are currently of considerable theoretical interest, and therefore it seemed highly desirable to attempt more detailed studies of such states, which are expected above about 1 Mev in ^{184}W.

From the Nilsson orbitals available for the odd neutron and odd proton in ^{184}Ta, a spin of 5^- is expected for this nucleus. We have, therefore, initiated a new study of levels in ^{184}W from the decay of 8-hr ^{184}Ta. Radioactive sources were prepared by the nuclear reaction ^{186}W$(d,\alpha)^{184}$Ta. Excellent resolution of the ^{184}Ta gamma rays has been achieved by use of *p-i-n* lithium-drifted germanium detectors. A list of the gamma-ray energies observed is shown in the first column of Table 1.8, and the corresponding relative intensities are given in the second column.

Extensive gamma-gamma coincidence measurements have been made by utilizing both NaI and germanium detectors in conjunction with a 100 ×

[46] N. R. Johnson, *Phys. Rev.* **129**, 1737 (1963).

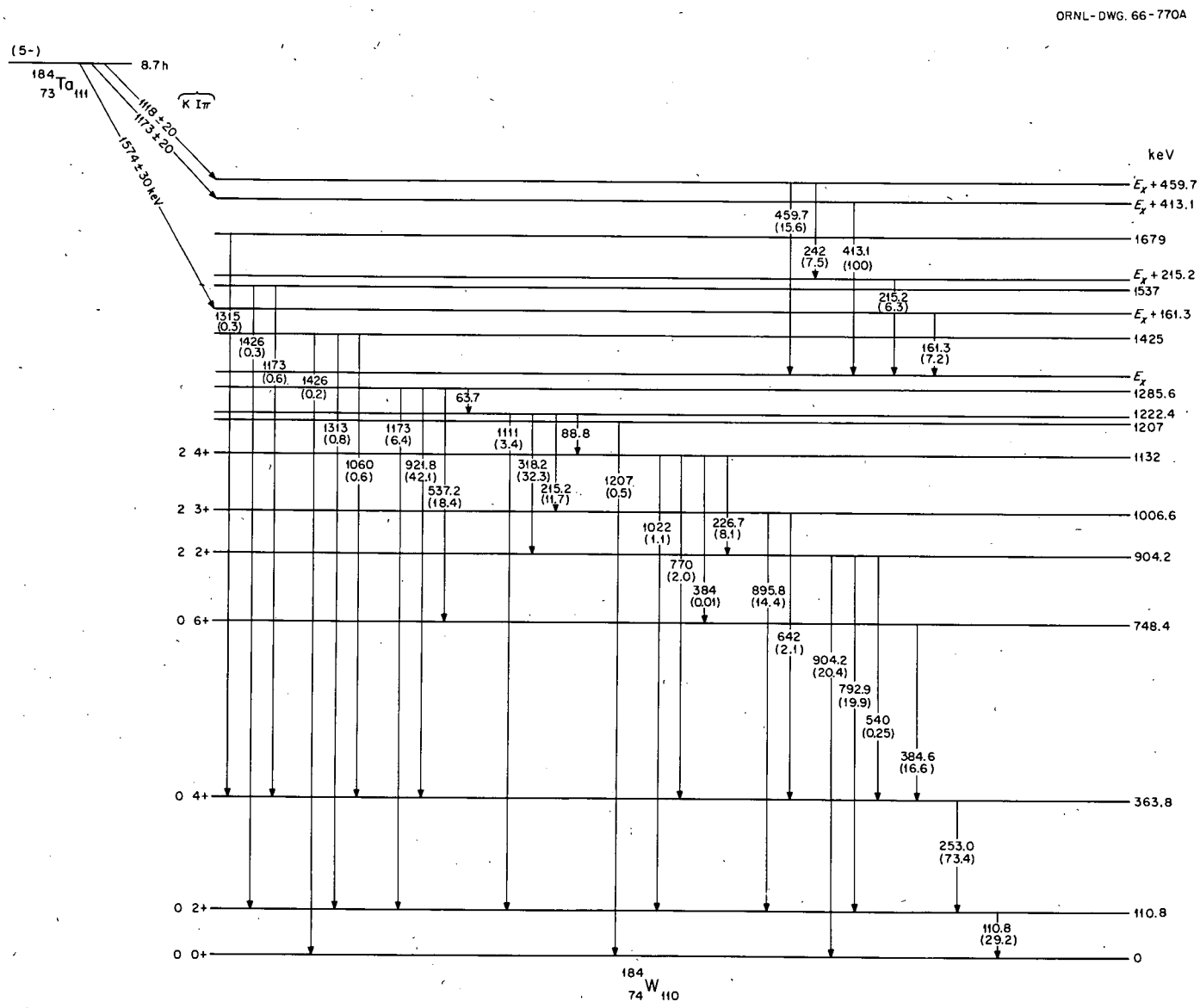

Fig. 1.12. Level Scheme in ^{184}W Populated by the Decay of 8.7-hr ^{184}Ta.

Table 1.8. ^{184}Ta Gamma-Ray Energies and Intensities

E_γ (kev)	Intensity $\gamma \times 100$ / Intensity 413-kev γ	E_γ (kev)	Intensity $\gamma \times 100$ / Intensity 413-kev γ
88.8 ± 1.2		642 ± 3	1.1
110.8 ± 0.8	29.2	770 ± 2	2.0
126 ± 3	1.5	792.9 ± 0.8	19.9
161.3 ± 0.9	7.2	810 ± 3	1.0
215.2 ± 1.0	18.0	872 ± 4	0.96
226.5 ± 1.0	8.1	895.8 ± 1.0	14.4
242 ± 2	7.5	904.2 ± 0.9	20.4
253.0 ± 0.7	73.4	921.8 ± 0.7	42.1
296 ± 2	2.3	970 ± 3[a]	1.0
318.2 ± 0.8	32.3	1022 ± 3[a]	1.1
384.6 ± 1.3	16.7	1111 ± 2[a]	3.4
413.1 ± 1.3	100	1154 ± 5[a]	0.33
459.7 ± 1.2	15.6	1173 ± 2[a]	6.0
537.2 ± 0.9	18.4	1207 ± 4[a]	0.53
		1315 ± 4[a]	0.31
		1340 ± 5[a]	0.14
		1426 ± 6[a]	0.38

[a]This peak appears broader than the expected Gaussian distribution.

200 channel multiparameter analyzer. Similarly, beta-gamma coincidence experiments have been performed with NaI and anthracene detectors. Although the data analysis has not been completed, broad new details of the ^{184}W level properties have been revealed in the analysis thus far. These are shown in the decay scheme of Fig. 1.12. The spin 0^+, 2^+, 4^+, and 6^+ members of the ground-state rotational band are seen to be populated in the decay. The group of states at about 1 Mev having $K = 2$ (K is the projection of the total angular momentum on the nuclear symmetry axis) and spins of 2^+, 3^+, and 4^+ are members of the γ-vibrational band. The reduced transition probabilities of the $E2$ transitions from these levels to members of the ground-state band are accounted for quite accurately by taking into account the admixture of the wave function of the γ-vibrational band into the wave function of the ground-state band.

The state at 1285.6 kev presents a most interesting situation because of the following facts: (1) the energy of the level occurs at just that expected for the 5^+ member of the γ-vibrational band; (2) this state populates members of the ground-state rotational band; (3) the gamma rays depopulating this state are not in prompt coincidence with those above it (experiments have shown the lifetime of the 1285.6-kev state to be longer than 1 μsec and less than 1 sec); and (4) the beta decay of ^{184}Ta appears to proceed only to ^{184}W states above 1285.6 kev, as no beta rays are in coincidence with any gamma rays below this level. From such a set of conditions it must be concluded that this state, or a state at some slightly higher energy (designated E_x in Fig. 1.12), is probably an intrinsic state produced by promoting either a pair of protons or a pair of neutrons into new Nilsson orbitals.

If level E_x exists at some small energy above the 1285.6-kev level in ^{184}W, then one should be able to observe conversion electrons in the transition between the two states. Attempts to measure such electrons by magnetic analysis with a beta-ray spectrometer have thus far proved unsuccessful. An additional attempt is planned for this measurement as well as for a direct determination of the lifetime of the 1285.6-kev state in order to further clarify the nature of these high-lying levels in ^{184}W.

DECAY PROPERTIES OF EUROPIUM-152[47]

J. H. Hamilton[48] L. L. Riedinger[48]
N. R. Johnson

The gamma rays from the decay of 12.4-year ^{152}Eu have been studied with an Li-Ge detector (3 mm deep and 2 cm^2 surface area) to obtain accurate gamma intensities and to search for unreported transitions, especially from the beta band. The preliminary results, energies (kev), and intensities in parentheses, are: 122.1 (125), 244.7 (29), 295.7 (1.3), 343.7 (100), 366.8 (2.1), 410.5 (8.1), 443.4 (13), 687.6 (2.7), 779.4 (52), 868.3 (15), 957.4 (2.0), 965.0 (55), 1006.1 (3.5), 1086.8 (44), 1113.0 (50), 1213.0 (4.6), 1249.0 (1.5), 1263.7 (1.1), 1298.4 (6.1), 1406.5 (79), 1454.9 (1.7), and 1524.6 (1.2). The energy errors are about 1 kev or less, and the intensity errors go from 5% for strong lines to 30% for weak lines. The 296-, 367-, 957-, 1006-, and 1455-kev transitions have not been reported previously. An estimate of 1% impurity of ^{154}Eu in the source was made from the 1274-kev transition observed. The 122- and 1006-kev gamma intensities were adjusted for this impurity. Multiparameter gamma-gamma coincidence measurements have been made and are being analyzed. At this point in the analysis, several new features of the level schemes of ^{152}Sm and ^{152}Gd are indicated, including the population of an additional member of the β-vibrational band. These features are illustrated in Fig. 1.13.

[47]From an abstract published in *Bull. Am. Phys. Soc.* 11(3), 407 (1966).

[48]Vanderbilt University, Nashville, Tenn.

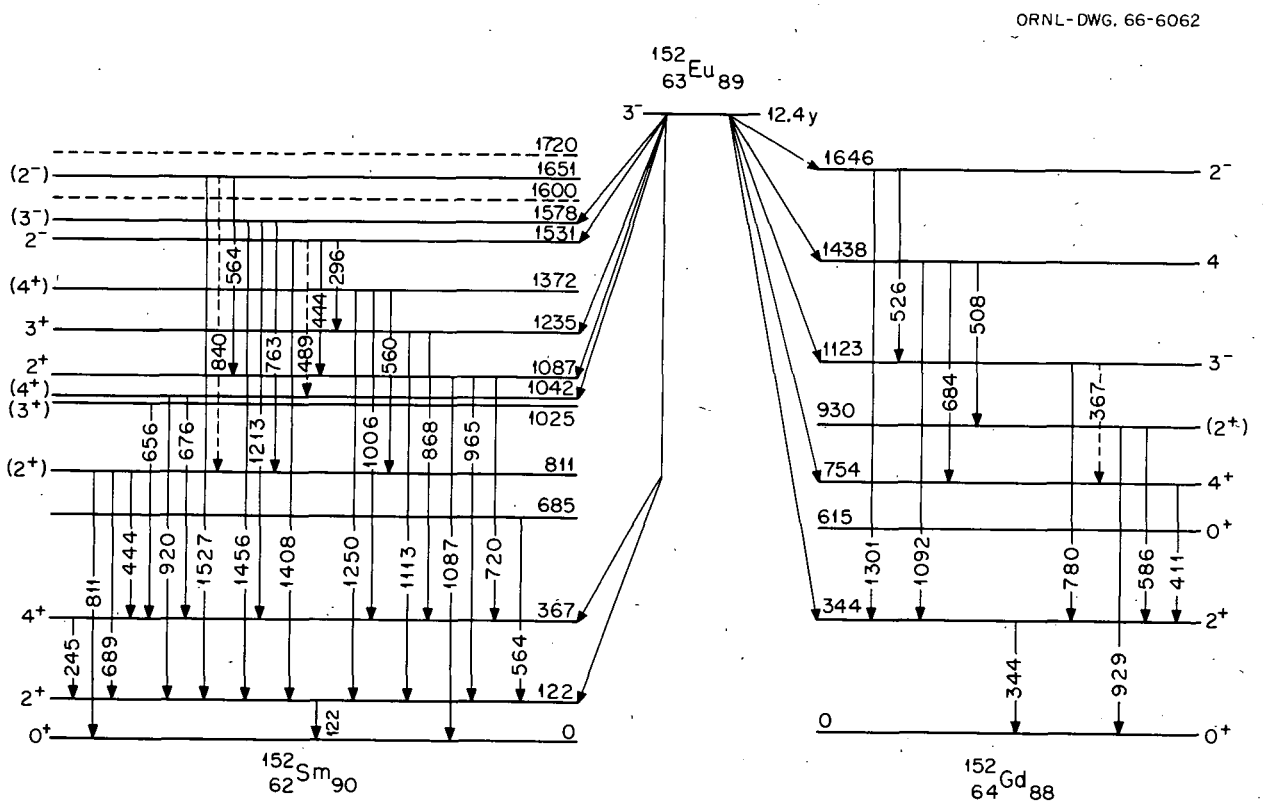

Fig. 1.13. Decay Scheme of 12.4-year ^{152}Eu. Both the new data from the present measurements and that existing in the literature have been utilized in the scheme.

STUDIES OF THE DECAY OF BROMINE-80m[49]

A. V. Ramayya[48] J. H. Hamilton[48]
B. van Nooijen[48] N. R. Johnson

The gamma-ray spectrum of ^{80m}Br was studied by means of a 3-mm-deep Li-Ge spectrometer; gamma-gamma coincidence measurements were performed with two 3 × 3 in. NaI(Tl) spectrometers and a three-dimensional (100 channels × 200 channels) multichannel analyzer. Gamma rays (relative intensities are in parentheses) of 617.5 ± 0.5 (100), 640.4 ± 0.7 (3.5), 666.7 ± 0.5 (15), 680.6 ± 0.7 (0.4), 691.0 ± 0.5, 706.9 ± 0.7 (3), 816.0 ± 0.7 (0.5), and 1257.5 ± 1.5 (1) kev were found in the decay of 4-hr ^{80m}Br. The 640.4- and 706.9-kev gamma rays are both in coincidence with the 617.5-kev transition; the 680.6- and 816.0-kev transitions are both coincident with the 666.7-kev transition. Levels at 667, 1347, and 1483 kev in ^{80}Se and at 618, 1258, and 1324 kev in ^{80}Kr are proposed. The level schemes in ^{80}Se and ^{80}Kr resulting from these measurements are shown in Fig. 1.14.

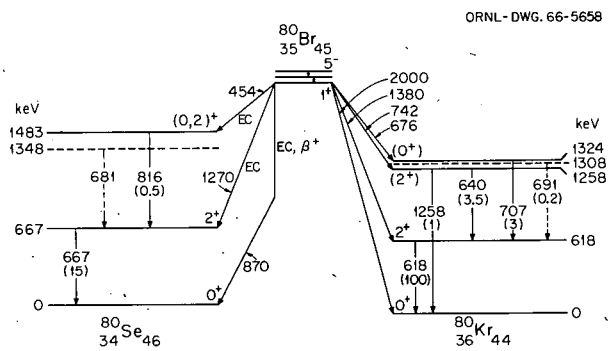

Fig. 1.14. Level Schemes in ^{80}Se and ^{80}Kr Populated from the Decay of ^{80m}Br.

GAMMA-RAY INTENSITIES IN THE DECAY OF EUROPIUM-154[50]

L. L. Riedinger[48] A. V. Ramayya[48]
J. H. Hamilton[48] B. van Nooijen[48]
N. R. Johnson

The absolute efficiency for gamma rays as a function of energy from 0.1 to 2.76 Mev was determined for a lithium-drifted germanium detector (3 mm depletion depth and 2 cm^2 surface area) for different source-detector distances. Thirteen sources of known strengths were used to determine the efficiencies. These efficiencies were used to determine gamma-ray intensities in the ^{154}Eu decay. The preliminary results, energies (kev), and intensities in parentheses, are: 248 (17), 444 (1.3), 555.9 (0.6), 590.5 (16), 693.0 (6.0), 724.2 (56), 759.1 (12), 817.1 (1.5), 848.0 (1.8), 876.0 (31), 906.2 (2.1), 999.6 (31), 1008.2 (50), 1249.3 (3.2), 1278.0 (100), 1495.8 (1.8), 1540 (0.1), and 1595.9 (4.5). The intensity errors are about 5% generally but extend to 30% in some cases. The 848-, 906-, 1249-, 1495-, and 1540-kev transitions have not been reported previously. Coincidence measurements to establish the nature of the high-energy levels in ^{154}Gd are in progress. A preliminary decay scheme illustrating the features observed in the present work as well as those in the existing literature is shown in Fig. 1.15.

DECAY SCHEMES OF PRASEODYMIUM-136 AND -137

A. R. Brosi B. H. Ketelle
J. R. Van Hise

Previously reported work resulted in reassignment of the praseodymium isotopes with mass numbers 136 and 137. An isotope with a half-life of 13.5 min instead of one with a half-life of 70 min was assigned to mass number 136. An isotope with a half-life of approximately 70 min instead of one with a half-life of 90 min was assigned to mass number 137. Further work has been done on ^{136}Pr and ^{137}Pr which has made it possible to construct diagrams of the energy levels populated by the decay of these isotopes. In addition, the total decay energy of ^{136}Pr, which appeared to be inconsistent with other praseodymium decay energies, has been redetermined. Work has also been done to eliminate some of the uncertainty in the ^{137}Pr half-life due to the wide variation in values obtained in previous measurements.

---

[49] Abstract published in *Bull. Am. Phys. Soc.* 11(3), 393 (1966).

[50] Abstract of a paper presented at the meeting of the American Physical Society — Southeastern Section, Charlottesville, Va., Nov. 1–3, 1965.

ORNL-DWG. 66-5657

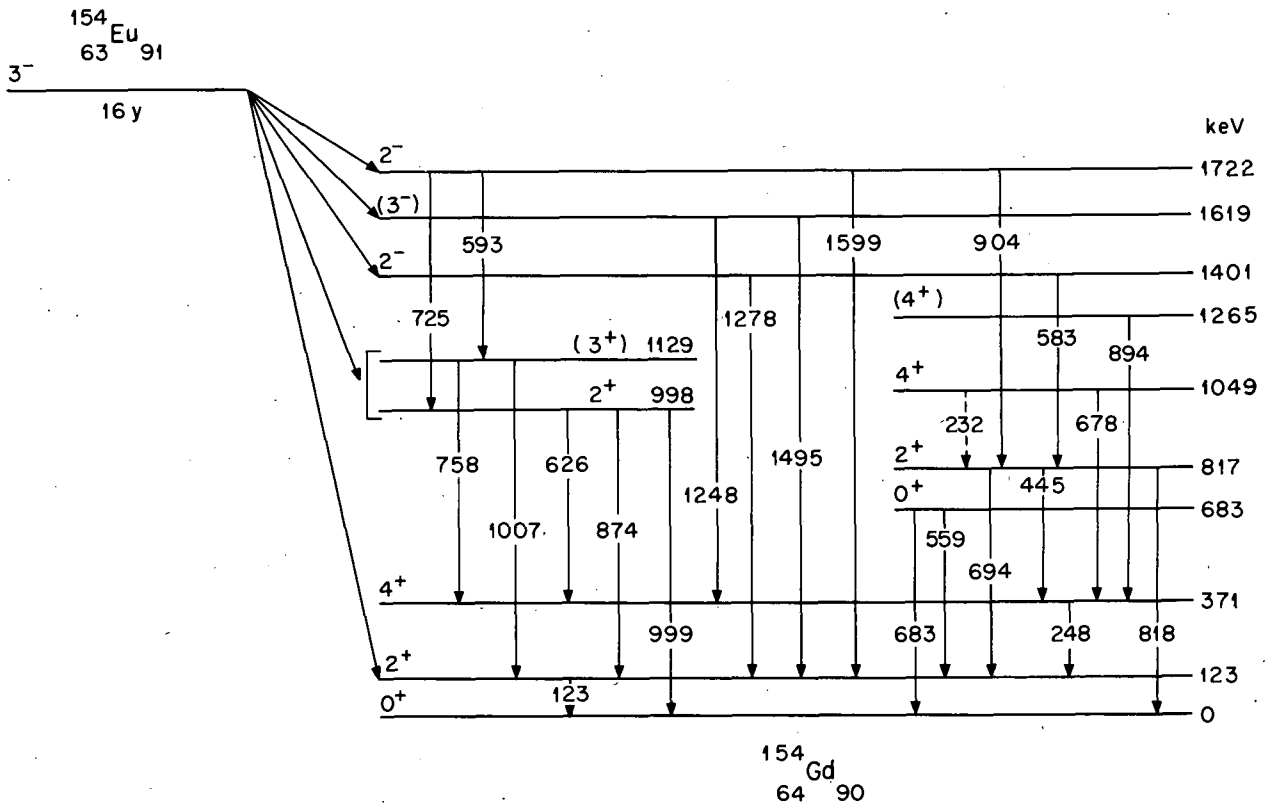

Fig. 1.15. Decay Scheme of ^{154}Eu Based on the Present Work and the Existing Information in the Literature.

The energies of the gamma-ray transitions following radioactive disintegration of both ^{136}Pr and ^{137}Pr were measured with a 5-cc lithium-drifted germanium detector. Twenty gamma rays were observed following ^{136}Pr decay and twenty-eight following ^{137}Pr decay. The energies of the most intense gamma rays were measured with a precision of a few tenths of a kilovolt and the relative intensities to about 10%. The energies of the low-intensity gamma rays have errors as high as a few kilovolts, and the relative intensities could be in error by a factor of 2.

Gamma-gamma coincidences following decay of ^{136}Pr and ^{137}Pr were measured using two 3 × 3 in. NaI(Tl) detectors. Nineteen pairs of coincident gamma rays were observed in the decay of ^{137}Pr. The coincidence results, together with the intensities and energies measured with the germanium detector, were used to construct the ^{137}Ce energy-level diagram shown in Fig. 1.16. None of the energy levels shown can be restricted to a single spin assignment on the basis of the work reported here. Several of the gamma rays emitted in ^{136}Pr decay have energies so nearly the same that they are not resolved by NaI detectors. The gamma-gamma coincidence data are not as definitive as in the case of ^{137}Pr decay but are consistent with the germanium detector data. The energy-level scheme of ^{136}Ce populated by the decay of ^{136}Pr is shown in Fig. 1.17. In this case spins were assigned to some of the levels on the basis of consistency with other even-even nuclei with similar neutron and proton numbers.

In earlier measurements of the decay energy of ^{136}Ce the positron energy spectrum was measured with an anthracene scintillation spectrometer. The anthracene crystal was placed between two NaI(Tl) detectors, and coincident 511-kev gamma-ray pulses in the NaI detectors were required before a pulse from the anthracene detector was gated to a multichannel analyzer. In this way a positron kinetic energy spectrum was obtained which was

ORNL-DWG. 66-5655

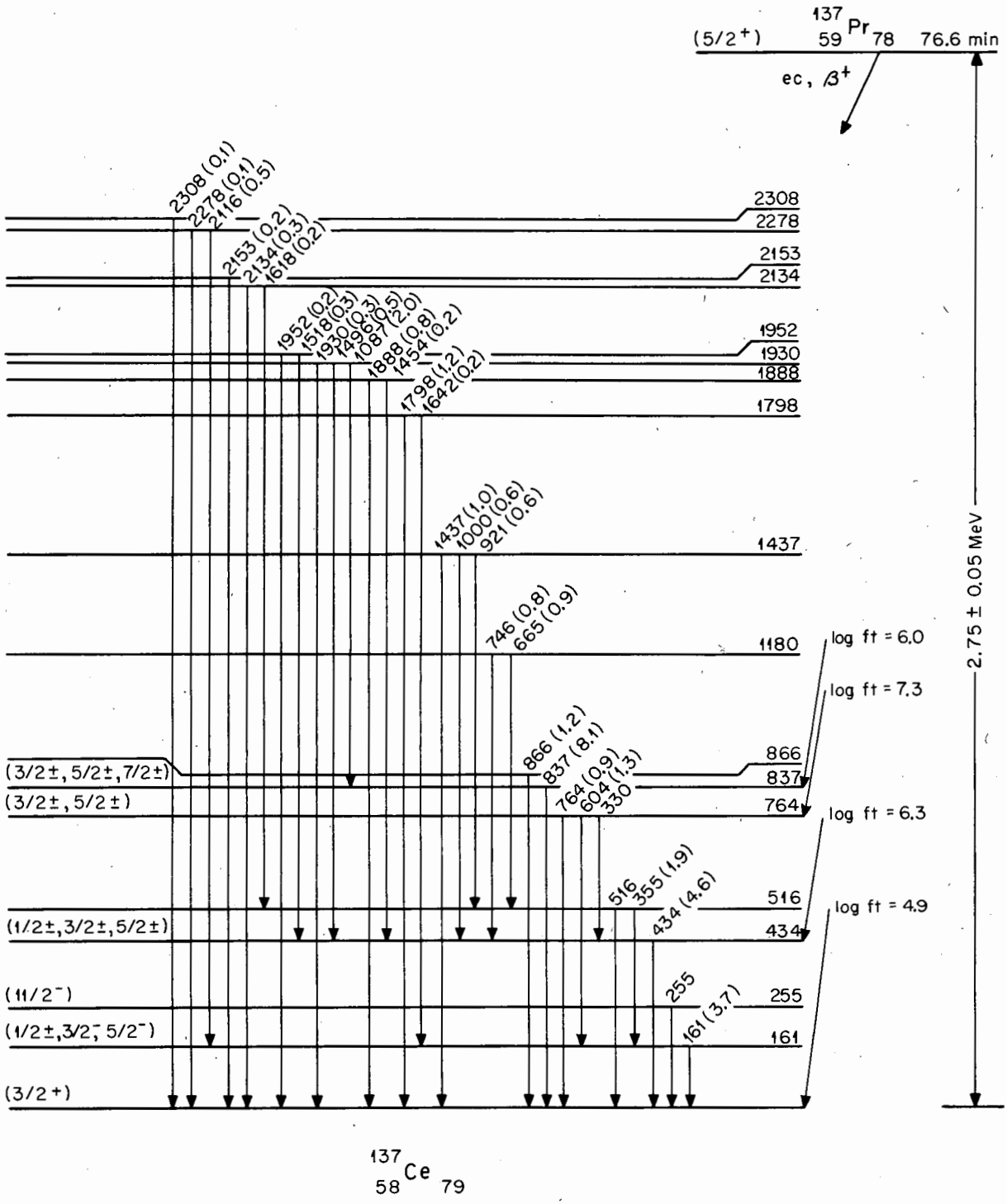

Fig. 1.16. Energy Levels of ^{137}Ce. Gamma-ray intensities are given in parentheses after the transition energies. The 255-kev level is populated by fewer than 0.1% of the ^{137}Pr disintegrations.

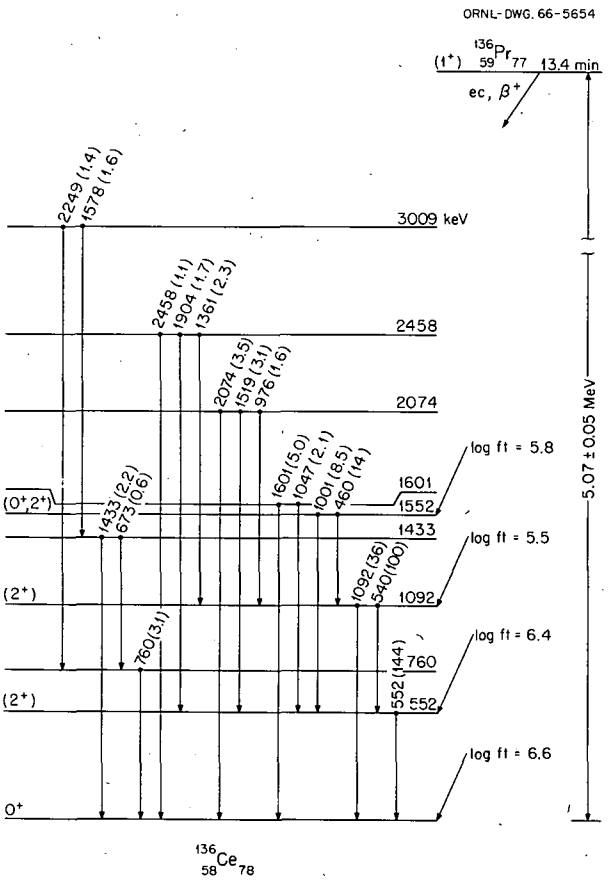

Fig. 1.17. Energy Levels of ^{136}Ce Populated by the Decay of ^{136}Pr. Gamma-ray intensities are given in parentheses after the transition energies.

undistorted by the occasional addition of the energy of an annihilation gamma ray. Because of the presence of four positron groups with an appreciable intensity, extrapolation of the Kurie plot to the maximum energy of the most energetic positron group was quite uncertain. A study of the coincidence system was made using the radiations of the 26-hr ^{72}As daughter of 8.4-day ^{72}Se. This study showed that with more efficient detectors, feasible counting rates were obtained when a fourth detector was used, with the additional requirement that a particular gamma ray be coincident with the positron in the anthracene detector and the two annihilation gamma rays in the NaI detectors.

Data were taken with a ^{136}Pr source where positron kinetic energy pulses were gated to an analyzer when they were coincident with two annihilation gamma rays and a 1092-kev gamma ray. A Kurie plot of the data gave a maximum positron kinetic energy of 2.954 ± 0.018 Mev for the positron group decaying to the 1.092-Mev level in ^{136}Ce. The error quoted is the standard deviation obtained from a least-squares analysis of the straight-line Kurie plot. Systematic errors involved in the energy calibration and data analysis are probably larger than the statistical error. Adding the rest mass and the coincident gamma-ray energies to the positron kinetic energy gives a total decay energy of 5.07 ± 0.05 Mev. This value is consistent with the decay energies of other praseodymium isotopes.

Some of the variation in the apparent half-life of ^{137}Pr has resulted from the contamination of sources by ^{135}Pr or ^{136}Pr, which have shorter half-lives, or ^{138}Pr or ^{139}Pr, which have longer half-lives than ^{137}Pr. Praseodymium-137 made by a (d,n) reaction on cerium enriched in ^{136}Ce was much purer than ^{137}Pr made by proton reactions. When the ^{137}Pr half-life was measured by following the decay of a peak in the Ge(Li) spectrum of a pure source there was still considerable variation in the results. This effect was found to be caused by the low intensities of the ^{137}Pr gamma rays and the high counting rate of the Compton continuum of the annihilation gamma ray. At peak counting rates high enough to give small statistical errors, random summing of pulses swept counts from the gamma-ray peak. This effect results in relatively fewer counts in a given photopeak at early counting times and hence leads to an increase in the apparent half-life. Therefore the apparent half-life obtained varies with the initial strength of the source.

A pulse generator peak taken with the Ge(Li) spectra was used to correct peak counting rates for summing effects. Least-squares analysis of the decay of the annihilation gamma-ray peak gave a half-life of 74.92 ± 0.16 min. Analysis of the decay of the most intense gamma-ray peak at 837 kev, with an intensity 60-fold lower than the annihilation gamma-ray peak, gave a half-life of 76.62 ± 1.54 min. Although the statistical error in the result for the 837-kev gamma ray is rather large, this gamma ray is more specific for ^{137}Pr than the annihilation gamma ray, and the result places a limit on the systematic error that could be caused by an impurity in the source.

2. Isotope Chemistry

NONAQUEOUS MICROTITRATION OF DIBENZOYLMETHANE AND OTHER WEAK ACIDS

D. A. Lee

In a continuing effort to separate the isotopes of lithium by chemical exchange techniques, a search was undertaken to find lithium species soluble in nonaqueous solvents. One such compound found was the chelate which lithium forms with dibenzoylmethane (DBM).[1] To study this complex, it was necessary to determine the DBM concentration in various nonaqueous solvents. A method was developed for the microtitration of DBM in those solvents.

DBM was titrated potentiometrically as a weak acid in pyridine or ethylenediamine. Tetrabutylammonium methylate dissolved in 90% benzene–10% methanol was the titrant. An investigation of several polarized bimetallic electrode systems produced a new electrode system. The indicating electrode was anodized platinum, and the reference electrode was cathodized antimony. Very stable, sensitive titration curves with sharp end points were obtained. Several other weak acids, succinimide, 4-nitrophthalimide, ethylacetoacetate, and benzenesulfonamide, were titrated to determine the scope of the method. Some very weak acids which were determined only with difficulty by other titration methods were successfully titrated. These compounds were cyanoacetamide, acetylurea, 2,3-butanedione, *sym*-diphenylurea, malonamide, dimethylglyoxime, and 2-nitropropane. A complete report of this work will be published in *Analytical Chemistry*.

[1] W. C. Fernelius and L. G. Van Uitert, *Acta Chem. Scand.* 8, 1726 (1954).

SEPARATION OF BORON ISOTOPES

A. A. Palko

A comparison was made of the temperature dependence of the isotopic equilibrium constants for the reaction

$$\text{donor} \cdot {}^{11}BF_3 + {}^{10}BF_3 = \text{donor} \cdot {}^{10}BF_3 + {}^{11}BF_3 ,$$

where donor represents various ethers, thioethers, and amines. Data for the systems in which the donors were Me_2S and Bu_2S appeared anomalous and were redetermined. The new equilibrium constants for these systems were given by

$$\log K_{eq}(Me_2S) = \frac{10.72}{T} - 0.01976 ,$$

$$\log K_{eq}(Bu_2S) = \frac{9.639}{T} - 0.01816 ,$$

where T is the absolute temperature. The new data correlated well with that for systems in which the donor formed weaker or stronger bonds with BF_3. A paper presenting an explanation for the isotope effect observed in these reactions and summarizing all of our research in this field is in preparation.

The fractionation of boron isotopes in the reaction

$$C_6H_5OCH_3 \cdot BF_3 \xrightarrow{50\%} C_6H_5OCH_3 + BF_3$$

was measured. A quantity of the 1 : 1 complex was prepared and was fractionally dissociated. After 50% of the initial complex was dissociated, the isotopic composition of the gas and the residual complex was compared. At 25°C the ratio, $({}^{10}B/{}^{11}B)\text{complex}/({}^{10}B/{}^{11}B)\text{gas}$, was 1.040.

This value is only slightly larger than that for the equilibrium exchange reaction. Consequently, this reaction does not warrant further consideration as a prospective isotope separation process.

CARBON ISOTOPE EFFECT IN THE DEPOLYMERIZATION OF PARALDEHYDE

L. L. Brown

There is an acid-catalyzed equilibrium between acetaldehyde and its trimer, paraldehyde. Paraldehyde has a six-membered ring structure with alternating C and O single bonds. When the trimer dissociates, three C–O bonds are broken and C=O bonds are formed. Thus, a kinetic isotope effect may be expected for the α carbon upon dissociating the trimer. The equilibrium oxygen isotope effect has already been reported.[2]

Depolymerization may be conveniently achieved by warming paraldehyde and stripping the more volatile acetaldehyde in a flowing nitrogen stream. If incremental samples of product are taken during the course of a reaction, the change in their isotopic composition is a measure of the kinetic isotope effect. As long as the individual sample is small compared with total product, the isotope effect can be found from Eq. (1):

$$\log r = (k^{13}/k^{12} - 1) \log (1 - f) + \log (k^{13}/k^{12}) , \qquad (1)$$

where $r = (^{13}C/^{12}C)\text{sample}/(^{13}C/^{12}C)\text{feed}$, and f = fraction reacted at the time sample is obtained. In practice, the least-square slope of the plot, $\log r$ vs $\log (1 - f)$, is used to find $(k^{13}/k^{12} - 1)$.

At 40 and 54°C, depolymerization was very slow, and little product resulted. By increasing the temperature to 64 and 69°C, samples sufficient for two determinations of the isotope effect were obtained. In both runs some discoloration of the liquid appeared, and some loss of product in the carrier stream was observed. Ratios for k^{12}/k^{13} of 1.006 and 1.012 were found. This kinetic isotope effect is not sufficiently large for an attractive carbon separation system based on current technology.

[2]L. L. Brown, *Chem. Div. Ann. Progr. Rept. June 20, 1961*, ORNL-3176, p. 19.

ATTEMPT TO REACT BORON HALIDES WITH CO

A. C. Rutenberg

Since CO is known to form the addition compound $BH_3 \cdot CO$, it was of interest to try to prepare an addition compound of a boron halide with CO. Mixtures of CO and BF_3, BCl_3, or BBr_3 were subjected to pressures up to 100 psig and temperatures from –80 to +145°C. There was no evidence that any significant amount of addition compound was formed.

ISOTOPE EFFECTS IN THE ALKALINE REDUCTION OF NO_3^-, NO_2^-, AND NH_2OH BY Fe(II)

L. L. Brown

Studies of the isotope effects occurring in the alkaline reduction of NO_3^-, NO_2^-, and NH_2OH have continued. The unexpected, reproducible, inverse ($k^{14}/k^{15} < 1$) isotope effect previously observed[3] in the Fe(II) reduction of nitrite, where MgO supplied the alkalinity, can now be explained. The system was characterized by a low yield of NH_3 and a very inefficient use of the reductant, Fe(II). Analysis of the product gas revealed that the major product was N_2O rather than NH_3.

There are two well-known reactions, 1 and 2,

$$NO_2^- + Fe(II) \longrightarrow NH_2OH , \qquad (1a)$$

$$NH_2OH + NO_2^- \longrightarrow N_2O , \qquad (1b)$$

$$2NO_2^- \rightleftharpoons N_2O_2^{2-} \longrightarrow N_2O , \qquad (2)$$

to account for the production of N_2O. If the isotope effect for the reduction of NO_2^- by either of these reactions is normal, that is, $k^{14}/k^{15} > 1$, then the unreacted NO_2^- remaining in solution would be enriched in ^{15}N with respect to its initial composition. The reduction of this residual NO_2^- by Fe(II) would then produce NH_3 enriched in ^{15}N and lead to an erroneous, inverse isotope effect. The observation that no NH_3 appeared until more than one-third of the necessary iron was

[3]L. L. Brown, *Chem. Div. Ann. Progr. Rept. May 20, 1965*, ORNL-3832, p. 37.

added, enough to convert all NO_2^- into $N_2O_2^{2-}$, suggested that the hyponitrite of reaction 2 was the most probable intermediate in the MgO system.

Further studies have also led to a better understanding of the reduction of NO_3^-, NO_2^-, and NH_2OH by Fe(II) in NaOH solutions. The observed isotopic fractionations may be explained in terms of (1) a slow rate-determining step operating in the reduction of NO_3^-, but not in the reduction of NO_2^- or NH_2OH and (2) a rate-determining step common to the conversion of both NO_2^- and NH_2OH to NH_3. At 25°C, the experimental ratio, k^{14}/k^{15}, for the slow step in (1) was 1.075 ± 0.004, and for that in (2), 1.032 ± 0.002. Isotope effects in good agreement with these values were computed on theoretical grounds, assuming cleavage of an N–O bond as the significant kinetic step in the reduction of each species. The mechanism suggested for the reduction of NO_3^-, NO_2^-, and NH_2OH in NaOH required irreversible reactions of the various species between N(5+) and N(3–). Compounds enriched in ^{15}N were used to establish the validity of this assumption and to identify unequivocally the slow rate-determining steps in the reduction reactions.

OXYGEN ISOTOPE ENRICHMENT

D. Zucker

The Oxygen-17 Facility performed satisfactorily during this report period. The Water Distillation Cascade remained on stream continuously except for a 25-min period on November 28 when an electrical transformer ignited. Normal operation was restored through the use of a standby transformer. Some mixing of the isotopic gradient occurred as a result of the electrical outage, but the productivity of the cascade was not seriously impaired. Peak concentrations of ^{17}O and ^{18}O in this system are currently 1.4 and 81.1% respectively. Operation of the Thermal Diffusion Cascade was normal during this period. The peak concentrations of ^{17}O and ^{18}O reached 24.0 and 99.8% respectively. More than 800 g of water, enriched in ^{18}O from 10 to 96%, was transferred to Isotope Division inventory for distribution to prospective users. Also transferred were 9.2 g of 99.6% ^{18}O gas, 25.0 g of 10% ^{17}O water, and 45.6 g of high-purity ^{16}O gas containing 10 to 40 ppm ^{17}O and ^{18}O. These products were valued in excess of $200,000.

A number of operating improvements were made during the report period. Several of the more important ones include (1) installation of a separate cooling system which increased the separative work capacity of the Thermal Diffusion Cascade ~25%, (2) installation of a constant-voltage transformer to provide a more constant power supply, and longer life, for the filaments in the Thermal Diffusion Cascade, (3) the virtual elimination of leakage into, or out of, the thermal diffusion column by the installation of newly designed top and bottom seals, and (4) the installation of new product collection equipment which minimized handling losses and maintained high purities in the collected products.

RAMAN AND INFRARED SPECTROSCOPY

During the current period, Raman and infrared spectral studies have proceeded on isotopic compounds and on several inorganic ions and complexes. Force-constant calculations have been performed in a number of cases, and isotopic partition function ratios have been calculated in order to estimate isotopic equilibrium constants. A number of these researches are reported below. Besides those reported, work is also being done on the spectra of a number of very reactive interhalogen ions which have interesting structures.

Ions for which the Raman spectra have been observed include the tetrafluorochlorate(III), the tetrafluorobromate(III), the hexafluorobromate(IV), and the hexafluoroiodate ions.

The use of a laser source in Raman spectroscopy offers the possibility of considerably better Raman spectral observations of many compounds. In order to proceed with such studies, we have undertaken to add a laser source and detector to our Cary model 81 Raman spectrophotometer.

Computed Carbon and Boron Isotopic Fractionation Factors for Exchange Reactions Involving Borine Carbonyl[4]

G. M. Begun

It has been suggested that the exchange equilibrium between carbon monoxide and its addition

[4]W. H. Fletcher and M. D. Danford aided in this work.

compound with diborane (borine carbonyl) might be used to fractionate the isotopes of carbon. Since borine carbonyl is thermally unstable, a simple heat reflux may be possible. For this reason a calculation of the equilibrium isotopic effects involving borine carbonyl was undertaken.

Bethke and Wilson[5] observed the infrared and Raman spectra of borine carbonyl and assigned fundamental vibrational frequencies for $^{10}BH_3CO$, $^{11}BH_3CO$, $^{10}BD_3CO$, and $^{11}BD_3CO$. They also did a normal coordinate analysis of the molecule and calculated a set of valence force constants that reproduce the observed frequencies quite well. There are, however, no data or calculations concerning the ^{13}C- or ^{18}O-containing species of the molecule. We have used the data of Bethke and Wilson and their normal coordinate analysis, and have calculated a set of valence force constants using the Wilson F- and G-matrix method. A machine-iterative, least-squares process similar to that of Overend and Scherer[6] was employed to converge on the best set of F-matrix elements. Table 2.1 compares our elements with those of Bethke and Wilson.[5] Agreement is good except for F_{78}, where the negative sign on the literature value is apparently in error.

The calculated isotopic frequencies for the various isotopic species are given in Table 2.2. Using these calculated frequency shifts and the observed isotopic frequencies for carbon monoxide[7,8] and for diborane,[9,10,11] we calculated the equilibrium fractionation factor for the isotopic exchange reactions. For these calculations we employed the formula given by Urey:[12]

$$\frac{Q_2\sigma_2}{Q_1\sigma_1} = \prod_i \frac{u_{2i}\exp(-u_{2i}/2)[1-\exp(-u_{1i})]}{u_{1i}\exp(-u_{1i}/2)[1-\exp(-u_{2i})]} . \quad (1)$$

Here the equilibrium constant for the exchange reaction between the molecule or species under consideration and its separated atoms is Q_2/Q_1, where the subscripts 1 and 2 refer to the different isotopic species, σ_1 and σ_2 are the symmetry numbers, $u_i = hc\omega_i/kT$, and ω_i is the ith normal vibrational frequency.

Table 2.3 lists the calculated isotopic equilibrium constants for the following reactions:

$$BH_3{}^{12}CO + {}^{13}CO \rightleftharpoons BH_3{}^{13}CO + {}^{12}CO , \quad (2)$$

$$BH_3C^{16}O + C^{18}O \rightleftharpoons BH_3C^{18}O + C^{16}O . \quad (3)$$

Table 2.1. F-Matrix Elements for Borine Carbonyl

Constant	Ref. 5	This Work
F_{11}	18.9660	17.9504
F_{22}	2.6289	2.7866
F_{33}	3.3925	3.2765
F_{44}	0.5281	0.5289
F_{24}	−0.2847	−0.2951
F_{55}	3.1575	3.1170
F_{66}	0.3440	0.3425
F_{77}	0.2905	0.2909
F_{88}	0.5175	0.5274
F_{78}	−0.1922	0.1967

The equilibrium constants were computed by first calculating the partition function ratios for the separate molecules, using formula (1), and then taking the ratio of the ratios for the two molecules involved.

At 25°C the $^{13}C-^{12}C$ and the $^{18}O-^{16}O$ separation factors were calculated to be 1.048 and 1.010 respectively. In both cases the heavy isotope concentrates in the borine carbonyl. Since borine carbonyl has the structure $H_3B:CO$, it is expected that the isotope effect will be considerably greater for the carbon atom than for the oxygen atom. This was, indeed, observed. The tabulated results are based on the harmonic oscillator approximation; data for anharmonic corrections were not available.

[5] G. W. Bethke and M. Kent Wilson, *J. Chem. Phys.* **26**, 1118 (1957).

[6] J. Overend and J. R. Scherer, *J. Chem. Phys.* **32**, 1289 (1960).

[7] E. K. Plyler, L. R. Blaine, and E. D. Tidwell, *J. Res. Natl. Bur. Std.* **55**, 183 (1955).

[8] I. M. Mills and H. W. Thompson, *Trans. Faraday Soc.* **49**, 224 (1953).

[9] R. C. Lord and E. Nielsen, *J. Chem. Phys.* **19**, 1 (1951).

[10] R. C. Taylor and A. R. Emery, *Spectrochim. Acta* **10**, 419 (1958).

[11] W. J. Lehmann, J. F. Ditter, and I. Shapiro, *J. Chem. Phys.* **29**, 1248 (1958).

[12] H. C. Urey, *J. Chem. Soc.* **1947**, 562.

Table 2.2. Calculated Fundamental Vibrational Frequencies of Isotopic Borine Carbonyl Molecules

	$^{10}BH_3{}^{12}C^{16}O$	$^{11}BH_3{}^{12}C^{16}O$	$^{10}BD_3{}^{12}C^{16}O$	$^{11}BD_3{}^{12}C^{16}O$	$^{10}BH_3{}^{13}C^{16}O$	$^{11}BH_3{}^{13}C^{16}O$	$^{10}BD_3{}^{13}C^{16}O$	$^{11}BD_3{}^{13}C^{16}O$
ν_1	2374.6	2372.0	2167.5	2167.0	2374.5	2371.9	2115.6	2115.1
ν_2	2167.0	2166.7	1701.0	1696.8	2115.2	2114.8	1701.0	1696.8
ν_3	1084.4	1072.9	882.8	860.7	1084.4	1072.9	882.5	860.4
ν_4	707.9	691.4	629.2	624.0	705.2	688.6	626.5	621.2
ν_5	2455.9	2440.8	1855.3	1834.0	2455.9	2440.8	1855.3	1833.9
ν_6	1096.8	1093.1	806.8	801.0	1096.8	1093.1	806.1	800.5
ν_7	818.9	812.7	712.2	709.5	808.0	801.7	699.4	696.4
ν_8	316.5	316.5	262.3	262.1	311.9	311.9	259.8	259.6
	$^{10}BH_3{}^{12}C^{18}O$	$^{11}BH_3{}^{12}C^{18}O$	$^{10}BD_3{}^{12}C^{18}O$	$^{11}BD_3{}^{12}C^{18}O$	$^{10}BH_3{}^{13}C^{18}O$	$^{11}BH_3{}^{13}C^{18}O$	$^{10}BD_3{}^{13}C^{18}O$	$^{11}BD_3{}^{13}C^{18}O$
ν_1	2374.5	2372.0	2121.2	2120.7	2374.5	2371.9	2068.0	2067.4
ν_2	2120.7	2120.4	1700.9	1696.7	2067.5	2067.2	1700.9	1696.6
ν_3	1084.4	1072.9	881.2	859.4	1084.4	1072.9	881.0	859.2
ν_4	698.3	681.7	620.9	615.4	696.1	679.4	618.6	612.9
ν_5	2455.9	2440.8	1855.3	1834.0	2455.9	2440.8	1855.2	1833.9
ν_6	1096.8	1093.1	806.7	800.9	1096.8	1093.1	806.0	800.4
ν_7	817.1	810.8	709.8	707.1	806.1	799.8	697.0	693.9
ν_8	313.7	313.7	260.0	259.8	309.0	309.0	257.3	257.2

Table 2.3. Calculated Equilibrium Constants for Isotopic Exchange in the Borine Carbonyl–Carbon Monoxide System

T (°K)	C^{13}/C^{12} Factor[a]	O^{18}/O^{16} Factor[b]
100	1.244	1.072
200	1.089	1.023
250	1.063	1.015
273.16	1.056	1.012
298.16	1.048	1.010
325	1.041	1.008
350	1.036	1.007
400	1.029	1.005
500	1.020	1.003
600	1.014	1.002

[a] $\frac{BH_3{}^{13}CO}{BH_3{}^{12}CO} \Big/ \frac{{}^{13}CO}{{}^{12}CO}$. [b] $\frac{BH_3C^{18}O}{BH_3C^{16}O} \Big/ \frac{C^{18}O}{C^{16}O}$.

Table 2.4. Calculated Equilibrium Constants for Boron Isotopic Exchange Between Diborane and Borine Carbonyl

T (°K)	Isotopic Separation Factor[a]
100	1.073
200	1.025
250	1.017
273.16	1.014
298.16	1.012
325	1.010
350	1.008
400	1.006
500	1.003
600	1.002

[a] $\frac{{}^{11}B}{{}^{10}B}(BH_3 \cdot CO) \Big/ \frac{{}^{11}B}{{}^{10}B}(B_2H_6)$.

Using the observed isotopic data for diborane[9,10] and the calculated boron shifts for borine carbonyl, we have also calculated the isotopic fractionation for the reaction

$$^{10}BH_3 \cdot CO + H_3{}^{11}B^{11}BH_3 \rightleftharpoons {}^{11}BH_3CO + H_3{}^{11}B^{10}BH_3 . \quad (4)$$

In calculating this separation factor, we have assumed that the partition function for the mixed molecule $H_3{}^{11}B^{10}BH_3$ is the geometric mean of that for the pure species $^{11}B_2H_6$ and $^{10}B_2H_6$. The calculated isotopic equilibrium constants are given in Table 2.4. It may be seen that the separation factor for boron isotopes is 1.012 at 25°C. This value compares unfavorably with factors near 1.03 for various BF_3, donor•BF_3 exchange reactions which have been studied recently. Thus it appears that the borine carbonyl systems offer the possibility of appreciable isotopic fractionation only in the case of carbon isotopes.

Raman and Infrared Spectra of the BF_3 Complex with Dimethyl Sulfide and the Isotopic Exchange of the Complex with BF_3[13]

G. M. Begun

Dimethyl sulfide forms a 1 : 1 molecular addition compound with boron trifluoride. The exchange of boron between this complex and gaseous BF_3 is the basis for a system for fractionating boron isotopes.[14] Since no infrared and Raman spectral data were available for the complex, we obtained these data in order to make theoretical calculations of the isotopic separation factor.

The boron trifluoride–dimethyl sulfide complex was synthesized from purified dimethyl sulfide and BF_3 enriched in ^{10}B or ^{11}B. The enriched isotopes were obtained from the Isotopes Division and contained 96% ^{11}B and 94% ^{10}B respectively. Raman spectra were obtained in sealed glass Raman cells containing about 5 ml of the complex.

[13] A. A. Palko and W. H. Fletcher aided this work.

[14] A. A. Palko and J. S. Drury, *J. Chem. Phys.* 33, 779 (1960).

A Cary model 81 Raman spectrophotometer was employed. Infrared spectra were obtained on liquid samples contained between silver chloride windows with very thin or no spacers between the windows. Cells were loaded in a dry box with fresh samples for each spectrum. A Perkin-Elmer 521 infrared grating spectrophotometer was used to observe the spectra.

The infrared spectrum of $^{10}BF_3 \cdot (CH_3)_2S$ liquid is shown in Fig. 2.1, and the Raman spectrum of $^{11}BF_3 \cdot (CH_3)_2S$ liquid is reproduced in Fig. 2.2. The other boron isotopic species produced similar spectra with some peaks slightly shifted. The infrared data are listed in Table 2.5, and the Raman data are listed in Table 2.6 along with a tentative assignment of the bands observed. The

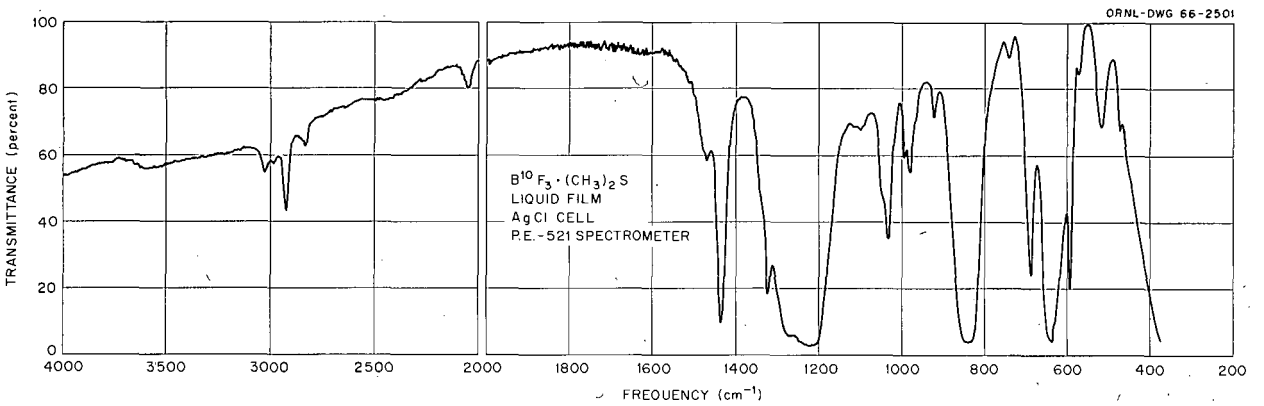

Fig. 2.1. Infrared Spectrum of Liquid $^{10}BF_3 \cdot (CH_3)_2S$.

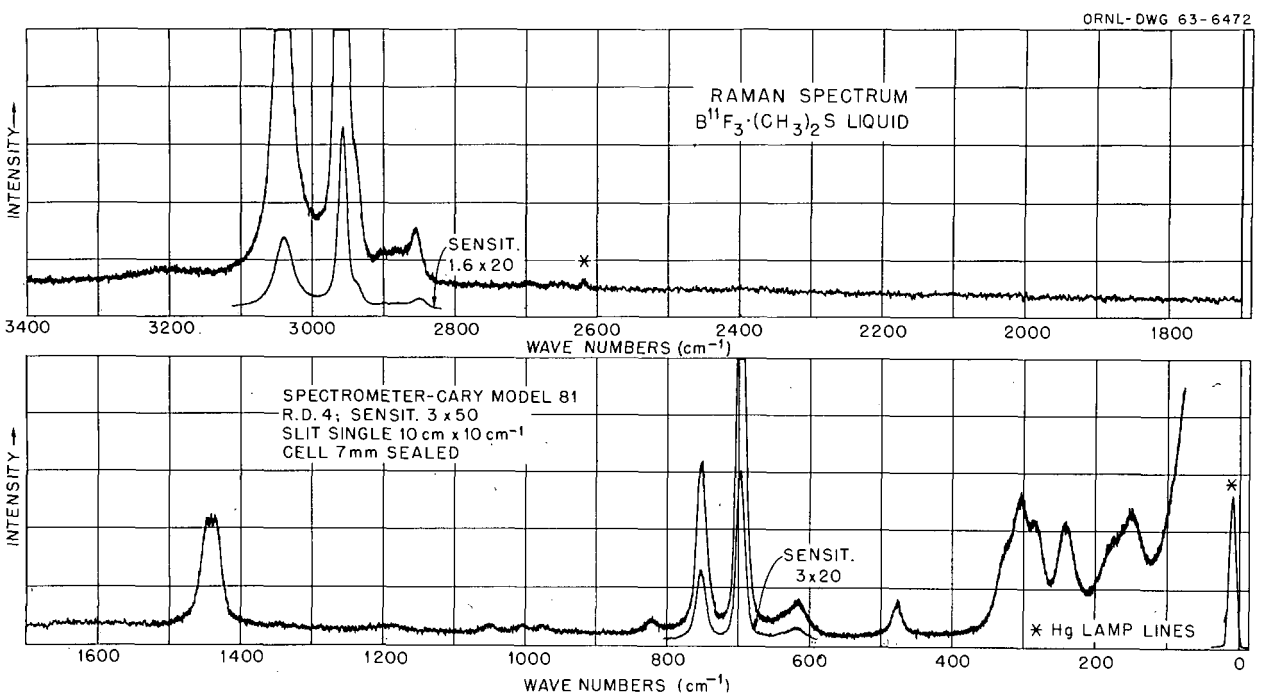

Fig. 2.2. Raman Spectrum of Liquid $^{11}BF_3 \cdot (CH_3)_2S$.

band numbering system is that described for the $BF_3 \cdot$ dimethyl ether complex in ref. 15.

Using these observed isotopic frequencies and those reported for BF_3,[16] we calculated the isotopic equilibrium constant for the reaction

$$^{10}BF_3 + {}^{11}BF_3 \cdot (CH_3)_2S \rightleftharpoons {}^{11}BF_3 + {}^{10}BF_3 \cdot (CH_3)_2S .$$

The method of calculation was similar to that described above in the section on the borine carbonyl systems. The calculated and observed values are given in Table 2.7.

As with the other BF_3, BF_3-complex systems, the ^{11}B was found to concentrate in the gaseous BF_3. Considering all the factors involved in both the experimental determination and the approximations in the calculation, the agreement between the observed and calculated equilibrium factors is good. The main discrepancy seems to be the slope of the temperature dependence. This lack of agreement may be due to a change in the species involved in the liquid complex as the temperature is changed. The spectral studies which were made at room temperature would not reflect such changes.

[15] G. M. Begun, W. H. Fletcher, and A. A. Palko, *Spectrochim. Acta* **18**, 655 (1962).

[16] J. Vanderryn, *J. Chem. Phys.* **30**, 331 (1959).

Table 2.5. Infrared Bands of $BF_3 \cdot (CH_3)_2S$ Liquid

Frequency (cm^{-1}) ^{11}B	Frequency (cm^{-1}) ^{10}B	Intensity[a]	Assignment and Vibration Type	
	432	w	ν_{18}, ν_{30}	Combination
468.5	471	w	ν_{13}, ν_{29}	BF_3 deformation (antisymmetrical)
	513	m	ν_{16}, ν_{30}	Combination
580	590	m	ν_{14}	BF_3 deformation (symmetrical) (A')
625	634	s	ν_{12}	B–S stretch (A')
	690	m	ν_{10}	C–S stretch (A')
	745	w	ν_{27}	C–S stretch (A'')
833	838	s	ν_{11}	B–F stretch (symmetrical)
	1035	m	ν_8	CH_3 rock (A')
1181	1223	vs	ν_7	B–F stretch (antisymmetrical) (A')
1222	1270	vs	ν_{25}	B–F stretch (antisymmetrical) (A'')
	1433	m	$\nu_{22}, \nu_{23}, \nu_{24}$	CH_3 deformation
	2838	w	$2\nu_5, 2\nu_6$	Overtone
	2933	m	ν_1	C–H stretch
	2994	w		C–H stretch
	3033	w		C–H stretch

[a] w = weak, m = medium, s = strong, v = very.

Table 2.6. Raman Bands of $BF_3 \cdot (CH_3)_2S$ Liquid

Frequency (cm^{-1}) ^{11}B	Frequency (cm^{-1}) ^{10}B	Relative Intensity	Polarization[a]	Assignment and Vibration Type	
	139	1	D	ν_{32}	BF_3 rock (A'')
	167 (sh)	1	P	ν_{18}	BF_3 rock (A')
	233	1	P	ν_{16}	$S(CH_3)_2$ wag (A')
	276	1	D (?)	ν_{30}	$S(CH_3)_2$ rock (A'')
	295	3	P	ν_{15}	C–S–C deformation (A')
	314 (sh)	1	P		
	470	0.5	D	ν_{13}, ν_{29}	BF_3 deformation (A', A'')
608	628	1	P	ν_{12}	B–S stretch (A')
	688	4	P	ν_{10}	C–S stretch (A')
	743	2	D	ν_{27}	C–S stretch (A'')
813	819	0.5	P	ν_{11}	B–F stretch (symmetrical) (A')
	965	0	D (?)	ν_9	$C \cdot H_3$ rock (A')
	994	0	D (?)	ν_{26}	CH_3 rock (A'')
	1041	0	P	ν_8	CH_3 rock (A')
	1047, 1436	3	D	ν_5, ν_6; $\nu_{22}, \nu_{23}, \nu_{24}$	CH_3 deformations
	2838	1	P	2×1427	Overtone
	2862	0.5	P	2×1436	Overtone
	2883	0.5	P		Overtone
	2920 (sh)	1		ν_2	C–H stretch (A')
	2942	10	P	ν_1	C–H stretch (A')
	3024	8	D (?)	$\nu_3, \nu_{19}, \nu_{20}, \nu_{21}$	C–H stretches

[a]P = polarized, D = highly depolarized, sh = shoulder.

Table 2.7. Boron Isotopic Equilibrium Constants Between BF_3 and $BF_3 \cdot (CH_3)_2S$

T (°K)	Calculated α^a	Observed α^b
253	1.044	1.056
263	1.042	1.048
273	1.040	1.041
299	1.036	1.031

[a] $\alpha = \dfrac{B^{11}/B^{10}\ (BF_3\ \text{gas})}{B^{11}/B^{10}\ [BF_3 \cdot (CH_3)_2S\ \text{liquid}]}$.

[b] Ref. 14.

INFRARED AND RAMAN SPECTRA OF THE HEXAFLUORIDE IONS OF SILICON, GERMANIUM, AND TIN

A. C. Rutenberg G. M. Begun

This work was initiated to establish the structures of SiF_6^{2-} and SnF_6^{2-} ions in the crystalline state. The most probable structure for these ions was a regular octahedron (point group O_h) or a distorted octahedron (point group D_{4h}), but data were not available to distinguish between these forms. The salts Na_2SnF_6, K_2GeF_6, and Na_2SiF_6 were prepared from the appropriate oxide or fluorosilicate, and crystals were grown by slow evaporation at room temperature. The Raman spectra of the crystals were run on samples in quartz or Pyrex conical tubes; observed frequencies are listed in Table 2.8. Several crystal size and tube combinations were tried to achieve the best signal-to-noise ratio. The infrared spectra were obtained using the KBr pellet technique. The spectra were recorded using a Cary model 81 Raman spectrophotometer and a Perkin-Elmer model 521 grating infrared spectrophotometer.

Table 2.8. Observed Raman and Infrared Frequencies for Na_2SnF_6, K_2GeF_6, and Na_2SiF_6 Crystals

	ν_1 Raman	ν_2 Raman	ν_3 IR	ν_4 IR	ν_5 Raman
Na_2SnF_6	591	480	566	300	253
K_2GeF_6	623	468	604	339, 359	335
Na_2SiF_6	663	478	738	483	407

Three Raman-active and two infrared-active fundamental vibrational frequencies were observed for each of the three compounds studied. These bands are characteristic of the spectra of point group O_h molecules, though D_{4h} symmetry is not unequivocally eliminated.

NUCLEAR MAGNETIC RESONANCE SPECTROSCOPY

A. C. Rutenberg

Low-Temperature NMR Study of the Species $(C_2H_5)_2O \cdot (BF_3)n$

Wirth, Jackson, and Griffiths[17] in their phase study of the system BF_3-$(C_2H_5)_2O$ report a compound containing $3BF_3/(C_2H_5)_2O$ with a melting point of −71°C. They also observed the well-known 1:1 addition compound melting at −59°C. An NMR experiment was performed to confirm and, possibly, characterize the newer addition compound. The sample container consisted of a 50-ml pipet bulb to which was sealed a 5-mm-OD capillary tube with a small piece of glass rod at the bottom to reduce the sample volume. A mixture of $3.5BF_3/(C_2H_5)_2O$ was introduced from a vacuum system. The sealed sample container had a pressure of about 1 atm at room temperature.

The sample was cooled slowly in the probe while the ^{19}F NMR spectrum was monitored. At room temperature a single peak due to the 1:1 addition compound was observed. At about −30°C a very small second peak was observed. This peak grew at the expense of the 1:1 peak, and at temperatures below −70°C had a greater area than the 1:1 peak. The new peak was ~24 ppm below the 1:1 peak, indicating a weaker interaction. The sample could be supercooled for short periods to temperatures as low as −110°C. The proton spectrum at −80°C consisted of an unsplit methyl and unsplit methylene peak from which no definite conclusions could be drawn. The ^{19}F spectra confirmed a second addition compound, but did not reveal the composition or the nature of the bonding.

[17] H. E. Wirth, M. J. Jackson, and H. W. Griffiths, *J. Phys. Chem.* 62, 871 (1958).

NMR Observations on BrF_3

The infrared and Raman spectra of ClF_3 and BrF_3 were measured by Claassen, Weinstock, and Malm.[18] Their data strongly support a planar *T* structure for ClF_3, and a like shape for BrF_3 based on less complete spectra. They also obtained evidence for association in liquid BrF_3. The ^{19}F NMR spectrum of gaseous and liquid ClF_3 was observed by Alexakos and Cornwell,[19] who measured the chemical shift and spin-spin coupling constant resulting from the two different fluorine sites. Only a single peak has been reported[20] in the NMR spectrum of BrF_3. We, therefore, made an attempt to obtain a more detailed NMR spectrum of BrF_3 to add to the structural information on this compound.

Matheson BrF_3 was distilled into a 5.6-mm-OD quartz tube attached to a nickel vacuum system. The sample (mp ~9°C) could be supercooled to near 0°C for a period sufficient to observe the NMR spectrum, which consisted of a single peak ~15 cps wide. In order to observe spectra at lower temperatures, a sample containing 2.5 ClF_3/BrF_3 was prepared. This mixture also contained a small amount of NaF to react with dissolved HF. Spectra were obtained at temperatures down to –37°C. Only a single peak was observed which broadened very little on cooling. It appears that all the fluorine atoms in the mixture were rapidly exchanging, perhaps by way of an intermediate such as ClF_2^+ or BrF_4^-.

NMR Study of Complexes Between Sn(IV) and F^-

There are not many data on F^- complexes of Sn(IV). The NMR method was investigated as a possible useful tool for characterizing and obtaining stability constant data on these species. Seven isotopes of tin have spin 0; the remaining three have spin ½. The ^{19}F NMR spectra of Sn-F species should have narrow lines in the absence of exchange, and the F-Sn spin couplings, if observed, would be smaller peaks with a simple, readily recognized pattern. Some preliminary observations indicated that the spectra were complicated because of the large number of species present in the solutions. A series of 20 solutions in 13-mm cellulose nitrate tubes were observed at room temperature. These solutions contained Sn(IV) and varying amounts of HF, from a trace to a large excess, and a small amount of CF_3COOH as an internal standard. Solutions low in HF had peaks in the CF_3COOH region of the spectrum. As more HF was added, additional peaks appeared at higher field, and the lower field peaks were reduced in area. After considerable HF was added, peaks appeared in the CF_3COOH region (+87 ppm from CF_3COOH in these solutions). In this series, 12 different major peak locations were observed.

If a small amount of Sn(IV) solution was added to a large excess of aqueous HF, two peaks could be observed in the ^{19}F NMR spectrum, attributable, presumably, to HF and SnF_6^{2-}. When, however, the smallest amount of HF that would give an NMR spectrum was added to a solution of $SnCl_4$, two small peaks appeared at –3 and +22 ppm from CF_3COOH. It is an unanswered question whether we have here two different compounds, such as $SnCl_3F$ and $SnCl_4F^-$, or two isomers of the same compound. Further information concerning the rate of exchange between species and the magnitude of the chemical shift between the two peaks can help to eliminate some of the possibilities. Additional information is needed from other forms of spectroscopy to characterize unambiguously the species in these solutions.

NMR Study of SbF_5 and AsF_5

The infrared and Raman spectra of SbF_5[21,22,23] and AsF_5[21] have been interpreted in terms of a trigonal bipyramid structure. In the SbF_5 case, the physical properties and the NMR study of Hoffman, Holder, and Jolly[24] indicate that this material is highly polymerized. Only a single

---

[18] H. H. Claassen, B. Weinstock, and J. G. Malm, *J. Chem. Phys.* **28**, 285 (1958).

[19] L. G. Alexakos and C. D. Cornwell, *J. Chem. Phys.* **41**, 2098 (1964).

[20] E. L. Muetterties and W. D. Phillips, *J. Am. Chem. Soc.* **81**, 1084 (1959).

[21] L. K. Akers, Ph.D. thesis, Vanderbilt University, June 1955.

[22] J. Gaunt and J. B. Ainscough, *Spectrochim. Acta* **10**, 57 (1957).

[23] W. D. Jones, Ph.D. thesis, Vanderbilt University, June 1963.

[24] C. J. Hoffman, B. E. Holder, and W. L. Jolly, *J. Phys. Chem.* **62**, 364 (1958).

broad line was observed by Muetterties and Phillips[20] in their study of the ^{19}F NMR spectrum of AsF_5. They postulated that impurities were in part responsible for the breadth of the AsF_5 resonance. It was felt that additional useful structural information might be obtained from higher-purity samples. Hoffman *et al.*[24] used Pyrex sample tubes, and it was found that SbF_5 attacks Pyrex. In addition, the present NMR equipment operating at 56.4 Mc offers an additional increase in sensitivity over the 40-Mc equipment used by Hoffman *et al.*[24]

The SbF_5 was obtained from three vendors, Ozark Mahoning, Harshaw, and City Chemical Company. Material from the last vendor gave the best NMR spectra. The samples were purified using a vacuum system constructed almost entirely of nickel, and were distilled into quartz NMR tubes. Some SbF_5 was purified by distilling the material in contact with NaF, treating it with F_2, then distilling it again. The best spectra were obtained from material distilled without any prior treatment. Although our spectra gave a better signal-to-noise ratio than the spectrum shown by Hoffman *et al.*,[24] no additional spin-spin splittings were observed. The present work confirms their observation of three different fluorine environments in the ratio of 1:2:2. This observation is not in accord with a trigonal bipyramid structure.

The ^{19}F NMR spectrum of AsF_5, in both gas and liquid phases, consisted of a single broad line. The liquid spectrum was observed in a 5.5-mm-OD quartz tube sealed to a 100-ml quartz bulb. The sample tube was cooled in the probe to condense the gas in the bulb. The AsF_5 gas sample was observed at ambient temperature. It was contained in a 15-mm-OD quartz tube at ~2.5 atm.

An inert diluent for SbF_5 was sought, but no suitable solvent was found. Fully fluorinated organic solvents did not dissolve appreciable amounts of SbF_5, and the almost completely fluorinated "Freons" reacted with SbF_5. In the process of seeking a solvent, an addition compound between SbF_5 and CF_3COOH was observed.

Antimony pentafluoride is very soluble and perhaps completely miscible with CF_3COOH. The lines in the room-temperature ^{19}F NMR spectrum were broad, and it was necessary to run the spectra below +10°C to get good detail. The chemical shifts varied with solution temperature and composition; the following description applies to a fairly concentrated solution of SbF_5 in CF_3COOH at +7°C. The higher field portion of the spectrum consisted of two peaks 1.2 ppm apart, resulting from the ^{19}F resonance in bound (lower field) and free CF_3COOH. The CF_3COOH molecules were rapidly exchanging, and at room temperature only a single broad peak was observed in this region of the spectrum. A doublet was measured +33.1 ppm from the free CF_3COOH, and a quintet was measured ~¼ the area of the doublet at +62.5 ppm from CF_3COOH. The multiplets had a spin-spin coupling constant of 95.5 cps. The spectrum described is consistent with an octahedral configuration around the antimony with a coordinated oxygen occupying one position and fluorines occupying the other five locations.

ISOTOPIC MASS SPECTRA

Lawrence Landau

Precise isotopic determinations were made of more than 900 boron-, carbon-, oxygen-, and nitrogen-containing samples during this report period. The substitution of VacIon pumps for mercury diffusion pumps, and the addition of a six-place digital voltmeter and printer to the mass spectrometer, made possible better analyses than before with a smaller investment in man-hours per sample.

MOLECULAR FORCE CONSTANTS

M. D. Danford

In force-constant determinations, many instances arise in which either insufficient frequency data are available, or there is no rigorous method for assignment of the observed frequencies. In the former case, there may be certain frequencies which are unobservable, or the number of force constants to be determined may be greater than the number of frequencies obtainable, as for tetrahedral XY_4 molecules. Sources for additional data include isotopic substitution, Coriolis coupling and centrifugal distortion constants, obtainable from spectroscopic or microwave techniques, and mean-square amplitudes of vibration (MSA) from diffraction studies. Of these, isotopic substitution, where one or more of the atoms is replaced by one of its isotopes, is the most powerful. The most commonly used method is that of replacing

the lighter atoms, such as hydrogen, by deuterium or tritium, and assuming the force constants to be the same in all species. Another method, proposed recently by McKean,[25] makes use of accurately measured frequency differences, obtained when the heavier atoms are replaced by their isotopes, as an additional data source. Coriolis coupling and centrifugal distortion constants provide additional data to define vibrational interactions, while the MSA define mainly the principal force constants.

The shapes of infrared bands and polarization measurements of Raman spectra often provide sources of information for making frequency assignments, but, frequently, there is no information obtainable from these sources. We have found it possible to obtain moderately precise principal force constants from MSA data. These data, while not sufficiently good to be useful in a quantitative sense, may sometimes be of value in making spectroscopic assignments. Conversely, we have found it possible to compute MSA data from spectroscopic results if the latter are available.

Other computer programs were also developed during this report period. One of these permits the extraction of harmonic force constants and Coriolis coupling constants from observed spectroscopic data. Another computer program includes the contributions of Coriolis coupling and centrifugal distortion constants in force-constant computations. The foregoing programs were used to compute (1) MSA for CH_4, CD_4, CCl_4, CF_4, $GeCl_4$, NH_3, ND_3, and PCl_3; (2) force constants for PCl_3; (3) fundamental vibrational frequencies for CH_4, CCl_4, and $GeCl_4$; and (4) force constants for $GeCl_4$.

[25] D. C. McKean, *Spectrochim. Acta* **22**, 269 (1966).

3. Radiation Chemistry

PULSE RADIOLYSIS AND FLASH PHOTOLYSIS

J. A. Ghormley J. F. Riley
C. J. Hochanadel J. W. Boyle

We have recently obtained a field emission source which provides 2-Mv electrons at 5000 amp in a 30-nsec pulse. This machine will be put into operation shortly and will allow study of short-lived transients with a unique capability, because of the very high current, for the study of transients in gases.

During the past year we assembled the fast-recording spectrographic-spectrophotometric detection apparatus and initiated studies of the flash photolysis of several aqueous systems. Flash photolysis studies will generally be carried out along with the pulse radiolysis studies. Much of our effort was expended in assembling this equipment and developing techniques for measuring transients on the shortest possible time scale. A brief summary of the equipment and of some preliminary studies is given below.

Equipment Development

The analyzing lamp is either a flash lamp for spectrographic detection of intermediates or a steady lamp for kinetic studies. The spectroflash lamp is a 10-j spark in air with a duration of ~ 0.5 μsec (Unilectron Corporation). The steady lamp is usually a high-pressure mercury-xenon lamp (Hanovia 901B-1) powered by a very stable supply (Electronic Measurements Company Regatran). The sample is contained in a cylindrical flow-through-type cell (Pyrocell Manufacturing Company) constructed of "suprasil" grade silica. The cell can be filled repeatedly with stock solution, which may be purged of air or saturated with a particular gas by continuous bubbling. After passing through the cell, the analyzing light goes through a collimator to minimize scattered light, and is then focused on the slit of a McPherson model 216, $f/9$ grating spectrograph-polychromator. The absorption spectrum can be photographed, or the instrument can be used as a polychromator with several photomultiplier tubes for monitoring several regions of the spectrum at the same time. The photomultiplier tubes are EMI 9558QA (S20 response), which have a large photocathode, high sensitivity, and low photocathode resistance. The output of these is fed to a dual-beam oscilloscope (Tektronix 555 with C-27 camera). For the photolysis flash, two lamps are used in series. These are placed alongside the sample cell inside a cylindrical reflector. An ignitron switch in series with the lamps is triggered by a thyratron discharge. The capacitors (Sangamo 1 μf, 25 kv), triggering circuits, and the flash apparatus are housed in steel cabinets to shield against electrical noise.

In order to examine the buildup and decay of intermediates on the shortest time scale, it is necessary to minimize the flash duration, the electrical noise, and the scattered light. We tested a number of lamp designs, using various rare-gas and rare-gas-quencher fillings. The lamp found to be best is constructed of a quartz tube with a coaxial rod between the stainless steel electrodes, which are sealed in place with Apiezon W wax. With 10-mm-ID tube and 7-mm rod the discharge is constrained to a $1\frac{1}{2}$-mm annulus. The resistance of two 25-cm lamps in series is adequate to provide critical damping, and essentially all of the electrical power is dissipated in the lamps. For a discharge of 300 j at 25 kv in krypton at 15 torrs, 90% of the light is emitted in 3.2 μsec, and for 600 j at 20 kv the duration is 5.8 μsec.

An example of the flash profile is given in Fig. 3.1, curve *a*, and the integrated light output is given by curve *b*.

ORNL-DWG. 66-6831

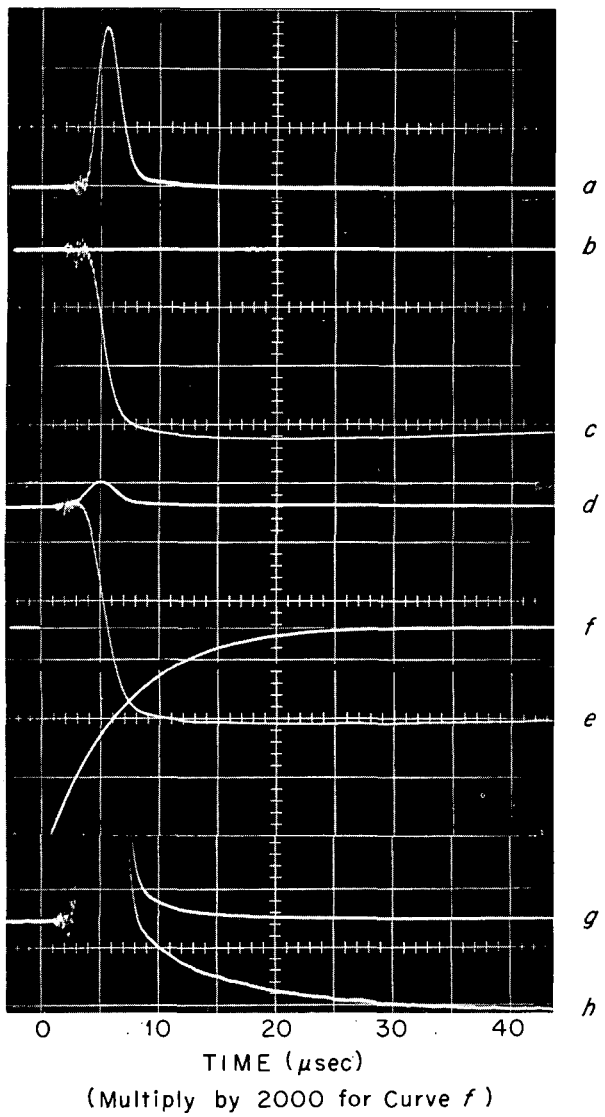

Fig. 3.1. Flash Characteristics and the Formation of Intermediates During and After the Flash in 6×10^{-5} *M* H_2O_2 Solution at pH 13. Curve *a* is the flash intensity as a function of time, *b-c* is the integrated light output, *d-e* is the formation of O_3^- in oxygen saturated solution (at 436 nm), *f* is the decay of O_3^-, *g-h* is the formation of O_2^- in oxygen-free solution (at 248 nm). The sensitivity for the absorption curves is 10% for each large division.

We also found that a concentric irradiation cell-lamp arrangement was efficient and gave a short flash, but considerable "noise" resulted from ultrasonic vibrations. A short flash was produced by a lamp lightly packed with quartz wool to quench the afterglow, and with a tungsten wire resistance to prevent ringing in the electrical circuit. However, the packing deteriorated on flashing, and the flashes were not reproducible. This arrangement suffered the further disadvantage that part of the power is dissipated in the wire, and the wire eventually burned out. The lamp was improved somewhat by Vigreaux-type indentations which held the quartz wool in place and also provided greater quenching surface. A lamp packed with fibers of boron nitride, which has a high melting range, also gave a short flash, but the boron nitride decomposed on flashing. A coaxial lamp constructed on the end of RG8/U coaxial cable also gave a short flash. The duration of the flash was determined by the internal diameter of the center tube and the width of the external annulus.

The scattered light from the photolysis flash and the electrical "noise" have been reduced to the extent that optical absorption can usually be measured during the flash. This permits us to compare the buildup of intermediates with energy input to within about 0.1 μsec even though the flash duration is 3 to 4 μsec. An example is shown in curves *d* and *e* of Fig. 3.1. With oxygen present during the photolysis of basic hydrogen peroxide solution, O_3^- is produced during the flash by the fast reaction[1] of O_2 with the O^- produced initially; with no oxygen present, O_2^- is produced by the somewhat slower reaction of HO_2^- with the O^- as shown by curve *h*.

Preliminary Studies

The flash photolysis of H_2O_2 solutions was studied at several flash intensities over the concentration range 5×10^{-5} to 10^{-2} *M*, and over the pH range 7 to 13. In neutral solution the absorption in the ultraviolet shows a fast decay attributed to reactions of the OH radical, followed by a slower decay attributed to reactions of HO_2.

[1] G. E. Adams, J. W. Boag, and B. D. Michael, *Proc. Roy. Soc. (London) Ser. A* **289**, 321 (1966).

A mechanism based on known reactions of the radicals with each other and with peroxide is consistent with the results. A kinetic analysis allowed the separation of the ultraviolet absorption into two components, giving the absorption spectra of O_2^- and OH as shown in Fig. 3.2. The spectrum of O_2^- agrees with that of Czapski and Dorfman.[2] Several workers[3] have found absorption in the ultraviolet which they attributed to the OH radical, but no spectrum had been reported. A similar OH spectrum was obtained by flashing pure water and OH^- solution. Additional evidence for its identity was provided by its reaction with H_2 and by the additional formation by reaction of N_2O with the e_{aq}^- produced on flashing OH^- solution. The kinetics for basic solutions have not been completely worked out. We do not find a second absorption band for O_3^- in the ultraviolet as reported by Adams *et al*.[1]

[2]G. Czapski and L. M. Dorfman, *J. Phys. Chem.* **68**, 1169 (1964).

[3]See, for example, J. K. Thomas, *Trans. Faraday Soc.* **61**, 702 (1965).

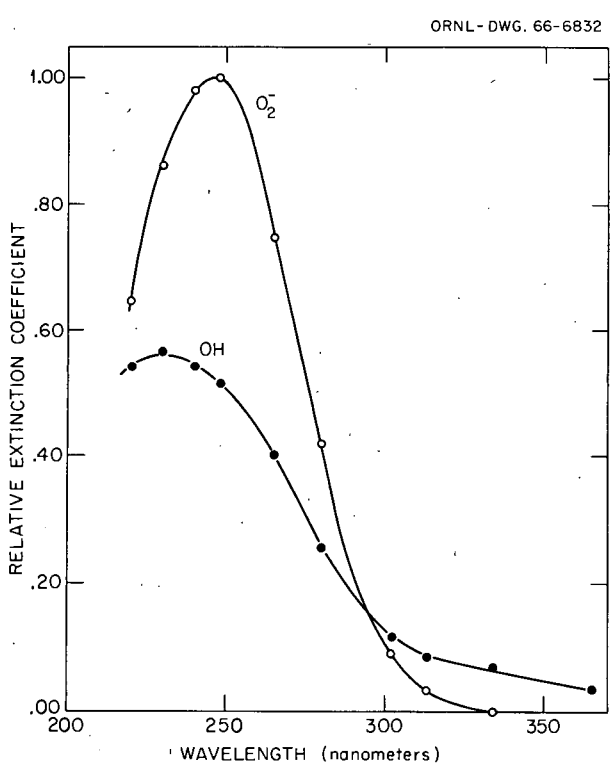

Fig. 3.2. Absorption Spectra of the OH Radical and the O_2^- Radical-Ion.

Preliminary studies were made of photoelectron transfer reactions in solutions of halides, nitrates, and sulfates. The NO_3 radical was observed in ceric nitrate solution as reported by Martin,[4] but it was not observed in HNO_3 or KNO_3 solution, even though the NO_3 radical would have been protected from back reaction by the fast reaction of e_{aq}^- with NO_3^-. This indicates that NO_3 is produced by electron transfer in the ionic complex, but not by charge transfer to solvent. In sulfate solutions, several absorption peaks were observed but not yet identified.

RADIOLYSIS OF NITROUS-OXIDE-SATURATED SOLUTIONS

H. A. Mahlman

The yield of molecular nitrogen produced during the ^{60}Co gamma radiolysis of N_2O-saturated solutions has been equated to the yield of hydrated electrons. However, H atoms have been shown to react with N_2O in aqueous solution and have also been considered as a possible contributor to the nitrogen yield. An evaluation and comparison of the nitrogen yields from N_2O-saturated aqueous solutions containing good H scavengers such as 2-propanol or formate ions with those from N_2O-saturated aqueous solutions containing a good electron scavenger such as nitrate ion will determine (1) if the H atom contributes to the nitrogen yield, (2) the G_H, and (3) the radical yield for which NO_3^- and N_2O compete.

2-Propanol and Sodium Formate Solutions

If H atoms react with N_2O, the N_2O and the organic solute will compete for the same intermediate in aqueous N_2O-saturated 2-propanol solutions. The competition established between N_2O and the organic solute would cause the nitrogen yields to decrease with a commensurate increase in the hydrogen yields as determined by the ratio of organic solute to nitrous oxide.

The nitrogen yield is unaffected by the addition of 2-propanol up to 5.9 *M*, and is in excellent agreement with that determined in N_2O-saturated water and in N_2O-saturated 10^{-3} *M* KBr solutions.

[4]T. W. Martin, R. E. Rummel, and R. C. Gross, *J. Am. Chem. Soc.* **86**, 2595 (1964).

Thus it is concluded that 2-propanol and N_2O are not competitive scavengers and that the $G(N_2)$ measured in N_2O-saturated water or aqueous solutions does not include the H atom yield.

The hydrogen yields, observed in aqueous N_2O-saturated 2-propanol solutions, are a linear function of the 2-propanol concentration, as shown in Fig. 3.3 by the least-squares line $G(H_2) = 0.95 + 0.54$ [2-propanol]. The $G(H_2)$ is considered to be the composite of three processes: (1) the G_{H_2} formed during the radiolysis of N_2O-saturated water and determined to be 0.34, (2) the G_H manifesting itself by hydrogen abstraction from the 2-propanol and evaluated to be 0.61, and (3) a "direct effect" directly proportional to the 2-propanol concentration and equal to 0.54 [2-propanol].

Also given in Fig. 3.3 are hydrogen yields observed in the radiolysis of aqueous N_2O-saturated sodium formate solutions. Interpreted similarly, the G_H is evaluated to be 0.57, while the "direct effect" has a concentration dependency of 0.16 [sodium formate]. If the hydrogen yields observed in the competitive study of O_2-saturated aqueous sodium formate solutions[5] are corrected for the "direct effect," the calculated G_H is lowered about 20% and is in excellent agreement with that determined in this work.

[5]G. Scholes and M. Simic, *Nature* **199**, 276 (1963).

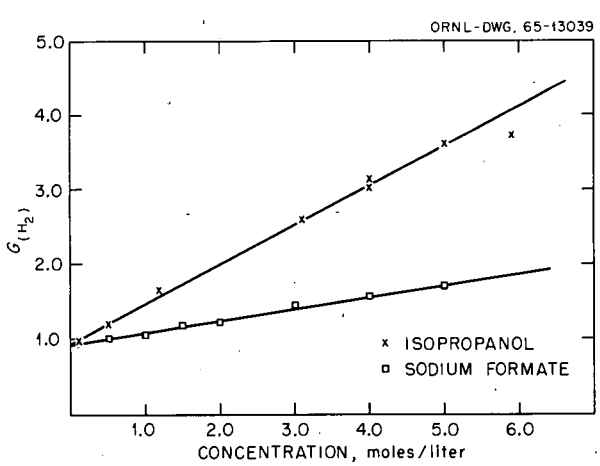

Fig. 3.3. Hydrogen Yields in N_2O-Saturated Solutions of 2-Propanol and Sodium Formate.

Sodium Nitrate Solutions

Competition between NO_3^- and N_2O in N_2O-saturated aqueous $NaNO_3$ solutions may be kinetically expressed by

$$\frac{1}{G(N_2)} = \frac{1}{G_{Red}}\left[1 + \frac{k_2(NO_3^-)}{k_1(N_2O)}\right]. \qquad (1)$$

The straight line drawn through the points in Fig. 3.4 represents the least-squares fit and has a calculated intercept of 0.313 and a slope of 0.451. Although these values are somewhat less than previously reported,[6] they are calculated from more precise data and are considered more accurate. The yield of reducing entities producing N_2 by reaction with N_2O is 3.19, and should not be construed to be the radical yield in the bulk of the solution. Supporting experiments have shown that the $G(H_2)$ is suppressed in an N_2O-saturated 10^{-3} *M* KBr solution by 0.12. With a 1:2 stoichiometry[7] the H_2 suppression would cause a commensurate increase in the $G(N_2)$ of 0.24. Thus the radicals which do not produce hydrogen and for which NO_3^- and N_2O compete have a yield of 2.95 in N_2O-saturated $NaNO_3$ solutions. This yield would include the reducing radicals in the

[6]A. M. Koulkes-Pujo and H. A. Mahlman, *Compt. Rend.* **259**, 788 (1964).

[7]J. T. Allan and C. M. Beck, *J. Am. Chem. Soc.* **86**, 1483 (1964).

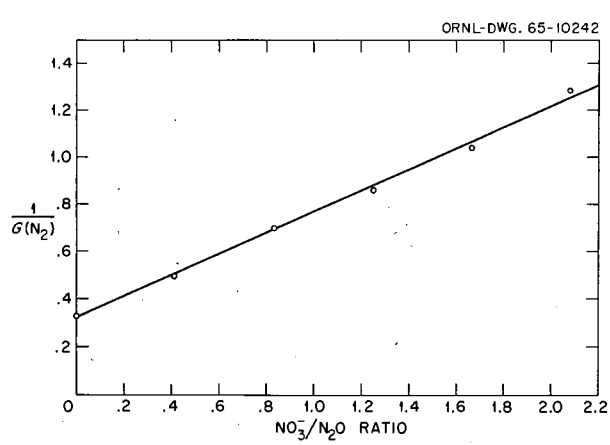

Fig. 3.4. $G(N_2)$ as a Function of the NO_3^-/N_2O Ratio in N_2O-Saturated Solutions.

bulk of the solution as well as those radicals that "normally" disappear by back reactions to form water, but now are reacting with the dissolved N_2O. The $G(N_2)$ calculated from the extrapolated intercept at zero NO_3^- concentration in the NO_3^--N_2O-H_2O system is the same (within experimental error) as that obtained in N_2O-saturated aqueous 2-propanol solutions, and indicates that the $G(N_2)$ does not include an H atom contribution.

The calculated rate constant ratio $k_2/k_1 = 1.44$ agrees very well with those calculated from pulsed radiolysis studies,[8,9] where hydrated electrons have been identified as the reducing radicals. In dilute solutions the reaction rate constants of reactions between hydrated electrons and reducible solutes have an ionic strength dependency[10] as given by

$$\log k/k_0 = 1.02 Z_a Z_b \frac{\mu^{1/2}}{1+\mu^{1/2}} . \qquad (2)$$

The "constant," 1.02, has been observed to decrease with increasing scavenging solute concentration at constant ionic strength,[11] and the absence of an ionic strength effect has been reported[12] at pH = 2. The variation of Eq. (2) was attributed to the reaction of the hydrated electron in a time shorter than that necessary to establish an ionic atmosphere. Thus the absence of an ionic strength effect observed in the radiolysis of N_2O-saturated 0.02 *M* $NaNO_3$ solutions containing 0.02 or 0.166 *M* Na_2SO_4 may be attributed to the fast reaction of the nitrate ions with the hydrated electrons. Consequently, agreement would be expected between the ratio k_2/k_1, determined in pulsed radiolysis studies at low ionic strengths, and that determined in this work at much greater ionic strength.

POSTIRRADIATION REDUCTION OF CERIUM(IV) IN THE ^{60}Co GAMMA RADIOLYSIS OF CONCENTRATED NITRATE SOLUTIONS. I. DEPENDENCE OF G_{HNO_2} ON SODIUM NITRATE CONCENTRATION

T. J. Sworski H. A. Mahlman

When concentrated sodium nitrate solutions in air-saturated 0.4 *M* sulfuric acid containing about 10^{-4} *M* cerium(IV) are irradiated in a kilocurie ^{60}Co source, postirradiation reduction of cerium(IV) is conveniently observable, as shown in Fig. 3.5. Changes in optical density of the solution with changes in cerium(IV) concentration were recorded as a function of time by a Cary recording spectrophotometer. Cylindrical Pyrocell spectrophotometer cells, with special silica windows which do not color under irradiation, were also used as irradiation cells. We reported previously[13] that this postirradiation reaction is due to slow reduction of cerium(IV) by nitrous acid.

The rate of reduction of cerium(IV) by nitrous acid conforms well to Eq. (1),

$$-d[Ce^{IV}]/dt = k[Ce^{IV}][HNO_2] . \qquad (1)$$

[8] S. Gorden *et al.*, *Discussions Faraday Soc.* **36**, 193 (1963).

[9] J. H. Baxendale *et al.*, *Nature* **201**, 468 (1964).

[10] G. Czapski and H. Schwarz, *J. Phys. Chem.* **66**, 471 (1962).

[11] E. Collinson *et al.*, *Proc. Chem. Soc.* **1962**, 40.

[12] P. J. Coyle, F. S. Dainton, and S. R. Logan, *Proc. Chem. Soc.* **1964**, 219.

[13] *Chem. Div. Ann. Progr. Rept. May 20, 1965*, ORNL-3832, p. 57.

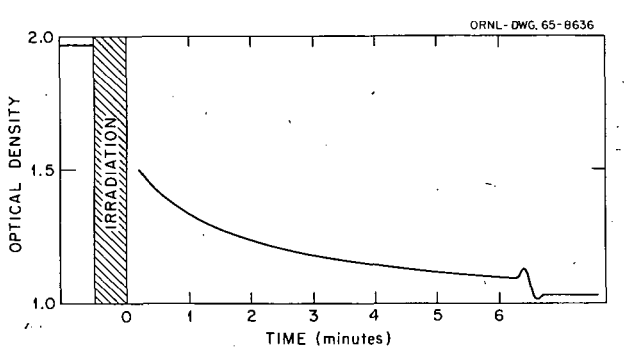

Fig. 3.5. Postirradiation Reduction of Cerium(IV) in the ^{60}Co Gamma Radiolysis of Air-Saturated 0.4 *M* Sulfuric Acid Containing 3.0 *M* Sodium Nitrate and 1.15×10^{-4} *M* Cerium(IV). Irradiation time was 30.2 sec. Optical densities at 340 mμ were 1.970 initially, 1.029 after postirradiation reaction was sensibly complete, and 0.855 due to absorption by 0.4 *M* sulfuric acid containing 3.0 *M* sodium nitrate in a 2-cm cell. All optical densities were measured relative to air.

Let $a = [Ce^{IV}]_{t=\infty}$, the concentration of cerium(IV) when reaction is sensibly complete, and let $a + x = [Ce^{IV}]_{t=t}$. Then $[HNO_2]_{t=t} = 0.5x$, and the rate of reduction of cerium(IV) is now given by Eq. (2).

$$-d[a + x]/dt = 0.5[a + x][x] \quad . \qquad (2)$$

Integration of Eq. (2) yields equation (3),

$$\ln\left[\frac{a+x}{x}\right]_{t=t} = 0.5akt + \ln\left[\frac{a+x}{x}\right]_{t=0} , \qquad (3)$$

in which $t = 0$ corresponds to the end of the irradiation time.

Figure 3.6 demonstrates the applicability of Eq. (3). The solid line in Fig. 3.6 corresponds to Eq. (3) with slope and intercept values obtained by the method of least squares. The least-squares analysis serves two purposes: k and $[HNO_2]_{t=0}$ are obtained from the slope and intercept respectively.

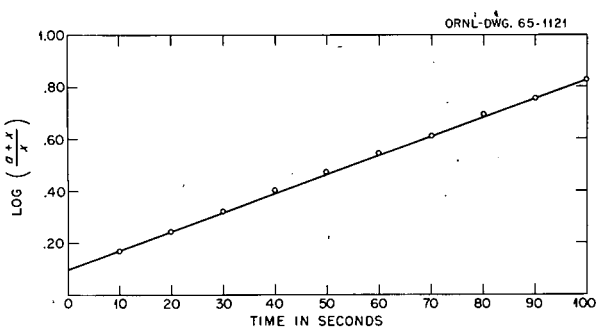

Fig. 3.6. Kinetic Evidence That the Reduction of Cerium(IV) by Nitrous Acid in Air-Saturated 0.4 *M* Sulfuric Acid is First Order in both Cerium(IV) and Nitrous Acid.

A significant amount of nitrous acid must disappear by reduction of cerium(IV) during irradiation. This is apparent from the rate for reduction of cerium(IV) at $t = 0$, which is indicated by Fig. 3.5. This must be quantitatively appraised in order to determine G_{HNO_2}.

We assume that reduction of cerium(IV) occurs by two processes: fast and slow processes with G values denoted by $G(Ce^{III})_{fast}$ and $G(Ce^{III})_{slow}$ and with $G(Ce^{III})_{slow} = 2G_{HNO_2}$. Therefore, $G(Ce^{III})$ is given by Eq. (4):

$$G(Ce^{III}) = G(Ce^{III})_{fast} + 2G_{HNO_2} \quad . \qquad (4)$$

The rates of change in concentration of cerium(IV) and nitrous acid during irradiation are then given by Eqs. (5) and (6):

$$d[Ce^{IV}]/dt = -0.01G(Ce^{III})_{fast}\, I/A - k[Ce^{IV}][HNO_2] \ , \qquad (5)$$

$$d[HNO_2]/dt = 0.01G_{HNO_2}\, I/A - 0.5k[Ce^{IV}][HNO_2] \ , \qquad (6)$$

in which I is the dose rate [ev l^{-1} sec^{-1}] and A is Avogadro's number. Equations (4), (5), and (6) contain five unknowns: $G(Ce^{III})_{fast}$, G_{HNO_2}, k, $[Ce^{IV}]$, and $[HNO_2]$.

By elimination of $G(Ce^{III})_{fast}$ and $[Ce^{IV}]$, Eqs. (4), (5), and (6) can be reduced to Eq. (7),

$$-d[HNO_2]/dt = b - c[HNO_2] - k[HNO_2]^2 + e[HNO_2]t \ , \qquad (7)$$

containing the following coefficients:

$$b = 0.01G_{HNO_2}\, I/A \ ,$$

$$c = 0.5k[Ce^{IV}]_{initial} \ ,$$

$$e = 0.005kG(Ce^{III})\, I/A \ .$$

Equation (7) contains three unknowns: k, $[HNO_2]$, and G_{HNO_2}. Since k and $[HNO_2]_{t=0}$ for each experiment are obtained by use of Eq. (3), G_{HNO_2} can be determined by use of Eq. (7). This was accomplished by an iterative process in which that value for G_{HNO_2} was found which yields $[HNO_2]_{t=0}$ by numerical integration of Eq. (7) by the Runge-Kutta method. A program SLOPULSE was written for ORNL's CDC 1604-A computer to determine k, $[HNO_2]_{t=0}$, and G_{HNO_2} from post-

irradiation data such as is shown in Fig. 3.5 by use of Eqs. (3) and (7).

The dependence of $G(Ce^{III})$ and G_{HNO_2} on sodium nitrate concentration is shown in Fig. 3.7. The results are very striking: an increase in $G(Ce^{III})$ with increase in sodium nitrate concentration is accompanied by an equal increase in $2G_{HNO_2}$. This confirms the original proposal[14] that the increase in $G(Ce^{III})$ with increase in sodium nitrate concentration is due to formation of nitrous acid and not due to reactions of OH radical with nitrate ion as previously proposed.[15] The lines in Fig. 3.7 are empirical: one is drawn to best represent the dependence of $G(Ce^{III})$ on sodium nitrate concentration, while the other is drawn to show that $G(Ce^{III}) - 2G_{HNO_2} = 1.77 \pm 0.25$ with an average deviation based on 24 experiments.

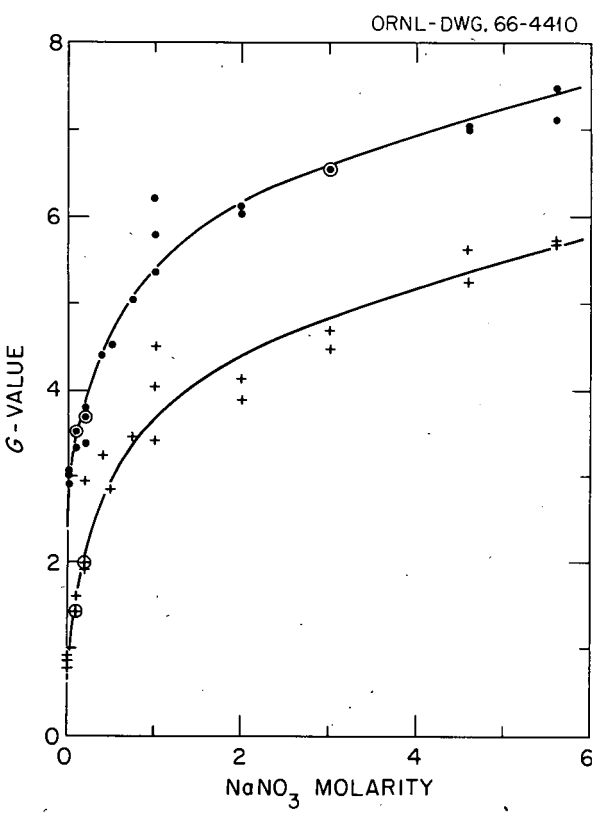

Fig. 3.7. Dependence of $G(Ce^{III})$ and G_{HNO_2} on Nitrate Concentration in Air-Saturated 0.4 *M* Sulfuric Acid: ● $G(Ce^{III})$; + $2G_{HNO_2}$. Two values which are so close to each other that they could not be differentiated by ● or + are denoted by ⊙ or ⊕ respectively.

We conclude that two overall processes must be used to denote formation of the earliest detectable intermediates in the radiolysis of concentrated sodium nitrate solutions in 0.4 *M* sulfuric acid:

$$H_2O \rightsquigarrow H_2, H_2O_2, H, OH \ ,$$

$$NO_3^- \rightsquigarrow NO_2^-, O_2 \ .$$

These are nonindependent processes, since G_{H_2} decreases[16,17] while G_{HNO_2} increases with increase in sodium nitrate concentration.

POSTIRRADIATION REDUCTION OF CERIUM(IV) IN THE ^{60}Co GAMMA RADIOLYSIS OF CONCENTRATED NITRATE SOLUTIONS. II. EFFECT OF 2-PROPANOL ON $G(Ce^{III})$ AND G_{HNO_2}

T. J. Sworski

A problem of both theoretical and experimental importance in the radiolysis of water is the dependence of G values for earliest detectable intermediates, on solute concentration. Since concentrated nitrate solutions have probably received more attention than any other concentrated solution, and in view of the conflicting reaction mechanisms proposed for nitrous acid formation, investigation of the postirradiation of cerium(IV) in the ^{60}Co gamma radiolysis of concentrated nitrate solutions is being extended to include the effects of those solutes which will be helpful in establishing the mechanism for nitrous acid formation.

Addition of 2-propanol to cerium(IV) solutions in air-saturated 0.4 *M* sulfuric acid increases $G(Ce^{III})$ from $2G_{H_2O_2} + G_H - G_{OH}$ to $2G_{H_2O_2} + G_H + G_{OH}$ just as previously reported for additions of thallium(I)[18] and formic acid.[19] This is consistent with a reaction mechanism in which reactions (1) and (2),

[14] T. J. Sworski, *J. Am. Chem. Soc.* **77**, 4689 (1955).

[15] G. E. Challenger and B. J. Masters, *J. Am. Chem. Soc.* **77**, 1063 (1955).

[16] R. G. Sowden, *J. Am. Chem. Soc.* **77**, 1263 (1957).

[17] H. A. Mahlman and J. W. Boyle, *J. Chem. Phys.* **27**, 1434 (1957).

[18] T. J. Sworski, *Radiation Res.* **4**, 483 (1956).

[19] T. J. Sworski, *Radiation Res.* **6**, 645 (1957).

$$OH + CH_3CHOHCH_3 \longrightarrow H_2O + CH_3\dot{C}OHCH_3 \ , \quad (1)$$

$$Ce^{IV} + CH_3\dot{C}OHCH_3 \longrightarrow Ce^{III} + CH_3COCH_3 \ , \quad (2)$$

inhibit oxidation of cerium(III) by OH radical through intermediate formation of HSO_4:[20]

$$OH + H_2SO_4 \longrightarrow H_2O + HSO_4 \ , \quad (3)$$

$$Ce^{III} + HSO_4 \longrightarrow Ce^{IV} + HSO_4^- \ . \quad (4)$$

Initial $G(Ce^{III})$ is independent of 2-propanol concentration in the range from 10^{-4} to 10^{-1} *M* as shown in Fig. 3.8. Comparison of these results with those published previously for thallium(I) and formic acid leads to the conclusion that HSO_4 can oxidize 2-propanol:

$$HSO_4 + CH_3CHOH \longrightarrow HSO_4^- + H^+ + CH_3\dot{C}OHCH_3 \ . \quad (5)$$

Since HSO_4 is a stronger oxidizing agent than cerium(IV), as evidenced by reaction (4), postulation of reaction (5) is consistent with the observation that cerium(IV) slowly oxidizes 2-propanol.

The effect of 2-propanol on $G(Ce^{III})$ and G_{HNO_2} in the radiolysis of concentrated sodium nitrate solutions is shown in Fig. 3.9. The 2-propanol does not alter the striking dependence of $G(Ce^{III})$ and G_{HNO_2} on sodium nitrate concentration; an increase in $G(Ce^{III})$ with increase in sodium nitrate concentration is accompanied by an equal increase in $2G_{HNO_2}$. The two curves in Fig. 3.9

[20] T. J. Sworski, *J. Am. Chem. Soc.* **78**, 1768 (1956).

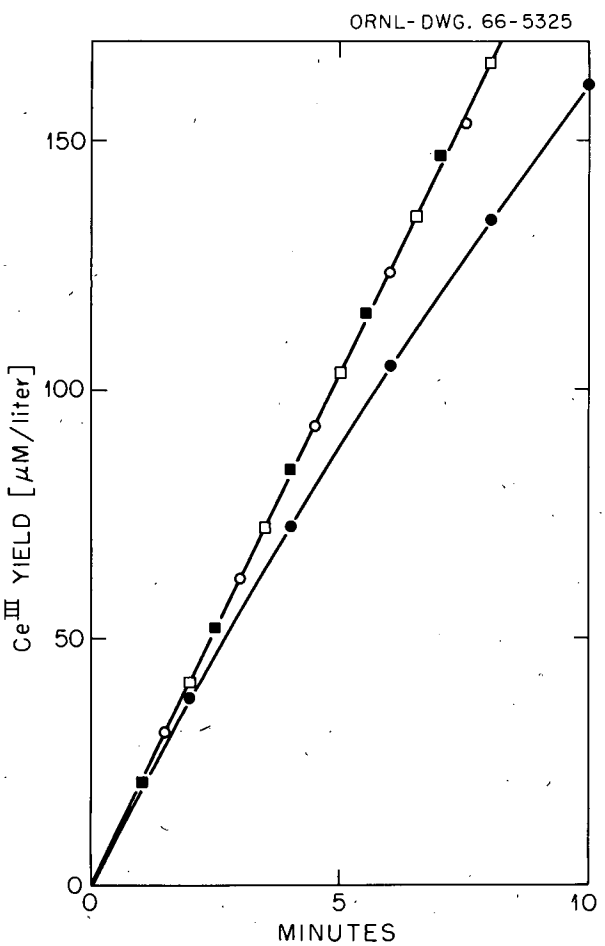

Fig. 3.8. Effect of 2-Propanol Concentration on Cerium(IV) Reduction in Air-Saturated 0.4 *M* Sulfuric Acid by ^{60}Co Gamma Radiation: 2-Propanol Concentrations: ● 9.85×10^{-5} *M*; ○ 9.85×10^{-4} *M*; □ 9.85×10^{-3} *M*; ■ 9.85×10^{-2} *M*. Dose rate in ferrous sulfate dosimeter: 1.54×10^{20} ev liter^{-1} min^{-1}.

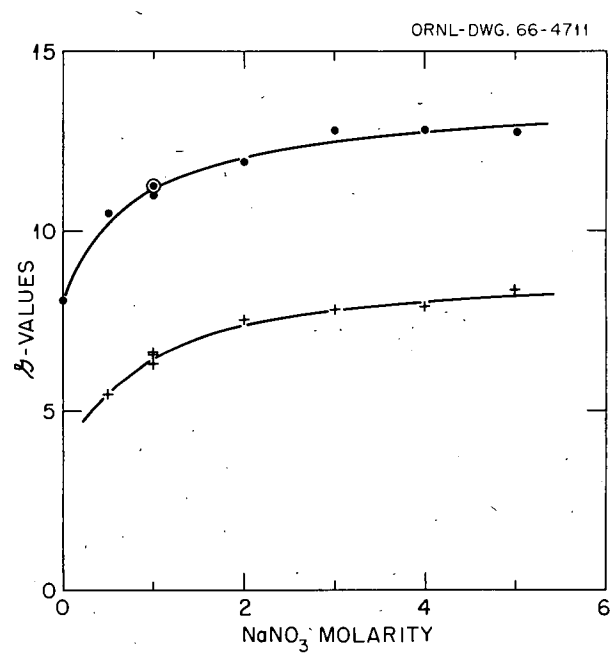

Fig. 3.9. Dependence of $G(Ce^{III})$ and G_{HNO_2} on Sodium Nitrate Concentration in Air-Saturated 0.4 *M* Sulfuric Acid Containing 2-Propanol: ● $G(Ce^{III})$; ○ Duplicate $G(Ce^{III})$ Values; + $2G_{HNO_2}$.

are empirical: one is drawn to best represent the dependence of $G(Ce^{III})$ on sodium nitrate concentration, and the other is drawn to show that $G(Ce^{III}) - 2G_{HNO_2} = G(Ce^{III})_{fast} = 4.67 \pm 0.21$.

The effect of 2-propanol is twofold: to increase $G(Ce^{III})$ by $2G_{OH}$ and to increase G_{HNO_2} by $0.5G_{OH}$, resulting in an increase in $G(Ce^{III})_{fast}$ of $G_{OH} = 2.90$. These effects reveal the nature of the free-radical processes in the absence of 2-propanol, and are consistent with reactions (1) and (2) inhibiting the oxidation of nitrous acid by HSO_4:

$$H + NO_3^- \longrightarrow OH^- + NO_2 \ , \qquad (6)$$

$$H_2O + 2NO_2 \longrightarrow HNO_2 + NO_3^- + H^+ \ , \qquad (7)$$

$$HSO_4 + HNO_2 \longrightarrow HSO_4^- + H^+ + NO_2 \ . \qquad (8)$$

This reaction mechanism indicates that NO_2 is inert toward the cerium(IV)-cerium(III) mixture in solutions and, therefore, that k for the reaction of cerium(IV) with nitrous acid is really the bimolecular rate constant k_{Ce^{IV},HNO_2}.

Since the effect of 2-propanol was investigated in air-saturated solutions, there is no evidence for reaction of NO_2 with O_2 as previously postulated[21,22] for neutral and alkaline solutions. This may not be conflicting since the e_{aq}^- is the principal reducing agent in neutral and alkaline solutions, and NO_3^{2-} may be capable of reducing O_2:

$$e_{aq}^- + NO_3^- \longrightarrow NO_3^{2-} \ ,$$

$$NO_3^{2-} + O_2 \longrightarrow NO_3^- + O_2^- \ .$$

RADIOLYSIS OF CARBON DIOXIDE

H. H. Carmichael[23] J. F. Riley

Although the radiation chemistry of carbon dioxide and its mixtures with other gases has been the subject of many studies, the mechanism of the radiolysis of carbon dioxide is not yet fully understood. Gaseous carbon dioxide shows a high radiation stability because of an efficient back-reaction of products. By irradiating carbon dioxide containing small amounts of other gases, we are able to intercept the species responsible for back-reaction and thereby permit a net production of carbon monoxide.

Our approach has been to examine the relative effectiveness of several added gases on the radiolysis of carbon dioxide. By looking at the radiolysis products from both carbon dioxide and the added gas, we seek to identify the intermediates involved.

Judging from the carbon monoxide yield in the radiolysis of carbon dioxide, hydrogen, methane, and ethylene show increasing efficiency of interception. The added methane, ethylene, and possibly hydrogen are consumed in interception, but at a lower rate than carbon monoxide is produced.

From the irradiation of pure carbon dioxide, $G(CO)$ was found to be ≤ 0.0016 molecule/100 ev. For carbon dioxide containing 10^3 to 26×10^3 ppm of hydrogen, $G(CO) = 4$ molecules/100 ev, but decreased for doses greater than 2×10^{19} ev g^{-1}. No dose rate dependence of $G(CO)$ was observed in a sixtyfold variation of the dose rate, the highest rate being 12×10^{17} ev g^{-1} min^{-1}.

For carbon dioxide containing 0.026 to 2.6% methane, $G(CO) = 5.1$ to 6.6 molecules/100 ev. The carbon monoxide yield decreased for doses greater than 2×10^{20} ev g^{-1}. For carbon dioxide containing 0.02 to 10% ethylene, $G(CO) = 6.6$ to 7.6 molecules/100 ev, with maximum yield observed at about 10^3 ppm of ethylene.

An oxygen material balance was not attained in these irradiations, and a determined search was made for other oxygen-containing products. The oxygen imbalance was not resolved, but methanol and formaldehyde do not appear to be important products.

Considerable energy transfer occurs in the radiolysis of methane–carbon dioxide mixtures. An ethane yield, $G(C_2H_6)$, of 1.5 molecules/100 ev was measured for a 2.6% CH_4 mixture. For comparison, for pure methane, $G(C_2H_6) = 2.1$ molecules/100 ev. The radiolysis of ethylene–carbon dioxide mixtures produced roughly equal quantities of CH_4, C_2H_6, and C_2H_2. The system

[21] V. A. Sharpatyi, V. D. Orekhov, and M. A. Proskurnin, *Dokl. Akad. Nauk SSSR* **122**, 122 (1958).

[22] M. L. Hyder, *J. Phys. Chem.* **69**, 1858 (1963).

[23] ORINS Summer Research Participant, North Carolina State University, Raleigh, N.C.

is complex, and both C_2H_6 and C_2H_2 yields passed through maximums as the dose was increased.

RADIATION-INDUCED SURFACE REACTIONS

H. W. Kohn

Hydrogen Atoms

Relative yields of hydrogen atoms formed by irradiating several adsorbents (silica gel, silica alumina, alumina, 0.05% platinized alumina, and several molecular sieves[24] with gamma rays at 77°K have been measured using the ESR technique.[25] If we assign a value of 1 to the lowest yields, those from the sodium sieves and from silica gel, the relative values for the other materials are as follows: Linde NH_4 sieve = 3, alumina = 5, silica alumina = 10, Linde H sieve = 40, Zeolon H sieve = 110. The yields are linear with dose out to 12 megarads, the highest dose used. The adsorbents except for the hydrogen sieves were degassed overnight at 250°C before irradiating. A range of degassing temperatures was used for these sieves which showed that maximum yields were obtained for Linde H if it was degassed at 100°C. For Zeolon H the best degassing temperature was 450°C.

If we accept a G value of ~0.06 for the hydrogen atom yield in silica gel,[26] this would make the yield for hydrogen atoms in the hydrogen sieves even greater than that previously observed in frozen acids.[27] So far our attempts to obtain absolute values for hydrogen atom yields have indicated that the estimates based on a value of 0.06 for silica gel for the yields in these adsorbents may be high by as much as a factor of 10.

The hydrogen atom signal disappears from all these adsorbents (except alumina) so quickly at 145°K that rates could not be measured. At 131°K the order of the initial rate of disappearance measured by pulse-annealing the samples in methylcyclopentane slush is hydrogen sieves > platinized alumina ≅ silica alumina > silica > alumina (see Fig. 3.10). This decay seems to take place in two steps, a very rapid loss of some (~20% for alumina, ~80 to 90% for the hydrogen sieves) hydrogen atoms followed by a slower disappearance of the residual atoms.

These adsorbents can be looked upon as acids. Since the strongest acids apparently give the biggest yields, the most eligible reaction for hydrogen atom formation is

$$H^+ + e \rightarrow H^* .$$

The observed H atom signal, however, is a function not only of the number of the hydrogen ions and

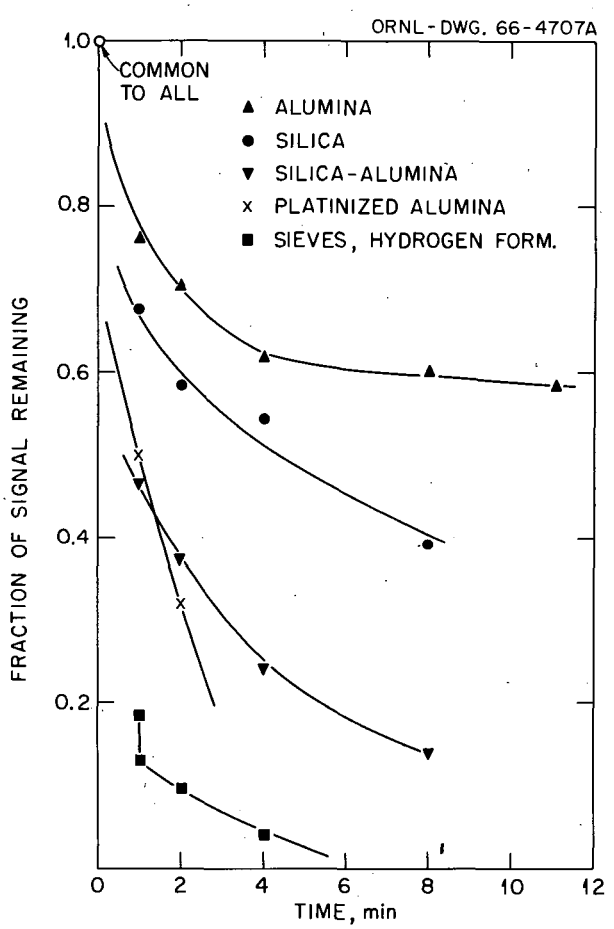

Fig. 3.10. Rate of Hydrogen Atom Disappearance from Several Irradiated Adsorbents at 131°K.

[24]Specifically Zeolon H and Zeolon Na, a hydrogen and sodium form of a mordenite sieve, and Linde Y, a faujasite sieve in sodium, hydrogen, and ammonium form.

[25]The electron spin resonance measurements were made at the Biology Division with the cooperation of M. L. Randolph and J. L. Hosszu.

[26]P. H. Emmett *et al.*, *J. Phys. Chem.* **66**, 921 (1962).

[27]R. Livingston and A. J. Weinberger, *J. Chem. Phys.* 33, 499 (1960).

their acid strengths but also of the number and depth of the available trapping sites. Hence these yields cannot be used directly as a measure of acid strength.

The trapped hydrogen atoms failed to react with molecular deuterium in the 77 to 145°K range to give a deuterium atom signal even though the atoms themselves were sufficiently mobile to disappear, presumably by recombination. Thus we might conclude that the low-temperature catalytic hydrogen-deuterium exchange does not take place on these irradiated materials by a free-atom mechanism. An alternative explanation[28] is that the atoms once rendered mobile enough to react will also disappear, presumably by recombination. Hence the D atoms resulting from the reaction

$$H^{\cdot} + D_2 \longrightarrow HD + D^{\cdot}$$

would also disappear and not be observable by ESR.

It was hoped that the yields from the following reactions, all of which showed energy transfer effect, could be related to the hydrogen atom yield:

$$N_2O \xrightarrow{\text{adsorbent}} N_2 + O_{(ads)} ,$$

$$HCOOH \longrightarrow CO_2 + H_2 ,$$

$$HCOOH \xrightarrow{\text{adsorbent}} CO + H_2O_{(ads)} ,$$

$$CH_3CHOHCH_3 \xrightarrow{\text{adsorbent}} H_2 + CH_4 + \text{others} .$$

Preliminary experiments, however, indicated no such relationship.

Nitrous Oxide Decomposition

Nitrous oxide is decomposed in the presence of silica gel to give principally nitrogen; most of the oxygen apparently remains adsorbed. If the same solid sample is reloaded with N_2O and reirradiated, a gradual buildup of oxygen yield through successive irradiations is noted, although in our experiments even after extensive ($\sim 10^{21}$ ev/g) irradiation, stoichiometry was never achieved. The samples which were degassed at high (above 325°C) temperature were purple after irradiation, showing that reaction with color centers or color center-like entities was not involved. Yield measurements at 195 and 77°K showed that the radiation reaction has a very low apparent activation energy.

If the silica gel sample is irradiated in vacuo at ambient ($\sim$35°C) temperature and nitrous oxide is then added, the color centers are, of course, not bleached, but the nitrous oxide reacts with some other trapped entity to give nitrogen in a very low yield ($G = \sim 0.05$ molecule/100 ev absorbed by the silica gel). Varying the time interval between radiation and analysis for both preirradiated silica gels and for gels irradiated in the presence of nitrous oxide indicated that no catalytic reaction and no other postirradiation effects, catalytic or otherwise, lead to measurable nitrogen formation. The reaction is insensitive to the pressure between 12 and 350 mm. Below 12 mm pressure the irradiation times become too short (and here they must be kept short to avoid appreciable depletion of the nitrous oxide) to give enough product for confident analysis. A small increase in yield appears as the pressure of nitrous oxide increases, however. This is due to direct gas phase radiolysis of the nitrous oxide.

Yields for nitrogen from nitrous oxide decomposition are plotted in Fig. 3.11. All yields

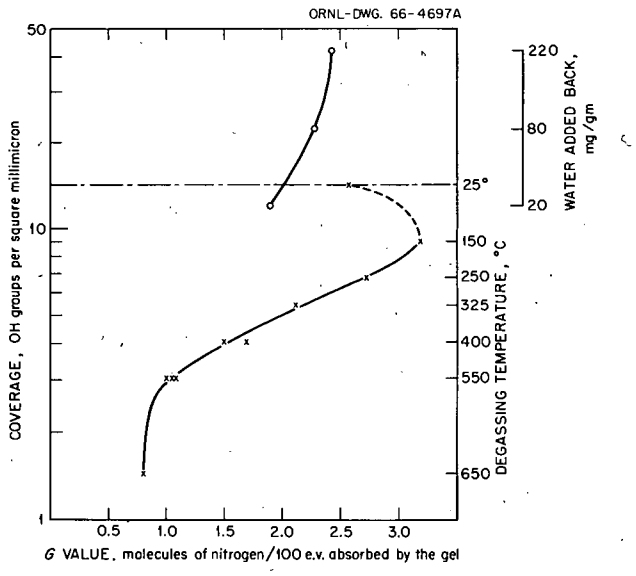

Fig. 3.11. Nitrogen Yields from Gamma Radiolysis of Nitrous Oxide in the Presence of Silica Gel (Effect of Water).

[28] I am indebted to J. A. Ghormley for suggesting this alternative.

are calculated on the basis of energy absorbed by the gel alone. They are obviously sensitive to hydroxyl content of the gel.[29] The crosses refer to degassed gels, the circles to gels to which water has been added back after degassing at 150°C (it is assumed that each water molecule gives two hydroxyl groups). The maximum near the eight to nine hydroxyl groups per square millimicron coverage is probably real, since this concentration corresponds to a fully silanol-covered surface. The reason for marked differences in value between the ~15 hydroxyls per square millimicron coverage obtained in two different ways is not yet clear. It is unfortunate that this portion of the curve which is most interesting is also the part for which it is most difficult to obtain reliable data.

Silica gel surfaces on which one to five monolayers of water have been adsorbed normally give big yields of hydrogen,[30] but they do not do so in the presence of nitrous oxide. The maximum yield of hydrogen obtained in this work in the presence of nitrous oxide was 0.3. Ordinarily one might expect hydrogen yields of 1.0 to 2.0. Thus the yields from reactions

$$H_2O_{(ads)} \rightsquigarrow H_2 ,$$

$$N_2O_{(ads)} \rightsquigarrow N_2$$

show that water and nitrous oxide apparently compete with each other for the same active intermediate.

We have also determined the yield of nitrogen from nitrous oxide in the presence of other adsorbents. These adsorbents were degassed at only a single temperature, 250°C. The values obtained were for alumina, $G_{N_2} = 2.6$; for Zeolon H, $G_{N_2} = 1.65$; for silica alumina, $G_{N_2} = 0.78$. Again only traces of oxygen were produced. Since wide variation in adsorbent properties, especially in the ability to produce hydrogen atoms, gave such little change, this was not pursued extensively.

Decomposition of Formic Acid

When formic acid adsorbed on silica gel at about 20% surface coverage is irradiated, H_2, CO, and CO_2 are formed. The G values (molecules/100 ev absorbed by the silica gel) for samples degassed in the 450 to 650°C range are, respectively, $G_{H_2} = 1.35 \pm 0.15$, $G_{CO} = 0.95 \pm 0.1$, $G_{CO_2} = 3.45 \pm 0.15$. Degassing at a lower (25 to 250°C) temperature gives a somewhat erratic performance; the hydrogen yields are virtually unchanged; the yields of carbon monoxide are definitely lowered to a value of 0.55 ± 0.1; and though we are not yet confident enough of the carbon dioxide yield to quote a number, the yield shows some sign of decreasing. If the radiation reaction is executed at 77°K, the formation of carbon monoxide is almost completely suppressed, whereas the carbon dioxide yield is cut in half. In all cases no color centers were visible after radiation. An important conclusion from this work is that the radiation does not operate simply by supplying energy for the thermally favored catalytic reaction, since, on silica gel, this would give predominantly carbon monoxide.

Decomposition of Isopropanol

Radiolysis of adsorbed isopropanol on silica gel at about 10% surface coverage gives $G_{CH_4} = 0.50 \pm 0.10$ and $G_{H_2} = 0.50 \pm 0.10$. We have not yet examined the effect of changing coverage or degassing temperature (these samples were degassed at 550 and 650°C). Traces of ethane and of acetaldehyde could also be detected in the chromatographs. Preliminary experiments on the simultaneous radiolysis of isopropanol and nitrous oxide over silica gel gave the yields of N_2, H_2, and CO expected from the previous individual radiolysis experiments. Hence isopropanol and N_2O apparently do not compete for the same reactive intermediate.

---

[29] Hydroxyl content has been calculated from the formula of W. K. Lowen and E. C. Broge, *J. Phys. Chem.* **65**, 16 (1961).

[30] N. A. Krohn, *Chem. Technol. Div. Ann. Progr. Rept. May 31, 1965*, ORNL-3830; *Chem. Technol. Div. Ann. Progr. Rept. May 31, 1966*, ORNL-3945, to be issued.

RADIATION AND HOT-ATOM CHEMISTRY OF INORGANIC CRYSTALLINE SOLIDS

Radiolysis of $LiNO_3$: Dose Rate Effects in the Molten State[31]

T. G. Ward, Jr.[32] G. E. Boyd
R. C. Axtmann[33]

The radiolysis of molten $LiNO_3$ by ^{60}Co gamma rays at temperatures slightly above its melting point of 254° was determined as a function of absorbed dose and dose rate. Steady-state concentrations of nitrite ion were approached at large doses, and, unexpectedly, these concentrations were found to pass through a maximum with increasing dose rate. The only additional radiolytic product formed in significant amounts was oxygen gas which was evolved in a 1:2 ratio with nitrite. A kinetic mechanism capable of yielding a quantitative description of the experimental results was developed. The dose rate dependence was described in terms of a rapid, monotonic increase in the concentrations of atomic and molecular oxygen which accelerated the reoxidation of nitrite ion.

[31] Submitted to *Journal of Physical Chemistry*.

[32] Oak Ridge Associated Universities Pre-doctoral Fellow.

Radiolysis of $LiNO_3$: LET and the Effect of the Solid-Liquid Phase Change

T. G. Ward, Jr.[32] R. C. Axtmann[33]
G. E. Boyd

Lithium nitrate containing added ^6Li was irradiated in the crystalline and in the molten state with nuclear reactor radiations to produce high LET tritons and alpha particles by ^6Li fission. The yield of nitrite ion in the crystal was linear with dose, and there was no dependence on dose rate over a threefold increase in this variable. The initial 100-ev yield for the solid was $G_0(NO_2^-) = 0.22 \pm 0.01$, which value is approximately an order of magnitude larger than for radiolysis by ^{60}Co gamma rays. The yield of NO_2^- in the radiolysis of molten $LiNO_3$ by ^6Li fission recoils was nonlinear with dose, and a "steady-state" concentration of about 3.1 mole % nitrite was approached when the dose rate was 5.2×10^{21} ev mole^{-1} min^{-1}. The initial yield was $G_0(NO_2^-) = 5.5 \pm 0.5$, and nitrite ion itself was not radiolyzed appreciably. The primary effect of melting crystalline $LiNO_3$ was to increase $G_0(NO_2^-)$ by a factor of 25 for radiolysis by ^6Li fission recoils, and by a factor of nearly 200 for ^{60}Co gamma radiolysis.

[33] Princeton University, Princeton, N.J.

4. Organic Chemistry

A METHOD FOR RELATING RATES OF INTERCONVERSION AND DESTRUCTION OF CLASSICAL CARBONIUM IONS

Vernon F. Raaen M. H. Lietzke
Clair J. Collins

How fast do equilibrating, classical ions interconvert with respect to the rates with which they react with entering groups or eject protons? This question goes to the heart of the debate[1–4] over nonclassical ions. Cram[2] implies, without saying why, that a factor of 100 in favor of phenyl migration would be too great for acetolysis, through classical ions, of *threo*-3-phenyl-2-butyl tosylate. Winstein[1] argues that a factor of 2000 in favor of interconversion of classical norbornyl ions would cause the rate of interconversion to exceed kT/h in the absolute rate equation.

The question is not easily answered, for we seek a ratio of two rates, the absolute values of which are unknown, and which can, conceivably, fluctuate over wide ranges. In addition, a determination of this ratio by ordinary[5] means strains the limits of experimental error for normal polarimetric, stoichiometric, or isotopic tracer techniques.

We attacked the problem first by studying reactions which are known[6] to proceed through equilibrating, classical ions, and outline here an approach which circumvents the need for extraordinary experimental precision.

Dehydration of either 1-*p*-tolyl-2,2-diphenylethanol (**1**) or 1,2-diphenyl-2-*p*-tolylethanol (**2**, *erythro* or *threo* forms) in boiling formic acid (containing a trace of *p*-toluenesulfonic acid) produces the olefins **3** and **4** (two geometrical isomers obtained in equal amounts) in yields of 76.0 and 24.0% respectively. By the use of a ^{14}C label, the four ions *a–d* (Chart I) can be recognized,

ORNL-DWG. 65-10245A

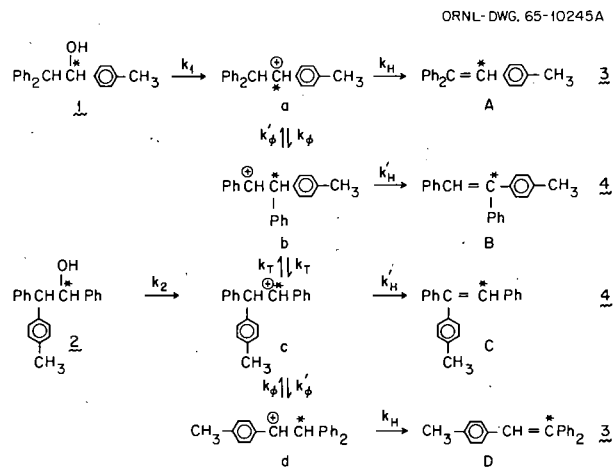

CHART I

and these go irreversibly to olefins **3** and **4** through paths *A–D*.[7] By a method previously reported,[3] Eqs. (1–4) were derived:

$$\frac{k_\phi}{k_H} m_a + \frac{k_T}{k'_H} m_c = m_b \left[\frac{k'_\phi}{k'_H} + \frac{k_T}{k'_H} + 1 \right], \qquad (1)$$

[1]S. Winstein, *J. Am. Chem. Soc.* **87**, 381 (1965).

[2]D. J. Cram, *J. Am. Chem. Soc.* **86**, 3767 (1964).

[3]C. J. Collins, B. M. Benjamin, and M. H. Lietzke, *Ann. Chem.* **687**, 150 (1965).

[4]H. C. Brown, K. J. Morgan, and F. J. Chloupek, *J. Am. Chem. Soc.* **87**, 2137 (1965).

[5]S. Winstein, E. Clippinger, R. Howe, and E. Vogelfanger, *J. Am. Chem. Soc.* **87**, 376 (1965), for example, measured the racemization of *exo*-norbornyl acetate with a precision they state to be within ±0.05%.

[6]C. J. Collins and W. A. Bonner, *J. Am. Chem. Soc.* **77**, 92, 6725 (1955).

[7]Although the ions *a–d* yield formate esters reversibly, all functions describing these processes cancel in the derivation of Eqs. (1–4).

$$\frac{k_T}{k'_H} m_b + \frac{k_\phi}{k_H} m_d = m_c \left[\frac{k_T}{k'_H} + \frac{k'_\phi}{k'_H} + 1 \right], \quad (2)$$

$$\frac{k'_\phi}{k'_H} m_c = m_d \left[\frac{k_\phi}{k_H} + 1 \right], \quad (3)$$

$$\frac{k_\phi}{k_H} (m_a + m_d) = (m_b + m_c) \left[\frac{k'_\phi}{k'_H} + 1 \right]. \quad (4)$$

These equations exactly describe the mechanism given in Chart I for the dehydration of **1**. Equation (4) relates the ratio $k'_\phi/k'_H : k_\phi/k_H$ to the yields of the two olefins, and the extent of ^{14}C rearrangement in **3** and **4** determines the mole fractions m_a, m_b, m_c, m_d (formed through paths *A*, *B*, *C*, and *D*), as well as the lower limits for k'_ϕ/k'_H and k_ϕ/k_H.

Given in Fig. 4.1 is a plot (obtained by use of a computer program for the IBM 7090) of k_T/k'_H vs $m_a/(m_a + m_d)$ for various values of k'_ϕ/k'_H for olefin yields of 76.0% (**3**) and 24.0% (**4**). Three separate determinations of $m_a/(m_a + m_d)$ (using both C-1 and C-2 labeled **1**) gave values of 0.5080, 0.5074, and 0.5060. Under identical conditions, $m_a/(m_a + m_d)$ after dehydration of **2** was 0.497 (slightly less than 0.500, a finding consistent with the mechanism).[8] The ratio k_T/k'_ϕ can be estimated from several different experiments[9] as 6 or greater. The total error in determining the ^{14}C distribution in **3** is certainly less than ±0.8%,

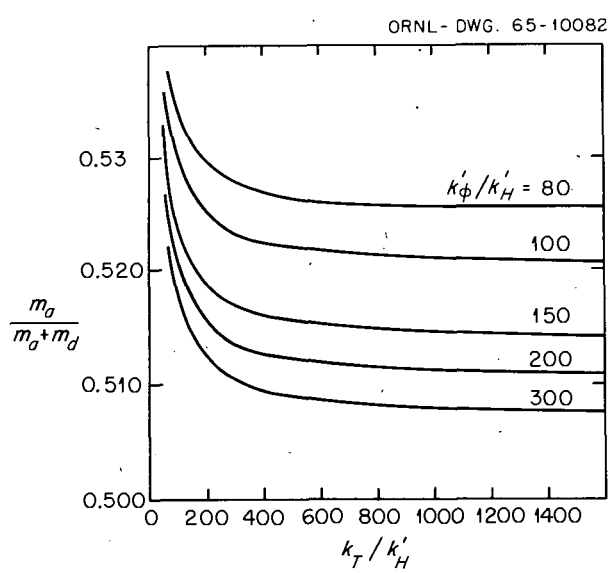

Fig. 4.1. Plot of ^{14}C Distribution in 3 vs k_T/k'_H (Chart 1) in the Reaction 1 → 3 (76.0%) and 4 (24.0%).

which means that $m_a/(m_a + m_d)$ can be no greater than 0.511. We can thus set the following minimum values for our three ratios: $k_\phi/k_H \geqq 63.5$, $k'_\phi/k'_H \geqq 200$, and $k_T/k'_H \geqq 1200$ (Fig. 4.1).[10]

We are unable at present to relate the rates of proton ejection (k_H and k'_H) to the rates of cation-anion collapse (to yield the formates of **1** and **2**). Since both the olefins and the formates can be isolated from reaction mixtures at lower temperatures, however, we presume that the differences in these rates are not great.

CONCERNING THE EFFECT OF A COMPETING EQUILIBRIUM ON A KINETICALLY CONTROLLED PROCESS

Clair J. Collins R. W. Stoughton
Ben M. Benjamin

It is a popular misconception[11–13] – until recently shared as well by us – that, in the absence

---

[8]Oxidation of **3** with chromic acid yielded benzophenone and *p*-toluic acid. Olefin **4** upon similar treatment yielded benzoic and *p*-benzoylbenzoic acids. The extent of ^{14}C rearrangements was determined by assay of these degradation fragments. The use of two different labels plus high radiochemical yield reduced error from isotope effects. Yields of the olefins **3** and **4** were determined by integration of the NMR plots to a precision of better than ±1%. The equilibration of label in **4** (from either **1** or **2**) was, within experimental error, complete. Authentic samples of **3** and **4** were stable under the reaction conditions.

[9]We have shown [C. J. Collins, W. T. Rainey, W. B. Smith and I. A. Kaye, *J. Am. Chem. Soc.* **81**, 460 (1959), Table 2; B. M. Benjamin and C. J. Collins, *J. Am. Chem. Soc.* **78**, 4332 (1956), Table IV] that the *p*-tolyl/phenyl ratio in compounds similar to **1** and **2** is 6 to 8 both in cold sulfuric and in formic acids. L. W. Kendrick, Jr., B. M. Benjamin, and C. J. Collins, *J. Am. Chem. Soc.* **80**, 4057 (1958), Table III, show that the ratio of secondary hydroxyl removal for erythro:threo-1,2-di-*p*-tolyl-1-phenylethylene-2-^{14}C glycol is 7:1 (sulfuric acid). In formic acid, $k_{tol}/k'_H : k_\phi/k'_H$ for rearrangement of VII and VIII (above reference) is 7.7:1. In the rearrangement in acetic-perchloric acids (0.1 to 0.86 *N*) of 1-phenyl-2-*p*-tolyl-ethylene-1-^{14}C glycol (B. M. Benjamin, unpublished work) the hydroxyl adjacent to *p*-tolyl is removed in preference to its neighbor in a ratio of 7:1 (*threo* form) and 10:1 (*erythro*-form).

[10]If the uncertainty in the yield of olefin **3** is expressed as 76 ± 1%, this corresponds to an error of only ±0.1% in $m_a/(m_a + m_d)$ (determined by a computer calculation using yields of 77.0 and 75.0% for **3**).

[11]S. Winstein and D. Trifan, *J. Am. Chem. Soc.* **74**, 1147, 1154 (1952).

[12]J. D. Roberts, C. C. Lee, and W. H. Saunders, Jr., *J. Am. Chem. Soc.* **77**, 3036 (1955), last paragraph of Discussion.

[13]D. J. Cram, *J. Am. Chem. Soc.* **74**, 2133 (1952).

of other mechanistic changes, the introduction of internal return[11] into a carbonium ion reaction scheme will necessarily alter the product ratio (or ^{14}C scrambling or extent of racemization) of the irreversibly formed products. In two recent studies[14,15] we indicated that the intervention of a competing thermodynamically controlled process has no effect on the product ratio to be expected from the kinetically controlled processes of a given carbonium ion mechanism. We now present both mathematical and experimental evidence in support of our view. Given in Chart II is a mechanism for the formic acid–catalyzed dehydration[16] of 1,2,2-triphenylethanol (**1a**) labeled both with ^{14}C and with deuterium in the 2-position.

ORNL-DWG. 66-2888A

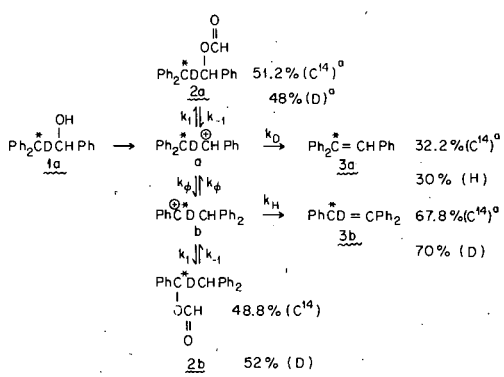

CHART II

The following relations become apparent (where the k_i have the significance given in Chart II, and m_{3a} and m_{3b} are the mole fractions of unrearranged and rearranged olefins produced):

$$\frac{d[b]}{dt} = k_\phi[a] - k_\phi[b] - k_H[b] - k_1[b] + k_{-1}[2b] , \quad (1)$$

$$\frac{d[2b]}{dt} = k_1[b] - k_{-1}[2b] , \quad (2)$$

$$\frac{d[3a]}{dt} = k_D[a] , \quad (3)$$

$$\frac{d[3b]}{dt} = k_H[b] ; \quad (4)$$

k_H is the rate of migration of hydrogen, k_D is the rate of migration of deuterium. Integrating between zero and infinite time and employing Hearon's area theorem,[17] we find

$$k_\phi S_a - k_\phi S_b - k_H S_b - k_1 S_b + k_{-1} S_{2b} = 0 , \quad (5)$$

$$k_1 S_b - k_{-1} S_{2b} = 0 , \quad (6)$$

$$m_{3a} = k_D S_a , \quad (7)$$

$$m_{3b} = k_H S_b , \quad (8)$$

where S_a, S_b, and S_{2b} are the appropriate integration areas.[17] From Eqs. (5)–(8) we easily obtain Eq. (9):

$$\frac{m_{3a}}{m_{3b}} = \frac{k_D}{k_H} + \frac{k_D}{k_\phi} , \quad (9)$$

which gives us the isotope effect (k_D/k_H) in terms of the product ratio, since we have evidence[15] indicating k_D/k_ϕ to be very small. Equation (9) tells us nothing about the relative yields of **3a** and **3b** before completion of reaction, but applies – in the general case – only after all of the two formates (**2a** and **2b**) have been converted irreversibly to olefin (**3a** and **3b**). If, however, k_ϕ is much greater than k_H and k_D, it can easily be shown that the ratio of **3a** to **3b** is constant throughout the reaction and equal to the final ratio $m_{3a}:m_{3b}$. Equation (9) can also be derived if we neglect the reversible processes leading to the formates **2a** and **2b**. This means that provided k_ϕ, k_D, and k_H remain constant, the final ratio of **3a** to **3b** will be the same whether or not the reversible formation of **2a** and **2b** takes place! The relationship of this result to the phenomenon of internal return[11] and to the widespread misconception[11–13] pertaining to internal return should be obvious. Thus our mathematical evidence is complete. The chemical evidence is demonstrated by the isotopic analyses shown by each of the products in Chart II. These particular data are for yields of 79% formate (**2ab**) and 21%

[14] C. J. Collins, B. M. Benjamin, and M. H. Lietzke, *Ann. Chem.* **687**, 160 (1965).

[15] V. F. Raaen, M. H. Lietzke, and C. J. Collins, *J. Am. Chem. Soc.* **88**, 369 (1966), footnote 8.

[16] C. J. Collins and W. A. Bonner, *J. Am. Chem. Soc.* **77**, 92 (1955).

[17] B. M. Benjamin and C. J. Collins, *J. Am. Chem. Soc.* **78**, 4332 (1956).

olefin (**3ab**) after **1a** was dissolved in formic acid and held at 98 to 99°C for 30 min. The results are identical – within experimental error – over wide ranges of yields of both olefin and formate. Thus both the reversible and irreversible processes go their separate ways, each independent of the other. When the reaction is allowed to proceed long enough (22 hr) to produce the olefin in quantitative yield, the ^{14}C distribution[18] in **3ab** is very nearly the same (34% **3a**; 66% **3b**) as that shown in Chart II. Similar experiments were carried out with 1,2,2-triphenylethanol labeled in the 1-position with ^{14}C and deuterium, and the results confirmed in every detail the data already presented.[18] Carbinol **1a**, when dehydrated for 2 to 5 min in sulfuric acid at 10°C, yielded olefin[18] quantitatively, with a ^{14}C distribution between the 1- and 2-positions of 33%:67%. 1,2,2-Triphenylethyl acetate, labeled in the 1-position with ^{14}C and deuterium, when heated at 50°C in acetic acid containing *p*-toluenesulfonic acid[16] produced no olefin, but yielded 1,2,2-triphenylethyl acetate with both ^{14}C and deuterium equally distributed between the 1- and 2-positions.[19,20]

CONSECUTIVE HYDRIDE SHIFTS DURING NORBORNYL REARRANGEMENTS

Ben M. Benjamin Clair J. Collins

6,2-Migrations of hydrogen have been unequivocally demonstrated by Roberts[21] and co-workers, and by Doering and Wolf[22,23] during carbonium ion rearrangements of *exo*-2-norbornyl tosylate and of O-deuterated fenchol respectively. In neither of these cases, however, is it possible to say if the hydrogen actually moves from the 6 to the 2 position, or whether a 6,1- and, subsequently, a 1,2-shift occurs. Berson and Grubb[24] recently showed that a 5-*endo* deuterium undergoes a transannular, intramolecular migration in the 2-carboxy-3-methyl-5-norbornyl cation (corresponding to a 6,2-shift in the norbornyl[21] case).

We discussed previously[25] the stereospecific elimination of deuterium, and the stereospecific 5,4-migration of deuterium (corresponding to 6,1-migration in unsubstituted norbornyl) during hydrolysis of the dideutero-2-*endo*-phenyl-2-hydroxy-3-norbornyl tosylate **1**, and mentioned that there were traces of another, then unidentified, diol in the product. We have already discussed the products arising from the presumed bridged ion intermediates *A* and *B* (Chart III) and the intermediate between them. The discovery of a very

[18] Upon prolonged heating in formic acid (or after a few minutes in sulfuric acid) 1,1,2-triphenylethylene-2-$^2H_1$ loses deuterium. Therefore when **1a** was placed in formic acid at 98 to 99° for 22 hr, the resulting olefin (**3ab**) contained 25% *less* deuterium than that isolated after ½ hr. We have also shown that 1,1,2-triphenyl-ethylene-1-^{14}C undergoes a very slow acid-catalyzed isotope position isomerization (S. F. Clark, unpublished work).

[19] Carbon-14 analyses were performed in the normal[14–17] manner, and the error in our determination is ±0.5%. The deuterium analyses were carried out by comparison of integrated areas of appropriate NMR spectra, and possess an inherent error of not more than ±3%.

[20] The reactions discussed here, as well as the treatment of the scheme outlined in Chart I, pertain to those systems (apparently in the majority) in which the products formed through the kinetic- and equilibrium-controlled processes involve the same intermediates. For an unusual example in which internal return leads to products which solvolyze through *different* intermediates than those through which they were formed, see P. von R. Schleyer, W. E. Watts, and C. Cupas, *J. Am. Chem. Soc.* **86**, 2722 (1964).

[21] J. D. Roberts and C. C. Lee, *J. Am. Chem. Soc.* **73**, 5009 (1951); J. D. Roberts, C. C. Lee, and W. H. Saunders, Jr., *J. Am. Chem. Soc.* **76**, 4501 (1954).

[22] W. von E. Doering and A. P. Wolf, *Chem. Abstr.* **46**, 7080 (1952).

[23] J. A. Berson, "Carbonium Ion Rearrangements in Bridged Bicyclate Systems," p. 141 in *Molecular Rearrangements*, chap. 3, ed. by P. de Mayo, Interscience, New York, 1963.

[24] J. A. Berson and P. W. Grubb, *J. Am. Chem. Soc.* **87**, 4016 (1965).

[25] B. M. Benjamin and C. J. Collins, *J. Am. Chem. Soc.* **88**, 1556 (1966); B. M. Benjamin, B. W. Ponder, and C. J. Collins, *J. Am. Chem. Soc.* **88**, 1558 (1966).

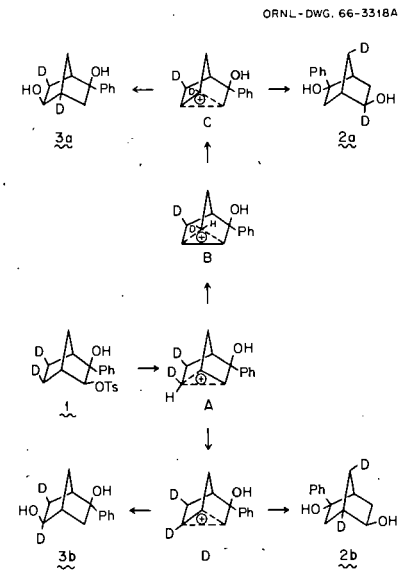

CHART III

ORNL-DWG. 66-5326

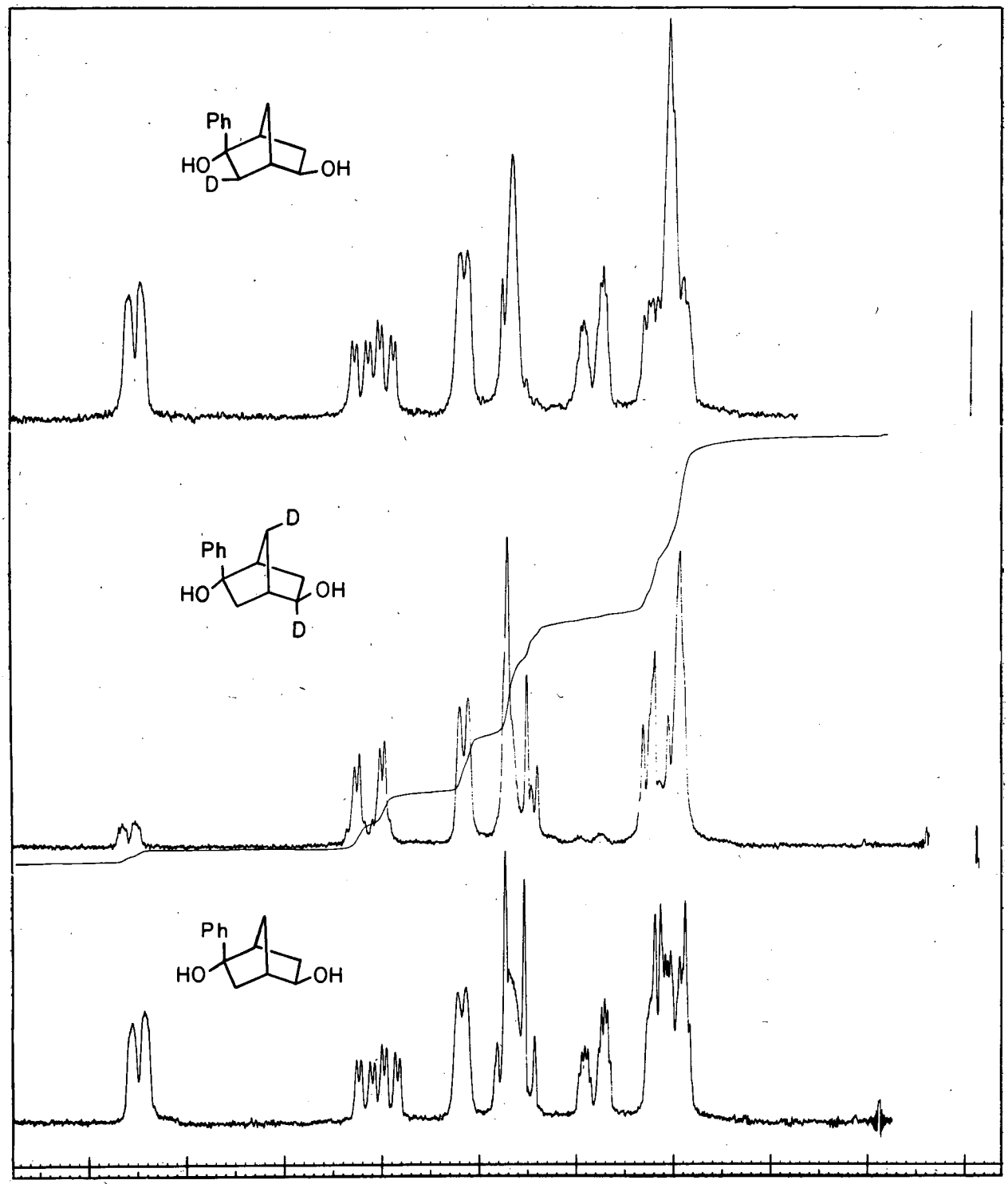

Fig. 4.2. The 100 Mc/sec Spectra of 2, 2ab, and 2cd Taken at 60°C in Pyridine Solution Using TMS as Standard at $\delta = 0$.

small yield, 4%, of an additional diol[26] during hydrolysis of **1a** led to the intriguing possibility that this diol might be either **2a** or **3a**, which conceivably *could be formed by consecutive shift of deuterium (A→B) and hydrogen (B→C).* The isotope position isomers **2b** and **3b** are also possible through a direct 5,3-migration of the *endo*-5 hydrogen (*A→D*). In fact, the diol turned out to be **2ab** which formed from *both* ions *C* and *D*, in the approximate proportions 9:1. This conclusion was confirmed by repeating the experiment with tosylate **1c**, and isolating the mixture **2cd** in about the same proportion.

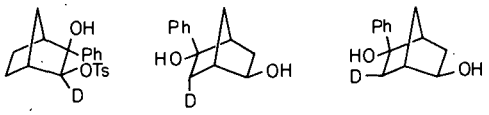

1c 2c 2d

The structure of **2** was confirmed by independent synthesis and by analysis of its 60 Mc/sec and

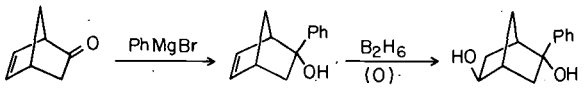

100 Mc/sec NMR spectra, Fig. 4.2. Assignments of the spectral parameters were made with the aid of spin decoupling in the frequency sweep mode. The signals at 1.94 ppm and 4.27 ppm arise from the 7-*syn* and 5-*endo* hydrogens respectively. In the spectrum of **2ab** the signal for 7-*syn*-H is almost totally absent, and the signal for 5-*endo*-H is only partly visible. From the integrated intensities of the signals, and because the starting tosylate contained about 10% protium in the 5-*exo* and 6-*exo* position, it is clear that approximately 90% of **2a** is formed through *A→B→C* and 10% of **2b** is formed through *A→D*. In the spectrum of **2cd** the quartet arising from 3-*exo*-H is considerably attenuated, thus further confirming the course of reaction. We believe this is the first demonstration of consecutive 1,2-hydride shifts in norbornyl-type cations.

[26]Melting point 163. Analysis calculated for $C_{13}H_{16}O_2$: C, 76.44; H, 7.90. Found: C, 76.55; H, 7.97.

Steric considerations[27] lead us to believe that the diol **3ab** should be formed in yields equivalent to those of compound **2ab**. We have thus far been unsuccessful, however, in isolating diol **3**.

Acknowledgment. We wish to thank Dr. H. W. Patton, Dr. V. W. Goodlett, and J. T. Dougherty, Tennessee Eastman Company, Kingsport, Tennessee, for obtaining the 100 Mc/sec spectra, decoupling data, and for helpful discussions.

THE ACETOLYSIS OF 2-exo-HYDROXY-2-PHENYL-3-exo-NORBORNYL-5,6-exo-d_2 TOSYLATE

Ben M. Benjamin Clair J. Collins

The acetolysis of the 3-*p*-toluenesulfonate ester of 2-phenylnorbornane-2,3-*cis*-*exo*-diol (**1**) has been shown[28] to give the acetate esters of three products, 7-phenylnorbornane-2-*exo*-7-*syn*-diol (**2**), 7-phenylnorbornane-2-*exo*-7-*anti*-diol (**3**), and 5-phenyl-5,6-norbornene-2-*exo*-ol (**4**). Compounds **2** and **3** are identical to two of the diols formed during hydrolysis,[29] and **4** appears to be a dehydration product of 2-*exo*-phenylnorbornane-2-*endo*-5-*exo*-diol (**5**) (also formed upon hydrolysis of **1**). No nortricyclic product was isolated. The relationship between hydrolysis and acetolysis of **1** and the greater complexity of the acetolysis experiment were demonstrated by studying the products of acetolysis of **1a**, the 5,6-di-*exo*-deutero form of **1**, using nuclear magnetic resonance spectroscopy.

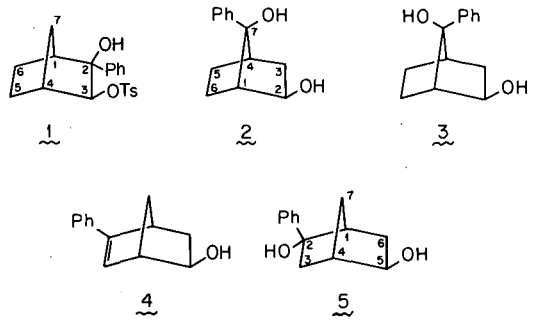

1 2 3

4 5

[27]J. A. Berson, A. W. McRowe, and R. G. Bergman, *J. Am. Chem. Soc.* **88**, 1067 (1966).

[28]B. M. Benjamin, B. W. Ponder, and C. J. Collins, *Chem. Div. Ann. Progr. Rept. May 20, 1965*, ORNL-3832, p. 66.

[29]B. M. Benjamin, B. W. Ponder, and C. J. Collins, *J. Am. Chem. Soc.* **88**, 1558 (1966).

Integration of the NMR spectrum of the *syn*-diol, **2a**, from **1a** showed that it contained 1.61 atoms of deuterium per molecule and that the deuterium was located in the 5 and 6 *endo* positions. Since the starting material contained 1.78 atoms of deuterium, it appears that some deuterium was lost during the reaction. The acetate ester of **2a** was produced by attack of solvent at the 4-position of the first-formed carbonium ion.

Analysis of the NMR spectrum of the *anti*-diol from **1a** showed that two isotope substitution isomers were present. One of the isomers, **3a**, contained deuterium in the *endo*-3 and *endo*-6

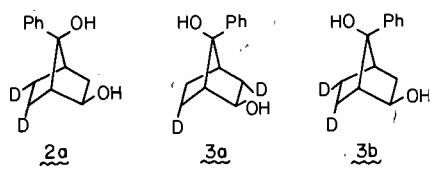

positions, and the other, **3b**, contained deuterium in the *endo*-5 and *endo*-6 positions. The acetate ester of **3a** was formed after 5,4-deuterium migration and attack of solvent at position 5, the acetate of **3b** after inversion of position 2 followed by solvent attack at position 4.

The olefinic product also consisted of more than one isotope position isomer. Although it was not possible to assign the position of the deuterium atoms in the molecules in pairs, the following distribution was determined:

0.30 atom at position 2

0.27 atom at position 1

0.88 atom at positions 3 and 7

Apparently 0.38 atom of deuterium was lost by exchange. Four routes can be described for the production of **4**. Migration of deuterium from the

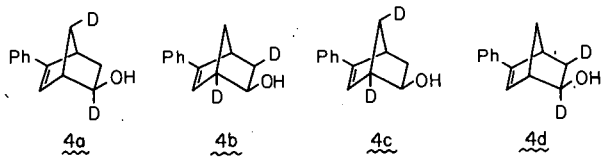

5- to the 4-position followed by migration of hydrogen from the 4- to the 3-position and then solvent attack at position 4 or 5 gives **4a** and **4b** respectively. Compounds **4c** and **4d** are formed after migration of hydrogen from the 5- to the 3-position followed by solvent attack at positions 4 and 5 respectively. The absence of good resolution in the appropriate signals of the NMR spectrum indicates that all four processes occur.

STEREOSPECIFIC 6,1 MIGRATION OF DEUTERIUM DURING REARRANGEMENT OF 2-PHENYLNORBORNANE-2,3-*cis*-exo-DIOL-5,6-d_2

Ben M. Benjamin Clair J. Collins

In 1961 Kleinfelter and Schleyer[30] reported that diol **I** (without deuterium) rearranges, in sulfuric acid, to produce 3-*endo*-phenylnorbornanone-2 (**II**, without deuterium). We showed[31] later that this rearrangement proceeds: (1) with inversion of configuration, (2) with intramolecular migration of the original 3-*endo*-hydrogen, and (3) without migration of phenyl (the asterisks denote appropriate labels with tritium and ^{14}C). These results are compatible with the presence of the bridged ion intermediates *A* and *B*. In the rearrangement *A*→*B* an intramolecular 6,1-hydride shift must take place.[31] We were curious as to whether this shift occurs (1) by a discrete shift of the *exo*-6-hydrogen, (2) through a "face-protonated" cyclopropane intermediate,[32,33] or (3) through some mechanism in which the three hydrogens in the 6 and 1 positions (of **I**) become involved in reversible migrations. We have now shown that it is the *exo*-6-hydrogen which undergoes a discrete 6,1 shift, and becomes the *exo*-5-hydrogen in **II**.

Glycol **Ia**, containing *exo*-5- and *exo*-6-deuterium, was obtained[30,31] starting with a mixture of deuterated 2-norbornanols which was prepared by catalytic deuteration of the mixed 2-norbornen-5-

[30] D. C. Kleinfelter and P. von R. Schleyer, *J. Am. Chem. Soc.* **83**, 2329 (1961).

[31] C. J. Collins, Z. K. Cheema, R. G. Werth, and B. M. Benjamin, *J. Am. Chem. Soc.* **86**, 4913 (1964).

[32] J. D. Roberts and C. C. Lee, *J. Am. Chem. Soc.* **73**, 5009 (1951).

[33] J. A. Berson and P. W. Grubb, *J. Am. Chem. Soc.* **87**, 4016 (1965), give a brief discussion of the stereochemistry of hydride shift in norbornyl compounds.

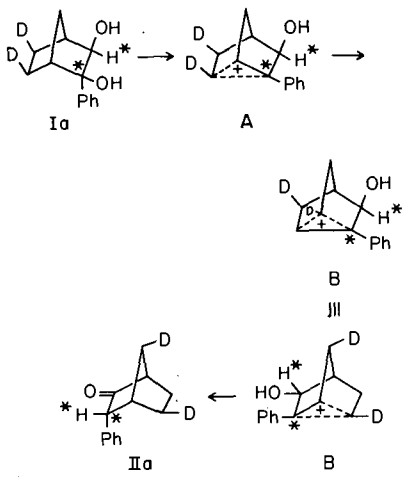

ols.[34] Ketone **IIa**, obtained upon rearrangement[30,31] of **Ia**, contained deuterium in the *exo*-5 and *anti*-7 positions. This was demonstrated through the arguments presented herein after reduction of **IIa** with lithium aluminum hydride to 3-*endo*-phenyl-2-*endo*-norbornanol (**IIIa**, mp 71°),[35]

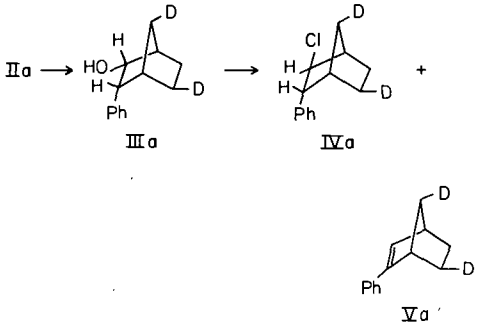

which was converted under S_N2 conditions to the chloride **IVa**, and 2-phenyl-2-norbornene-*exo*-6-*anti*-7-d_2 (**Va**). Confirmation of the structure of **III** is obtained from its NMR spectrum (Fig. 4.3). The signal for the *exo*-2-hydrogen is a quartet (δ = 4.12 ppm, $J_{1,2}$ = 4.6 cps, $J_{2,3}$ = 10.0 cps). The signal assigned to the *exo*-3-hydrogen is also a quartet (δ = 2.87 ppm, $J_{3,4}$ = 4.0 cps, $J_{2,3}$ = 10.0 cps).[36] This signal shows an additional splitting in each component of 0.9 cps (inset, Fig. 4.3) which is attributed to long-range coupling with the *exo*-5-hydrogen.[36,37] The corresponding signal for **IIIa** is a sharp quartet; the width of each component at half height is 1.5 cps (inset, Fig. 4.3). Compound **IIIa** therefore contains deuterium in the *exo*-5 position. The two bridgehead protons (1 and 4) of **III** exhibit signals centered at δ = 2.25 ppm. The integrals of these signals compared with integrals of corresponding signals from **IIIa** show that not more than 3% deuterium could be in the two bridgehead positions. The bridgehead protons of ketones **II** and **IIa** also exhibit isolated signals centered at δ = 2.65 ppm. Comparison of the pertinent integrals further indicated less than 3% deuterium at the bridgeheads. Thus at least 94% of the original *exo*-6-deuterium of **Ia** migrated during the rearrangement **Ia**→**IIa**.

The structure of compound **IV** was confirmed by its NMR spectrum. A signal at 4.00 ppm is due to the *endo*-2-hydrogen. Splittings of 4.2 and 1.9 cps result from couplings with the *exo*-3 and *anti*-7-hydrogens[38] respectively. The *anti*-7-hydrogen gives a doublet of components at 1.38 ppm, and double irradiation at this position removes the splitting of 1.9 cps exhibited by the *endo*-2-hydrogen (4.00 ppm). A broadened doublet, J_{gem} = 10.1 cps, for the *syn*-7-hydrogen appears at 2.06 ppm. The downfield shift of this signal is attributed to the anisotropic effect of the *exo*-2-chlorine. The appearance of the *exo*-3-hydrogen

[34]The high preference for *exo* deuteration was demonstrated by an analysis of NMR spectrum of *exo*-5,6-dideuterio-2-phenylnorbornene-2,[31] an intermediate in the synthesis of **Ia**. Comparison of pertinent integration areas showed that not more than 3% *endo* deuteration took place.

[35]Satisfactory carbon and hydrogen analyses were obtained for **III** and **IV**. Dr. D. C. Kleinfelter (University of Tennessee) has independently synthesized and characterized **III** (3-*endo*-phenyl-2-*exo*-norbornanol has been previously prepared[31] through hydroboration of **V**). The *cis* character of the phenyl and hydroxyl of **III** is confirmed by demonstrating hydrogen[31] bonding of the OH...Ph type; $\Delta\nu$ is 12 cm^{-1} relative to the frequency of the OH band of *endo*-2-norbornanol [also measured and communicated to us by Dr. Kleinfelter, who informs us he has, in addition, synthesized and characterized the three other (2,3) isomers of **III** by NMR: Master's thesis, J. E. Mallory, 1966].

[36]These signals were further shown to be mutually coupled by double resonance. A range of 8.9 to 11.4 cps is expected for *exo-exo* couplings, while 5.8 to 7.7 cps is usually found for *endo-endo* couplings [P. Laszlo and P. von R. Schleyer, *J. Am. Chem. Soc.* **86**, 1171 (1964)]. Coupling between *endo* and bridgehead hydrogens is ordinarily not observed.

[37]F. A. L. Anet, *Can. J. Chem.* **39**, 789 (1961).

[38]J. Meinwald and Y. C. Meinwald, *J. Am. Chem. Soc.* **85**, 2514 (1963).

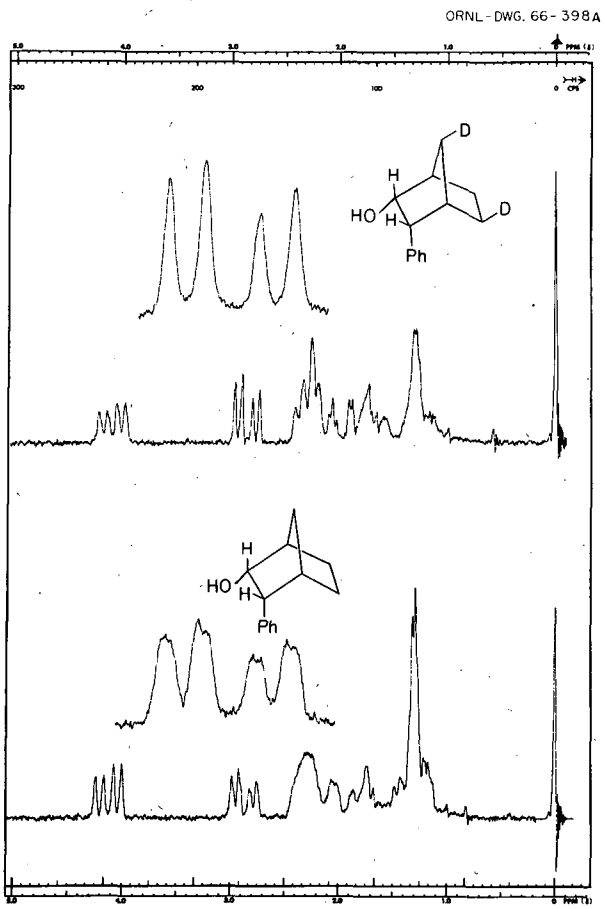

Fig. 4.3. The NMR Spectra of III and IIIa in Benzene Solution Recorded at 60 Mc/sec. The aromatic proton signals are not shown. The OH signal was removed by shaking the sample with D_2O.

at 3.44 ppm as a triplet is expected from the almost equal $J_{4,exo\text{-}3}$ and $J_{endo\text{-}2,exo\text{-}3}$.[39] In the spectrum of **IVa** the signal for the *endo*-2-hydrogen is a simple doublet, $J_{2,3}$ = 4.2 cps; the signal for the *syn*-7-hydrogen is collapsed to a single line, and the doublet at 1.38 ppm for the *anti*-7-hydrogen is absent.

Finally, additional quantitative evidence for the *exo*-5-deuterium in **IIa** is found in the NMR spectrum of **Va** (see also ref. 34). The *syn*-7 proton of **V** gives a multiplet centered at δ = 1.51 ppm, whereas the signals for the *exo*-5 and *exo*-6 protons are centered at 1.71 ppm. Comparison of pertinent integration areas of **V** and **Va** confirms that at least 95 to 96% of the deuterium originally in the *exo*-6 position of **Ia** resides in the *exo*-6 position of **Va**.

[39]If a Wagner-Meerwein rearrangement had taken place during treatment of **III** with PCl_5, the formation of 7-*anti*-phenyl-2-*exo*-norbornyl chloride might be expected. Its NMR spectrum should be considerably different from that observed for **IV**.

THE DEAMINATION OF 3-*endo*-AMINO-2-*exo*-PHENYLNORBORNANOL-2

Vernon F. Raaen Clair J. Collins

In our continuing[40] effort to determine the identities and yields of the products of deamination of 3-*endo*-amino-2-*exo*-phenylnorbornanol-2 (**1**), we changed the solvent from water to glacial acetic acid. This change was made after isotopic dilution studies showed us that the products previously[40] reported represented an overall conversion of only 11%. We have some evidence that the bulk of the material unaccounted for was converted to a water-soluble material (probably the amine nitrite) which decomposed on attempted workup to yield oily mixtures which could not easily be separated. The results of the deamination of **1** in acetic acid were much more satisfactory and after treatment of the reaction product with $LiAlH_4$, allowed us to isolate and identify compounds **2**–**7** in the approximate yields shown under each formula. The diol **8**, produced

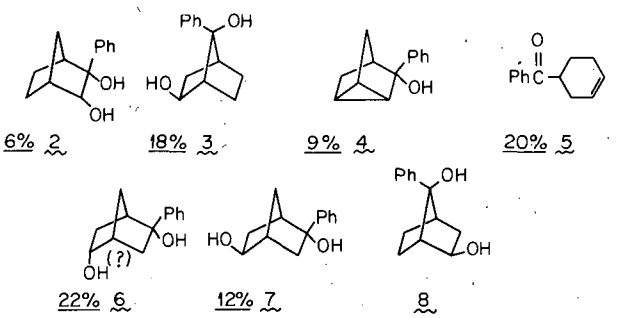

when the reaction was conducted in water, was not isolated during the present experiments, but we suspect it is present in the approximately 15%

[40]I. T. Glover, B. M. Benjamin, and C. J. Collins, *Chem. Div. Ann. Progr. Rept. May 20, 1965*, ORNL-3832, p. 74.

of material which is as yet unaccounted for. Compounds **2–7** were laboriously separated by column chromatography (alumina). The production of these compounds can only be explained through the intervention of open carbonium ions. An interesting conclusion to be drawn from these data is that hydride shifts must take place during interconversion of open (or classical) carbonium ions. We have previously shown[41] that such hydride shifts take place during interconversion of ions which are presumed to be nonclassical.

STEREOSPECIFIC ELIMINATION AND MIGRATION OF DEUTERIUM DURING HYDROLYSIS OF A SUBSTITUTED NORBORNYL TOSYLATE

Ben M. Benjamin B. W. Ponder[42]
Clair J. Collins

Hydride shifts (6,1 and 6,2)[43] occur during solvolyses of 2-*exo*-norbornyl derivatives. We recently established the intramolecularity and stereochemistry of one of these shifts.[44,45] During hydrolysis of the dideuterated[46] tosylate **1a** we now report (1) a stereospecific elimination and (2) a stereospecific 5,4 migration, respectively, of the 5-*exo* deuterium. Hydrolysis of **1a** in aqueous acetone (containing sodium carbonate) led to the 85% production of compounds **2a**, **3a**, and **4a** with deuterium in the positions shown. The three products were easily separated by chromatography on alumina in yields of 25, 60, and 15% respectively. Traces of another diol have been detected.

The structures of compounds **2**, **3**, and **4** (without deuterium) were established through their NMR and infrared spectra and by their chemical reactions.[47] In addition, **2** was independently synthesized by reaction of nortricyclenone with phenylmagnesium bromide. Compounds **3** and **4** were also prepared by solvolysis of **1** which contained a deuterium in the *endo*-3 position, and each, as expected, contained one atom of deuterium per mole in the 1

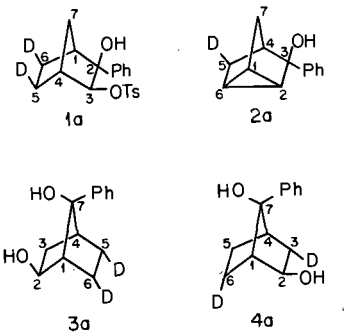

(bridgehead) position. Deuterium contents in all cases were determined by integration of the appropriate signals of the NMR spectra.

Most of the signals in the NMR spectrum of **2** are well separated and can be assigned on the basis of expected inductive and anisotropic effects. In addition to five aromatic hydrogens and one exchangeable hydrogen (OH), the following are observed: (1) A one-proton doublet, J = 10.1 cps at 2.13 ppm, due to the *syn*-7 hydrogen. It is deshielded by the hydroxyl and therefore appears at lowest field. The latter doublet is reciprocated by a doublet at 1.29 ppm (7-*anti*-H). (2) A one-proton (4 H) broadened signal at 1.73 ppm. (3) Signals for the remaining five hydrogens in two bands at 1.23 ppm (3 H) and at 1.07 ppm (2 H).

In the spectrum of **2a** the band at 1.07 ppm had an intensity of only one hydrogen. The relative intensities of all other lines were the same. Thus at least 95 to 96% of a deuterium atom was lost during the reactions **1a**→**2a**. In addition, the signal for the C-4 hydrogen of **2a** exhibits a width at half height of 4.6 cps, whereas the same signal for **2** has a width of 5.2 cps, and the deuterium atom in **2a** results in the removal of one coupling constant. Double irradiation shows that the C-4

[41] B. M. Benjamin and C. J. Collins, *J. Am. Chem. Soc.* **88**, 1556 (1966); B. M. Benjamin, B. W. Ponder, and C. J. Collins, *J. Am. Chem. Soc.* **88**, 1558 (1966).

[42] Summer research participant of the Oak Ridge Institute of Nuclear Studies from the University of Alabama.

[43] J. Berson, pp. 138–55 in *Molecular Rearrangements*, ed. by P. de Mayo, vol. 1, Interscience, New York, 1963.

[44] B. M. Benjamin and C. J. Collins, *J. Am. Chem. Soc.* **87**, 1556 (1965).

[45] See also J. A. Berson and P. W. Grubb, *J. Am. Chem. Soc.* **87**, 4016 (1965).

[46] Not more than 3% *endo* deuteration took place (see ref. 44).

[47] All gave satisfactory carbon and hydrogen analyses, performed by Huffman Microanalytical Laboratories, Wheatridge, Colo.

hydrogen of **2** is weakly spin coupled to hydrogens, contributing to the signals at 1.23 and 1.07 ppm. The latter are assigned to the methylene hydrogens at C-5. Double irradiation of the one-proton signal at 1.07 ppm had no effect upon the signal for the C-4 hydrogen of **2a**. The deuterium atom in **2a** is thus located at C-5 and *anti* to the phenyl substituent at C-3.

The spectra of **3** and **4** both exhibit one-proton signals appearing as X parts of ABX systems. The pattern is characteristic for an *endo*-hydrogen of an H-C-O group.[48] The signal is centered at 3.64 ppm for compound **3** and at 3.56 ppm for compound **4**. In the upfield region of the spectrum of **3** there are two bands at 1.39 and at 1.21 ppm, assigned to the *exo*-5- and -6- hydrogens and confirmed through spin decoupling from the 1- and 4-hydrogens at 2.24 and 2.47 ppm. Two bands at 0.99 and at 0.82 ppm are assigned to the 5- and 6-*endo*-hydrogens. The *exo* and *endo* protons at C-3 appear at 1.89 ppm, and these were spin decoupled from the *endo* hydrogen at C-2 (3.64 ppm). In **3a** the signals for the 5- and 6-*endo*-hydrogens (0.99 and 0.82 ppm) are absent and the pair of signals for the 5- and 6-*exo*-hydrogens is collapsed into a single broadened peak centered at 1.25 ppm. None of the other spectral features is altered. Neither of the two deuterium atoms originally at the 5- and 6-*exo* positions of **1a** migrated, and they now appear at the 5- and 6-*endo* positions of **3a**.

Integration of the spectrum of **4a** shows the molecule contains two deuterium atoms. The signal of **4** which appears at 3.56 ppm is a well-resolved quartet. The separation of the outer peaks is 12.2 cps, and that of the inner peaks is 4.4 cps. The same signal for **4a** appears as a doublet, while a set of sharp signals centered at 1.68 ppm, originally due to the *endo*-3 proton of **4**, is now absent. The doublet of **4a** at 3.56 ppm represents the smaller coupling constant (J_{ax} = 3.5 cps) of the ABX system. The two coupled hydrogens are therefore in a *trans* configuration, and placement of one deuterium atom at C-3 and *endo* is confirmed. A pair of signals at 1.21 and at 1.08 ppm is due to the 5- and 6-*endo*-hydrogens. Their intensity in **4a** is half that of **4**, and therefore there is one *endo*-deuterium in these positions.

From these data we cannot rigidly exclude deuterium from the *endo*-5 position. Integration of the signals for the hydrogens (of **4a**) at C-1 (2.42 ppm) and C-2 (3.56 ppm) shows that neither of these positions contains a measurable amount of deuterium. Thus at least 97% of the deuterium originally *exo*-5 in **1a** has left that position, and a discrete 5,4 shift of deuterium has taken place. Any rational mechanism producing an *endo*-5-deuterium should also affect the *endo*-3 label; we conclude our assignment of an *endo*-6-deuterium is correct.

All of the results are nicely rationalized by the sequences **1a**→**5a**→**3a**; **1a**→**5a**→**6a**→**2a**; and **1a**→**5a**→**6a**→**7a**→**4a**. The intermediate (or transition state) **6a** can lose a deuterium to yield the phenylnortricyclanol **2a**, or it can proceed to **7a** with completion of the 5,4 shift. Structure **6a** is similar to that proposed earlier by Aboderin and Baird.[49]

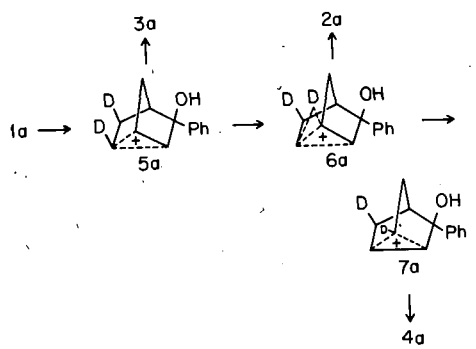

An alternate explanation involving a homo-E2 elimination will be shown later to be untenable.

ORGANIC COMPOUNDS IN NUCLEAR TECHNOLOGY. EXTRACTION WITH 2-ETHYL-HEXANOHYDROXAMIC ACID

W. H. Baldwin C. E. Higgins

Solvent extraction techniques are ubiquitously employed in nuclear technology. In one solvent extraction system tributyl phosphate in an organic diluent is contacted with an aqueous nitric acid solution of reactor fuels. Certain hydrocarbon

[48] T. J. Flautt and W. F. Erman, *J. Am. Chem. Soc.* **85**, 3212 (1963).

[49] A. A. Aboderin and R. L. Baird, *J. Am. Chem. Soc.* **86**, 252 (1964).

diluents react with nitric acid in this system to produce undesirable products. Lane[50] has presented arguments for hydroxamic acids being an important but low-yield component of the reaction mixture. Hydroxamic acids are known to form complexes with many cations.[51] However, the hydroxamic acids containing aryl rings or unbranched aliphatic chains are solids and too insoluble in nonpolar solvents to be useful in solvent extraction. Our earlier experiences with other solvents have led to the generalization that branched aliphatic chains impart desirable solubility characteristics. We prepared the branched chain 2-ethyl-hexanohydroxamic acid [C_4H_9-$CH(C_2H_5)C(O)NHOH$] and found it to be soluble in chloroform.

[50]E. S. Lane, *Nucl. Sci. Eng.* 17, 620 (1963).
[51]H. L. Yale, *Chem. Rev.* 33, 209 (1943).

The hydroxamic acid in chloroform (0.2 *M*) was equilibrated with 10^{-3} *M* concentrations of cations in aqueous hydrochloric or nitric acid. Distribution coefficients (concentration in organic phase over concentration in aqueous phase) were greater than 20 for zirconium, niobium, and hafnium when the concentration of nitric acid was 2 *M*. Equilibrium distribution coefficients for cobalt II, uranyl II, thorium IV, and iron III were greater than 1 when the aqueous phase was buffered with sodium acetate, but were significantly lower from 2 *M* nitric or hydrochloric acid.

On the basis of our preliminary results, it appears unlikely that the properties of a simple hydroxamic acid can be used to explain the properties of the nitric acid reaction products that were reported by Lane.[50] A more complex hydroxamic acid with other functional groups in the molecule cannot be rejected.

5. Chemistry of Aqueous Systems

THE THERMODYNAMIC PROPERTIES OF HCl-$BaCl_2$ MIXTURES

M. H. Lietzke R. W. Stoughton

The thermodynamic properties of HBr-KBr mixtures[1] and of HCl-NaCl mixtures[2] have been described in previous papers. In the present work emf measurements of the cell

$$\text{Pt-H}_2\ (p)\ |\ \text{HCl}\ (m_2),\ \text{BaCl}_2\ (m_3)\ |\ \text{AgCl-Ag}$$

have been combined with values of the osmotic coefficient of $BaCl_2$[3,4] to compute the thermodynamic properties of both HCl and $BaCl_2$ in HCl-$BaCl_2$ mixtures.

In treating the results, the hydrogen pressure was calculated by subtracting the vapor pressure of the solution from the observed total pressure, while the vapor pressure of the solution was obtained by taking the vapor pressure of pure water at the temperature of measurement from the steam tables[5] and correcting for the presence of $BaCl_2$ and HCl in solution by Raoult's law. Each emf value was corrected to 1.00 atm of hydrogen pressure by subtracting $(RT/2\mathfrak{F})\ \ln f_{H_2}$, where the hydrogen fugacity f_{H_2} was taken equal to the hydrogen pressure. The solubility of AgCl was neglected, and the ionic strength was taken to be equal to $m_{HCl} + 3m_{BaCl_2}$. The corrected emf values E at each ionic strength were plotted as a function of temperature, and the values were corrected to the round values of the temperature, 25, 60, 90, 125, 150, and 175°. The temperature of measurement was never more than 1° from the corresponding round temperature.

The activity coefficient $\gamma\pm$ of HCl at each temperature and set of concentrations in the mixtures was evaluated by using the Nernst equation and previous values[6] of the standard potential $E°$ of the Ag, AgCl electrode, except that 0.2223 v was used instead of 0.2220 v at 25°:

$$E = E° - \frac{RT}{\mathfrak{F}} \ln [m_2(m_2 + 2m_3)] - \frac{2RT}{\mathfrak{F}} \ln \gamma\pm . \quad (1)$$

In this equation m_2 and m_3 are the molalities of HCl and $BaCl_2$.

A plot of $\ln \gamma\pm$ vs ionic strength fraction of $BaCl_2$ was made at each temperature and at the total ionic strengths 0.5 and 1.0. Also included in these plots were the values for pure HCl[6] at all temperatures and for 0.01 m HCl in $BaCl_2$[7] at 25 and 60°. (The values at 60° were obtained by extrapolations of data from 0 to 50°.) In all cases the plots were linear within experimental error, in conformity with Harned's rule.

Expressions for $\gamma\pm$ of HCl and $BaCl_2$ in the Mixtures

The activity coefficients of HCl were smoothed as to HCl and $BaCl_2$ concentrations and tempera-

[1] M. H. Lietzke and R. W. Stoughton, *J. Phys. Chem.* **67**, 2573 (1963).

[2] M. H. Lietzke, H. B. Hupf, and R. W. Stoughton, *J. Phys. Chem.* **69**, 2395 (1965).

[3] R. A. Robinson and R. H. Stokes, *Electrolyte Solutions*, p. 471, Academic, New York, 1955.

[4] C. S. Patterson, L. O. Gilpatrick, and B. A. Soldano, *J. Chem. Soc.* **1960**, 2730.

[5] *VDI-Wasserdampftafeln*, ed. by E. Schmitt, 4th ed., Springer, Berlin, 1956.

[6] M. H. Lietzke and R. W. Stoughton, *J. Phys. Chem.* **68**, 3043 (1964).

[7] H. S. Harned and B. B. Owen, *The Physical Chemistry of Electrolytic Solutions*, 3d ed., Appendix A, p. 748, Reinhold, New York, 1958.

ture, and those of $BaCl_2$ were evaluated as follows. In accordance with the treatment in the previous papers,[1,2] the excess free energy of the solution G^e, that is, excess over the molality and Debye-Hückel terms, was expressed as

$$\frac{G^e}{RT} = 2n_2 \ln \gamma_2^e + 3n_3 \ln \gamma_3^e = 2 \sum_{ij} B_{ij} \frac{n_i n_j}{w} + 2 \sum_{ijk} C_{ijk} \frac{n_i n_j n_k}{w^2}, \quad (2)$$

where n represents the number of moles of each solute, w is the number of kilograms of water, and the sums are taken over each solute i, j, k = 2 (for HCl) to 3 (for $BaCl_2$); B_{ij} and C_{ijk} are interaction coefficients to be determined from the data.

Then for the HCl

$$2 \ln \gamma_2^e = \frac{\overline{G}_2^e}{RT} = \frac{\partial}{\partial n_2}\left(\frac{G^e}{RT}\right) = 4 \sum_i B_{2i} m_i + 6 \sum_{ij} C_{2ij} m_i m_j , \quad (3)$$

while for the $BaCl_2$

$$3 \ln \gamma_3^e = \frac{\overline{G}_3^e}{RT} = 4 \sum_i B_{i3} m_i + 6 \sum_{ij} C_{ij3} m_i m_j . \quad (4)$$

Hence

$$\ln \gamma_2^e = 2I \left[B_{22} + \left(\frac{B_{23}}{3} - B_{22} \right) X_3 \right] + 3I^2 \left[C_{222} + 2 \left(\frac{C_{223}}{3} - C_{222} \right) X_3 + \left(C_{222} + \frac{C_{233}}{9} - 2 \frac{C_{223}}{3} \right) X_3^2 \right], \quad (5)$$

and

$$\ln \gamma_3^e = \frac{4}{3} I \left[\frac{B_{33}}{3} + \left(B_{23} - \frac{B_{33}}{3} \right) X_2 \right] + 2I^2 \left[\frac{C_{333}}{9} + 2 \left(\frac{C_{233}}{3} - \frac{C_{333}}{9} \right) X_2 + \left(\frac{C_{333}}{9} + C_{223} - 2 \frac{C_{233}}{3} \right) X_2^2 \right]. \quad (6)$$

In Eqs. (5) and (6), X represents the ionic strength fraction of the designated component in the mixture and I represents the ionic strength of the solution, given by $I = m_2 + 3m_3$. Since, as mentioned above, Harned's rule appears to hold for the HCl in the mixtures, the coefficient in parentheses of the X_3^2 term in Eq. (5) is zero.

The total $\ln \gamma_q$ is obtained by adding the Debye-Hückel term to Eqs. (5) and (6). This term was assumed to be $\mathcal{A}\rho^{1/2} \sqrt{I}/(1 + 1.5\sqrt{I})$ for the HCl and $2\mathcal{A}\rho^{1/2} \sqrt{I}/(1 + 1.5 \sqrt{I})$ for the $BaCl_2$, where $\mathcal{A}$ is the limiting slope for a 1-1 electrolyte and ρ is the density of water, which corrects the ionic strength to a volume basis as required by the Debye-Hückel theory.

The activity coefficients of HCl in the HCl-$BaCl_2$ mixtures were fitted by the method of least squares using Eq. (5) with the coefficient of the X_3^2 term set to zero. In the first attempt the B and C coefficients were assumed to vary with temperature according to equations of the type

$$B_{iq} = B'_{iq} + B''_{iq}/T + B'''_{iq} \ln T \quad (7)$$

and

$$C_{ijq} = C'_{ijq} + C''_{ijq}/T + B'''_{ijq} \ln T . \quad (7')$$

These equations would give rise to excess enthalpies varying linearly with temperature and excess entropies varying linearly with ln T. However, convergence difficulties were encountered in the resulting 12-parameter fit, just as in the case of the HCl-NaCl mixtures studied previously.[2] This was probably caused by the parameters in Eqs. (7) and (7′) being too strongly correlated. When C_{ijq} was expressed as in Eq. (8) with only two parameters,

$$C_{ijq} = C'_{ijq} + C''_{ijq}/T , \quad (8)$$

and Eqs. (7) and (8) used in Eq. (5), then no difficulties were encountered in the least-squares determination. Equation (8) is consistent with temperature-independent excess enthalpies and entropies. In the ionic strength range studied, the contribution of the B terms is much more important than that of the C terms (and hence the difficulty in determining as many parameters in the C coefficients).

The values of B'_{22}, B''_{22}, B'''_{22}, B'_{23}, B''_{23}, B'''_{23}, C'_{222}, C''_{222}, C'_{223}, and C''_{223} were obtained directly by the least-squares fit, while the values of C'_{233} and C''_{233} were obtained by the application of Harned's rule: $C_{222} + (C_{233}/9) - (2C_{223}/3) = 0$. The additional parameters needed for calculating γ_3^e by Eq. (6), namely the coefficients B_{33} and C_{333}, were evaluated by the method of least squares using osmotic coefficient data[3,4] on $BaCl_2$ solutions. Since osmotic coefficients of $BaCl_2$ solutions have been measured only at 25 and 100°, the values of B_{33} and C_{333} were determined separately at these two temperatures and the appropriate values used in Eq. (6) to compute the activity coefficients of $BaCl_2$ in the mixtures only at these two temperatures.

The parameters for calculating the various B and C coefficients are given in Table 5.1. Activity coefficients of HCl and $BaCl_2$ in the mixtures (I = 0.5 and 1.0) calculated using these parameters are shown as the solid lines in Figs. 5.1 and 5.2. The values of the activity coefficient of HCl calculated from the observed emf values are shown as data points in Fig. 5.1.

The relationship between the B and C coefficients, as defined by Eqs. (7) and (8), and the α coefficient of Harned's rule, as well as the expressions for the partial molal free energy $\bar{G}_q$, the partial molal enthalpy $\bar{H}_q$, and the partial molal entropy $\bar{S}_q$ for component q, may be calculated using the expressions previously reported[2] in the study of HBr-KBr mixtures.

Our results at 25° may be compared with those of Harned and Gary[8] and of Rush and Johnson[9]

[8]H. S. Harned and R. Gary, *J. Am. Chem. Soc.* **76**, 5924 (1954).

[9]R. M. Rush and J. S. Johnson, *J. Phys. Chem.* **68**, 2321 (1964).

Table 5.1. Parameters of the B and C Coefficients [Eqs. (7) and (8)] for the HCl-$BaCl_2$ System over the Range 25 to 175°

$B'_{22} = 6.09924$	$B''_{22} = -227.202$	$B'''_{22} = -0.914405$
$B'_{23} = 25.62597$	$B''_{23} = -1176.159$	$B'''_{23} = -3.77226$
$C'_{222} = 0.0740066$	$C''_{222} = -23.6361$	
$C'_{223} = 0.1459287$	$C''_{223} = -51.0375$	
$C'_{233} = 0.2095128$	$C''_{233} = -93.5001$	
At 25°		
$B_{33} = 0.1310844$	$C_{333} = 0.0168507$	
At 100°		
$B_{33} = 0.0911783$	$C_{333} = 0.0105197$	

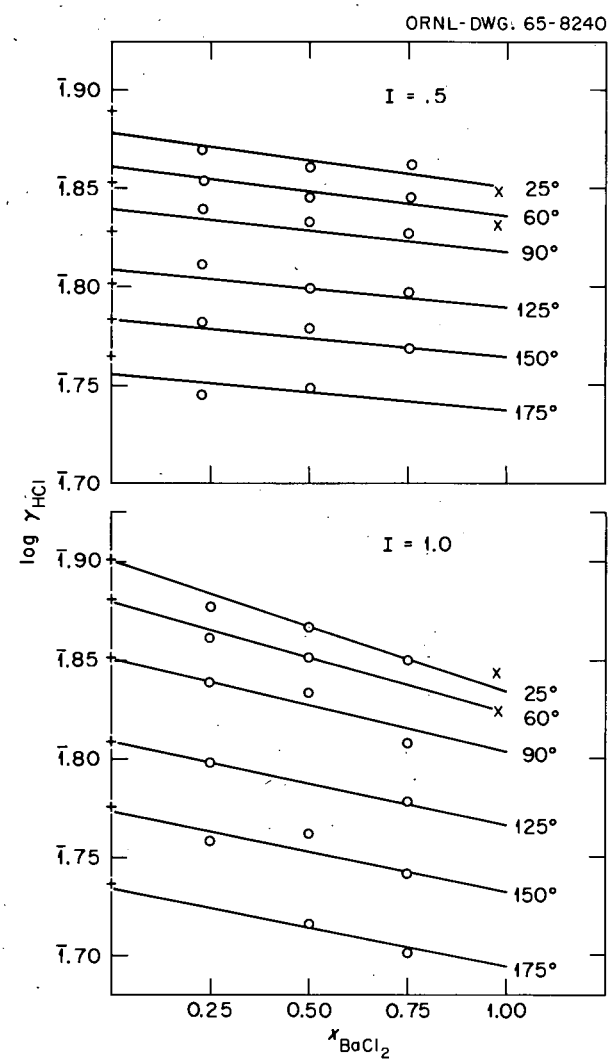

Fig. 5.1. Log γ_{HCl} vs X_{BaCl_2} in HCl-$BaCl_2$ Mixtures. Data: o this paper, + ref. 6,[2] and × ref. 7.

after expressing them in terms of Harned's α coefficients:

$$\log \gamma_2 = \log \gamma_2^0 - \alpha_{23} I_3 , \qquad (9)$$

$$\log \gamma_3 = \log \gamma_3^0 - \alpha_{32} I_2 , \qquad (10)$$

where the ionic strength ($I = I_2 + I_3$) is held constant and the superscript zero indicates a two-component or single-solute solution. The α coefficients are given by the negatives of the right-hand sides of Eqs. (5) and (6) respectively, after deletion of the first term inside each of

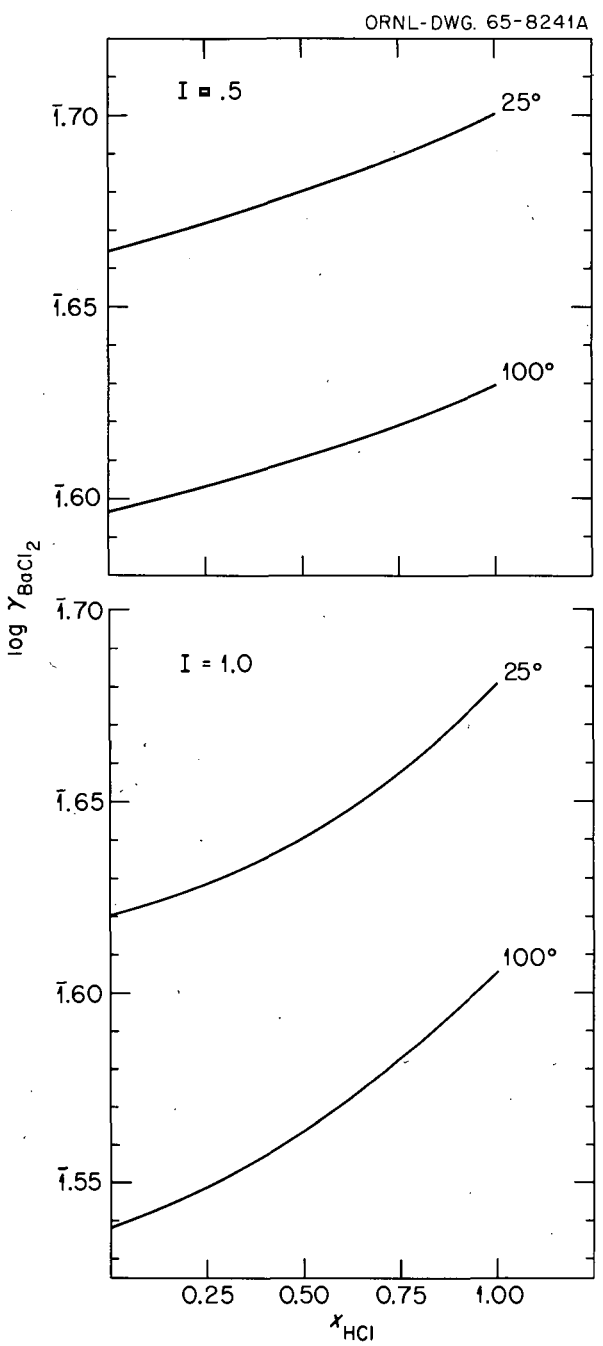

Fig. 5.2. Log γ_{BaCl_2} vs X_{HCl} in $HCl\text{-}BaCl_2$ Mixtures.

the brackets, dividing by 2.303 I_3 or 2.303 I_2, and deletion of the coefficient of X_3^2 in (5) in conformance with Harned's rule. Thus

$$\alpha_{23} = 2\left[\left(B_{22} - \frac{B_{23}}{3}\right) + I\left(3C_{222} - C_{223}\right)\right] \Big/ 2.303 \,, \quad (11)$$

and

$$\alpha_{32} = \left[\frac{4}{3}\left(\frac{B_{33}}{3} - B_{23}\right) + 4I\left(\frac{C_{333}}{9} - \frac{C_{233}}{3}\right) + 2m_2\left(\frac{2C_{233}}{3} - \frac{C_{333}}{9} - C_{223}\right)\right] \Big/ 2.303 \,. \quad (12)$$

The coefficient α_{23} depends only on ionic strength, while α_{32} depends on both I and composition (i.e., on $I_2 = m_2$). Harned and Gary[8] reported 0.0651 for α_{23} at $I = 1.0$ and 25°; on the assumption that α_{32} was independent of m_2, they found a value of -0.0716 for α_{32}. Rush and Johnson[9] by using ultracentrifuge techniques found $\alpha_{23} = 0.0666$ for data at $I = 1.0$ only. They found 0.0617 at $I = 1.0$ when all their data were treated together (I = 1.0, 2.0, 3.0, and 4.0). They obtained an essentially constant value (independent of m_2) of -0.0740 for α_{32} at $I = 1.0$. In our work Eq. (11) gives $\alpha_{23} = 0.0642$ at $I = 1.0$ and 25°, while Eq. (12) gives $\alpha_{32} = -0.0202$ at $m_2 = 0$ and -0.0602 at $m_2 = 1.0$.

It is interesting to compare the activity coefficient behavior observed in the present system with that observed in the HCl-NaCl and in the HBr-KBr systems. The plots of ln γ_2 vs X_3 (Fig. 5.1) are very similar to the corresponding plots in the HBr-KBr system in that the slopes are negative at all temperatures and at both total ionic strengths. In contrast the plots of ln γ_2 vs X_3 in the HCl-NaCl system showed a positive slope at the higher temperatures. The plots of ln γ_3 vs X_2 in the present system are very similar to those observed in the HCl-NaCl system.

THE SOLUBILITY OF Ag_2SO_4 IN $AgNO_3$ SOLUTIONS

M. H. Lietzke R. W. Stoughton

In a series of previous papers,[10] the solubility of Ag_2SO_4 in a variety of electrolyte solutions has

[10] M. H. Lietzke and R. W. Stoughton, *J. Phys. Chem.* **63**, 1183, 1186, 1188, 1190, 1984 (1959); **64**, 133, 816 (1960); **66**, 2264 (1962).

been investigated. In all of these solutions, whether the supporting electrolyte was a single salt or a salt mixture, it was shown that single-parameter empirical expressions of the Debye-Hückel type, such as

$$\ln S = \ln S_0 + \mathcal{S}_T \left[\frac{\sqrt{I}}{1 + A\sqrt{I}} - \frac{\sqrt{I_0}}{1 + A\sqrt{I_0}} \right], \quad (1)$$

could be used to describe the variation of the solubility product of Ag_2SO_4 over a wide range of temperature and ionic strength. In this equation $S_0 = 4s_0^3$, where s_0 is the solubility of Ag_2SO_4 in pure water; $\mathcal{S}_T$ is the appropriate Debye-Hückel slope; I is the ionic strength of the solution; $I_0 = 3s_0$, the ionic strength of a saturated solution of Ag_2SO_4 in pure water; and A is an adjustable parameter. As previously[10] noted, good agreement between calculated and observed solubilities was obtained when the A parameter was assumed to be temperature independent and to be either ionic strength independent or to decrease slowly with increasing ionic strength.

Although some of the Ag_2SO_4 solubility systems mentioned above contained the common anion SO_4^{2-}, none contained the common cation Ag^+. Accordingly, a study of the solubility of Ag_2SO_4 in $AgNO_3$ solutions has been undertaken to determine whether Eq. (1) could be used in describing this system also.

All solubility measurements were performed using the synthetic technique.[10] At each of the three concentrations of $AgNO_3$ used, the measurements were extended to as high a temperature as possible. Decomposition occurred in 0.056 m $AgNO_3$ solution above 125° and in 0.109 m $AgNO_3$ solution above 150°. In the case of the 0.242 m $AgNO_3$ solution, it was possible to observe both the disappearance of the crystals of Ag_2SO_4 at the lower temperatures and the reappearance of Ag_2SO_4 crystals at the higher temperatures. These latter solutions were stable to above 200°. Values of the solubility of Ag_2SO_4 in H_2O up to 100° were taken from the work of Barre,[11] while values above 100° were taken from previous work.[10]

In carrying out the calculations, it was assumed that only the species Ag^+, NO_3^-, and SO_4^{2-} existed in a solution containing Ag_2SO_4 and $AgNO_3$ dissolved in H_2O. If s is the molal solubility of Ag_2SO_4 in an $AgNO_3$ solution of molality m, then the molal solubility product of the Ag_2SO_4 is given by

$$S = (2s + m)^2 s \,. \quad (2)$$

The variation of the solubility product with ionic strength was assumed to be given by

$$\ln S = \ln 4s_0^3 + 6\mathcal{S}'_T \left[\frac{\sqrt{I}}{1 + A\sqrt{I}} - \frac{\sqrt{3s_0}}{1 + A'\sqrt{3s_0}} \right], \quad (3)$$

where $\mathcal{S}'_T$ is the Debye-Hückel limiting slope for a univalent ion and the other terms have the same significance as in Eq. (1) except that the parameter A' was set either to A, 1.0, or 1.5. In terms of the assumed species, the ionic strength of the solution is given by

$$I = m + 3s \,. \quad (4)$$

The overall calculation involved the estimation of the A parameter in Eq. (3) by the method of least squares subject to the criterion that $\sum_i (s_{obsd} - s_{calcd})_i^2$ be a minimum. For convenience in carrying out this calculation, the experimental solubility values were plotted and values of the solubility read from the curves at 25° intervals from 25 to 150°. These values were then used in all subsequent calculations.

Two different approaches were tried in estimating the value of A in Eq. (3).

1. An attempt was made to find the value of A (with A' set equal to A) which fitted the solubility of Ag_2SO_4 in the three different concentrations of $AgNO_3$ at 25° intervals from 25 to 150°. This involved the numerical evaluation of $(\partial s/\partial A)$, the partial derivative of the solubility of Ag_2SO_4 with respect to the A parameter, at each temperature and at each concentration of $AgNO_3$, so that the original estimate of the value of A could be adjusted to satisfy the least-squares criterion. Values of A ranging from 0.4 at 25° to 1.0 at the higher temperatures were obtained. No mathematical convergence difficulties were encountered in this approach. However, the agreement between the observed and calculated values of the solubility of Ag_2SO_4 was poor at the lowest concentration of $AgNO_3$. Depending on the temperature, the calculated solubilities were 10 to 25% higher than the observed solubilities. This indicated that an ionic-strength-independent value of A could not be used in describing the data.

[11] M. Barre, *Ann. chim. phys.* [8] **24**, 211 (1911).

2. A temperature-independent value of A was obtained for Eq. (3) at each of the three concentrations of $AgNO_3$ separately. With A' set to 1.0, the values of A in this case were 1.38 at 0.056 m $AgNO_3$ and 0.97 at both the higher concentrations of $AgNO_3$. The corresponding calculated values of the solubility of Ag_2SO_4 in the three different concentrations of $AgNO_3$ are plotted (solid lines) in Fig. 5.3 along with the experimental values. As can be seen, the agreement between the calculated and observed solubilities is very good. With A' set to 1.5, the values of A were 2.00 at 0.056 m $AgNO_3$ and 1.38 at 0.109 m $AgNO_3$; convergence (computational) difficulties were encountered with the 0.242 m $AgNO_3$ solution. In the two cases which did converge, the agreement between the calculated and observed solubilities of Ag_2SO_4 was almost the same as in the cases where A' was set to 1.0.

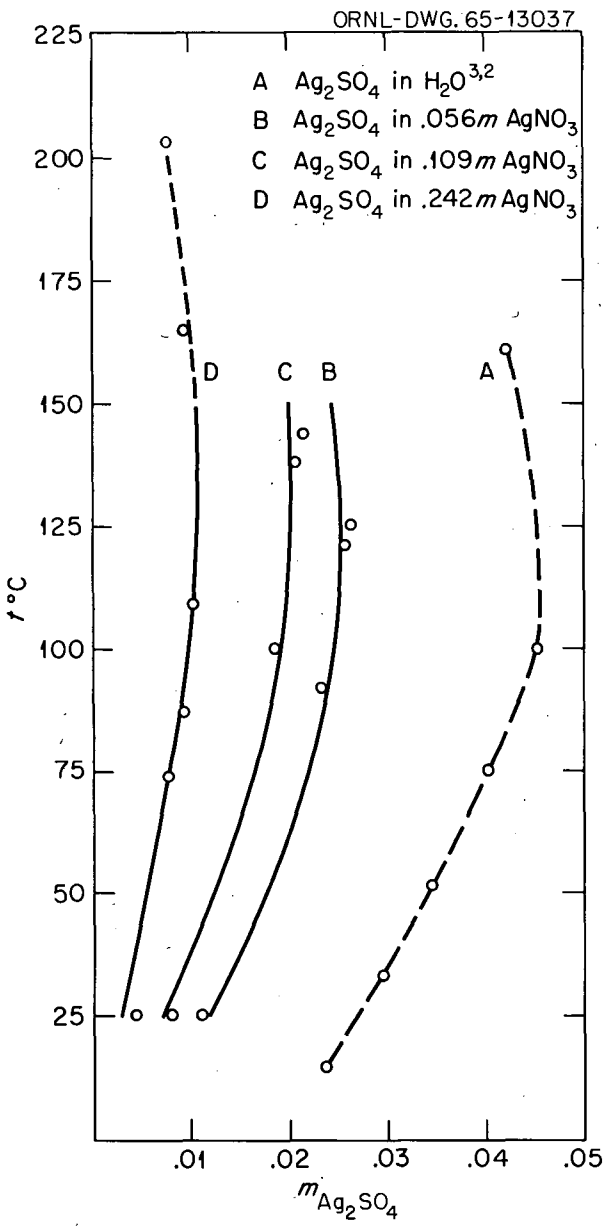

Fig. 5.3. The Solubility of Ag_2SO_4 in 0.056, 0.109, and 0.242 m $AgNO_3$ Solutions. O = observed solubilities, — = calculated solubilities.

Hence the Ag_2SO_4-$AgNO_3$ system is similar in some respects to the Ag_2SO_4-K_2SO_4 system[10] in that the molal solubility product of Ag_2SO_4 in both systems may be described using a single-parameter Debye-Hückel expression. In both cases the assumption of a temperature-independent, ionic-strength-dependent A parameter, which decreases in value as the ionic strength of the solution increases, gives the best fit of the data. However, there is a distinct difference in behavior depending on whether the Ag^+ or SO_4^{2-} is the common ion. When SO_4^{2-} is the common ion (e.g., in the Ag_2SO_4-K_2SO_4 system[10]), the effect of increasing the ionic strength (adding more K_2SO_4) is to increase the solubility of Ag_2SO_4 except at low temperatures at low concentrations (e.g., below 80° in 0.1 m K_2SO_4). Thus the activity coefficient (or ionic strength) effect is greater than the common ion effect. When Ag^+ is the common ion, an increase of Ag^+ (by adding $AgNO_3$) causes a decrease in the solubility of Ag_2SO_4 under all conditions. This difference probably results from the fact that the solubility product depends on the square of the Ag^+ activity and the first power of the SO_4^{2-} activity and from a greater activity coefficient effect of the bivalent SO_4^{2-} ion than of the monovalent Ag^+ ion.

THE SOLUBILITY OF LANTHANUM SULFATE IN SULFURIC ACID SOLUTIONS AT ELEVATED TEMPERATURES

M. H. Lietzke R. W. Stoughton

In a previous series of papers, a study of the solubility of Ag_2SO_4 in a variety of electrolyte media has been described.[12] In this work it

[12] M. H. Lietzke and R. W. Stoughton, *J. Phys. Chem.* **63**, 1183, 1186, 1188, 1190, 1984 (1959); **64**, 133, 816 (1960).

was shown that the concentration dependence of the logarithms of the equilibrium quotients and solubility products could be expressed by single-parameter expressions of the Debye-Hückel type, $\mathscr{S}\sqrt{I}/(1 + A\sqrt{I})$, where $\mathscr{S}$ is the appropriate limiting slope, I is the ionic strength of the solution, and A is an adjustable parameter. These expressions were shown to hold for ionic strengths as high as 4.0 and from 25 to 275°. In all cases best agreement between observed and calculated solubilities was obtained when each single A parameter was assumed to be temperature independent and to be either ionic strength independent or to decrease slowly with increasing ionic strength.

In the present study the solubility of $La_2(SO_4)_3$ in aqueous H_2SO_4 solutions was measured. The study was undertaken to determine whether an expression of the type used to describe the concentration dependence of the logarithm of the solubility product of Ag_2SO_4 could be used in a system where the ionic strength effect was much greater ($I = 15m$) and the limiting slope was 15 times the limiting slope for a 1-1 electrolyte (five times as high as the limiting slope used in the Ag_2SO_4 calculations).

The solubility of $La_2(SO_4)_3$ was measured in 0.234, 0.471, and 0.714 m H_2SO_4 solutions in the temperature range approximately 120 to 175° using the synthetic technique. In all cases the solubility of the $La_2(SO_4)_3$ decreased as the temperature increased. The measurements were not extended below 120° because the solubility of the $La_2(SO_4)_3$ became so high that the synthetic method employed could not be used. In order to produce a set of solubility values for use in the subsequent calculations, the raw data were plotted vs temperature and values read from the curves at 5° intervals from 135 to 160°. These values were then cross-plotted vs H_2SO_4 concentration and solubilities corresponding to concentrations of H_2SO_4 from 0.2 to 0.7 m at 0.1 m intervals read from these curves. The resulting smoothed $La_2(SO_4)_3$ solubilities are shown as the s_{obs} values in Table 5.2.

In carrying out the calculations, it was assumed that only the species La^{3+}, SO_4^{2-}, H^+, and HSO_4^- existed in a solution of $La_2(SO_4)_3$ dissolved in H_2SO_4. If s is the molal solubility of $La_2(SO_4)_3$ in H_2SO_4 of molality m, and x and y are taken as the SO_4^{2-} and H^+ concentrations, then the molality solubility product of the $La_2(SO_4)_3$ is given by

$$S = 4s^2x^3 . \tag{1}$$

By conservation of acid hydrogen, the HSO_4^- concentration is seen to be equal to $2m$ less the H^+ concentration y, and the bisulfate dissociation quotient becomes

$$Q_2 = \frac{xy}{2m - y} . \tag{2}$$

The equation for the conservation of total sulfate is

$$m + 3s = 2m - y + x ,$$

or

$$3s + y - x - m = 0 . \tag{3}$$

Equations (1), (2), and (3) represent three equations in the three unknowns (s, x, and y) which may be solved for any particular values of S and Q_2.

In accordance with previous calculations,[12] it was assumed that

$$\ln Q_2 = \ln K_2 + 4S_T \left[\frac{\sqrt{I}}{1 + A_2\sqrt{I}}\right] \tag{4}$$

and

$$\ln S = \ln (108 s_0^5) + 30\mathscr{S}_T \left[\frac{\sqrt{I}}{1 + A_S\sqrt{I}} - \frac{\sqrt{15 s_0}}{1 + A_S\sqrt{15 s_0}}\right], \tag{5}$$

where K_2 is the bisulfate acid constant, $\mathscr{S}_T$ is the Debye-Hückel limiting slope at temperature T for a singly charged ion, s_0 is the solubility of $La_2(SO_4)_3$ in water at temperature T, A_2 and A_S are adjustable parameters, and I is the ionic strength of the solution, given by

$$I = m + 9s + 2x . \tag{6}$$

The value of $\ln K_2$ as a function of temperature is known from previous work[13] to be given by the equation

[13] M. H. Lietzke and R. W. Stoughton, *J. Phys. Chem.* 65, 2247 (1961).

Table 5.2. A Comparison of Calculated Values of the Solubility of $La_2(SO_4)_3$ in H_2SO_4 with Smoothed Observed Values

$m_{H_2SO_4}$	s_{calc}	s_{obs}	$m_{H_2SO_4}$	s_{calc}	s_{obs}
	$t = 135$			$t = 140$	
0.2	0.0087	0.0100	0.2	0.0070	0.0083
0.3	0.0105	0.0108	0.3	0.0083	0.0087
0.4	0.0139	0.0131	0.4	0.0110	0.0102
0.5	0.0173	0.0162	0.5	0.0137	0.0125
0.6	0.0206	0.0202	0.6	0.0162	0.0157
0.7	0.0238	0.0248	0.7	0.0187	0.0198
	$t = 145$			$t = 150$	
0.2	0.0060	0.0072	0.2	0.0053	0.0063
0.3	0.0071	0.0074	0.3	0.0063	0.0065
0.4	0.0093	0.0085	0.4	0.0081	0.0074
0.5	0.0113	0.0103	0.5	0.0098	0.0090
0.6	0.0133	0.0128	0.6	0.0114	0.0111
0.7	0.0152	0.0162	0.7	0.0128	0.0136
	$t = 155$			$t = 160$	
0.2	0.0046	0.0056	0.2	0.0044	0.0050
0.3	0.0055	0.0057	0.3	0.0051	0.0052
0.4	0.0071	0.0065	0.4	0.0064	0.0059
0.5	0.0087	0.0079	0.5	0.0076	0.0071
0.6	0.0101	0.0098	0.6	0.0087	0.0086
0.7	0.0115	0.0123	0.7	0.0097	0.0102

$$\ln K_2 = \frac{-1283.108}{T} + 12.31995 - 0.04223215T \,. \quad (7)$$

The value of s_0, the solubility of $La_2(SO_4)_3$ in H_2O, is not known in the temperature range studied because of hydrolysis difficulties.

Thus, the overall problem involves the evaluation of A_2, A_S, and s_0 by a nonlinear least-squares procedure, subject to the restrictions represented by Eqs. (1), (2), (3), and (6).

The criterion adopted in solving the above set of equations was that $\sum_i (S_{obs} - S_{calc})_i^2$ be a minimum, where the summation is taken over the different solubilities (at different values of m) at any temperature.

When the attempt was made to determine the three parameters A_2, A_S, and s_0 on a high-speed computer, convergence difficulties were encountered which could be attributed to strong correlation between the parameters A_2 and A_S. Hence the calculation was carried out for fixed values of A_2. It was observed that when the value of A_2 was varied from 1.0 to 2.0 the value of A_S determined by least squares adjusted itself correspondingly higher, so that the overall standard error of fit was not significantly affected and the computed solubilities in all cases were practically identical.

A comparison between the smoothed observed and the calculated solubilities of $La_2(SO_4)_3$ in H_2SO_4 solutions is shown in Table 5.2, while the values of the parameters A_S and s_0 (along with their standard errors) computed with $A_2 = 1.0$ are shown in Table 5.3. As can be seen, the calculated values of the solubility of $La_2(SO_4)_3$ are slightly lower than the smoothed observed values at the lower concentrations of H_2SO_4 at all temperatures and slightly higher at the intermediate concentrations. At the highest concentration of H_2SO_4 (0.7 m), the calculated value

Table 5.3. Values of the Parameters A_S and s_0 Obtained with $A_2 = 1.0$

t	A_S	σ_{A_S} [a]	s_0	σ_{s_0} [b]
			$\times 10^{-4}$	$\times 10^{-4}$
135	1.35	0.07	2.19	0.25
140	1.38	0.09	1.73	0.26
145	1.43	0.11	1.46	0.24
150	1.48	0.10	1.26	0.18
155	1.47	0.11	1.00	0.15
160	1.56	0.09	0.92	0.11

[a]Standard error in A_S.
[b]Standard error in s_0.

of the solubility is again lower than the observed value. Adding a term linear in ionic strength to Eq. (5) in an attempt to obviate this systematic trend in the calculated solubilities caused convergence difficulties. In view of the difficulty in weighing the small amounts of $La_2(SO_4)_3$ (a few milligrams) in preparing the solubility tubes for the determinations at low acid concentrations and in view of the small concentrations involved, the overall fit of the assumed model to the data is about as good as can be expected. Hence the applicability of expressions of the type given by Eqs. (4) and (5) even in systems involving a salt of higher valence type seems to be warranted.

THE APPARENT MOLAL VOLUMES IN AQUEOUS SOLUTION OF LiCl AND NaCl AT 5 AND 35°

Fred Vaslow

The densities of aqueous solutions of LiCl and NaCl have been measured at 5° and for LiCl also at 35°. Apparent molal volumes (ϕ_V) calculated from the densities, minus the theoretical limiting law slope, are shown as functions of $\sqrt{c}$ in Fig. 5.4 for LiCl and in Fig. 5.5 for NaCl. The curve at 25° has been previously reported.[14] Point-to-point differentiations, that is, $\Delta\phi_V/\Delta\sqrt{c}$ for each successive pair of points have been made for the

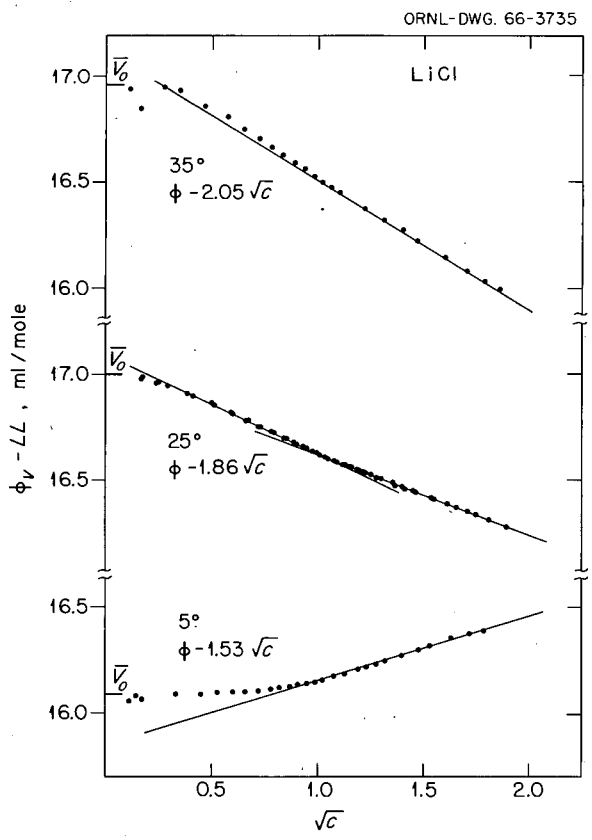

Fig. 5.4. The Apparent Molal Volumes of LiCl at 5, 25, and 35° with Limiting Law Subtracted from Experimental Points.

curves and are shown in Fig. 5.6 for each individual LiCl run and in Fig. 5.5 for the 5° NaCl run. The point-to-point differentiation requires data of a very high precision and consistency in order that the derived curve be reasonably coherent. The 25° NaCl runs were the first experiments of this work, and the results are judged as not justifying the differentiation, which later improvements in technique and apparatus made possible.

Although the number of points is too small and the lowest concentration too high for an accurate confirmation of the limiting law, the data are not inconsistent with it, and, in fact, provide a better confirmation than previously available. Using the theoretical slopes[15] for extrapolation to zero concentration, values of $\bar{V}_2^0$ are 16.09, 16.99, and

[14]F. Vaslow, *Chem. Div. Ann. Progr. Rept. May 31, 1965*, ORNL-3832, p. 87.

[15]O. Redlich and D. M. Meyer, *Chem. Rev.* **64**, 221 (1964).

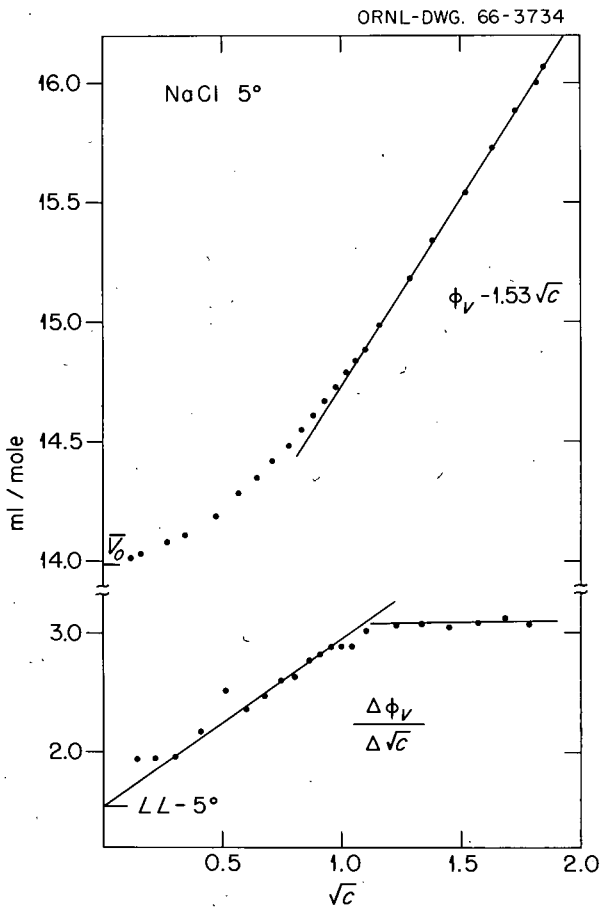

Fig. 5.5. The Apparent Molal Volume of NaCl at 5° Minus Limiting Law and $\Delta\phi_V/\Delta\sqrt{c}$ vs $\sqrt{c}$ for each successive Pair of Points.

16.95 ml/mole at 5, 25, and 35°, respectively, for LiCl, and 13.99 and 16.63 ml/mole at 5 and 25° for NaCl. A preliminary result for NaCl at 35° gives $\bar{V}_2^0$ as 17.62 ml, probably valid to ±0.03 ml and also apparently consistent with the theoretical slope.

In the previous annual report,[14] the existence of a salt-induced transition of liquid structure was suggested on the basis of well-defined changes in the curve of ϕ_V vs $\sqrt{c}$ for LiCl.[16] In particular, the apparent molal volume of LiCl above 0.1 *m* appeared to be accurately a linear function of $\sqrt{c}$ with the exception of a short region around 1 *N* where a small change in slope occurred.

[16]F. Vaslow, *J. Phys. Chem.*, in press.

The results at 5 and 35° do not show this linearity below 1 *N*; nevertheless the transition is still clearly evident in the differential curves. Each of the LiCl curves shows an abrupt increase in slope at about 1 *N*, while the NaCl differential curve suggests a sudden change in curvature of the apparent volume curve. While the statistics for any individual curve do allow other interpretations, the appearance at the same concentration of the abrupt changes points to some real phenomenon in the solution in this region of concentration.

The results obtained from the density measurements may be compared with results based on NMR work,[17,18] where curves with transitions are also reported, although with a different interpretation. For LiCl at 20° the NMR work gives 1.13 *M* as the transition point, compared with the density value of 1.14 at 25°. From the NMR work the transition appears strongly at 10° but disappears at 0°. The transition in the differential volume curve at 5° does appear substantially more diffuse than at higher temperatures, apparently consistent with the NMR work.

[17]P. A. Zagarets, V. J. Ermakov, and A. P. Grunau, *Zh. Fiz. Khim.* **39**, 9 (1965) [*Russ. J. Phys. Chem.* (1965) 4].

[18]P. A. Zagarets, V. J. Ermakov, and A. P. Grunau, *Zh. Fiz. Khim.* **39**, 1552 (1965) [*Russ. J. Phys. Chem.* (1965) 826].

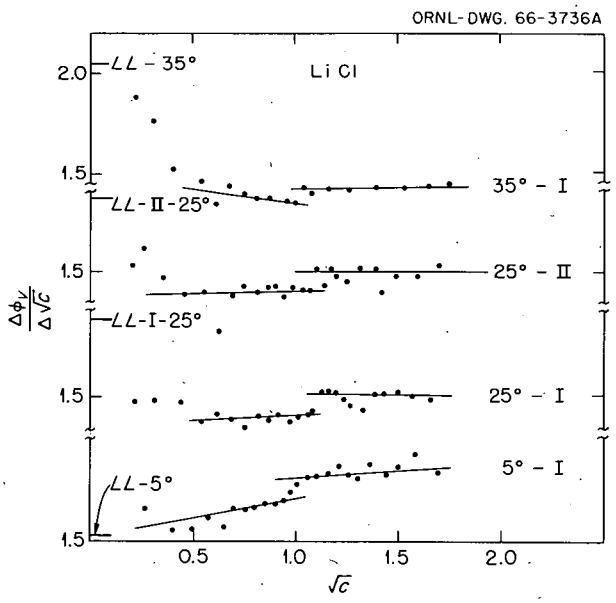

Fig. 5.6. $\Delta\phi_V/\Delta\sqrt{c}$ vs $\sqrt{c}$ for Each LiCl Run.

For $NaCl^{17}$ and KCl^{17} the temperatures of the NMR runs are not given. However, the transitions are given as at 0.98 and 0.82 *M* respectively, compared to 0.85 and 0.81 *M* from the density measurements. The 5° NaCl transition (density measurements) appears to be about at 1.0 *N*. These results exhibit a surprising consistency between the NMR and the density measurements, but a judgment as to the importance of the agreement must await resolution of some questions about the NMR results, specifically the effect of the added Co^{2+} ion and the real precision of the data. It is desirable that the 25° NaCl runs be repeated using the more developed apparatus and techniques now available.

HYDROLYSIS OF THORIUM(IV)

Forest C. Hentz, Jr.[19] J. S. Johnson

We have completed an investigation of Th(IV) hydrolysis which has been under way off and on for more than a decade. During the past year, measurements by equilibrium ultracentrifugation (interference optics) of thorium perchlorate aggregation were repeated and expanded. The range from hydroxyl number, **n** [average number of hydroxides bound per Th(IV)], 0 to 3 was covered; Th(IV) concentrations were 0.025 to 0.1 *M* over most of the range, and the solutions contained $NaClO_4$ as supporting electrolyte, total perchlorate being 1 *M*. The aggregates appeared to reach chemical equilibrium for **n** $\lesssim$ 2.5, but, at **n** = 3, average degrees of polymerization were much higher and were continuing to increase with time. In general, the dependence of sedimentation on Th(IV) concentration indicated that the average charge per monomer unit, z', is not the maximum 4 − **n**, that is, that there is complexing of perchlorate by Th(IV) species. For example, at **n** = 2, the average degree of polymerization, N_w, appeared to be ~3.6 and $z' \sim 1.3$ (Fig. 5.7).

The values of N_w obtained from the intersection of graphs similar to Fig. 5.7 are summarized in Fig. 5.8. In general, agreement with the results of a light-scattering study[20] is fairly good. From these results, several hydrolysis schemes in the literature can be eliminated from consideration. Agreement with two rather different proposals (Fig. 5.8), based on potentiometric data,[21,22] however, indicates that studies by other techniques will probably be necessary to establish definitively the major species formed when Th(IV) hydrolyzes.

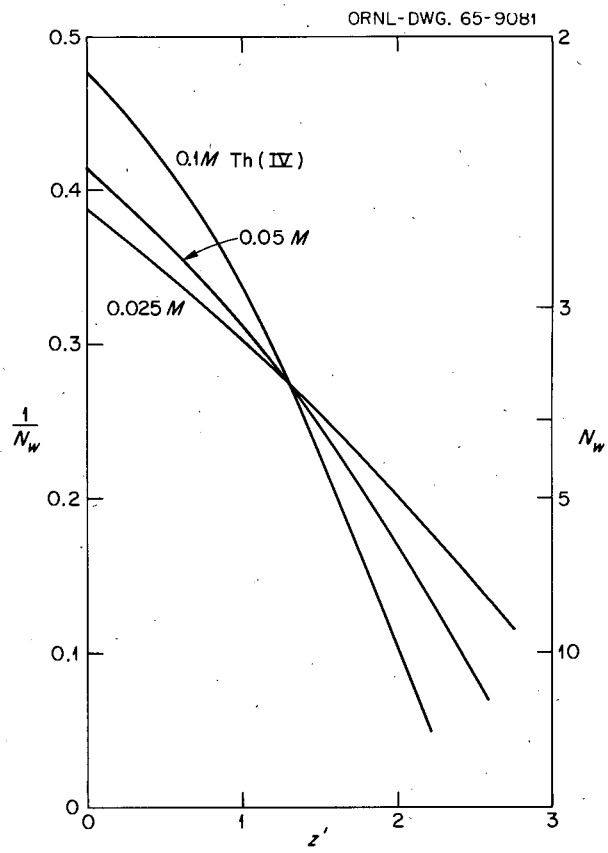

Fig. 5.7. Degree of Polymerization of Hydrolyzed Thorium Perchlorate (n = 2.0) Computed as a Function of Assumed Charge, z'. Supporting Electrolyte, $NaClO_4$; solution 1 *M* in total perchlorate. 11,273 rpm.

[19]North Carolina State University, Raleigh. Summer Research Participant, Oak Ridge Institute of Nuclear Studies, 1965.

[20]F. C. Hentz and S. Y. Tyree, *Inorg. Chem.* 4, 873 (1965).

[21]S. Hietanen and L. G. Sillén, *Acta Chem. Scand.* 18, 1018 (1964).

[22]C. F. Baes, N. J. Meyer, and C. E. Roberts, *Inorg. Chem.* 4, 518 (1965).

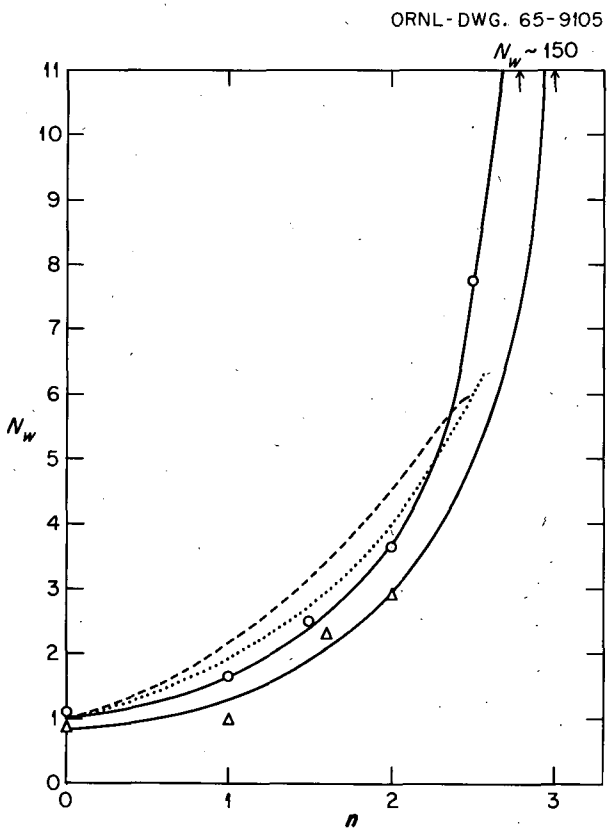

Fig. 5.8. Weight Average Degree of Polymerization of Hydrolyzed Th(IV) Solutions as a Function of Hydroxyl Number (25°).

—O— equilibrium ultracentrifugation } 1*M* perchlorate
—△— light scattering (Hentz and Tyree) }

Interpretation of acidity measurements in terms of species $Th_N OH_{nN}$: ..... Baes *et al.*, 1*M* perchlorate, [*N*, *nN*] of [1,1] [1,2] [2,2] [4,8] [6,15]. ----- Hietenan and Sillén, 3*M* chloride, [*N*, *nN*] of [1,2] [2,2] [2,3] [6,14] [6,15].

ION EXCHANGE SEPARATIONS

F. Nelson H. O. Phillips
D. C. Michelson K. A. Kraus

Cation Exchange of the Elements in HBr Solutions

A systematic study of the adsorption behavior of elements on a Dowex 50 cation exchange resin in dilute to concentrated (12 *M*) HBr has been carried out. The adsorption data are summarized in Fig. 5.9, a "periodic table" arrangement of plots of log D_v vs molarity of HBr. The adsorption functions are comparable, since they refer to the same batch of Dowex 50-X4 resin and were determined under conditions of low loading, *L* (usually less than 1% capacity of the resin) by the elements. The principal features of the adsorption functions may be summarized as follows:

1. Many elements which form very stable bromide complexes, for example, platinum elements, are not significantly absorbed from *ca.* 0.5 to 12 *M* HBr; presumably they also are nonadsorbable at HBr concentrations lower than 0.5 *M* provided adsorbable hydrolytic species are not formed. Similar low adsorbability is shown by most of the nonmetallic elements as their common acids, for example, HF, H_2SO_4, H_3PO_4, and $HClO_4$.
2. Several elements, for example, Mg(II), Zn(II), Cd(II), Pb(II), Al(III), and V(IV), are strongly adsorbed from very dilute HBr solutions. Adsorbability decreases with increasing HBr concentration and becomes negligible in dilute to moderately concentrated HBr solutions. For some of these elements, particularly those which form stable and moderately stable but weakly adsorbed bromide complexes, for example, Cd(II) and Pb(II), adsorption decreases very steeply with increasing *M* HBr and becomes negligible at relatively low HBr concentrations.
3. Most elements in HBr solutions show adsorption minima. Many of these elements,

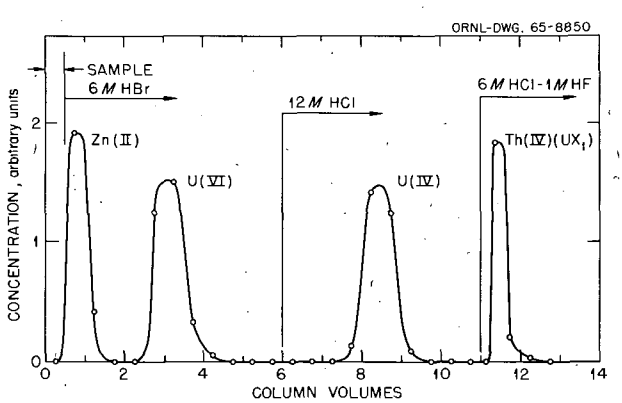

Fig. 5.9. Separation of Zn(II), U(VI), U(IV), and Th(IV) by Cation Exchange. Dowex 50-X4, 0.28 cm^2 × 4 cm column, 25°C.

Ca(II), R.E.(III), Th(IV), etc., presumably are adsorbed at all HBr concentrations as cationic species. Others, however, for example, Fe(III), Ga(III), and In(III), apparently are adsorbed as cationic species at low HBr concentrations and as anionic species at high HBr concentrations.

4. Some elements, for example, Au(III), Tl(III), and Po(IV), which presumably exist in HBr solutions as negatively charged bromide complexes over a wide range of HBr concentration, show the expected low adsorbability in dilute HBr solutions, but are significantly adsorbed from strong HBr solutions apparently as negative complexes.

Numerous column separations may be designed from the data given in Fig. 5.9. The wide differences in adsorption behavior in dilute HBr solutions permit many separations in which elements are adsorbed from dilute HBr (or other media) and sequential elution is accomplished with HBr solutions of progressively increasing HBr concentration. Conversely, many elements may be adsorbed from concentrated HBr solutions and sequential elution achieved with solutions of decreasing HBr concentration or with other acids or acid mixtures, for example, HCl, HNO_3, HBr-HF, and HCl-HF solutions.

Two typical separations involving elution with HBr solutions are shown in Figs. 5.10 and 5.11; the first separation involves the six alkaline-earth elements, and the second illustrates separation of different oxidation states of the same element [U(IV) and U(VI)] from each other and from Zn(II) and Th(IV). Details for these and many other column separations are described in a paper recently submitted to the *Journal of Chromatography*.

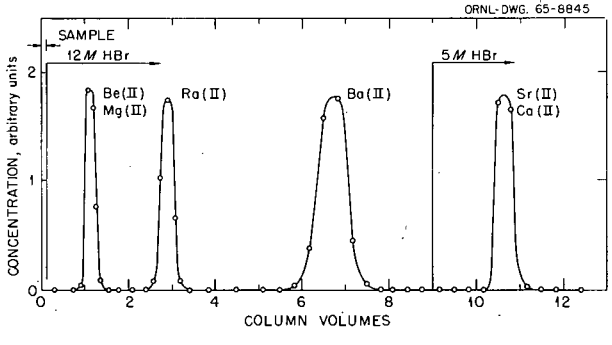

Fig. 5.10. Separation of Alkaline Earths in HBr Solutions. Dowex 50-X4, 0.25 $cm^2 \times 6$ cm column, 60°C.

Comparison of Adsorbabilities in HCl, HBr, and $HClO_4$ Solutions

Adsorption data for the elements in 9 *M* HBr are compared in Table 5.4 with similar previously published data for 9 *M* HCl and 9 *M* $HClO_4$ solutions.[23] In general, the elements are more strongly adsorbed from 9 *M* $HClO_4$ solutions and, if adsorbed at all, are more strongly adsorbed from 9 *M* HBr solutions than from 9 *M* HCl solutions.

Separation of Alkali-Metal Ions

A systematic study of the cation exchange behavior of alkali-metal ions, Li^+ to Fr^+, in HCl-water and HCl-methanol-water solutions has been carried out with sulfonic acid cation exchangers of the polystyrene-divinylbenzene and phenol-formaldehyde types. Separability of potassium, rubidium, and cesium in HCl solutions has also been investigated with a zirconium phosphate cation exchanger. The results of these studies along with detailed procedures for separating alkali-metal ions from each other have been published.[24]

PHYSICAL CHEMISTRY OF POLYELECTROLYTE SYSTEMS

Structural Effects on the Enthalpy and Entropy of Dilution of Aqueous Solutions of the Quaternary Ammonium Halides at 25°C[25]

G. E. Boyd J. W. Chase Fred Vaslow

Heat of dilution and solution measurements were performed at 25° on the quaternary ammonium halides derived from tetramethylammonium chloride and bromide by substituting either a β-hydroxyethyl or a benzyl group, or both, for methyl groups.

[23] F. Nelson, T. Murase, and K. A. Kraus, *J. Chromatog.* 13, 503 (1964).

[24] F. Nelson, D. C. Michelson, H. O. Phillips, and K. A. Kraus, *J. Chromatog.* 20, 107 (1965).

[25] Presented before the Division of Physical Chemistry, 152nd National Meeting of the American Chemical Society, New York, September 1966.

ORNL-DWG. 66-1162

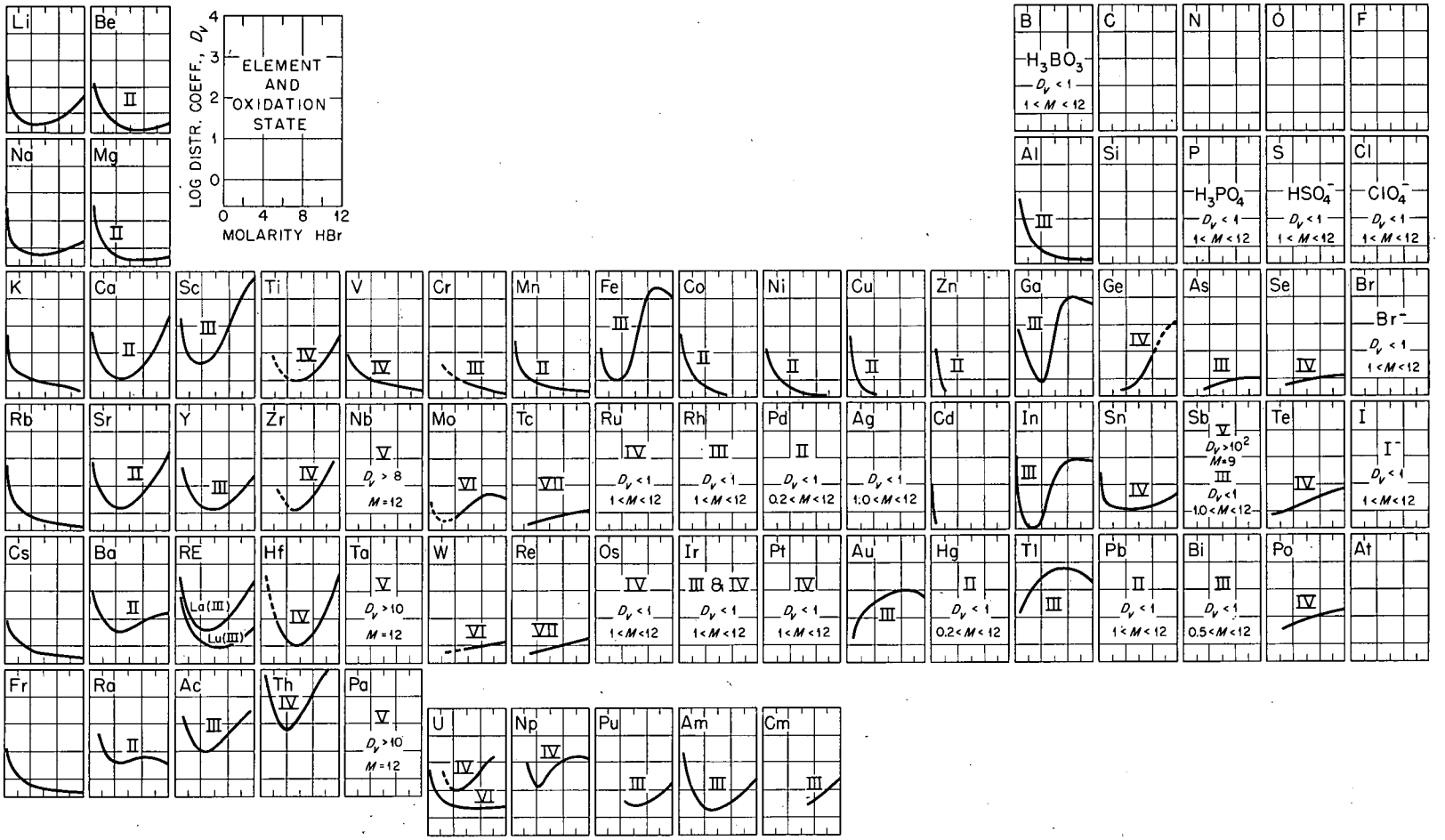

Fig. 5.11. Adsorption of the Elements from HBr Solutions by a Cation Exchange Resin.

Table 5.4. Distribution Coefficients of Elements in 9 *M* HCl, 9 *M* HBr, and 9 *M* $HClO_4$ (Dowex 50-X4)

Element	Distribution Coefficient, D_v		
	9 *M* HCl	9 *M* HBr	9 *M* $HClO_4$
Ac(III)	8.5	7.8×10^1	1×10^4
Ag(I)	<1	<1	2.4
Al(III)	0.6	0.3	3.8
Am(III)	1.2	5.9	2.0×10^3
As(III)	<1	<1	0.4
As(V)	<1		1.4
Au(III)	1.2×10^2	6.1×10^1	
B (H_3BO_3)	<1	<1	1
Ba(II)	4.5	1.1×10^1	4.9
Be(II)	0.3	<1	1.3
Bi(III)	<1	<1	8.6×10^2
Br (Br^-)	<1		<1
Ca(II)	3.2	6.4	1.4×10^2
Cd(II)	<1	<1	1.7×10^1
Cl (Cl^-)	<1	<1	<1
Cl (ClO_4^-)		<1	
Cm(III)	1	6.4	$>1 \times 10^3$
Co(II)	0.3	<1	1.5
Cr(III)	<1	<1	2.0
Cr(VI)	<1		$>1.0 \times 10^2$
Cs(I)	<1	<1	0.6
Cu(II)	0.4	<1	1.2
F (HF)	<1	<1	<1
Fe(III)	3×10^2	2.5×10^3	1.8×10^1
Fr(I)	<1	<1	<1
Ga(III)	3.3×10^2	1×10^3	1.3×10^1
Hf(IV)	<1	5.4	9.6×10^1
Hg(II)	<1	<1	7
I (I^-)	<1	<1	<1
In(III)	<1	8.0×10^1	9.5
Ir(III)	<1	<1	
Ir(IV)	<1	<1	
K(I)	<1	<1	0.3
Li(I)	<1	1.0	1.8
Mg(II)	0.3	<1	1.9
Mn(II)	0.4	<1	1.9×10^1
Mo(VI)	<1	4.5	8.7×10^2
N (NO_3^-)	<1		1.5
Na(I)	<1	<1	<0.5
Nb(V)	1.6	>3	$>1 \times 10^3$
Ni(II)	<1	<1	1.0
Np(IV)		1.6×10^2	
Np(VI)	<1		$>1.0 \times 10^2$
Os(IV)	<1	<1	
P (H_3PO_4)	<1	<1	1
Pa(V)	<1	$>1 \times 10^1$	$>1 \times 10^3$
Pb(II)	<0.5	<1	1.9×10^1
Pd(II)	<1	<1	
Po(IV)	<1	1.2×10^1	<1
Pt(IV)	<1	<1	
Pu(III)		6	
Pu(VI)	<1		$>1 \times 10^2$
R.E.(III)			
La(III)	4.5	1.7×10^1	3.3×10^3
Eu(III)		7.2	2.0×10^3
Yb(III)	1.0		1.3×10^2
Lu(III)	0.8	1.3	8.7×10^1
Ra(II)	2.5	5.6	2.0
Rb(I)	<1	<1	<0.5
Re(VII)	<0.8	1.3	<1
Rh(III)	<1	<1	
Ru(IV)	<1	<1	
S (HSO_4^-)	<1	<1	1
Sb(III)	<1	<1	1
Sb(V)	2×10^3	$>1 \times 10^2$	
Sc(III)	1.7×10^1	3.3×10^2	7.2×10^5
Se(IV)	<1	1.2	0.7
Sn(IV)	<1	1.7	
Sr(II)	3.5	8.7	2.9×10^1
Ta(V)	1	$>1 \times 10^1$	$>1 \times 10^3$
Tc(VII)	<0.5	<2	<1
Te(IV)	<1	4.0	2.8
Th(IV)	2.8×10^1	3.6×10^3	$>1 \times 10^7$
Ti(IV)	1	3.0	1.9×10^3
Tl(III)	5.3	6.0×10^2	1
U(IV)		$>1 \times 10^2$	
U(VI)	0.5	2.3	3.8×10^3
V(IV)	<1	<1	2.1×10^1
V(V)	2		$>1 \times 10^2$
W(VI)	<1	<1	$>5 \times 10^2$
Y(III)	1.6	3.5	5.8×10^2
Zn(II)	<1	<1	1.8
Zr(IV)	1	8	2.1×10^2

Heat was absorbed on dilution of all the salts except with (β-hydroxyethyl)benzyldimethylammonium fluoride, whose solutions evolved heat. The measured apparent molal heat contents, ϕ_L, were combined with free energy data (osmotic and activity coefficients) to obtain $\overline{S}_1$-S_1°, the relative partial molal entropy of the solvent. The concentration dependence of $\overline{S}_1$-S_1° indicated that the substitution of a β-hydroxyethyl or a benzyl for a methyl group in tetramethylammonium cation increased its water-structure-breaking properties. Apparent molal heat content differences, $\Delta\phi_L$, were compared with standard heats of anion exchange, ΔH°, for several cross-linked strong-base exchangers based on the (β-hydroxyethyl)benzyldimethylammonium group.

Structural Effects on the Osmotic and Activity Coefficients of the Quaternary Ammonium Halides in Aqueous Solutions at 25°[26]

G. E. Boyd A. Schwarz[27] S. Lindenbaum

The quaternary ammonium halides derived from tetramethylammonium chloride and bromide by substituting either a β-hydroxyethyl or a benzyl group, or both, for methyl groups were employed in a study of the effect of cation structure on electrolyte behavior in aqueous solution. The osmotic and mean molal activity coefficients of the (β-hydroxyethyl)trimethylammonium (choline) salts were slightly smaller than those for the corresponding tetramethylammonium salts at all concentrations. The coefficients for benzyltrimethylammonium chloride and bromide were appreciably smaller than those for Me_4NCl and Me_4NBr, respectively, while those for (β-hydroxyethyl)benzyldimethylammonium chloride and bromide were slightly smaller than those for the benzyltrimethylammonium salts at all concentrations. The "water-structure-breaking" action of the β-hydroxyethyl group was assumed to be the cause for the lower coefficients of the choline halides relative to the tetramethylammonium salts. The very small activity coefficients of the benzyl- and the ethanolbenzyl-substituted derivatives have provided a basis for understanding the relatively large selectivity coefficients for bromide over chloride ion shown by cross-linked strong-base anion exchangers.

[26]Published in *J. Phys. Chem.* **70**, 821 (1966).

[27]Visiting Scientific Staff Member from Israel.

Thermodynamics of Aqueous Solutions of Tetra-*n*-alkylammonium Halides. Enthalpy and Entropy of Dilution[28]

S. Lindenbaum

Heats of dilution of tetramethyl-, -ethyl-, and -*n*-propylammonium chloride, bromide, and iodide and tetra-*n*-butylammonium chloride and bromide were measured at 25° from near saturation to 0.2 *m*, or lower, to final concentrations of less than 0.003 *m*. The apparent molal heat contents, ϕ_L, were combined with the previously reported free energy data (osmotic and activity coefficients) to obtain the excess apparent molal entropies. A comparison of the apparent molal free energy, enthalpy, and entropy reveals that the values of the free energy are small compared to the enthalpy and entropy. It is suggested, therefore, that structural inferences drawn from free energy information alone can be misleading and that structural models describing these solutions must account for the very pronounced entropy and heat effects observed.

Thermodynamic Quantities in the Exchange of Lithium with Cesium Ion on Cross-Linked Phosphonic Acid Cation Exchangers[29]

K. E. Becker[30] S. Lindenbaum G. E. Boyd

Calorimetric measurements showed that heat was absorbed in the preferential uptake of lithium ion from dilute alkaline aqueous solutions in exchange reactions with cesium ion in cross-linked nuclear and methylene phosphonic acid–type cation exchangers. Standard heats, ΔH°, and entropies, ΔS°, of exchange were 0.89 and 1.20 kcal/mole and 4.1 and 6.4 eu respectively. As with cross-linked polymethacrylic acid ion exchangers, the increase in ΔS° was attributed principally to the decrease in Li^+ ion hydration in the exchange reaction. Site binding of Li^+ ion was postulated as the cause for the alkali-metal cation ion exchange affinity sequence: $Li^+ > Na^+ > K^+ > Rb^+ > Cs^+$.

[28]Published in *J. Phys. Chem.* **70**, 814 (1966).

[29]Submitted to the *Journal of Physical Chemistry*.

[30]Temporary summer employee, 1965.

WATER RESEARCH PROGRAM

Hyperfiltration Studies[31]

W. H. Baldwin K. A. Kraus
C. E. Higgins A. E. Marcinkowsky
J. S. Johnson H. O. Phillips
A. J. Shor[32]

Salt Filtration by a Porous Glass. – Dresner and Kraus[33] have analyzed theoretically the equilibrium distribution of electrolyte solutes between a solution and a porous body having charged (ion exchange) walls. They found that one might expect substantially lower concentration of salt inside pores of diameters of the order of 100 A than in the solution phase, though, of course, the exclusion is not expected to be as strong as with an ion exchanger having the same charge homogeneously distributed. As a consequence of this exclusion, if solution is forced through the porous body at a rapid enough rate, salt should be filtered out.

Since unfired Vycor glass has pores of remarkable uniformity and is composed of an inorganic ion exchanger, silica, we have attempted to test Dresner's predictions with it. We cut membranes of 0.5 to 1 mm thickness from stock having pores peaking at 50 A diameter and tested them in a hyperfiltration apparatus, in which pressurized (35 to 100 atm) salt solution is circulated by the supported frits. The concentration of effluent, c_ω, is compared with that of the feed, c_f, to obtain rejection,

$$R_{obs} = (c_f - c_\omega)/c_f .$$

Some typical results are summarized in Table 5.5.

At the acidity of air-equilibrated salt solutions (no additives), silica is a cation exchanger of low capacity. As one would predict from this, Vycor rejects a small fraction of NaCl and somewhat more of Na_2SO_4 (which has a divalent coion) at the same equivalent concentration. Less predictably, the effluent solutions with 0.015 *M* $MgCl_2$ were more concentrated than the feed; similar negative rejections were observed with $CaCl_2$ and $La(NO_3)_3$, which like the $MgCl_2$ have polyvalent counterions.

Table 5.5. Hyperfiltration Properties of Unfired Vycor Glass

Feed	Additive	Salt Rejection (%)
0.03 *M* NaCl		5–10
0.01 *M* NaCl	pH 10	55
0.03 *M* NaCl	pH 10, silicate	35
0.03 *M* NaCl	Th(IV)	55
0.015 *M* Na_2SO_4		20
0.005 *M* Na_2SO_4	pH 10, silicate	70
0.015 *M* $MgCl_2$		–10
0.02 *M* $MgCl_2$	Th(IV)	45

We have investigated the effect on rejection of two manipulations which should vary the charge density of the pore walls. Increase of pH should increase the cation exchange capacity, and in Table 5.5 it appears that rejection indeed increases when the pH of the solution was increased to ~10; furthermore, increase of NaCl rejection with decreasing feed concentration is qualitatively in accord with an ion exchange mechanism. The other method of increasing charge density is adsorption of multivalent ions; here we used 0.001 *M* Th(IV), added to the feed as $ThCl_4$, and rejection increased substantially.

Although these observations (except those involving polyvalent counterions) can be understood qualitatively in terms of ion exchange properties of the solid and of their modification, we have not yet progressed to the point of testing to what extent theory predicts the observations quantitatively. The permeation rates we observed are too slow (of the order of 0.5 cm/hr) for practical use of these frits in desalination. However, if usable membranes could be prepared in much thinner configurations, in which the benefits in permeation rates expected from their looser structure would be realized, they might be of interest in treatment of dilute feeds, even with the low rejections attained.

[31]Research sponsored by the Office of Saline Water, U.S. Department of the Interior, under Union Carbide Corporation's contract with the U.S. Atomic Energy Commission.

[32]Reactor Chemistry Division.

[33]L. Dresner and K. A. Kraus, *J. Phys. Chem.* **67**, 990 (1963); L. Dresner, *J. Phys. Chem.* **69**, 2230 (1965).

Hyperfiltration by Dynamically Created Membranes. – During the past year, we have found that hyperfiltration by porous materials can occur not only with bodies having holes similar in size to those of unfired Vycor, but with pores of much larger size, if the feed solution contains suitable additives. An example is given in Fig. 5.12, which outlines the results of a hyperfiltration experiment with a 0.2-μ (pore sizes listed in this account are nominal values specified by the manufacturer) silver filter, a *ca.* 0.02 *M* NaCl feed, and 0.002 *M* $ThCl_4$ additive. As solute was rejected, concentration varied more than could be conveniently controlled by additions, and the ranges are listed in the legend. The initial, very high, permeability dropped about three orders of magnitude in the first hour and leveled off at about 100 gpd/ft^2; concurrently, the rejection of NaCl and thorium increased, that of NaCl being about 40% and of Th(IV) about 80% after 1 hr. Permeation dropped and rejection rose more slowly after this, rejection of thorium becoming virtually complete in a few days.

We have observed similar behavior with many different porous bodies and additives; Table 5.6 summarizes several examples. Besides the substrates mentioned in the table, rejecting layers have been formed on Millipore filters, on sintered glass (ultrafine), on other porous metals, and on porous carbon tubes. Pore sizes have ranged up to 5 μ. Other additives with which rejecting membranes have been prepared include humic acid, ground-up ion exchange beads of low ($\frac{1}{2}$%) cross linking, other hydrolyzable ions and their hydrous oxides, and other polyelectrolytes. The most successful additives to date have been those which might be expected to give an ion exchange layer. Rejections have also been obtained with neutral additives (e.g., polyvinylpyrrolidone), but values have been so low (*ca.* 20%) that they could possibly be ascribed to corrosion products or other impurities rather than to the neutral polymers.

Properties of these membranes are not very reproducible; rejections and flows obtained for a given set of conditions frequently are different, and decreases of permeation rates, accompanied by low rejections, occasionally occur when no additive is intentionally present. We do not understand many aspects of these phenomena, but some statements can be made with reasonable confidence. For salt to be filtered, a rejecting

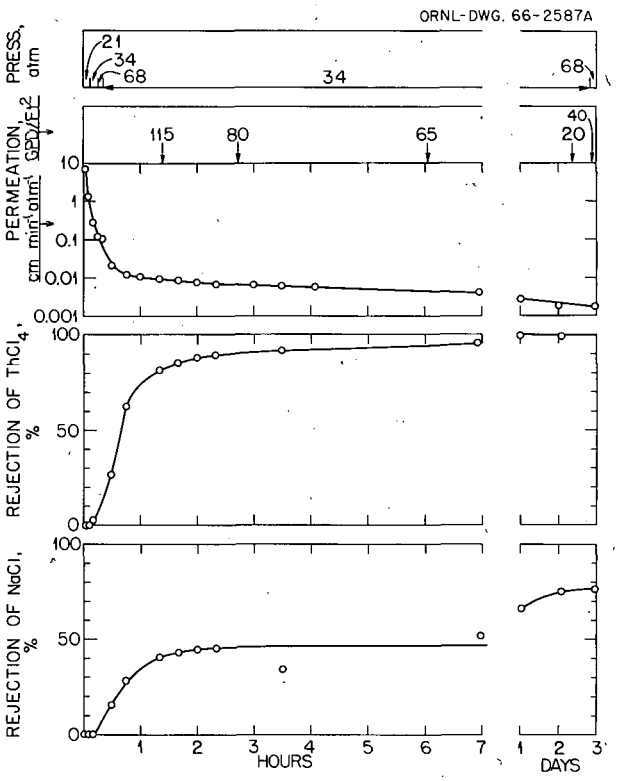

Fig. 5.12. Hyperfiltration with Silver Frit, Th(IV) Additive. Nominal pore size, 0.2 μ; feed, 0.018 to 0.026 *M* NaCl with 0.0014 to 0.0026 *M* $ThCl_4$.

layer much more compact than implied by the pore sizes (0.1 to 5 μ) must be dynamically formed. To be consistent with the high permeation rates observed, the layer must be much thinner than the thicknesses of the porous bodies, and, in fact, usually must be no thicker than a few microns. It must also be formed at the pressurized-feed–porous-body interface – otherwise the salt concentration buildup at the interface when rejection occurs would not be dissipated by the circulating stream, and observation of rejection would be masked by concentration polarization. The alpha activity of the two sides of 40-μ-thick silver frits after formation of a dynamic membrane with $ThCl_4$ containing feed confirms this; in the cases checked, the counting rate from the feed side was 5 to 40 times higher than that from the effluent side. Since frequently the size of the additive molecules is clearly far less than the pore sizes, it seems likely that

Table 5.6. Hyperfiltration with Dynamically Created Membranes

Feed	Additive	Membrane, Pore Size (nominal)	Pressure (atm)	Permeation[a] (cm/min)	Rejection (%)
0.02 *M* NaCl	0.002 *M* $ZrOCl_2$	0.2 μ silver	140	0.9	85
0.02 *M* NaCl	0.0001 *M* $ThCl_4$	0.5 μ porcelain	25	0.3	75
0.02 *M* NaCl	0.000003 *N* BTMAC[b]	0.2 μ silver	35	0.25	62
0.01 *M* $MgCl_2$	0.000003 *N* BTMAC	0.2 μ silver	35	0.25	81
0.025 *M* Na_2SO_4	0.001 *N* PSS[c]	0.3 μ carbon	40	0.25	45
0.01 *M* NaCl	0.0001 *M* HZO[d]	0.8 μ silver	35	0.8	80
0.1 *M* NaCl	0.0001 *M* HZO	0.8 μ silver	35	0.8	44
0.01 *M* $MgCl_2$	HZO[e]	0.8 μ silver	35	0.7	90
0.02 *M* NaCl	Bentonite (45 mg/liter)	0.2 μ silver	135	0.3	50

[a]1 cm/min is equivalent to 354 gpd/ft^2.
[b]Polybenzyl trimethyl ammonium chloride.
[c]Polystyrene sulfonic acid.
[d]Hydrous zirconium oxide, colloidally dispersed.
[e]No additive was present in this feed; the membrane had been formed previously with HZO.

at least sometimes the compact layer is formed of corrosion products or other impurities in the feed, and that the additives adsorb on the layer and activate it for rejection. Concentration dependence of rejection and the greater rejection observed for salts having polyvalent coions than for 1.1 solutes are consistent qualitatively with an ion exchange model.

The high permeation rates of these dynamically created layers, coupled with substantial rejections, impel consideration for practical applications, at least for processing of dilute solutions. In one instance, a transmission rate through a membrane of 1000 gpd/ft^2 was accompanied by an appreciable rejection (17%), and several hundred gpd/ft^2 are not uncommon. (The highest permeations usually attributed to rejecting cellulose acetate membranes are 50 gpd/ft^2, and values for films suggested for desalination are as much as a factor of 10 lower.) The observed rejections are in many cases less than the values of which the membranes are intrinsically capable, because our circulation rates have not always been sufficiently high to eliminate concentration polarization. The additive concentrations necessary to maintain rejecting properties are frequently small (e.g., as little as 1 ppm) after the membrane is established with a feed containing a high concentration of additive. The chief problem standing in the way of practical application (besides learning to control conditions well enough for reproducible results) is the sensitivity of these barriers to the presence of polyvalent counterions in the feeds. Rejection is frequently sharply decreased, sometimes to zero, and the films occasionally are even destroyed when such ions are present. However, some additives (e.g., humic acid) are not so sensitive to polyvalent counterions, and in other cases the presence of a polymeric neutral additive in the feed seems to alleviate the difficulties.

Osmotic Coefficients of Sea Salt Solutions[34]

R. M. Rush J. S. Johnson

An isopiestic apparatus has been constructed, primarily to measure osmotic coefficients of

[34]Research jointly sponsored by the Office of Saline Water, U.S. Department of the Interior, and by the U.S. Atomic Energy Commission.

multicomponent solutions. Our initial objective is to establish in representative cases the best procedures for computation of free energies of multicomponent systems from free energies of the limiting two-component systems. Although we are particularly interested in perchlorate salts, because of their extensive use in the study of complexing reactions, the first systems undertaken had the solute composition of sea water and its concentrates. We selected these solutions because practical implications have led to a recent computation by Stoughton and Lietzke of their thermodynamic properties from data on NaCl.[35] In effect they obtained a semiempirical equation for the osmotic coefficient of NaCl, ϕ_{NaCl}, in terms of a Debye-Hückel term and a power series in molality, m; their equations also covered a range of temperatures. They then computed seawater osmotic coefficients, ϕ_{sw}, from the equation for ϕ_{NaCl} (with the appropriate correction to the Debye-Hückel term for the bivalent ions in seawater) by inserting into the power series terms seawater concentrations expressed in different ways. From comparison of boiling-point elevations of seawater computed from ϕ_{sw} with what they took to be the best values in the literature, they concluded that the best seawater osmotic coefficients were obtained by expressing the concentration as "osmolality," $\frac{1}{2}\sum_i m_i$, the summation being over all ionic species. There is, however, considerable disagreement between values of seawater boiling-point elevations measured in different laboratories, and a direct experimental determination of ϕ_{sw} seemed desirable.

We have measured the osmotic coefficients at 25° of synthetic seawater solutions in the ionic strength range 0.6 to 7. The solutions contained Na^+, Mg^{2+}, K^+, Cl^-, and SO_4^{2-} in the ratios reported for seawater, with Ca^{2+} being replaced by an equivalent amount of Mg^{2+} and HCO_3^- and Br^- by Cl^-. Some measurements were made at low concentrations on solutions in which Ca^{2+} was present. The results of these measurements are shown in Fig. 5.13. These results show that the substitution of Mg^{2+} for Ca^{2+} had little effect on the values of ϕ_{sw}.

The curves in Fig. 5.13 represent the values of ϕ_{sw} calculated from an equation for ϕ_{NaCl} at

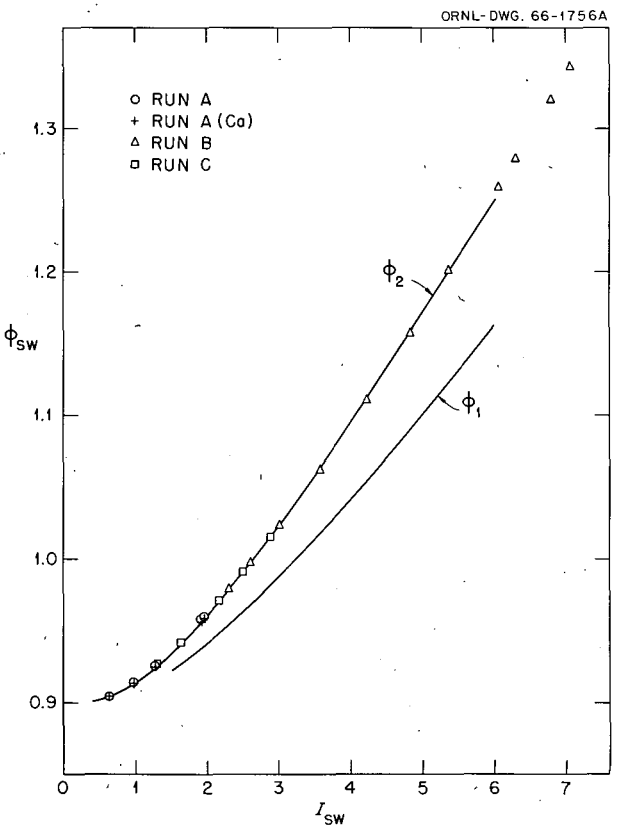

Fig. 5.13. Osmotic Coefficients of Synthetic Seawater Solutions.

25° with seawater concentrations inserted as "osmolality" (ϕ_1) or as ionic strength, $\frac{1}{2}\sum_i m_i z_i^2$ (ϕ_2). It is clear that, at least at 25°, much better agreement between computed and experimental values is obtained by insertion of ionic strength of seawater in the equation for ϕ_{NaCl} than by insertion of "osmolality."

Thermodynamic Properties of Sea Salt Solutions

R. W. Stoughton M. H. Lietzke

In previous work[35,36] vapor pressures of sea salt solutions were calculated from 25 to 175°C and from 1 to 28 wt % solids by using the following extended Debye-Hückel equation and parameters obtained from measured osmotic coefficients of sodium chloride solutions:

[35] R. W. Stoughton and M. H. Lietzke, *J. Chem. Eng. Data* **10**, 254 (1965).

[36] R. W. Stoughton, M. H. Lietzke, and R. J. White, *J. Tenn. Acad. Sci.* **39**, 109 (1964).

$$\phi = 1 - \frac{\mathcal{S}}{A^3 I}\left[(1 + A\sqrt{I}) - 2\ln(1 + A\sqrt{I}) - \frac{1}{1 + A\sqrt{I}}\right] + BI' + CI'^2 . \quad (1)$$

In Eq. (1), $\mathcal{S}$ is the appropriate Debye-Hückel limiting slope for either a single electrolyte or an electrolyte mixture, A is the Debye-Hückel parameter (here set equal to 1.5), I is the ionic strength, I' is a concentration term discussed below, while B and C are adjustable parameters. The latter parameters for NaCl solutions were evaluated to 270°C[35,36] from osmotic or activity coefficients from the literature up to 4 m to 100°[37] and up to 3 m from 100 to 270°C.[38]

In applying Eq. (1) to sea salt solutions, the values of B and C for NaCl solutions were used with three different concentration terms for I':

$$I' = \frac{1}{2}\sum_i m_i Z_i^2 = I \quad (2a)$$

$$= \frac{1}{2}\sum_i m_i \mid Z_i \mid \quad (2b)$$

$$= \frac{1}{2}\sum_i m_i . \quad (2c)$$

(For a 1-1 electrolyte all three expressions are equal to the molality.)

The calculated vapor pressures were compared with the measured vapor pressures of Arons and Kientzler[39] at 25 and 35° and those of Higashi *et al.*[40] from 25 to 175°C and to 28 wt % solids. The agreement was best when Eq. (2c) was used and poorest when (2a) was used. Vapor pressure measurements of Forrest and Worthley[41] from 25 to 100°C gave better agreement with Eq. (2a) than with (2b) or (2c), although the scatter of the various experimental values[39–41] was much greater than the difference between the values calculated using Eqs. (2a) and (2c); even at 28 wt % solids, the scatter was greater by at least a factor of 2 than the difference between the two sets of calculated values. Because the measurements of Arons and Kientzler[39] appeared to be the most precise ones available, we concluded[35,36] that Eq. (2c) gave best results for the thermodynamic properties of sea salt solutions.

Recently Rush and Johnson[42] have measured osmotic coefficients of synthetic sea salt solutions in the ionic strength range 0.6 to 7.0 at 25°C by using NaCl as a standard and the osmotic coefficients of ref. 37 for the standard. These were compared with values of ϕ calculated by using Eqs. (2a) and (2c) and Eq. (1) with the addition of a cubic term DI'^3 in which the B, C, and D parameters were evaluated from osmotic coefficients[37] at 25° only. Throughout the whole concentration range Eq. (2a) gave the best agreement, showing a maximum deviation of 0.003. By contrast, Eq. (2c) showed a deviation of 0.001 at the lowest and about 0.1 at the highest concentration.

We believe that the measurements of Rush and Johnson are the best available. Hence we now conclude that Eq. (2a) should be used to calculate the thermodynamic properties of sea salt solutions, at least at and near room temperature. We therefore now recommend that unless and until good experimental measurements suggest otherwise, Eq. (2a) should be used at all temperatures, that is, that it is best to set $I' = I = \frac{1}{2}\sum m_i Z_i^2$ at all temperatures.

We have reevaluated the B and C parameters of Eq. (1) by the method of least squares on the assumption that their variation with absolute temperature T was the same as that given in Eq. (3) for B,

$$B = \frac{B_1}{T} + B_2 + B_3 \ln T . \quad (3)$$

At 15 and 35°C we used osmotic coefficients at 0.5, 1.0, 2.0, 3.0, and 4.0 m which had been calculated[43] from activity coefficients presented by

[37] R. A. Robinson and R. H. Stokes, *Electrolyte Solutions*, Appendices 8.3 and 8.8, Academic, New York, 1955.

[38] E. R. Gardner, P. T. Jones, and H. J. de Nordwall, *Trans. Faraday Soc.* **59**, 1994 (1963).

[39] A. B. Arons and C. F. Kientzler, *Trans. Am. Geophys. Union* **35**(5) (1954).

[40] K. Higashi, K. Nakamura, and R. Hara, *Sci. Rept. Tohoku Univ.* **10**, 433 (1931–32).

[41] W. W. Forrest and S. R. Worthley, *Australian J. Appl. Sci.* **15**, 53 (1964).

[42] R. M. Rush and J. S. Johnson, submitted to the *Journal of Chemical and Engineering Data*.

[43] M. H. Lietzke and R. W. Stoughton, *J. Phys. Chem.* **65**, 508 (1961).

Harned and Owen.[44] At 60, 80, and 100°C we used osmotic coefficients at the same concentrations, while at 25°C we also included the value at 5 m – all from ref. 37. Between 125 and 250°C (inclusive) at every 25° interval we used the results of ref. 38 plus some additional and some corrected experimental values.[45] Unit weights were assigned to all values except those at 25°C; at 25° weights of 3.0 were assigned in the least-squares fit, since these were the result of a critical evaluation of measurements from different sources. The resulting values of the B and C parameters are given as follows:

$$B_1 = -330.332 \qquad C_1 = 32.6806$$
$$B_2 = 6.31446 \qquad C_2 = -0.553679$$
$$B_3 = -0.909395 \qquad C_3 = 0.0790215$$

Additional fits were made by using different weights, by fixing the values of the parameters at 25° to be consistent with the 25° data, and by using seven temperature-dependent parameters (i.e., by adding a term B_4T). None of these gave a fit to the measured values which was significantly better than that using the parameters noted above. They all appeared to fit the data well within the apparent uncertainties.

Recalculated BPE's, Minimum Energies of Recovery, and Osmotic Pressures. – We have recalculated the boiling-point elevations (BPE's) of sea salt solutions to 260°C and to 28 wt % solids, the minimum energies of recovery of water from standard seawater to 200°C and to 100% recovery, and the osmotic pressures of sea salt solutions to 100°C and to 25 wt % solids using the current recommendation [i.e., Eq. (2*a*)] and the new NaCl parameters (i.e., table above).

The new values all show the greatest deviations from the previous calculations[35] at low temperatures and high concentrations (100% recovery in the case of the free energy of recovery). The largest change is a 12% increase in BPE at 25°C at 28 wt % solids. The largest change at 12 wt % solids and below is a 4% increase in BPE at 25°C. In general where there is a change the new values are higher. The BPE values at the highest concentrations and temperatures are exceptions to this general observation; a 2% decrease occurs at 28 wt % solids at 260°C.

[44]H. S. Harned and B. B. Owen, *The Physical Chemistry of Electrolyte Solutions*, 3d ed., p. 726, Reinhold, New York, 1958.

[45]E. R. Gardner, private communication.

Use of Cationic Glass Electrodes to Measure the Activity of KCl Solutions

M. H. Lietzke R. W. Stoughton

The Beckman 39137 cationic glass electrode has been used in the temperature range 15 to 55° to measure the activity of KCl solutions in the concentration range 0.01 to 2.5 m. It was found that successive measurements of the emf of the cation-indicating glass electrodes (against an Ag, AgCl reference electrode) were usually reproducible to within a few tenths of a millivolt, although over a period of hours or days drifts of several millivolts were often observed. For convenience in computing the activity coefficient of KCl, all the emf values measured in a given solution with one electrode were averaged. In all, three different glass electrodes were used in conjunction with one Ag, AgCl reference electrode. The averaged emf values for each glass electrode were then fitted against the molality of the KCl solution m by the method of least squares using the equation

$$E = E^\circ - \frac{RT}{\mathfrak{F}} \ln m + \frac{RT}{\mathfrak{F}} \left[\frac{\mathcal{A}\sqrt{m}}{1 + 1.5\sqrt{m}} - Bm - Cm^2 \right], \quad (1)$$

where E°, R, T, and $\mathfrak{F}$ have their usual significance; $\mathcal{A}$ is the Debye-Hückel limiting slope at temperature T given by

$$\mathcal{A} = \frac{4.18859 \times 10^6 \, \rho^{1/2}}{(DT)^{3/2}};$$

D and ρ are the dielectric constant and density of water at temperature T respectively; and E°, B, and C are the adjustable parameters. Three values of the activity coefficient of KCl were then calculated for each KCl solution at each temperature, corresponding to the three sets of B and C parameters obtained at each temperature with each of the three glass electrodes. Most of these

values were then averaged for each solution at each temperature, although a few obviously deviant values were not included in the averages. The values of log γ_{KCl} vs $1/T$ for each concentration of KCl are plotted in Fig. 5.14. As can be seen there is good agreement between the values obtained by the glass electrodes (circles) and literature values[46] (solid lines) obtained by vapor pressure measurements, except at 1.0 and 2.5 *m* KCl at 15°, where the activity coefficients obtained from the glass electrode measurements appear to be too low. Since there are no literature values at 55°, no comparison is possible at this temperature. A possible explanation for the low values at 15° in the 1.0 and 2.5 *m* solutions is that the attainment of emf equilibrium is slow in these solutions and that, therefore, the values of log γ_{KCl} plotted do not represent equilibrium values.

Measurements were also made at 5° at all the above concentrations plus 0.001 *m* and at 0.001 *m* at all the above temperatures. The observed emf values were much more erratic than those reported, and the resulting activity coefficients at 0.001 *m* were 15 to 40% different from those in the literature.

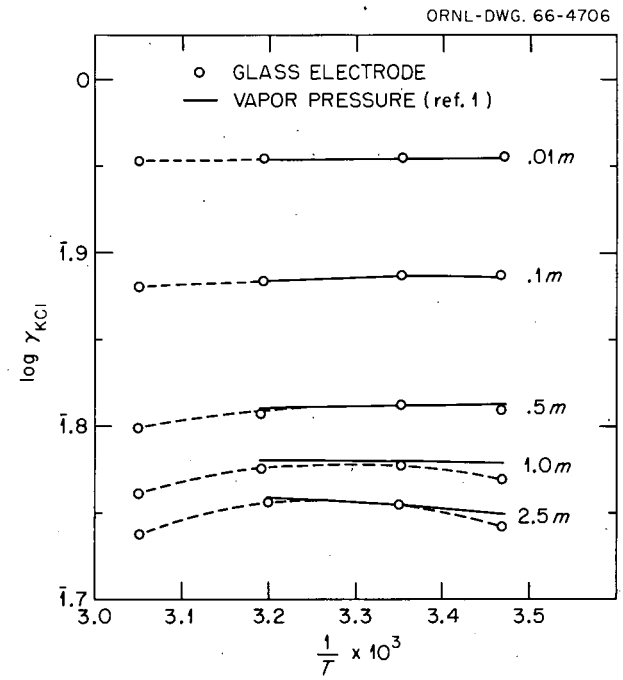

Fig. 5.14. The Activity Coefficient of KCl Solutions.

[46] H. S. Harned and B. B. Owen, *The Physical Chemistry of Electrolyte Solutions*, 3d ed., p. 727, Reinhold, New York, 1958.

6. Electrochemical Kinetics and Its Application to Corrosion

STUDIES ON THE INHIBITION OF CORROSION

G. H. Cartledge

There have been three principal types of hypotheses to account for the inhibiting action of inorganic substances of the general formula XO_4^{n-}. A purely chemical mechanism was based on repair of defects in an isolating film by oxidation and buffering at the interface. An electrochemical hypothesis ascribed the effect to polarization of the metal to a passive potential by the cathodic action of the reducible inhibitor. A third hypothesis was based on adsorption of the inhibitor, but without specification of the way in which the kinetics of dissolution is thereby altered.

The electrostatic polarization hypothesis developed in this Laboratory in 1952 sought to find the kinetic effect of adsorption in the influence of an induced electric field arising from the polarity of the bonds within the XO_4^{n-} particle. It was this point of view which led to the discovery of the extreme effectiveness of the pertechnetate ion, TcO_4^-, as an inhibitor. Subsequently, it was demonstrated that inhibitors of this type do, in fact, produce an effect which enables oxygen to induce passivation, even when the inhibitor itself is too weak an oxidizing agent to passivate the metal. During the past year, an investigation of this effect was conducted with TcO_4^-, CrO_4^{2-}, and MnO_4^- as inhibitors. By working at controlled potentials that were too noble to permit reduction of the inhibitor, it was found in each case that the current density and accumulated charge required before passivation is produced are greatly diminished by the inhibitor. It was shown also that none of these inhibitors is capable of supplying sufficient cathodic current to passivate the metal in the absence of the newly identified noncathodic effect. Some suggestions regarding the way in which this noncathodic effect enters specifically into the kinetics were presented at the Symposium on Inhibition in Birmingham, England, in March 1966. The full paper will be published in the *British Corrosion Journal*. The first part of the experimental work is published,[1] and a second paper has been submitted for publication.

MECHANISM OF CORROSION INHIBITION

E. J. Kelly

Earlier investigations[2] have established that in noninhibiting media, such as acidic sulfate solutions, active dissolution of iron follows the mechanism represented by Eqs. (1–5):

$$Fe + H_2O \rightleftharpoons Fe(H_2O)_{ad}\,, \qquad (1)$$

$$Fe(H_2O)_{ad} \rightleftharpoons Fe(OH^-)_{ad} + H^+\,, \qquad (2)$$

$$Fe(OH^-)_{ad} \rightleftharpoons (FeOH)^\circ_{ad} + e^-\,, \qquad (3)$$

$$(FeOH)^\circ_{ad} \longrightarrow (FeOH)^+ + e^- \text{ (rate-determining)}\,, \qquad (4)$$

$$(FeOH)^+ + H^+ \rightleftharpoons Fe^{2+} + H_2O\,. \qquad (5)$$

[1] G. H. Cartledge, *J. Electrochem. Soc.* 113, 328 (1966).

[2] E. J. Kelly, *J. Electrochem. Soc.* 112, 124 (1965).

On the basis of this mechanism, one may derive the experimentally verified equation for the steady-state anodic current density, i_n, corresponding to iron dissolution, Eq. (I):

$$i_n = k_n a_{(OH^-)} \exp(3FE/2RT) . \qquad \text{(I)}$$

Active dissolution of cobalt appears to conform to the same mechanism.[3]

In the presence of an adsorbed inhibitor, such as the benzoate anion (Bz^-), the noninhibited reaction system described above must be augmented by the following set of reactions:

$$x \cdot Fe(H_2O)_{ad} + Bz^- \rightleftharpoons Fe_x(Bz^-)_{ad} + x \cdot H_2O , \qquad (6)$$

$$Fe_x(Bz^-)_{ad} + (FeOH)^\circ_{ad} \rightleftharpoons [Fe_x(Bz)(FeOH)]^-_{ad} \equiv S^- , \qquad (7)$$

$$S^- \longrightarrow Fe_x(Bz^-)_{ad} + (FeOH)^+ + e^- \text{ (fast)} , \qquad (8)$$

$$S^- \longrightarrow Fe(Bz)(OH) + x \cdot Fe + e^- \text{ (slow)} . \qquad (9)$$

These postulates, together with Eqs. (1–5), enable the derivation of Eqs. (II) and (III):

$$i_\theta = k_n a_{(OH^-)}(1-\theta)\exp(3FE/2RT) + k a_{(OH^-)}\theta(1-\theta)\exp(FE/RT) , \qquad \text{(II)}$$

$$\frac{d\theta}{dt} = k_a a_{(Bz^-)}(1-\theta) - k_d\theta - k_f a_{(OH^-)}\theta(1-\theta)\exp(FE/RT) , \qquad \text{(III)}$$

where i_θ represents the anodic current density corresponding to iron dissolution, θ represents the fraction of the iron surface occupied by the adsorbed inhibitor, and other terms have their customary significance. Equation (6) shows the non-Faradaic adsorption-desorption reactions which account for the first two terms on the right-hand side of Eq. (III). Interaction of the adsorbed inhibitor with the surface intermediate generated by the noninhibited reaction sequence, Eqs. (1–3), is shown in Eq. (7). Equation (8) represents an anodic decomposition of the resultant surface complex (S^-) with the inhibitor remaining in an adsorbed state; the reaction portrayed by Eq. (9) corresponds to a Faradaic desorption of the inhibitor and is responsible for the last term on the right-hand side of Eq. (III).

According to Eq. (III) the Faradaic desorption reaction results in a decrease in the steady-state value of θ as the potential becomes increasingly positive. If the first and second terms on the right side of Eq. (II) are designated by i_1 and i_2, respectively, then $i_\theta \to i_2$ as $\theta \to 1$ and $i_\theta \to i_1$ as $\theta \to 0$, as evidenced by the change in the experimental value of the Tafel slope, $(dE/d\ln i_\theta)_{\theta,(OH^-)}$, from RT/F to $2RT/3F$ as θ decreases from 1 to 0. A comparison of Eqs. (I) and (II) reveals that $i_1 = (1-\theta)i_n$; that is, i_1 corresponds to the anodic current density developed by the noninhibited reaction system on that fraction of the surface not occupied by the inhibitor. The term i_2 arises as a consequence of the reaction shown in Eq. (8). The current density associated with the Faradaic desorption reaction, Eq. (9), is always insignificant compared to $(i_1 + i_2)$ and therefore does not appear in Eq. (II). Were it not for the reaction of Eqs. (7–9), the degree of inhibition, i_θ/i_n, resulting from the non-Faradaic adsorption of the inhibitor would be equal to the "ideal" value of $i_1/i_n = (1-\theta)$. Unfortunately, the reactions of Eqs. (7–9) limit the effectiveness of the inhibitor to $i_\theta/i_n < i_1/i_n$.

Equations (II) and (III) have been successfully applied to the analysis of a wide variety of transient and steady-state polarization data. For example, at constant potential, Eq. (III) may be solved for θ as a function of time. Subject to certain restrictions, the result may be combined with Eq. (II) to yield Eq. (IV),

$$\log \frac{(1+\beta i_{ss} i_0)(i_t - i_{ss})}{(1+\beta i_{ss} i_t)(i_0 - i_{ss})} = -W_{ss} t/2.303 , \qquad \text{(IV)}$$

where i_0, i_t, and i_{ss} represent the observed values of i_θ at times 0, t, and ∞ (steady state), respectively, and β and W_{ss} are constants. Experimental potentiostatic current-time transients have been found to follow Eq. (IV). If Eq. (III) is solved for

[3] E. J. Kelly, *Chem. Div. Ann. Progr. Rept. May 20, 1965*, ORNL-3832, p. 101.

the steady-state value of θ as a function of potential and the result combined with Eq. (II), then it may be shown that there exists a potential of unpolarizability, E_u, at which $d \log i_\theta/dE$ is a maximum, and, as a limiting case, E_u is given by Eq. (V):

$$E_u = 0.060 \log a_{(Bz-)} - 0.060 \text{ pH} + \text{constant} . \quad \text{(V)}$$

The potential of unpolarizability has been observed for the benzoate system, but, more importantly, Eq. (V) has been found to apply to the inhibition of iron dissolution by iodide ions,[4] and this suggests that the mechanism and equations described here are applicable to a variety of inhibited systems. The applicability of Eqs. (II) and (III) to inhibited dissolution of cobalt is currently being investigated.

ELECTROCHEMISTRY OF ZIRCONIUM

R. E. Meyer

In all aqueous solutions, zirconium rapidly forms thin passivating films of ZrO_2. From the point of view of aqueous oxidation and corrosion, the thickness of films of interest ranges from 10 to 100 A at room temperature to about 1000 A at higher temperatures. If sufficient HF is present in solution, a steady-state dissolution reaction occurs in which the film is dissolved as rapidly as it is formed. Study of this reaction therefore provides kinetic data on both the dissolution reaction and the film-formation reaction.

Dissolution by HF

During the past year, attention has been centered upon anion effects, largely because previous work showed surprising differences in rates between mixtures of HF-HNO_3 and HF-H_2SO_4 when the rotating disk electrode assembly was used to separate mass transfer effects from the surface reaction.[5] It was therefore of interest to determine if nitrate or sulfate ions or both had any specific effect on the reaction. Previous evidence indicated that nitrate had little effect but that sulfate was adsorbed in such a way as to inhibit the reaction with HF.[5] Experimental measurements were made on the systems HF-HCl and HF-H_3PO_4 for comparison with observations on the HF-HNO_3 and HF-H_2SO_4 systems. The rotating disk electrode assembly was also used in these experiments to separate mass transfer effects from the surface reaction. The results show that below the pitting potential for chloride ion, the rates of dissolution in HF-HCl and HF-HNO_3 mixtures are identical. This indicates that neither Cl^- nor NO_3^- ions have any specific effect on the reaction below the chloride pitting potential.

Zirconium forms insoluble compounds with phosphate ion, and adsorption of phosphate on ZrO_2 films might be expected to occur along with possible specific effects on the dissolution by HF. The experiments show that the rates in HF-H_3PO_4 are reduced by several orders of magnitude in comparison with rates at equal concentrations of HF-HNO_3. The reaction rate is reduced so much that it no longer depends on the rate of mass transfer of HF to the surface, and stirring effects are noted only when the phosphoric acid concentration is considerably reduced. In addition, the rates are not a function of potential in the range studied but are remarkably constant. The effect of phosphate ions is therefore similar to that of sulfate ions except that it is much more pronounced.

Effects of Chloride Ions

In aqueous media, zirconium ions hydrolyze readily to form solutions in which the metal ion is variously described as ZrO^{2+}, $ZrOOH^+$, etc. Fluoride ion forms stable complexes in aqueous solution of the general formula $ZrF_n^{(4-n)+}$. One might expect that, although both fluoride and chloride ions attack the metal under anodic conditions, only the fluoride ion will attack the oxide. The data show that the rates of dissolution in HF-HCl and HF-HNO_3 are identical below the pitting potential. Above the pitting potential the corrosion rate in the HF-HCl system rises very rapidly, as shown in Fig. 6.1. Capacity measurements showed that in some of these experiments the films must have been in the 10-to-20-A range, but even here no differences were detected. The corrosion rate also

[4] K. E. Heusler and G. H. Cartledge, *J. Electrochem. Soc.* **108**, 732 (1961).

[5] R. E. Meyer and S. M. Zettl, *J. Electrochem. Soc.* **112**, 1092 (1965).

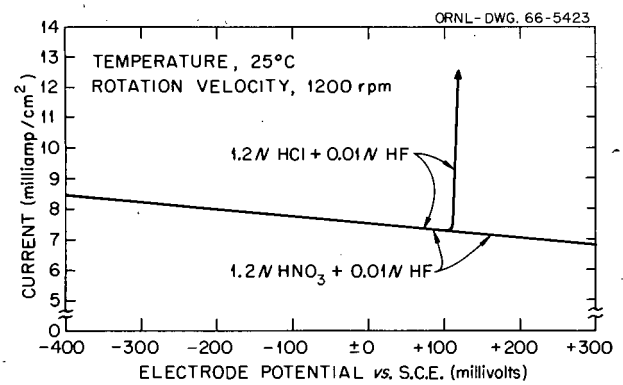

Fig. 6.1. Comparison of Rates of Dissolution of Crystal-Bar Zirconium in 1.2 *N* HCl–0.01 *N* HF and 1.2 *N* HNO_3–0.01 *N* HF as Determined with a Rotating Disk Electrode Assembly.

rises above the pitting potential in solutions containing only HCl, but a time delay usually occurs before pitting begins. It seems reasonable to assume that the chloride ion attacks the metal directly and must first be transported through the film either by field-assisted ionic migration or through flaws.

Diffusion Coefficient of HF

Attempts to determine mechanisms of reactions involving mass transfer of HF usually require a knowledge of the diffusion coefficient of HF. Since reliable values were not available, experiments were initiated to determine the diffusion coefficient by the open-ended capillary method. Initial results gave values of about 2.2×10^{-5} cm^2/sec at 25°C, but this value must be regarded as tentative until appropriate checks on the experimental method are carried out.

ROTATING DISK STUDIES ON THE DISSOLUTION OF ALUMINUM IN CHLORIDE SOLUTIONS[6]

S. S. Misra[7] F. A. Posey

The rate of the anodic dissolution reaction of aluminum in alkaline solutions is determined by the rate of mass transfer of hydroxide ions to the interface.[8] Classical electrochemical measurements cannot provide information on the specific rate of the interfacial reaction itself because the hydroxide ion concentration at the interface is not known and is not related simply to the concentration in the bulk of the solution.

It has been shown[9] that if an electrode is used in the form of a disk spinning about its axis, the pertinent mass transfer equations may be solved exactly. If a number of experimental conditions are met, the anodic dissolution current (i, amp) of the aluminum rotating disk electrode may be expressed by Eq. (1):

$$i = \frac{nFSkC^0}{1 + k/A\sqrt{\omega}}, \qquad (1)$$

where n is the electron number (equivalents/mole), F is Faraday's constant (coulombs/equivalent), S is electrode surface area (cm^2), k is the desired formal specific rate constant of the anodic dissolution reaction (cm/sec), C^0 is the hydroxide ion concentration in the bulk of the solution (moles/cm^3), ω is the rotational velocity (rpm), and $A = 1.91D^{2/3}\gamma^{-1/6}$ is a constant [D is the diffusion coefficient of hydroxide ions (cm^2/sec) and γ is the kinematic viscosity (cm^2/sec)]. Equation (1) may be rearranged to the following useful form:

$$\frac{1}{i} = \frac{1}{nFSkC^0} + \frac{1}{nFSC^0A\sqrt{\omega}}. \qquad (2)$$

Equation (2) shows that a plot of $1/i$ vs $1/\sqrt{\omega}$ should be linear and that the intercept at $1/\sqrt{\omega} = 0$ is given by $i(1/\sqrt{\omega} \to 0) = nFSkC^0$, where all quantities are known or measurable except the desired specific rate constant (k).

A rotating disk electrode assembly was constructed, and measurements were initiated on aluminum in 1 *M* NaCl at 25°C. Figure 6.2 shows the effect of pH on polarization curves of the anodic reaction which were obtained by the extrapolation procedure discussed above. At constant electrode

---

[6]Research jointly sponsored by the Office of Saline Water, U.S. Department of the Interior, and by the U.S. Atomic Energy Commission under contract with the Union Carbide Corporation.

[7]Visiting scientific staff member from India.

[8]H. Kaesche, *Z. Physik. Chem. (Frankfurt)* **34**, 87 (1962); *Werkstoffe Korrosion* **14**, 557 (1963).

[9]V. G. Levich, *Physicochemical Hydrodynamics*, Prentice-Hall, Englewood Cliffs, N.J., 1962.

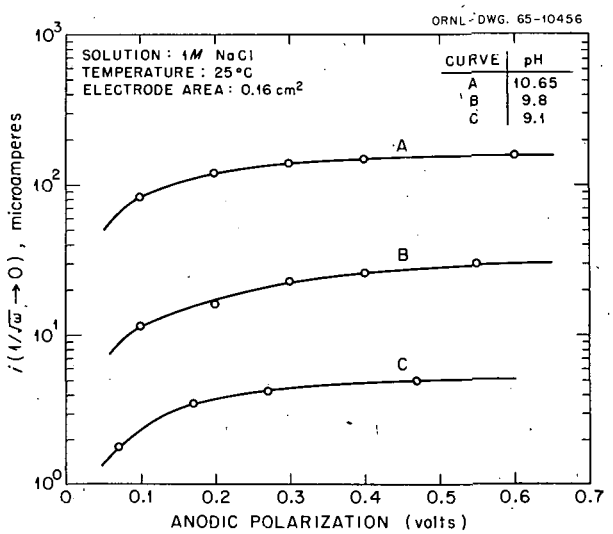

Fig. 6.2. Effect of Rapid Changes of pH on the Anodic Dissolution of Aluminum Corrected for Concentration Polarization by Use of a Rotating Disk Electrode.

potential the rate of the interfacial reaction is directly proportional to the hydroxide ion concentration, so that the assumption of first-order kinetics is justified experimentally. The position of the extrapolated polarization curves depends on the elapsed time following insertion of the electrode into solution. This effect is shown in Fig. 6.3, which presents polarization curves corrected for concentration polarization as a function of time.

The aspect of these polarization curves suggested that the observed decrease in dissolution rate with time might be due to formation of a porous aluminum oxide layer on the electrode surface. This hypothesis was verified by electron micrographs of oxide layers formed on aluminum electrodes which were corroded for approximately one week in 1 *M* NaCl solutions. Pictures obtained by use of both replica and transmission techniques showed the existence of a relatively thick (*ca.* 2000 A) porous layer on the electrode surface. These results support the view that growth kinetics of the porous layer, which serves as a diffusion barrier for reactant ions, determines the variation of corrosion rate with time.

A simplified model of the corrosion of aluminum in alkaline solutions was developed which incorporates the growth kinetics of a porous oxide layer. Predictions of the model are in reasonable agreement with experiment and allow rationalization of observations of others on such items as the effect of the ratio of specimen area to solution volume and the effect of solution flow rate and refreshment rate on corrosion kinetics.

KINETICS OF PITTING ATTACK OF TITANIUM IN CHLORIDE SOLUTIONS[6]

S. S. Misra[7] F. A. Posey

Experiments were initiated on electrochemical aspects of the formation and growth of pits on titanium in chloride solutions in order to increase our understanding of factors responsible for the values and the unusual temperature dependence of the pitting potentials of titanium and its alloys. A number of observations were made on titanium of type 150A (2.8% Cr, 0.3% Fe) by use of a rotating disk electrode assembly in 1 *M* NaCl at temperatures from 23 to 95°C, and some of these are summarized below.

No significant effect of solution velocity on the initiation and growth of pits on titanium was observed up to approx 3500 rpm. Evidently the layer of hydrolysis products formed during pit growth prevents convection of the external solution from diluting the concentrated acid chloride solution in the interior of the pits.

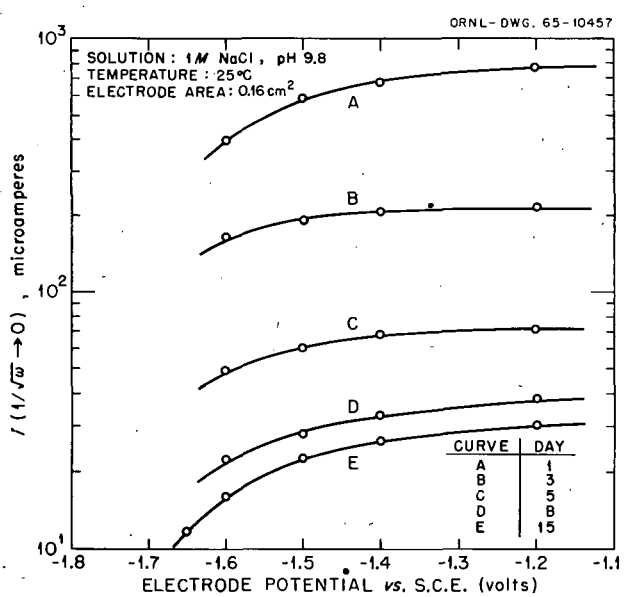

Fig. 6.3. Effect of Potential and Time on the Anodic Dissolution of Aluminum Corrected for Concentration Polarization by the Use of a Rotating Disk Electrode.

On application of a constant anodic current (galvanostatic polarization), titanium is anodized and the thickness of the passive oxide layer and the electrode potential increase essentially linearly with time. In the presence of a sufficient concentration of chloride ions, the passive layer is eventually penetrated by the chloride ions, a pit forms, and the electrode potential suddenly plunges from a high value (breakdown potential) down to a value which depends on the composition of the alloy and on the temperature (pitting potential). The final pitting potential is essentially independent of the anodic current over wide limits. Pits can exist simultaneously with passive areas at and above the pitting potential. We find that the value of the breakdown potential depends to some extent on the initial thickness of the passive layer as well as on other factors; fresh electrodes with thin films exhibit lower breakdown potentials than aged electrodes having thicker films, although the final pitting potential is about the same in either case.

Addition of sulfate ions to 1 *M* NaCl at 23°C gradually increases the breakdown potential of titanium (type 150A) from approx +13.5 v vs S.C.E. with no SO_4^{2-} present to approx +25.0 v with 0.4 *M* Na_2SO_4 (+ 1 *M* NaCl). However, the final pitting potential (approx +8.0 v) is unaffected over the same range of sulfate ion concentration. Higher SO_4^{2-} concentrations cause a sudden shift of the breakdown potential up to approx +80 v, a value characteristic of Na_2SO_4 solutions with no chloride present. Evidently SO_4^{2-} ions affect the time necessary for initiation of a pit on the electrode surface, possibly by competing with Cl^- ions for adsorption at the oxide-solution interface.

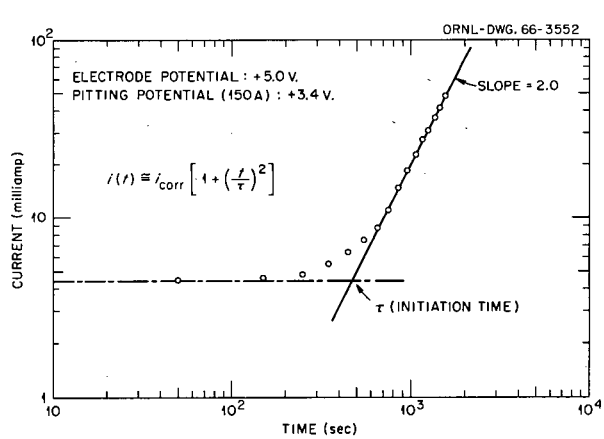

Fig. 6.4. Growth of Single Pit on Titanium (150A) in 1 *M* NaCl. pH 3, 90°C.

Experiments at constant electrode potential are capable of providing information on the kinetics of the pit growth process. Figure 6.4 shows the growth law of a single pit initiated potentiostatically at +5.0 v on titanium of type 150A in 1 *M* NaCl, pH 3, at 90°C. A finite time is required for chloride ions to penetrate the passive oxide layer during the process of pit initiation. After initiation, the current due to pit growth varies with the square of the time, indicating pit growth at constant current density over the pit interior. The dependence of initiation time on electrode potential, chloride ion concentration, temperature, alloy composition, and other factors is being studied.

EFFECT OF TEMPERATURE ON PITTING CORROSION OF TITANIUM IN CHLORIDE SOLUTIONS[6]

F. A. Posey E. G. Bohlmann[10]

Titanium is one of the favorite modern materials of construction which is being considered for use in large desalination plants. Years of accumulated experience at low temperatures have disclosed no tendency of titanium to undergo catastrophic forms of corrosion, like pitting and crevice attack. However, a number of long-term experiments in dynamic loops on corrosion of titanium in high-temperature chloride solutions have now demonstrated drastic, but sometimes extremely erratic, pitting attack at temperatures from 100 to 200°C.[11]

Polarization curves of titanium and some of its alloys were measured in chloride solutions at temperatures up to 200°C by use of a titanium loop facility which provides good control over temperature, pH, and solution velocity and refreshment rate. Typically the rate of the anodic or corrosion reaction of titanium is quite independent of the electrode potential up to very high potentials in such media as sulfate and nitrate solutions. However, in the presence of a sufficient concentration of chloride ions, titanium and its alloys exhibit a pitting potential which in some cases is low enough to allow pitting attack to proceed spontaneously.

---

[10]Reactor Chemistry Division.

[11]E. G. Bohlmann and F. A. Posey, "Aluminum and Titanium Corrosion in Saline Waters at Elevated Temperatures," *Proceedings of the First International Symposium on Water Desalination* (in press).

Pits form on the electrode surface at and above the pitting potential and exist simultaneously with passive areas. Experience with this and other systems shows that pitting potentials are independent of the pH of the external solution but depend significantly on temperature. At the pitting potential the total area of the surface undergoing pitting attack is directly proportional to the anodic current over wide limits.

Each titanium alloy was found to have a characteristic pitting potential. Increase of temperature profoundly affects the value of the pitting potential; plots of pitting potential as a function of temperature are quite reproducible and show clearly which alloys are superior in tendency towards pitting attack. Some alloys exhibit striking changes (as much as 2 v or more) in the value of the pitting potential over a temperature range of only a few degrees. These sudden changes appear to be connected with the presence of minor constituents in the alloys, but the reason for this is not yet known with certainty. In general, the higher the percentage of alloying elements, the lower the pitting potential. These observations show that pitting corrosion can be expected to occur on titanium alloys in chloride solutions at sufficiently high temperatures if conditions of dissolved oxygen concentration and pH allow the metal to corrode spontaneously at the pitting potential.

CORROSION OF ALUMINUM IN SALINE WATERS AT ELEVATED TEMPERATURE[6]

F. A. Posey E. G. Bohlmann[10]

The corrosion of aluminum alloys, particularly types 5454 and 6061, was studied in 1 *M* NaCl solution at 150°C in titanium loop facilities with special emphasis on the electrochemical aspects. Corrosion rates were determined by weight loss and by measurements of the polarization resistance of the specimens. The results show that the 5454 alloy is superior in corrosion resistance to the generally recommended 6061 alloy in high-temperature saline solutions. Polarization curves of the alloys were measured under a variety of conditions in order to determine the nature of the difference in corrosion properties. The results are generally similar to those obtained by other workers at lower temperatures, except for certain effects which appear mainly at the higher temperature of this study.

A pronounced minimum exists in the corrosion rate of aluminum and its alloys in chloride solutions in the vicinity of neutrality. Changes in the polarization curves of anodic and cathodic processes occurring at the aluminum-electrolyte interface with pH provide a kinetic basis for understanding this and other aspects of the corrosion behavior. At low potentials the rate of the anodic or corrosion reaction is independent of the electrode potential, but increases with increasing pH. The rate of the anodic process is controlled by the rate of mass transport of hydroxide ions to the oxide-solution interface. At higher potentials, in the presence of chloride ions, the anodic polarization curve exhibits a pitting potential which is independent of the anodic current density. The pitting potential does not vary with pH but decreases with increasing chloride concentration. The cathodic reaction in alkaline solution consists of the reduction of water molecules to form molecular hydrogen; this process is pH-independent. With increasing acidity, reduction of hydrogen ions becomes increasingly important. The minimum corrosion rate represents a compromise between the decrease with increasing acidity of the rate of the transport-controlled anodic reaction and the increase in the rate of the cathodic hydrogen-evolution. reaction. Oxygen in solution may also increase the corrosion rate by providing an additional cathodic process.

The transport-controlled rate of the anodic process depends on solution velocity and on the rate of the cathodic process, both of which affect the local pH at the oxide-solution interface. The rate of the anodic reaction decreases with time at constant pH and solution velocity and is affected by the rate of refreshment of the solution in the loop and by the ratio of area of corroding specimens to solution volume. These effects can probably be understood on the basis of growth and dissolution kinetics of a porous outer layer, which is known to exist on aluminum in high-temperature aqueous solutions.

Comparison of polarization curves of the 5454 and 6061 alloys shows that the rate of the cathodic hydrogen-evolution reaction on the 6061 alloy is considerably greater than that of the 5454 alloy. The enhanced rate of the cathodic process on the 6061 alloy accounts for its greater corrosion rate at any pH and for its susceptibility to pitting attack. Catalysis of the cathodic process on the 6061 alloy may be attributable to its copper content.

7. Nonaqueous Systems at High Temperatures

CONDENSED-PHASE BEHAVIOR OF THE ALUMINUM CHLORIDE–ZIRCONIUM CHLORIDE SYSTEM

A. J. Shor[1] William T. Smith, Jr.[2]
M. A. Bredig

The phase relations in the aluminum chloride–zirconium chloride system had been judged to be of some interest in connection with the reprocessing of nuclear fuels by the volatility chloride process.[3] Experimental data were reported previously.[3,4] These were subjected to a careful review, and, with the cooperation of A. S. Dworkin and the advice of Professor J. E. Ricci,[5] some additional thermoanalytical tests were carried out on specially heat-treated samples. A revised phase diagram for this system resulted (Fig. 7.1). We have discussed the new phase relationships thoroughly in a recent publication[6] in which they were summarized as follows:

"According to thermal, differential thermal, and X-ray analysis, Al_2Cl_6 and $ZrCl_4$ form a simple eutectic system, without solid intermediary compounds but possibly with some limited solid solution. The composition of the eutectic at 165° is approximately 75 mole % Al_2Cl_6. In disagreement with earlier literature data, visual observation above the liquidus showed the presence of only one liquid phase. Semiquantitative interpretation, with the use of the heats of fusion of the components, of the liquidus in terms of activities suggests that these largely molecular chlorides interact in the liquid to form mixtures of essentially un-ionized complex molecules $ZrCl_4 \cdot (AlCl_3)_n$, n = 1, 2, 3, and 4, with higher values of n possible at high aluminum chloride concentration."

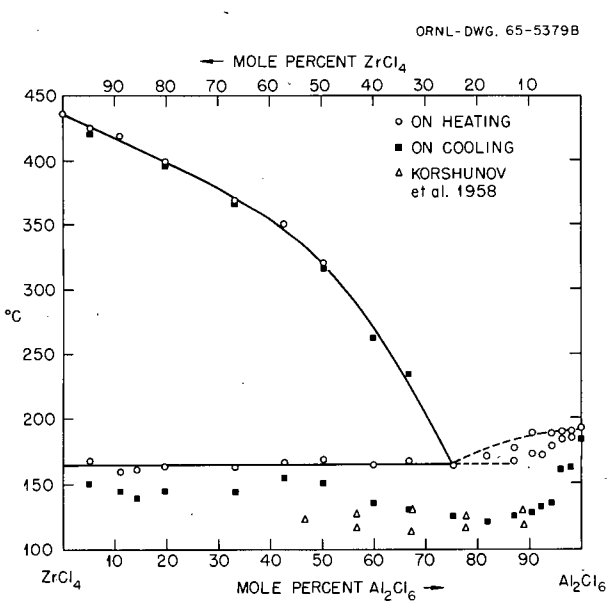

Fig. 7.1. The Aluminum Chloride–Zirconium Chloride Phase Diagram.

PRETRANSITION BEHAVIOR OF SOLID POTASSIUM AND THALLIUM SULFATES FROM HEAT CONTENT AND THERMAL EXPANSION

A. S. Dworkin M. A. Bredig

Entropy changes associated with phase transitions in salts have interested us especially in

---

[1]Reactor Chemistry Division.

[2]University of Tennessee.

[3]*Reactor Chem. Div. Ann. Progr. Rept. Jan. 31, 1965*, ORNL-3789, pp. 94–96.

[4]A thesis by A. J. Shor, submitted in partial fulfillment of the requirements for the degree of Master of Science, University of Tennessee, December 1964.

[5]Consultant, New York University.

[6]A. J. Shor, W. T. Smith, Jr., and M. A. Bredig, *J. Phys. Chem.* 70, 1511 (1966).

connection with the application of the thermodynamics of freezing to the interpretation of molten salt–metal solutions in terms of solute species. In this connection we have previously discussed the unusually low entropies of fusion of salts possessing the fluorite or antifluorite type of crystal structure, for example, CaF_2, $SrCl_2$, and K_2S.[7,8] The small entropies were attributed to a high degree of disorder characteristically existing in the solid salts at their melting points. This disorder develops over a large temperature range in a high-temperature lambda type of transition resembling "premonitory" effects that precede some first-order transitions.[9]

Recently, Majumdar and Roy[10,11] reported that the enthalpy of the transition in K_2SO_4 at 584°C from the orthorhombic to the hexagonal crystal structure, as determined by means of the Clausius-Clapeyron equation $\Delta H_{tr} = (\Delta V_{tr} \cdot T_{tr})/(dT_{tr}/dp)$, from x-ray diffraction patterns $[\Delta V_{tr}(\text{x ray})]$ and the pressure dependence of the transition temperature (dT_{tr}/dp) disagreed by almost a factor of 2 with ΔH_{tr}(cal) determined calorimetrically.[12] We felt that the explanation given in terms of several, not specified intermediate crystal transformations in K_2SO_4, which were said to invalidate the assumption of the presence of the orthorhombic structure at 584° and thus the calculation of ΔV_{tr}(x ray) based upon it, was entirely untenable for various reasons. Instead, we suspected as the cause for the discrepancy the occurrence of a gradual excess heat absorption just below the transition temperature, that is, a "premonitory" effect[9] caused by disordering of one kind or another. Such an effect appeared to be indicated by the early heat content measurements[12] (Fig. 7.3) and other observations.[13] It might have caused Majumdar and Roy inadvertently to compare two incongruous enthalpy values, namely, the isothermal one from ΔV_{tr} and (dT_{tr}/dp) in which the pretransition enthalpy was not included, and the calorimetric one, 2140 cal/mole, which was obtained by extrapolation of an equation and did include it.[12] However, the other possibility also existed that the pretransition effect observed in the calorimetric study was not an intrinsic structural effect, but due to the presence of a eutectoid produced by impurities. This would require an explanation of the enthalpy discrepancy in terms of an erroneous ΔV_{tr}, possibly even the implausible one of additional crystal structure transformations.[10] In an attempt to resolve this question, we remeasured the heat content of K_2SO_4 in our own copper-block drop calorimeter. For comparison of K_2SO_4 with Tl_2SO_4, iso-dimorphous with, but chemically quite different from K_2SO_4,[10] we also measured, for the first time, the heat content of Tl_2SO_4 up into the liquid range.

Figure 7.2 represents the results obtained. They are also expressed (cal/mole) by the empirical (least-squares) equations that follow:

Tl_2SO_4 [recrystallized; SO_4^{2-}: 19.02 ± 0.02% (theoretical 19.03); no foreign metals]

Orthorhombic: $H_T - H_{298} = -7710 + 19.39\ T + 22.18 \times 10^{-3}\ T^2$ (±0.2%) (298 – 774)

Transition: $\Delta H_{tr}(774°K) = 210 \pm 50$; $\Delta S_{tr} = 0.27 \pm 0.05$

Hexagonal: $H_T - H_{298} = -14{,}700 + 45.84\ T$ (±0.1%) (774 – 916)

Melting: $\Delta H_m(916°K) = 5880 \pm 50$; $\Delta S_m = 6.42 \pm 0.05$

Liquid: $H_T - H_{298} = -8600 + 45.60\ T$ (±0.2%) (916 – 1000)

K_2SO_4 (analytical grade)

Orthorhombic: $H_T - H_{298} = -7450 + 19.78\ T + 18.17 \times 10^{-3}\ T^2$ (±0.3%?) (298 – 857)

Transition: $\Delta H_{tr} = 1990 \pm 50$; $\Delta S_{tr} = 2.32$ (±0.1%)

Hexagonal: $H_T - H_{298} = -13{,}910 + 45.22\ T$ (±0.1%) (measured 857 – 980)

There is very little if any indication of the pretransition effect in K_2SO_4 immediately below T_{tr} = 584° (857°K). With a ΔH_{tr} value of 1990 cal/mole the value 1940 reported originally[12] (or 2140 cal/mole, presently accepted)[10,14] is essentially confirmed. The heat content at 580°

[7] M. A. Bredig, "Mixtures of Metals with Molten Salts," p. 396 in *Molten Salt Chemistry* (ed. by M. Blander), Interscience, New York, 1964.

[8] A. S. Dworkin and M. A. Bredig, *Chem. Div. Ann. Progr. Rept. May 20, 1965*, ORNL-3832, p. 110.

[9] See, for example, A. R. Ubbelohde, *Melting and Crystal Structure*, Clarendon Press, Oxford, 1965.

[10] A. J. Majumdar and R. Roy, *J. Phys. Chem.* **69**, 1684 (1965).

[11] A. J. Majumdar, Ph.D. thesis, Pennsylvania State University, 1958. University Microfilms, Inc., Ann Arbor, Mich., L. C. Card No. Mic 58-7290.

[12] C. H. Shomate and B. F. Naylor, *J. Am. Chem. Soc.* **67**, 72 (1945).

[13] M. A. Bredig, *J. Phys. Chem.* **47**, 587 (1943).

[14] K. K. Kelley, *Bur. Mines Bull.* **584** (1960).

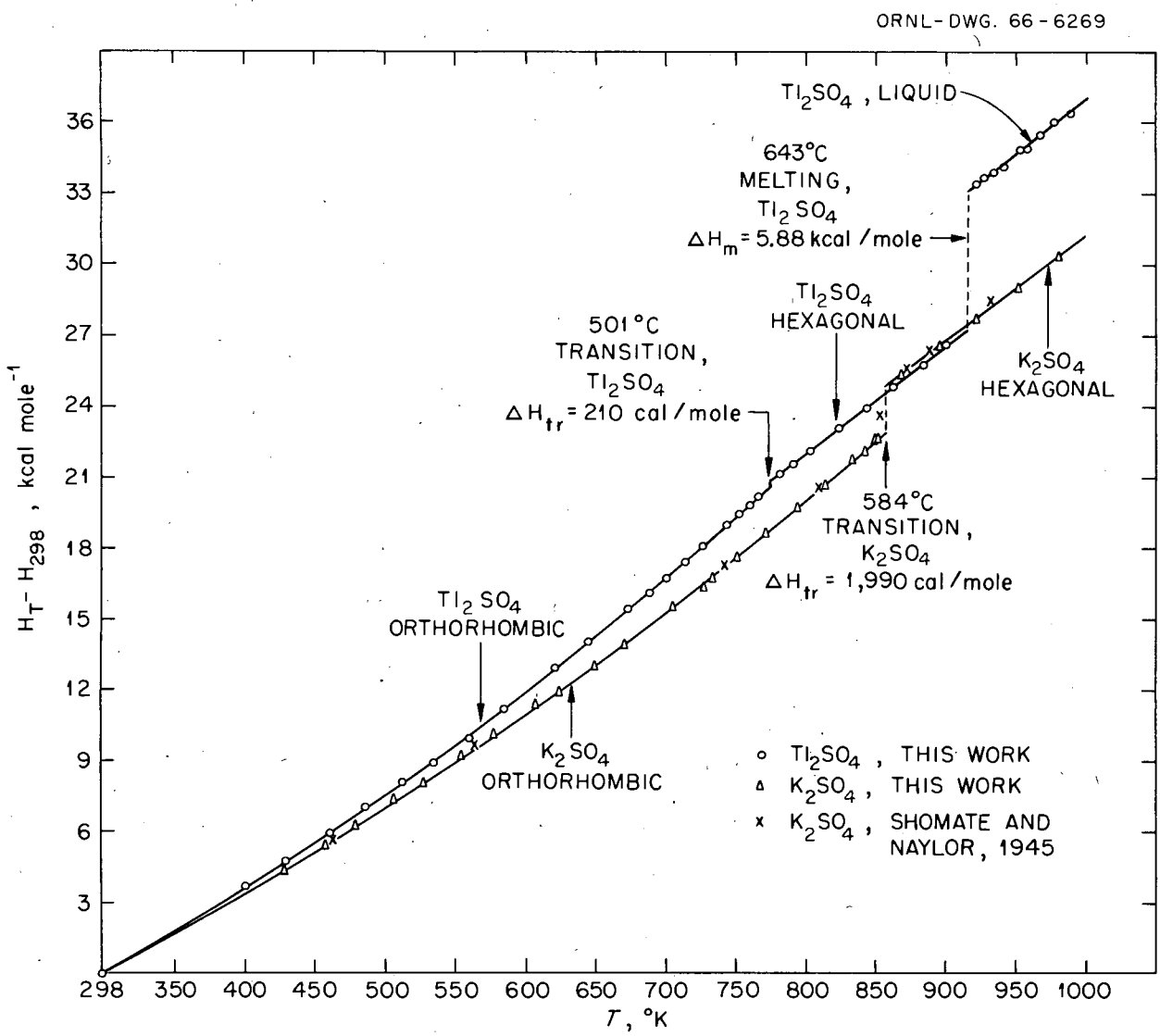

Fig. 7.2. Heat Content ($H_T - H_{298}$) of Potassium Sulfate and Thallium Sulfate (New Data).

reported earlier as "pretransition"[12] actually must have reflected partial transition (eutectoid) caused by an impurity. (This seems to have been realized by Shomate and Naylor[12] in arriving at ΔH_{tr} = 1940 cal/mole). It cannot have been an effect intrinsic to pure K_2SO_4, and we are forced to look for another explanation of the discrepancy in ΔH_{tr} reported by Majumdar and Roy. Such an explanation seems now to be forthcoming from a scrutiny of their x-ray data which revealed that several errors had entered the deviation of the volume change on transition, ΔV_{tr}, some of which are indicated in Fig. 7.3. However, final clarification must await a repetition of the high-temperature x-ray diffraction study.

The calorimetric results for thallium sulfate (Fig. 7.2) exhibit a rather significant difference from the potassium salt, quite in contrast to the structural similarity stressed by Majumdar and Roy.[10] Both the enthalpy (210 cal/mole) and the entropy (0.28 cal deg^{-1} mole^{-1}) of the transition are an order of magnitude smaller than in K_2SO_4 (1990 and 2.7 respectively). This is in excellent agreement with the high-temperature x-ray data:[10]

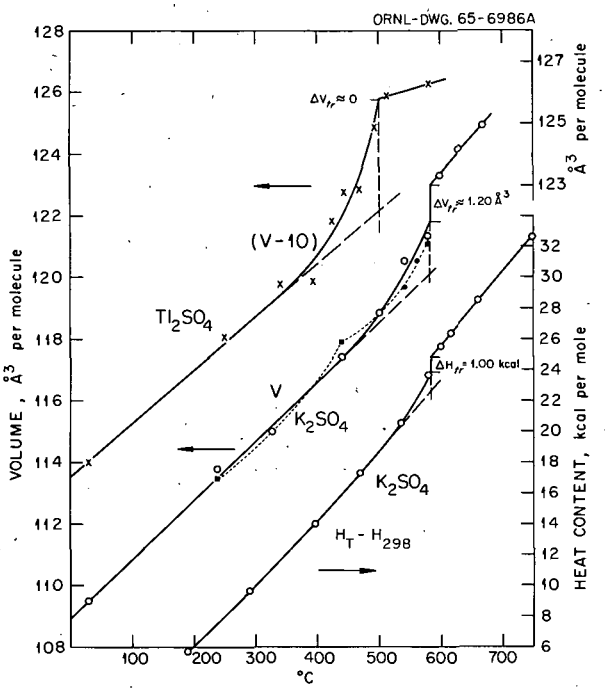

Fig. 7.3. Volume Expansion (K_2SO_4; Tl_2SO_4) and Heat Content (K_2SO_4) as a Function of Temperature (Based on X-Ray Diffraction and Calorimetric Data from Refs. 10 and 12 Respectively; Dotted Line Through Full Squares and Circles Representing Computational and Plotting Errors Is from Fig. 3 of Ref. 11). ΔH_{tr} = 1.00, rather than reported 1.94 kcal, would have represented isothermal enthalpy if "pretransition" heat content at 580°C had been found to be intrinsic.

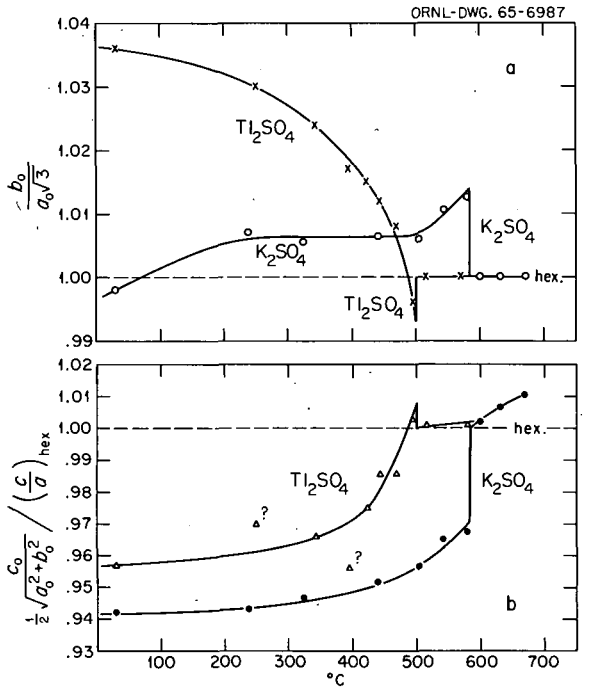

Fig. 7.4. Continuous and Discontinuous Deformation of the Orthorhombic Low-Temperature Structure of K_2SO_4 and Tl_2SO_4 (Based on Data from Ref. 10). (*a*) Deviation from hexagonal symmetry of base plane. (*b*) Change in pseudohexagonal axis ratio.

Fig. 7.3 shows that the considerable volume change ΔV_{tr} in K_2SO_4 is contrasted by a negligibly small one in the Tl_2SO_4, a fact which the previous authors ignored. Figure 7.3 further shows for Tl_2SO_4 an abnormal volume expansion, resulting largely from an increase in the pseudohexagonal c axis of the orthorhombic structure, in the temperature range 150° below the transition point, while a corresponding pretransition expansion in K_2SO_4 is much smaller. Figure 7.4 further demonstrates how gradual the change is in Tl_2SO_4 from the pseudohexagonal symmetry of the base plane of the orthorhombic structure to the truly hexagonal symmetry of the high-temperature phase, and shows for K_2SO_4 the largely *isothermal* change of 3% from the pseudohexagonal axis ratio $c_0/(\frac{1}{2}\sqrt{a_0^2 + b_0^2})$ to the hexagonal c/a in contrast to the gradual change in Tl_2SO_4.

The foregoing demonstration of the different structural behavior of the two sulfates is in accord with an early brief discussion by Fischmeister,[15] who attributed the far more gradual nature of the structure change in Tl_2SO_4 – as little as was known about it at the time – to the high polarizability of the Tl^+ ion.

MOLTEN-SALT–METAL SOLUTIONS

EMF Measurements in Molten Rare-Earth-Metal–Metal Halide Solutions

H. R. Bronstein

Studies of phase equilibria and electrical conductivity of solutions of metals in their molten

[15] H. F. Fischmeister, *Z. Physik. Chem.* (Frankfurt) 7, 91 (1956).

halides[16,17] led to their classification into two broad categories: (1) the metal furnishes mobile electrons to its solution in the salt, and (2) chemical reaction (oxidation-reduction) occurs between metal and salt with little or no electron mobility. The division between 1 and 2 is not a sharp one, and in some systems both mechanisms of dissolution may apply.

The rare-earth-metal–metal halide solutions show this transition in the series La-$LaCl_3$, Ce-$CeCl_3$, Pr-$PrCl_3$, and Nd-$NdCl_3$, where the electrical properties change from those of solutions of mobile electrons to those of almost purely ionic systems.

The measurement of properties closely related to the existence of metal ions in various valence states can possibly clarify this distinction. A method suitable for this purpose is an electrochemical study of the equilibrium potentials of cells of the type

$$\text{Ce liquid}|\text{molten } CeCl_3 + CeCl_{(3-n)}\text{sat}||\text{molten } CeCl_3 + x\, CeCl_{(3-n)}|\text{Ta},$$

$$E = \text{const} + \frac{RT}{nF}\ln\frac{a_{Ce^{3+}}}{a_{Ce^{(3-n)+}}},$$

where

$$\text{the const} = -\frac{RT}{nF}\ln\left[\frac{a_{Ce^{3+}}}{a_{Ce^{(3-n)+}}}\right]_{\text{metal-sat'd}},$$

$$E = \text{const} + \frac{RT}{nF}\ln\frac{\gamma_{Ce^{3+}}}{\gamma_{Ce^{(3-n)+}}} + \frac{RT}{nF}\ln\frac{[Ce^{3+}]}{[Ce^{(3-n)+}]}.$$

Studies of the Ce-$CeCl_3$[18,19] and La-$LaCl_3$[20,21] systems have been made, but the results obtained have been invalidated by the reaction of the solutions with the ceramic container material.[22] How badly the results were falsified by this reaction is shown by the obtainment of zero emf in concentration cells of the above type at concentrations of 29 mole % Ce in $CeCl_3$[19] and of 33 mole % La in $LaCl_3$,[20] whereas the saturation limit is 9 and 10 mole % in the Ce-$CeCl_3$[23,24] and La-$LaCl_3$[25,26] respectively.

With the recent development of a metal-cell technique for measuring emf,[27] the study of the emf of the rare-earth systems was undertaken. Figure 7.5 illustrates the all-metal tantalum cell used. The electrode tube contains a weighed quantity of rare-earth halide sufficient to give a liquid height as illustrated. All operations in handling the anhydrous salt and metal were performed in a helium dry box. By means of suitable seals, the center tube of the cell assembly is used both as a stirrer and as a means of adding accurately weighed metal to the salt melt. The end of the center tube has a small hole in the bottom and slots on opposite sides. Small blades were welded to the tube as illustrated to give stirring action. In operation the center tube is lifted out of the melt by slightly loosening the upper seal, releasing the argon pressure in the tank by means of a nullmatic valve, removing the sealing rubber tube, and immediately dropping an accurately weighed piece of rare-earth metal down the tube and resealing with the rubber tube. The tube is then reinserted into the melt, the upper seal retightened, and the argon pressure adjusted.

---

[16] M. A. Bredig, "Mixtures of Metals with Molten Salts," in *Molten Salt Chemistry* (ed. by Milton Blander), Interscience, New York, 1964.

[17] J. D. Corbett, "The Solutions of Metals in their Molten Salts," in *Fused Salts* (ed. by B. R. Sundheim), McGraw-Hill, New York, 1964.

[18] S. Senderoff and G. W. Mellors, *J. Electrochem. Soc.* **105**, 224 (1958).

[19] M. V. Smirnov and V. S. Lbov, *Elektrokhimiya* **1**, 833 (1965); English translation, *Soviet Electrochem.* **1**, 740 (1965).

[20] M. V. Smirnov, P. M. Usov, and T. F. Khazemova, *Dokl. Akad. Nauk SSSR* **151**, 591 (1963); English translation, *Dokl. Chem. Proc. Acad. Sci. USSR* **151**, 583 (1963).

[21] M. V. Smirnov and P. M. Usov, *Dokl. Akad. Nauk SSSR* **151**, 862 (1963); English translation, *Dokl. Chem. Proc. Acad. Sci. USSR* **151**, 606 (1963).

[22] H. R. Bronstein, A. S. Dworkin, and M. A. Bredig, *J. Phys. Chem.* **64**, 1344 (1960).

[23] G. W. Mellors and S. Senderoff, *J. Phys. Chem.* **63**, 1111 (1959).

[24] H. R. Bronstein, A. S. Dworkin, and M. A. Bredig, *J. Phys. Chem.* **66**, 44 (1962).

[25] F. J. Keneshea, Jr., and D. Cubicciotti, *J. Chem. Eng. Data* **6**, 507 (1961).

[26] A. S. Dworkin, H. R. Bronstein, and M. A. Bredig, *Discussions Faraday Soc.* **32**, 188 (1961).

[27] H. R. Bronstein, *J. Electrochem. Soc.* **112**, 1032 (1965).

ORNL-DWG. 66-5666

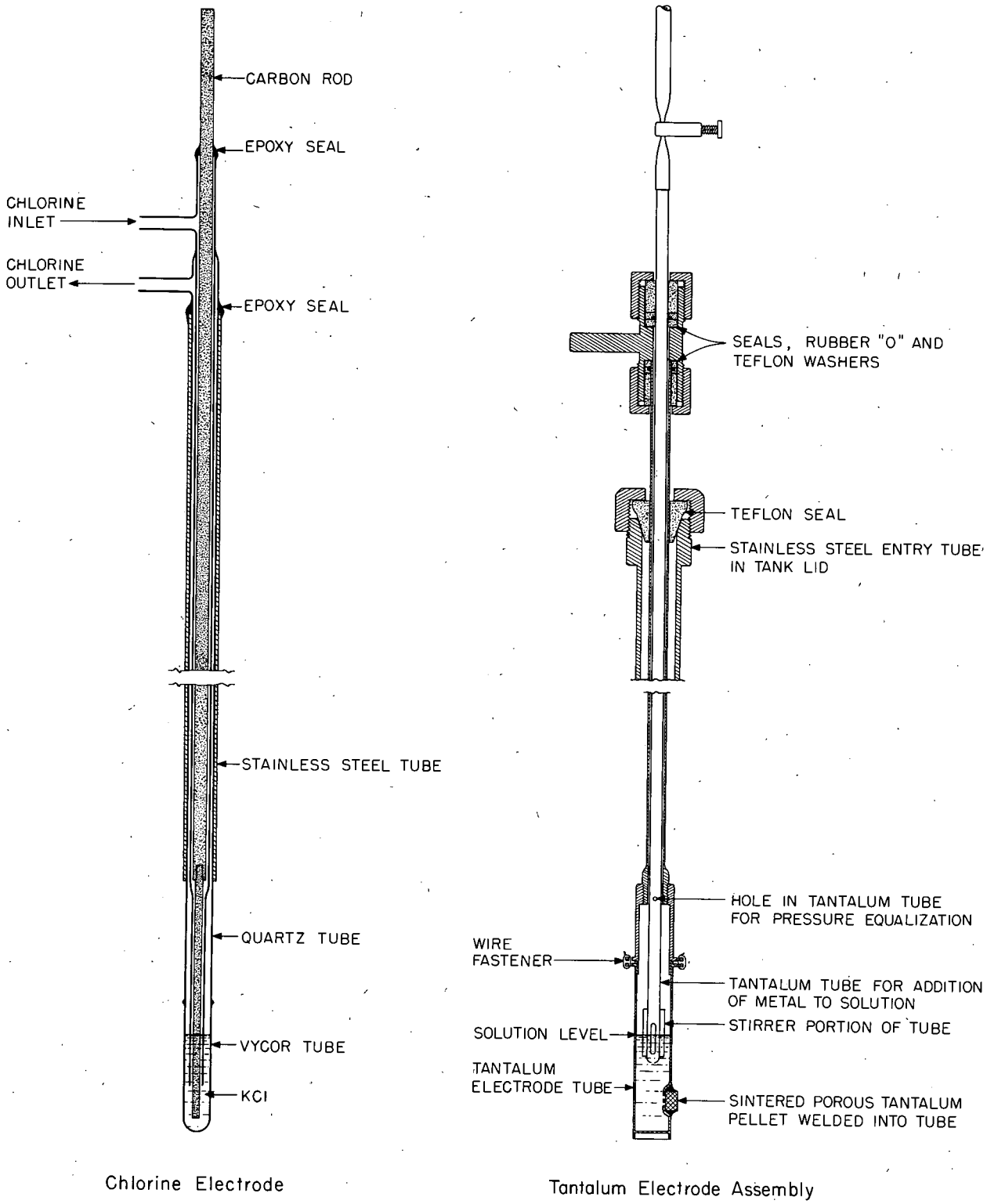

Fig. 7.5. Electrodes of the EMF Apparatus for Corrosive Metal–Metal Halide Solutions.

By this means the metal is added so that splashing is avoided, which could cause a change in concentration. The solution can be stirred by slightly loosening the seal and manually rotating the tube. Figure 7.5 is self-explanatory with respect to the construction of the chlorine electrode assembly. The use of a solid Vycor membrane instead of a porous barrier for electrical contact is necessary to avoid leakage of chlorine gas into the tank. The Vycor glass acts as a salt bridge, since it contains very small quantities of alkali-metal ions which at high temperature become mobile enough to impart conductivity. Since the molten salt on both sides of the Vycor barrier is potassium chloride or, in the case of the Ag-AgCl (7 mole %) electrode, the lithium chloride–potassium chloride eutectic, junction potentials can be considered negligible or nonexistent.[28,29] A potentiometric voltmeter bridge in conjunction with a Hewlett-Packard model 426 dc microvolt-ammeter and recorder was used to measure the emf of the cells.

Figure 7.6 and 7.7 represent the results of the emf investigation for the Ce-$CeCl_3$ and Nd-$NdCl_3$ systems. The emf is plotted against the logarithm of the ratio of the concentrations of the postulated cation species taking part in the electrode reaction

$$M^{2+} \rightleftharpoons M^{3+} + e^- .$$

Both systems yield a slope corresponding to a one-electron process as postulated above. The linearity of the plots implies that the logarithm of the ratio of the activity coefficients remains constant, or that the ratio is equal to unity. This has been observed in mixtures of molten salts[30] and in the Sb-SbI_3 system.[31] Also, the emf increase with metal concentration ceases at the saturation concentration for each system.[23–26] In the Nd-$NdCl_3$ investigation an Ag|AgCl (7 mole %), LiCl-KCl eutectic reference electrode and the LiCl-KCl eutectic as the bridging liquid were used for one series of measurements. In another measurement the C, Cl_2 |KCl| Vycor electrode and KCl as the bridging liquid were used.

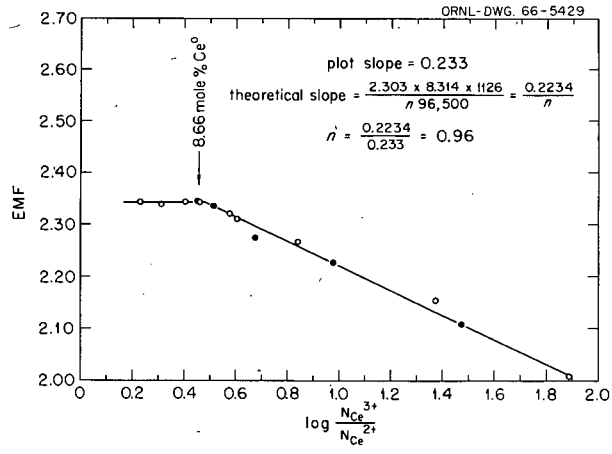

Fig. 7.6. E in Relation to Log_{10} ($N_{Ce^{3+}}/N_{Ce^{2+}}$) (853°C) for the Cell Ta| $CeCl_3$, $xCeCl_{(3-n)}$|KCl| Vycor Glass |KCl|C, Cl_2.

The difference of 1 v between the two series of measurements is in agreement with the known difference between the two types of reference electrodes.[28,32]

The rather surprising feature of these measurements is the similarity in behavior of the Ce-$CeCl_3$ and Nd-$NdCl_3$ systems. In both, the electrode reaction seems to be $M^{2+} = M^{3+} + e^-$. In contrast, the electrical conductivity differs greatly for the two systems.[24,26] In the Ce-$CeCl_3$ system the conductivity increases to a value, in the saturated metal solution (9 mole % Ce^0), approximately five times that of the salt. In the Nd-$NdCl_3$ system, this ratio amounts to only 1.7 (saturation 25 mole % Nd^0), which may be mostly attributed to the greater mobility of the Nd^{2+} vs Nd^{3+} ions. However, most of the difference between Nd and Ce solutions may be explained by assuming that while in the Nd system the equilibrium $M^{2+} \rightleftharpoons M^{3+} + e^-$ lies far to the left, it is shifted in the Ce system to the right providing more mobile electrons. Even in the Ce system, however, the number of mobile electrons appears to be small, and while able to affect the electrical conductivity greatly, has little or no effect upon the thermodynamic activity of the species that determine the emf. While in the preceding these

[28] R. Littlewood, *Electrochim. Acta* 3, 270 (1961).

[29] A. Boozenny, *Trans. AIME* 224, 950 (1962).

[30] S. Senderoff, G. W. Mellors, and R. I. Bretz, *J. Electrochem. Soc.* 108, 93 (1961).

[31] J. D. Corbett and F. C. Albers, *J. Am. Chem. Soc.* 82, 533 (1960).

[32] L. Yang and R. G. Hudson, *Trans. AIME* 215, 589 (1959).

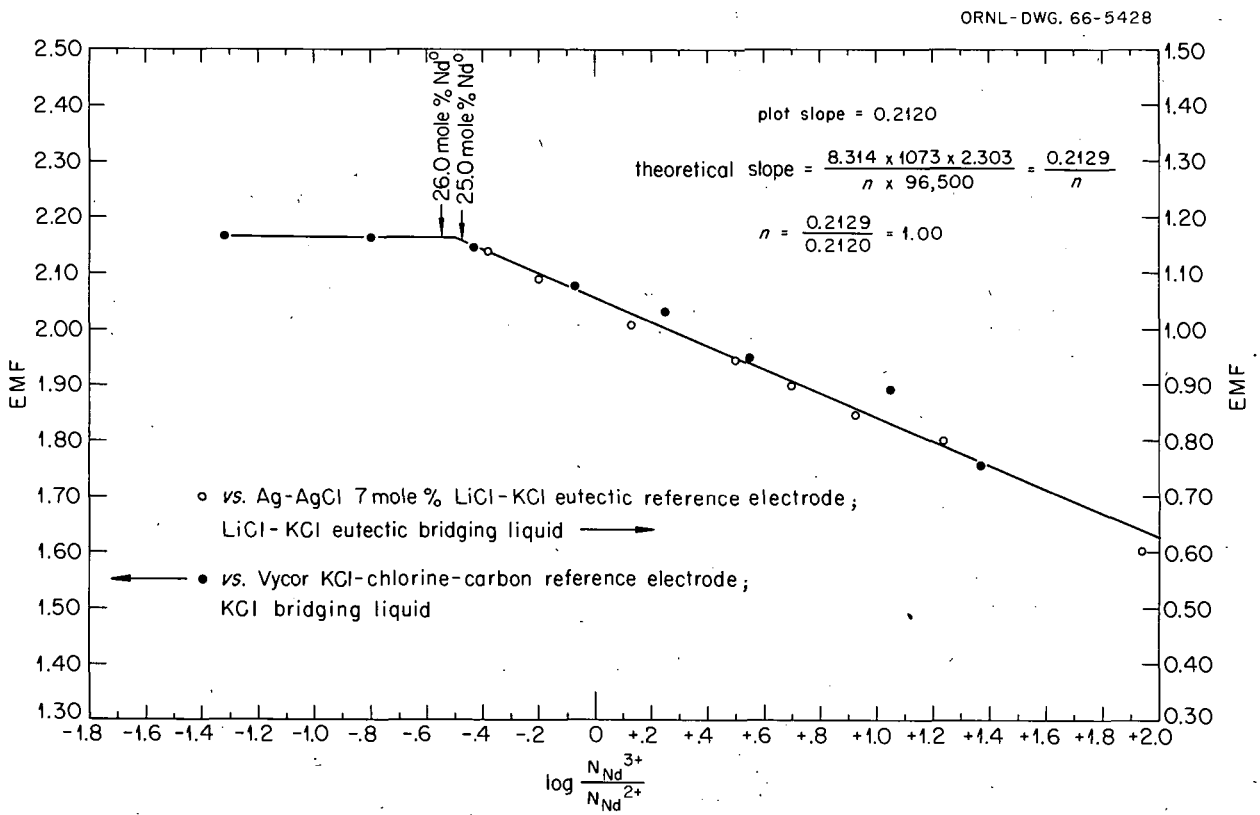

Fig. 7.7. E in Relation to Log ($N_{Nd^{3+}}/N_{Nd^{2+}}$) (800°C) for the Cells Ta | $NdCl_3$, $xNdCl_{(3-n)}$ | KCl | Vycor Glass |KCl| C, Cl_2 and Ta | $NdCl_3$ $xNdCl_{(3-n)}$|LiCl-KCl| Vycor Glass |LiCl-KCl, AgCl(7 Mole %)| Ag.

species have been named M^{2+} (and M^{3+}), there appears to be no reason why a mobile "solvated," F-center-like electron[33] might not behave similarly to M^{2+} with respect to the emf dependence on concentration.

The evaluation of thermodynamic quantities such as the free energy, heat, and entropy of formation of these metal solutions will be made as soon as the experiments now under way are completed. The C, Cl_2 |KCl| Vycor electrode is to be measured vs an $NdCl_3$ | C, Cl_2 and a $CeCl_3$ | C, Cl_2 electrode so that by combination with the present data, potentials of the cells

$$Ce^0_{liquid}|CeCl_3, CeCl_{(3-n)} \text{ sat'd}||CeCl_3|C, Cl_2 ,$$

$$Nd^0_{solid}|NdCl_3, NdCl_{(3-n)} \text{ sat'd}||NdCl_3|C, Cl_2 ,$$

pertaining to the reaction $M^0_{liquid} \rightarrow M$ dissolved in MCl_3 can be calculated.

Strontium Metal–Strontium Halide Systems

A. S. Dworkin M. A. Bredig

We have continued the study of metal-salt miscibility in systems of the type M-MX_2 with a determination of the phase equilibria between strontium metal and its halides (X = Cl, Br, I). The results are compared in Fig. 7.8 with those obtained earlier for the corresponding barium systems.[34] As more or less expected, the strontium systems are intermediate between the calcium and barium systems, but closer to the latter. This is

[33] M. A. Bredig, *J. Chem. Phys.* 37, 914 (1962).

[34] A. S. Dworkin, H. R. Bronstein, and M. A. Bredig, *Chem. Div. Ann. Progr. Rept. June 20, 1964*, ORNL-3679, p. 91.

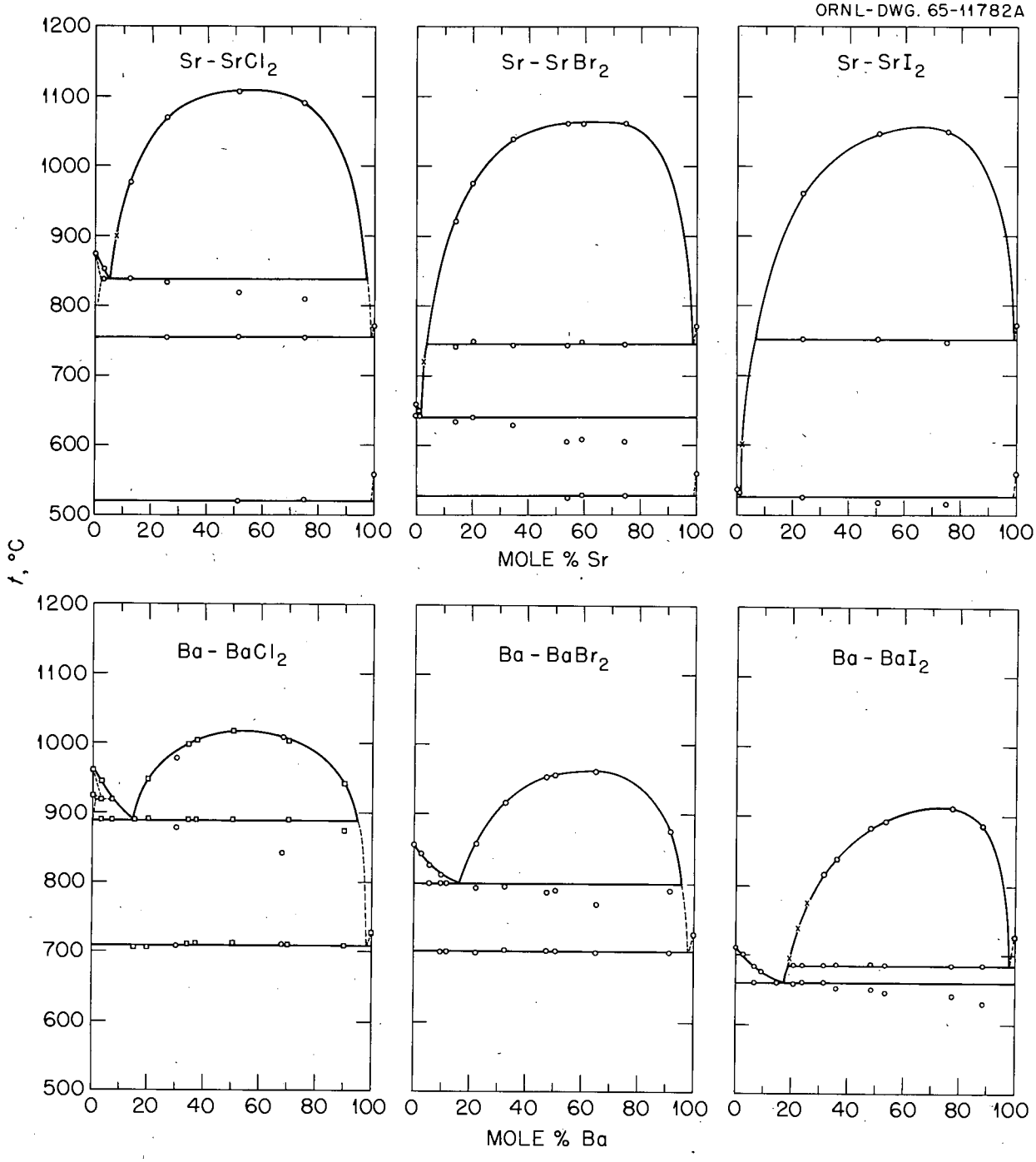

Fig. 7.8. Strontium Metal–Strontium Halide Systems in Comparison with the Corresponding Barium Systems.

reflected by the critical solution temperature, which may be used as a good criterion of the miscibility. Strontium is also intermediate with respect to the dependence of the miscibility on the nature of the halide ion. This miscibility which for calcium slightly decreases from the fluoride to the iodide systems, increases slightly in this halide series for strontium, but less so than for barium.

Combination of the solubility of $SrCl_2$ in liquid strontium metal with vapor pressure data yields the result that in the metallic solution $SrCl_2$ by dissociation produces two (new) particles, probably separate Cl^- ions.

A more detailed discussion of these various results is given in a paper which is being prepared for publication.

Metal–Metal Fluoride Miscibility in Liquid and Solid Phase

A. S. Dworkin M. A. Bredig

We have shown earlier[35] that the original data[36] on the phase relations in the calcium metal–calcium fluoride system required a reinterpretation in terms of complete miscibility of the metal with the salt in the liquid state. We have performed a few additional tests in this system and confirmed our conclusion that there is no monotectic reaction; that is, there are no two-liquid phase equilibria in this system, making CaF_2-Ca the first metal–metal halide system outside the alkali-metal systems for which this has been observed. This result suggested that barium fluoride, because of its lower lattice energy compared with calcium fluoride, would be considerably more soluble in liquid barium metal than CaF_2 in Ca. Figure 7.9, based on cooling curves for BaF_2-Ba mixtures contained in tantalum capsules, shows this indeed to be the case by as much as a factor of 4. Figure 7.10 is a plot of the partial molar excess free energy or excess chemical potential of BaF_2, $\Delta\mu^E(BaF_2)$, vs the square of the barium-metal mole fraction, N_{Ba}. In this test of

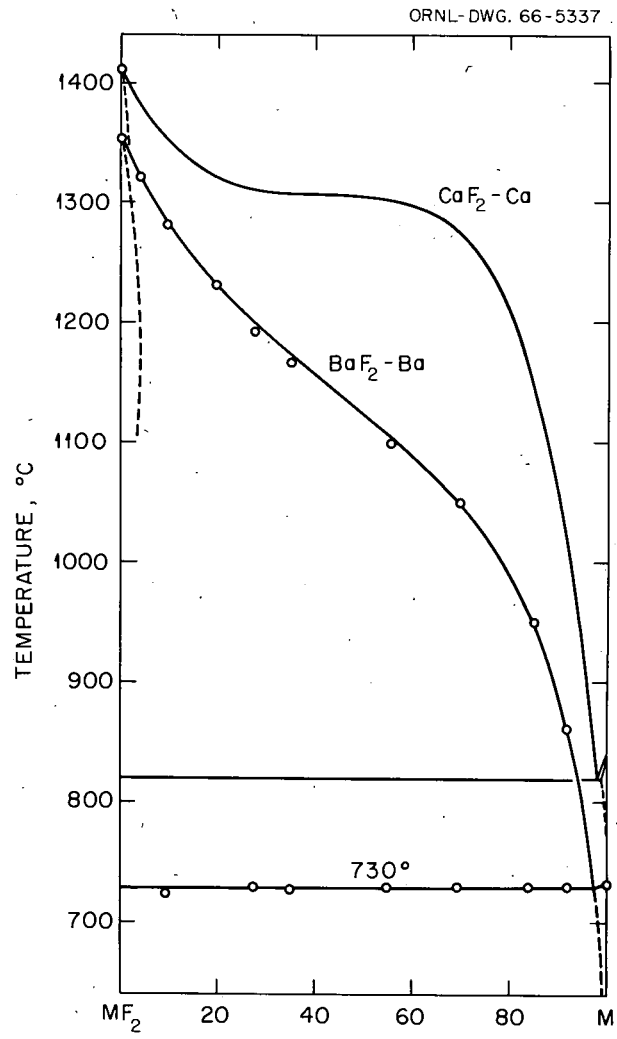

Fig. 7.9. Phase Equilibrium Diagram of the BaF_2-Ba System Compared with CaF_2-Ca.

the most simple form of the dependence of the activity coefficient on concentration according to regular solution theory, the experimental points should have fallen on a straight line. Its slope and intercept at $N_{Ba} = 1$ would equal the parameter B in $\ln \gamma_{BaF_2} = BN_{Ba}^2/RT$. This plot for the BaF_2-Ba solutions greatly resembles earlier plots for several alkali-metal–metal halide systems, Rb-RbBr, Cs-CsI, and the other cesium systems[37]

[35] B. D. Lichter and M. A. Bredig, *J. Electrochem. Soc.* 112, 506 (1965).

[36] P. S. Rogers, J. W. Tomlinson, and F. D. Richardson, p. 909 in *Proceedings of the International Symposium on Physical Chemistry of Process Metallurgy, Pittsburgh, 1959*, Interscience, New York, 1961.

[37] M. A. Bredig, "Mixtures of Metals with Molten Salts," p. 379 in *Molten Salt Chemistry* (ed. by M. Blander), Interscience, New York, 1964.

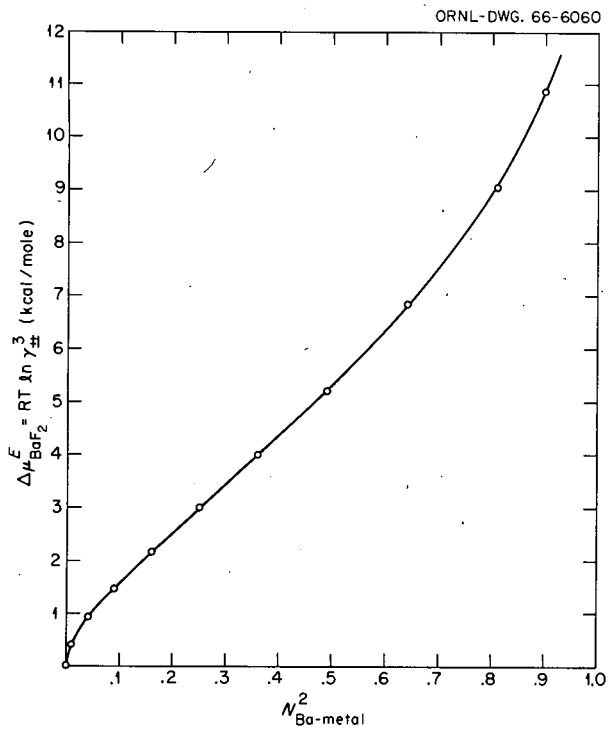

Fig. 7.10. Excess Chemical Potential of BaF_2 as Functions of Concentration.

in two important aspects: (1) The actual nonlinear character of the curve indicates considerable deviation from simple regular solution behavior,[38] that is, nonideal entropy of mixing and very likely also a temperature dependence of this entropy. (2) The value of *B* from an approximate straight line through the experimental points, 6 kcal per equivalent of BaF_2, compares with the 3.5 to 4.5 kcal/mole for the alkali-metal systems above.

A further interesting observation in the BaF_2-Ba system is the relatively high solubility of BaF_2 in *solid* barium metal, approximately 2.5 mole % as estimated from the intercept of the liquidus with the eutectic horizontal, the difference between the eutectic temperature and the melting point of pure barium metal, and the entropy of fusion of the latter. It compares with little more than 1 mole % of CaF_2 in solid calcium metal, and is ascribed to the lower lattice energies of the components in the barium system.

An attempt was also made to study the magnesium metal–magnesium fluoride system. However, additions of magnesium metal up to a concentration of 20 mole % Mg lowered the freezing point of MgF_2, 1256°, to 1253°. With the entropy of fusion of 9 cal deg^{-1} $mole^{-1}$ this indicates that the solubility of Mg in MgF_2 at the monotectic temperature of 1253° is only about 0.5 mole %.

Since an extrapolation of the behavior of the alkali- and alkaline-earth-metal–metal fluoride solutions to the behavior of the trivalent metal–metal fluoride systems appears to be very uncertain, we have begun to study the latter systems experimentally, starting with lanthanum metal–lanthanum fluoride. Difficulties due to the high liquidus temperatures in these systems, approaching 1500°C, are being overcome.

[38] K. S. Pitzer, *J. Am. Chem. Soc.* 84, 2025 (1962).

8. Chemical Physics

THE ABSORPTION SPECTRUM OF AMMONIA IN THE NEAR-INFRARED REGION AS A FUNCTION OF TEMPERATURE FROM BELOW THE FREEZING POINT TO ABOVE THE CRITICAL POINT

W. C. Waggener A. J. Weinberger
R. W. Stoughton

We are studying the temperature dependence of the NH_3 spectrum in the condensed state between 0.6 and 1.4 μ. This spectrum, arising from harmonics and combinations of vibrational modes of the NH_3 molecule, is especially complex because the four fundamental and the combination bands resulting are all infrared active. We have accounted for the general features of the spectrum by a plot of all of the possible summation bands, the positions and relative intensities of the bands being indicated by means of vertical lines on the wavelength scale. The frequencies of bands out to quintary terms were calculated from literature values of the fundamentals and estimated anharmonicity constants, and the relative intensities were assumed to decrease regularly with the number of terms in the summation. The principal band maxima occurring near 1.04, 0.93, 0.89, 0.80, and 0.65 μ have molar absorptivities of 16.2, 0.85, 1.22, 1.93, and 0.19 liters $mole^{-1}$ $cm^{-1} \times 10^{-3}$ in the liquid at the freezing point (–77.7°C). Freezing causes an abrupt decrease in the position of these band maxima of from 62 to 116 cm^{-1} as compared with about 200 cm^{-1} for comparable bands of H_2O. Upon warming liquid NH_3 the above maxima increase slowly and linearly (0.06 to 0.14 $cm^{-1}/°C$) from the freezing point to 60°. For liquid H_2O and D_2O the shifts in the position of respective maxima at the freezing point are initially very large (3 to 5 $cm^{-1}/°C$) and nonlinear, decreasing with increasing temperature to linear shifts (0.2 to 0.3 $cm^{-1}/°C$) above about 100°C. These large shifts observed for H_2O and D_2O near the freezing point are consistent with the presence of and breaking of strong H bonds with increasing temperature. The difference in behavior between water and ammonia is also consistent with the presence of fewer and weaker H bonds in the latter liquid. The NH_3 bands at 1.04 and 0.8 μ are sufficiently well defined as to allow study of their widths as a function of temperature. Both show a broadening of 16 and 55%, respectively, in going from the freezing point (–77.7°C) to the critical point (132.4°C), which must be due to kinetic effects characteristic of relatively weak intermolecular association. The widths of the broad water bands studied previously decrease 50 to 55% in going from the freezing point to 250°C, which is again indicative of relatively strong intermolecular H-bonding and the concomitant bond-breaking with increasing temperature.

THE ABSORPTION SPECTRUM OF NORMAL HEXANE AND CYCLOHEXANE IN THE NEAR-INFRARED REGION AS A FUNCTION OF TEMPERATURE FROM BELOW THE FREEZING POINT TO ABOVE THE CRITICAL POINT

W. C. Waggener A. J. Weinberger
R. W. Stoughton

We are studying the near-infrared spectra of normal hexane and cyclohexane in the wavelength region between 0.6 and 1.6 μ. We have measured the former solvent from –100 (freezing point –94°C) to 250° (critical point 235°C), and the latter from below its freezing point (5.5°C) to 250° (critical point 279°C). Both liquids have a similar spectrum which consists of complex bands centered at 1.4, 1.2, 1.02, 0.92, and 0.75 μ. The 1.2-, 0.92-, and

0.75-μ bands arise from the third, fourth, and fifth harmonic absorptions of the C–H stretch fundamentals, while the broader 1.4 and 1.02 bands probably involve combinations of the stretching harmonics and the bending modes. Our measurements are not complete, but several features of the temperature dependences of these spectra are apparent. The band maxima exhibit extremely small and essentially linear shifts ($\sim$0.05 $cm^{-1}/°C$) to higher frequencies over the entire liquid range from the freezing point to within 6° of the critical point (*n*-hexane). The band intensities are relatively insensitive to temperature changes compared to those of NH_3, H_2O, D_2O, and CO_2. We also have been unable to detect any measurable change in the spectral parameters of cyclohexane due to solidification at its freezing point. These observations agree with the behavior to be expected for C–H bonds as compared to more polar N-H and O-H bonds.

CALORIMETRY

The Heat Capacity of Potassium Hexaiodorhenate(IV) from 6 to 320°K

R. B. Bevan, Jr. R. A. Gilbert
R. H. Busey

The low-temperature heat capacity measurements on K_2ReI_6 reported here are a continuation of a series of such measurements on the compounds K_2ReX_6. The chloride[1] and bromide[2] complexes have been reported. The latter two complex salts have the K_2PtCl_6 face-centered cubic structure at room temperature, whereas the iodide salt has orthorhombic symmetry.[3,4] Pure quadrupole resonance data[5] on K_2ReI_6 indicate no structure change from room temperature to liquid-nitrogen temperatures, but they do indicate a crystal structure change at 160°C. The structure above 160°C is not cubic, however, as might be expected from the crystal structure behavior of the chloride and bromide salts. For these reasons no heat capacity anomalies arising from structural changes like the ones exhibited by the chloride and bromide salts[1,2] were anticipated. The possibility existed, however, that K_2ReI_6 might exhibit thermal history behavior similar to that shown by K_2ReBr_6.

Results of the heat capacity measurements are given in Figs. 8.1, 8.2, and 8.3. Figure 8.1 shows the lambda-type heat capacity anomaly associated

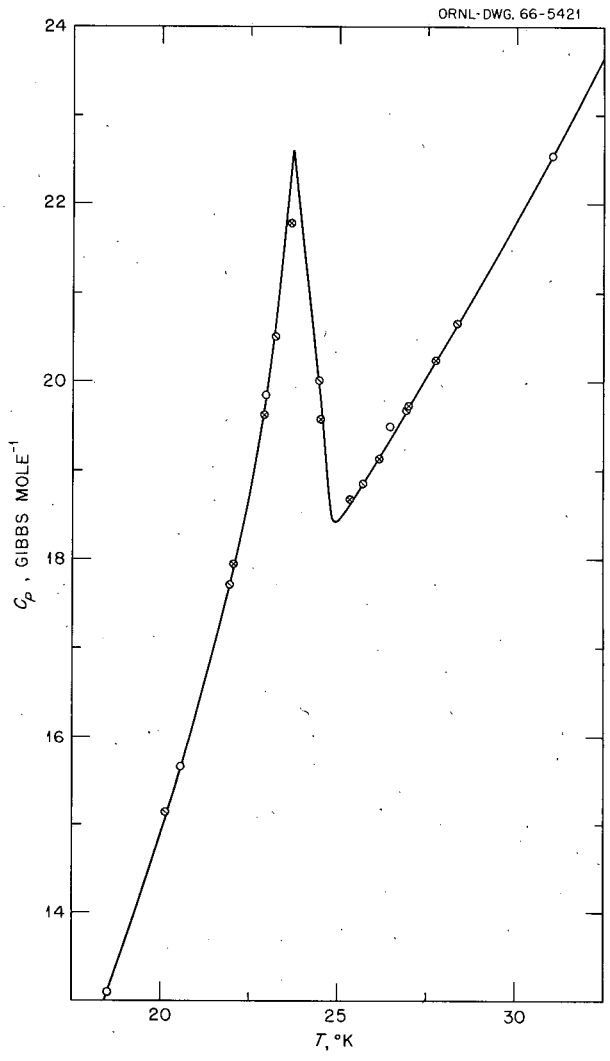

Fig. 8.1. Cooperative Transition of K_2ReI_6 with Heat Capacity Maximum at 23.7°K. The transition is from an ordered antiferromagnetic state below 23.7°K to the disordered paramagnetic state above this temperature.

[1] R. H. Busey, H. H. Dearman, and R. B. Bevan, Jr., *J. Phys. Chem.* **66**, 82 (1962).

[2] R. H. Busey, R. B. Bevan, Jr., and R. A. Gilbert, *J. Phys. Chem.* **69**, 3471 (1965).

[3] J. Dalziel, N. S. Gill, R. S. Nyholm, and R. D. Peacock, *J. Chem. Soc.* **1958**, 4012.

[4] J. C. Morrow, *J. Phys. Chem.* **60**, 19 (1956).

[5] R. Ikeda, D. Nakamura, and M. Kubo, *J. Phys. Chem.* **69**, 2101 (1965).

with the transition from the disordered paramagnetic state above 23.7°K (Néel temperature) to the ordered antiferromagnetic state below this temperature. This anomaly is not as sharp and well defined as the similar anomalies shown by the chloride and bromide salts, a circumstance which may be due to the fact that K_2ReI_6 cannot be prepared as pure as K_2ReCl_6 and K_2ReBr_6.

Figure 8.2 shows the anomalous behavior of the heat capacity from 190 to 240°K. When the sample was cooled to 180°K and measurements were made over this temperature interval, the results fell on the dotted portion of the curve. The sample spontaneously evolved heat over the temperature interval 150 to 160°K; only when this heat evolution was allowed to go to completion did the heat capacity results show the anomalous behavior. In this respect the K_2ReI_6 resembles the behavior of the K_2ReBr_6, which exhibits a small heat capacity anomaly at 214°K only after heat evolution at 150°K has been allowed to go to completion.[2] The entropy associated with the anomalous behavior is 0.09 cal $deg^{-1} \cdot mole^{-1}$ for the K_2ReI_6, which is similar in magnitude to that of the K_2ReBr_6. Contrary to the behavior of the 214°K anomaly of K_2ReBr_6, however, the anomalous behavior of

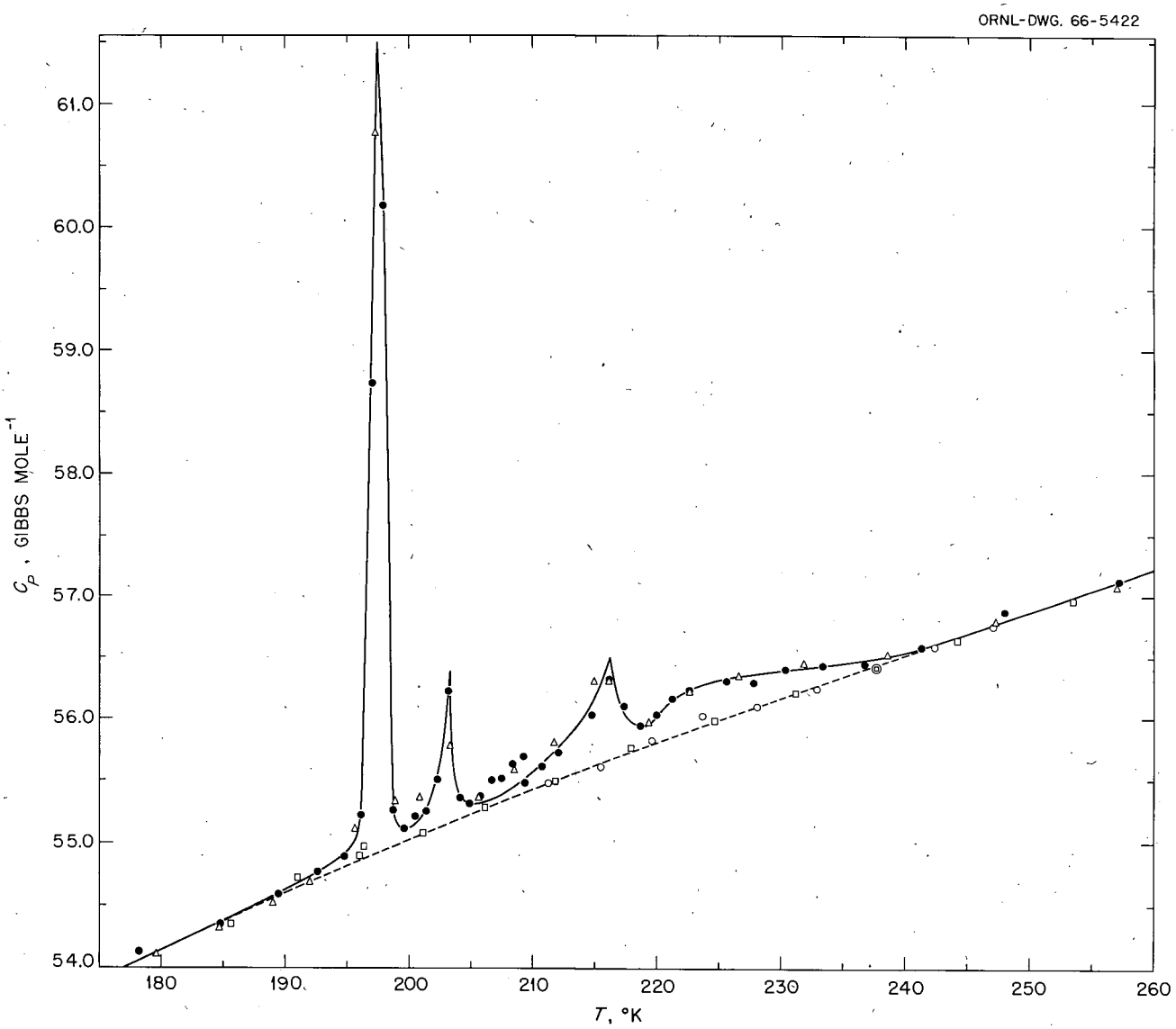

Fig. 8.2. Heat Capacity of K_2ReI_6 Showing Details of the Anomalous Region from 190 to 240°K.

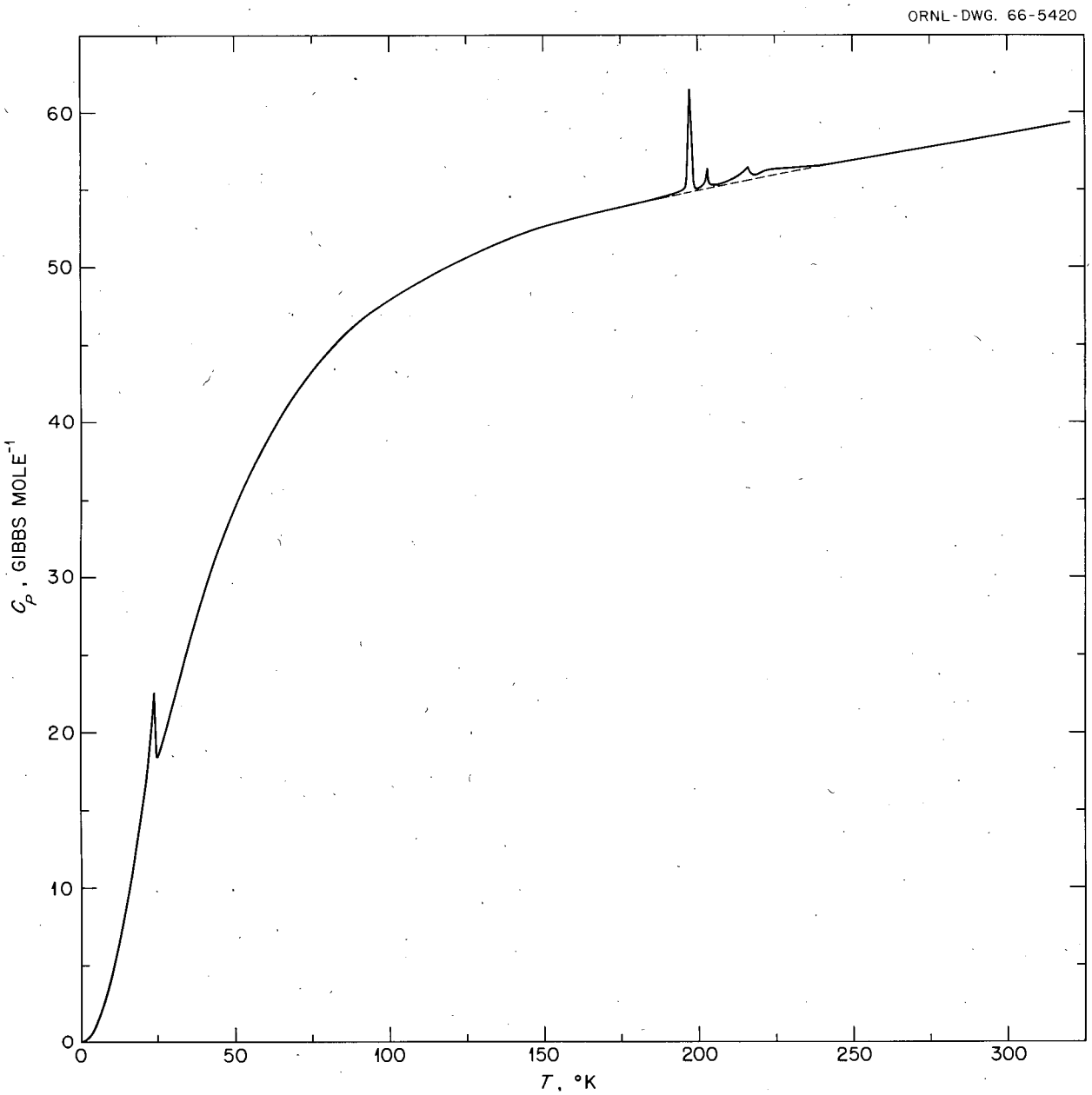

Fig. 8.3. Heat Capacity of K_2ReI_6 Showing the Anomalies in Relation to the Remainder of the Heat Capacity Curve.

K_2ReI_6 in the region 190 to 240°K does not diminish and disappear after many coolings to the region of heat evolution.

It has been suggested[2] that in the case of K_2ReBr_6 the 214°K anomaly is associated with a low concentration of a metastable crystalline phase, and that this phase is "annealed out" of the sample by many coolings through a low-temperature region where three crystal structure changes occur. Similarly, the anomalous heat capacity of K_2ReI_6 in the interval 190 to 240°K may be due to a metastable phase (or phases); but in this case, consistent with the observations, no diminution of the anomalous behavior is expected with multiple cool-

ings because the salt has no low-temperature crystal structure changes and thus has no mechanism for "annealing out" the metastable phase.

The metastable phase hypothesis might be tested by attempting to anneal the phase out at higher temperatures, for example, by thermally cycling the sample through the 160°C transition. Unfortunately, preliminary experiments indicate that some decomposition occurs in a sample of K_2ReI_6 even at 100°C. Decomposition products in a thermally treated sample might complicate the interpretation of further heat capacity measurements made to detect changes resulting from the thermal treatment.

From plots of the Néel temperatures (determined from low-temperature heat capacity data) of K_2ReI_6, K_2ReBr_6, and K_2ReCl_6 vs appropriate parameters (reciprocal of the electronegativity or electron affinity of the halide), the Néel temperature of K_2ReF_6 is estimated to be approximately 7°K. This requires that the planned heat capacity measurements on K_2ReF_6 be extended to as low a temperature as possible with our present calorimeter in order to obtain accurate entropy results.

The thermodynamic functions of K_2ReI_6 at 298.15°K in cal deg^{-1} mole^{-1} are: $C_p^\circ = 58.53$, $S^\circ = 118.16$, $(H^\circ - H_0^\circ)/T = 46.35$, $(F^\circ - H_0^\circ)/T = -71.80$.

High-Temperature Enthalpy of Potassium Pertechnetate. Second-Order Transition with a Heat Capacity Maximum at 750°K

R. A. Gilbert R. H. Busey

The relative enthalpy of $KTcO_4$, $(H_T - H_{273.15})$, has been measured to 1200°K using a Bunsen ice calorimeter and a silver-core furnace. The meas-

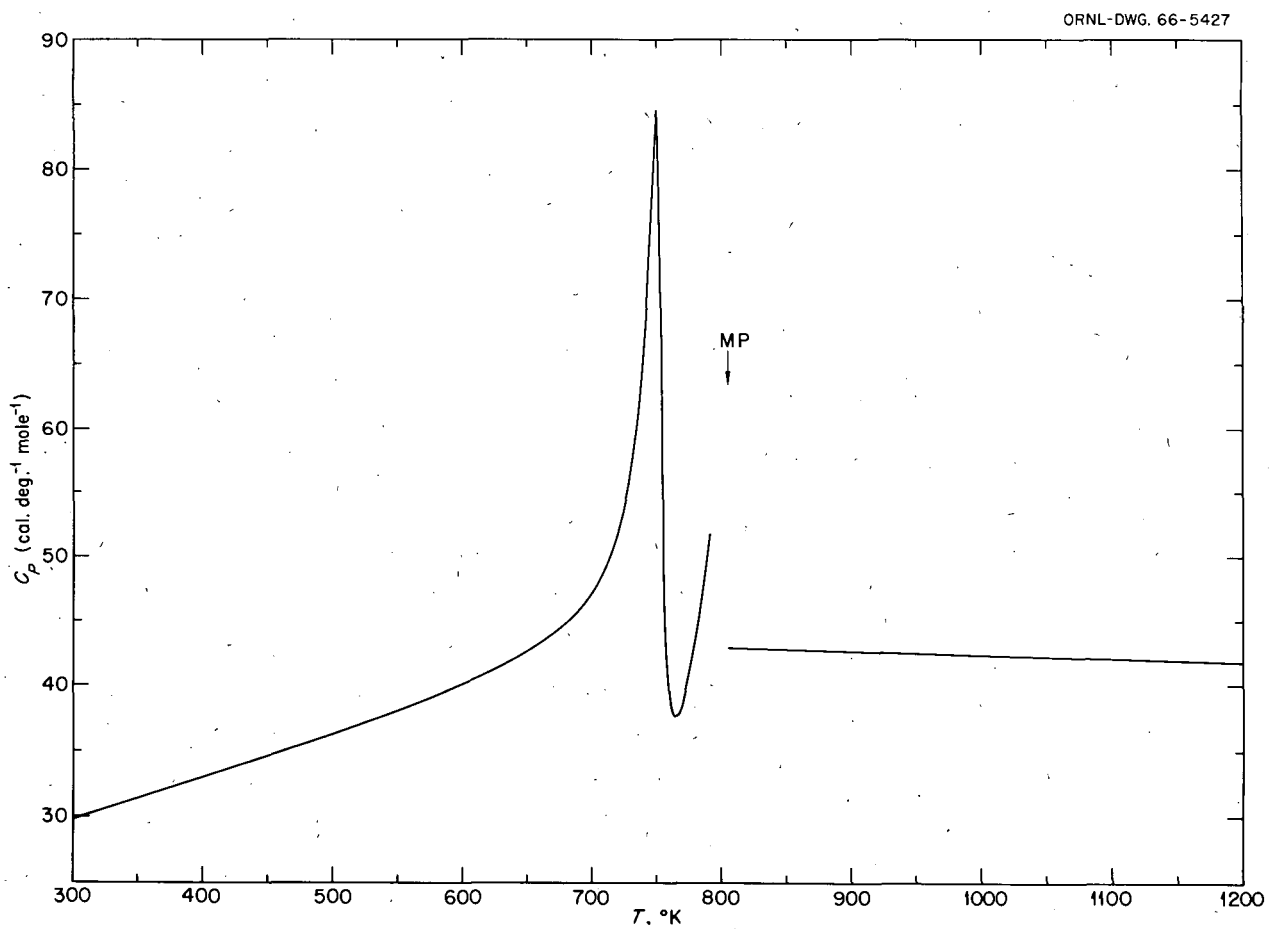

Fig. 8.4. High-Temperature Heat Capacity of $KTcO_4$, Derived from High-Temperature Enthalpy Data, Showing Lambda-Type Transition with a Maximum at 750°K.

urements were made on a gold-encapsulated 14-g sample.

The results are presented in Fig. 8.4, which gives the heat capacity from 300 to 1200°K derived from the high-precision enthalpy results. The lambda-type transition with a maximum at 750°K (only 50° below the melting point) dominates the high-temperature heat capacity curve.

At room temperature $KTcO_4$ has the $CaWO_4$-type structure (scheelite structure, space group $C_{4h}^6 - I4_1/a$).[6] A cursory search of the literature reveals that very little is known concerning the high-temperature behavior of salts possessing the scheelite structure at room temperature. The lambda transition might represent a crystal structure change, possibly to a cubic structure similar to that of $KClO_4$ at high temperatures.

Enthalpy and Free Energy of Formation of the Hexachlororhenate(IV) Ion and Its Enthalpy of Hydrolysis

R. H. Busey R. A. Gilbert
K. H. Gayer[7] R. B. Bevan, Jr.

The following is an abstract of a paper accepted for publication[8] in the *Journal of Physical Chemistry*.

The entropy of the aqueous hexachlororhenate(IV) ion, $ReCl_6^{2-}(aq)$, has recently been determined from low-temperature heat capacity, enthalpy of solution, and solubility measurements on K_2ReCl_6.[9] Since this ion represents one of the most stable and important species of rhenium in hydrochloric acid, the determination of its thermodynamic properties is of primary importance to a study of the thermochemistry of this element.

The standard enthalpy of the reaction

$$K_2ReCl_6(c) + \frac{3}{2}ClO^- + 5OH^- = ReO_4^- + \frac{15}{2}Cl^- + 2K^+ + \frac{5}{2}H_2O \qquad (1)$$

was determined to be $\Delta H_1^\circ = -152.7 \pm 0.6$ kcal per mole at 25°C by solution calorimetry. The stoichiometry of the reaction was established by oxidizing several samples of K_2ReCl_6 with excess standard alkaline hypochlorite solution and determining the unreacted hypochlorite iodometrically after acidifying the solution with hydrochloric acid. During the course of the calorimetric measurements, it was observed that a restriction [in addition to the obvious ones dictated by Eq. (1)] had to be placed on the concentrations of hypochlorite and hydroxide relative to the sample weight in order to obtain complete reaction. If all initial concentrations are expressed in molarity, the additional restriction required that the concentration ratio given by the expression $R = [OH^-][Re]/[ClO^-]$ be greater than approximately 0.015 in order to obtain complete reaction in a reasonable length of time. When $R \sim 0.013$ the reaction was observed to be only 60 to 70% complete an hour after the reaction was initiated. Spectrophotometric examination of a 0.5-g sample in a 450-ml solution which was 0.32 N in ClO^- and 0.14 N in OH^- (giving $R \sim 0.002$) showed that 75% of the $ReCl_6^{2-}$ was still unreacted three days after initiating the reaction. It should be emphasized that $ReCl_6^{2-}$ slowly hydrolyzes even in water. Separate titration experiments confirmed these observations.

The standard enthalpy of the reaction

$$K_2ReCl_6(c) + 4OH^- = ReO_2 \cdot 2H_2O(c) + 6Cl^- + 2K^+ \qquad (2)$$

was determined to be $\Delta H_2^\circ = -63.6 \pm 0.2$ kcal per mole. With less than a fivefold excess of OH^-, larger, but erratic, exothermic enthalpies were observed. Apparently with smaller excesses of OH^- the enthalpy observed is not that represented by Eq. (2).

The above ΔH_1° and ΔH_2° combined with the enthalpy of solution of K_2ReCl_6[9] give the following:

$$ReCl_6^{2-} + \frac{3}{2}ClO^- + 5OH^- = ReO_4^- + \frac{15}{2}Cl^- + \frac{5}{2}H_2O\,,$$

$$\Delta H_3^\circ = -163.1 \pm 0.8 \text{ kcal/mole}\,; \qquad (3)$$

[6] B. J. McDonald and G. J. Tyson, *Acta Cryst.* **15**, 87 (1962).

[7] Oak Ridge Institute of Nuclear Studies research participant at Oak Ridge National Laboratory during 1965 from Wayne State University, Detroit, Mich.

[8] R. H. Busey, K. H. Gayer, R. A. Gilbert, and R. B. Bevan, Jr., *J. Phys. Chem.* **70**, in press.

[9] R. H. Busey, H. H. Dearman, and R. B. Bevan, Jr., *J. Phys. Chem.* **66**, 82 (1962).

$$ReCl_6^{2-} + 4OH^- = ReO_2 \cdot 2H_2O(c) + 6Cl^- ,$$

$$\Delta H_4^\circ = -74.0 \pm 0.2 \text{ kcal/mole} . \quad (4)$$

The enthalpy of formation of $ReCl_6^{2-}(aq)$ at 25°C is calculated from ΔH_3° to be $\Delta H_f^\circ[ReCl_6^{2-}(aq)] = -183.0 \pm 0.8$ kcal/mole, using values from the literature[10] for the required thermodynamic properties of the other species.

If $\Delta H_f^\circ[ReCl_6^{2-}(aq)] = -183.0$ kcal/mole and an estimated $S^\circ[ReO_2 \cdot 2H_2O(c)] = 37 \pm 5$ cal deg^{-1} mole^{-1} are combined with ΔH_4°, the free energy of formation of $ReO_2 \cdot 2H_2O(c)$ is computed to be -197.3 ± 1.5 kcal/mole. This result differs significantly from that calculated from the potential observed by Hugus[11] for the $ReO_2 \cdot 2H_2O(c)$-ReO_4^- couple, -202.4 kcal/mole. Unless the estimated entropy of $ReO_2 \cdot 2H_2O(c)$ is grossly in error,[12] the thermal data for reactions (3) and (4) indicate either that Hugus' potential may be in error, or that the free energies of the hydrolytically produced and the electrolytically produced $ReO_2 \cdot 2H_2O(c)$ do indeed differ by approximately 5 kcal/mole. Since there is preliminary evidence[13] that Hugus' potential is substantially correct, the second hypothesis seems more likely. It should be pointed out that ΔH_4° corresponds to the enthalpy change when *freshly* precipitated $ReO_2 \cdot 2H_2O(c)$ is obtained. On the other hand, the dioxide employed in an electrolytic cell potential measurement is usually "aged," since often days are required to reach equilibrium. The hypothesis may be expressed by the equation:

$$ReO_2 \cdot 2H_2O(c)\text{(freshly precipitated)} = ReO_2 \cdot 2H_2O(c)\text{(aged)} ,$$

$$\Delta F = -5.1 \text{ kcal/mole} .$$

The free energy of formation of $ReCl_6^{2-}(aq)$ at 25°C is:

$$\Delta F_f^\circ[ReCl_6^{2-}(aq)] = \Delta H_f^\circ - T\Delta S_f^\circ = -183.0 + 41.4 \text{ (ref. 9)} = -141.6 \text{ kcal/mole} .$$

The standard electrode potentials of the half reactions,

$$ReCl_6^{2-} + 4H_2O = ReO_4^- + 8H^+ + 6Cl^- + 3e^-$$

and

$$Re + 6Cl^- = ReCl_6^{2-} + 4e^- ,$$

are computed to be -0.19 ± 0.01 v and -0.50 ± 0.01 v respectively. These potentials show that the $ReCl_6^{2-}(aq)$ is thermodynamically unstable with respect to disproportionation into Re metal and $ReO_4^-(aq)$. Since the ion is quite stable, the Re(III) and Re(V) species on each side of it in the redox scheme in hydrochloric acid probably have free energies of formation that stabilize it.

Table 8.1 summarizes the thermodynamic properties derived from the data presented, together with those previously available.

Table 8.1. Thermodynamic Functions for the Formation of K_2ReCl_6, $ReCl_6^{2-}(aq)$, and $ReO_2 \cdot 2H_2O$ at 25°C

	$\Delta H_f^{\circ a}$	$\Delta F_f^{\circ a}$	$S^{\circ b}$
$K_2ReCl_6(c)$	−313.5	−280.7	88.84
$ReCl_6^{2-}(aq)$	−183.0	−141.6	60.8
$ReO_2 \cdot 2H_2O(c)$	−241.8	−202.4	37[c]

[a]In kcal/mole.
[b]In cal deg^{-1} mole^{-1}.
[c]Estimated.

[10]The thermodynamic properties of various species required in the thermochemical calculations were taken from W. M. Latimer, *Oxidation Potentials*, 2d ed., Prentice-Hall, New York, 1962, with the following exceptions:

(*a*) ReO_4^-: G. E. Boyd, J. W. Cobble, and W. T. Smith, Jr., *J. Am. Chem. Soc.* **75**, 5783 (1953);

(*b*) ClO^-: J. E. McDonald, J. P. King, and J. W. Cobble, *J. Phys. Chem.* **64**, 1345 (1960);

(c) Re: U. Piesbergen, *Z. Naturforsch.* **19A**, 1075 (1964).

[11]Z. Z. Hugus, cited by Latimer.[10]

[12]To obtain agreement between ΔH_3°, ΔH_4°, and Hugus' potential, the entropy of $ReO_2 \cdot 2H_2O(c)$ would have to be 54.2 cal deg^{-1} mole^{-1}, which seems excessive.

[13]Private communication from G. H. Cartledge of this Laboratory.

MICROWAVE AND RADIO-FREQUENCY SPECTROSCOPY

Paramagnetic Resonance Studies of Single Crystals

Robert W. Holmberg José Ezratty[14]
Ralph Livingston

A paramagnetic resonance spectrometer has been designed and constructed so that samples can be gamma irradiated at 4°K and resonance spectra observed without warming the sample. The spectrometer operates at a nominal frequency of 9 gHz and uses a microwave cavity operating in the TE_{102} mode. The cavity, which is located in a double Dewar system for liquid helium and liquid nitrogen, has variable coupling, which may be adjusted while the cavity is at 4°K. In present usage, a sample is placed in the cavity before cooling and irradiation, but a connecting tube from the cavity to the exterior of the Dewar system gives future provision for withdrawing a sample from the cold cavity, introducing a new sample from a region of higher temperature, piping light to the sample for photolytic studies, etc. The spectrometer employs a microwave circulator, and the microwave frequency may be locked on the cold cavity or upon an external cavity so that dispersion signals may be seen. Irradiations at 4°K are made by transferring the entire Dewar system containing the cavity and sample at 4°K to a large ^{60}Co irradiation facility.

Several years ago a study was made[15] of paramagnetic species formed at 77°K in single crystals of calcium hydroxide irradiated with gamma rays from ^{60}Co. The principal species gave rise to a single anisotropic line described by an axially symmetric g tensor. The line width was anisotropic with respect to the orientation of the crystal in the magnetic field, and there were satellites which indicated upon analysis that the species occupied an OH^- vacancy. It was finally concluded that the species was probably O^-. It disappeared when the crystal was warmed to 0°C. Crystals of calcium hydroxide have now been studied at 4°K. Crystals irradiated at 77°K but examined at 4°K gave a spectrum exactly like that attributed to O^- in the earlier work. However, a crystal irradiated and examined at 4°K gave a different spectrum. This new species was apparently a precursor of O^-, for as the sample was allowed to slowly warm to 77°K the new spectrum disappeared while that of O^- appeared. A precise assay has not been made, but the correspondence appeared to be 1:1.

Detailed measurements of the new spectrum have been made. Calcium hydroxide crystals are hexagonal with space group D^3_{3d}. We have chosen an orthogonal system of axes designated 1, 2, and 3 where axis 1 is the threefold axis (hexagonal c axis), axis 2 is a twofold axis, and axis 3 lies in a mirror plane. The spectrum was measured for various directions of the magnetic field parallel to the 1, 2 and also the 1, 3 planes. Principal values found for the g tensor were 2.001, 2.069, and 2.110. The direction corresponding to g = 2.069 was parallel to axis 2, while those corresponding to 2.001 and 2.110 were parallel to the 1, 3 plane, making angles of 37 and 53°, respectively, with axis 1. Hyperfine effects were also present. The most prominent feature was a doublet splitting which was anisotropic. This interaction was probably due to a single nearby interacting proton. The maximum splitting was about 8 gauss. The hyperfine effects could not be fitted to a simple spin Hamiltonian, and there was a peculiar intensity anomaly. The species most reasonably is the OH radical, although the hyperfine interaction is smaller than expected, and there remain theoretical problems to be resolved.

When crystals of calcium hydroxide were irradiated at 77°K, warmed to room temperature, and again cooled to 77°K, the spectrum of O^- disappeared. However, if the crystal was further cooled to 4°K, a new, third spectrum appeared. There were no resolved hyperfine interactions, and the g tensor had principal values 2.310, 1.967, and 1.978 with principal directions parallel to axes 2, 1, and 3 respectively. This spectrum was undoubtedly due to O_2^-, which could only be observed at 4°K even though the species is stable at room temperature.

Paramagnetic Resonance Study of Free Radicals Formed in Liquids During Ultraviolet Photolysis

Ralph Livingston Henry Zeldes

A study of the paramagnetic resonance spectra in liquid acetone and acetone solutions during

[14]Visitor from CEN, Saclay, France.

[15]R. Livingston and H. Zeldes, *Chem. Div. Semiann. Progr. Rept. June 20, 1956*, ORNL-2159, p. 89.

the course of intense irradiation with ultraviolet light has been completed and will be published shortly. Acetone is excited by the irradiation, presumably to a triplet state, whereupon it is capable of extracting hydrogen from suitable donors. Another molecule of acetone may serve as the donor, and accordingly both radicals of the reaction

$$CH_3COCH_3 + CH_3COCH_3 \longrightarrow (CH_3)_2\dot{C}OH + \dot{C}H_2COCH_3$$

were studied during the photolysis of pure acetone. A small amount of $\dot{C}H_3$ was also observed, which was thought to result from the reaction

$$\dot{C}H_2COCH_3 \longrightarrow H_2C{=}C{=}O + \dot{C}H_3 .$$

Higher concentrations of $\dot{C}H_2COCH_3$ and $\dot{C}H_3$ were also prepared by another method, the photolysis of acetone containing 1% H_2O_2. The OH radical was produced from H_2O_2, and then abstracted hydrogen from the acetone.

Many substances are more suitable donors of hydrogen than acetone. When solutions of these substances with acetone were photolyzed, higher yields of radicals were obtained. For example, with ethyl alcohol both radicals of the reaction

$$CH_3COCH_3 + CH_3CH_2OH \longrightarrow (CH_3)_2\dot{C}OH + CH_3\dot{C}HOH$$

were seen. Moreover, high yields of radicals could often be obtained in solutions containing large amounts of water, say, up to 80% H_2O. Accurate measurements of g values and hyperfine parameters for $(CH_3)_2\dot{C}OH$, $\dot{C}H_2OH$, and $CH_3\dot{C}HOH$ in both acetone-rich and water-rich solutions were made at room temperature by choosing the appropriate alcohol as a constituent of the solution. The radical $CH_3\dot{C}HOCH_2CH_3$ was studied in an acetone solution containing ether. Similarly, in an acetone solution of dioxane the radical formed by abstraction of a hydrogen atom from dioxane was studied.

In earlier work[16] we found that hyperfine interactions for hydroxyl hydrogens were highly temperature dependent, and in some cases temperatures were found for which the interaction became zero. The mechanism proposed for these changes implied that at more extreme temperatures the interaction would once again become nonzero, but we were unable for practical reasons to attain such temperature extremes. We have now studied a case, $CH_3\dot{C}HOH$ in a water-rich solution, where the hydroxyl proton hyperfine interaction was carried through the value zero by changes in temperature.

The rate of exchange of hydroxyl protons of radicals is catalyzed by acid. A spectroscopic study of this exchange for $\dot{C}H_2OH$ and $(CH_3)_2\dot{C}OH$ in water-rich solutions was made, and the mean lifetime of a radical between exchanges was measured.

In earlier work[16] a study was made of radicals formed by abstracting hydrogen from simple alcohols. A solution of a small amount of H_2O_2 in the alcohol was photolyzed. Here, OH radical was the intermediate that abstracted hydrogen. The abstraction, generally, was highly specific for the hydrogen in the position alpha to the hydroxyl group. We were unable to obtain radicals, for example, from *t*-butyl alcohol, which has no alpha hydrogens. An extension of the original work has now been completed where the solutions were modified by the addition of water and acid. The addition of water to *t*-butyl, isopropyl, and ethyl alcohols enhanced the formation of the radicals resulting from abstraction of beta hydrogens. The principal effect of acidifying the solutions was the enhancement of the rate of exchange of hydroxyl protons. Hyperfine couplings and g values were measured for $(CH_3)_2(\dot{C}H_2)COH$ and CH_3-$(\dot{C}H_2)CHOH$. The primary product from ethylene glycol with or without water was $\dot{C}HOHCH_2OH$, but with small amounts of acid this radical was not obtained. In its place was $\dot{C}H_2CHO$. Hyperfine couplings and the g value were measured for this radical.

[16] R. Livingston and H. Zeldes, *J. Chem. Phys.* 44, 1245 (1966).

NEUTRON AND X-RAY CRYSTALLOGRAPHY

X-Ray Determination of the Crystal Structure, Molecular Structure, and Absolute Configuration of Leucoxine Hydrobromide

G. M. Brown

A complete x-ray crystal-structure analysis has been performed on the hydrobromide of leucoxine, an alkaloid extracted from the leaves and stems

of *Ocotea leucoxylon* (family Lauraceae). The preliminary characterization[17,18] of the alkaloid leucoxine, $C_{20}H_{21}O_5N$, by chemical, ultraviolet spectroscopic, and NMR methods indicates that it is a member of the aporphine series (based on the ring system **1**) with two methoxy groups, a methylene dioxy group, and a phenolic hydroxyl group. The structure **2** was postulated,[18] in which the asterisks indicate the probable points of attachment of the two CH_3O- groups and the $OH-$ group. The

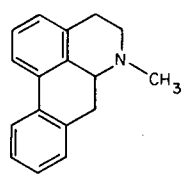

1

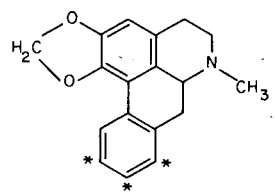

2

x-ray analysis of crystalline leucoxine hydrobromide, $C_{20}H_{22}O_5NBr$, confirms the postulated structure and completes the elucidation of molecular structure, including the absolute stereochemical configuration.

Two crystals, one about 0.2 × 0.1 × 0.1 mm and the other about 0.4 × 0.4 × 0.4 mm, were cut from prismatic specimens of leucoxine hydrobromide furnished by Dr. S. Goodwin and used in data collection on the new Oak Ridge automatic computer-controlled x-ray diffractometer.[19,20,21] The smaller crystal was used for reflections with 2θ values under 85°, and the larger one was used for the remaining reflections with 2θ angles up to 159.5°. Intensity data of 2204 independent reflections were recorded (copper $K\alpha$ radiation) by the θ-2θ step-scan method, with background counts measured at 2θ settings above and below each reflection peak. At the beginning of data recording, approximate parameters for the orthorhombic unit cell (space group $P2_12_12_1$, $Z = 4$) from preliminary precession photography were used; by least-squares adjustment, these were refined from high-angle reflection data recorded on the diffractometer to the following values: $a = 7.1929 \pm 0.0008$ A, $b = 18.3715 \pm 0.0024$ A, $c = 13.8490 \pm 0.0009$ A. The intensity data were converted in preliminary processing, which included correction of absorption errors,[22] to a set of values of structure-factor squares $|F_o|^2$ and standard errors $\sigma_{|F^2|}$ for the structure analysis.

The solution to the phase problem for this crystal was found by the classic heavy-atom method,[23] making use of the bromide ion as the heavy atom. Eventually all 49 atoms in the asymmetric unit ($C_{20}H_{22}O_5NBr$) were included in full-matrix least-squares refinement.[24] The absolute configuration[25] was established at the stage at which the parameters of the 27 heavier atoms had been extensively refined but the hydrogen atom parameters had not been refined. When the imaginary component of the Br^- scattering factor,[26] $\Delta f'' = 1.4$, was included in the structure-factor calculations, the reliability indices[27]

$$R(F) \equiv \frac{\Sigma\left|\,|F_o| - |F_c|\,\right|}{\Sigma|F_o|}$$

were 0.035 and 0.046 for the correct and the inverted configuration, and the values of the standard deviation of fit,[27] σ_1, were 1.48 and 2.11. These differences in goodness-of-fit parameters are highly

[17] S. Goodwin, A. F. Smith, and E. C. Horning, *Chem. Ind.* **1960**, 691.

[18] S. Goodwin, private communication.

[19] W. R. Busing, R. D. Ellison, C. K. Johnson, and H. A. Levy, *Chem. Div. Ann. Progr. Rept. June 20, 1964*, ORNL-3679, p. 100.

[20] W. R. Busing, R. D. Ellison, and H. A. Levy, *Chem. Div. Ann. Progr. Rept. May 20, 1965*, ORNL-3832, p. 128.

[21] W. R. Busing, R. D. Ellison, S. P. King, and H. A. Levy, "The Oak Ridge Computer-Controlled X-Ray Diffractometer," this report.

[22] D. J. Wehe, W. R. Busing, and H. A. Levy, "OR ABS, a Fortran Program for Calculating Single Crystal Absorption Corrections," ORNL-TM-229 (1962).

[23] See discussion in H. Lipson and W. Cochran, *The Determinations of Crystal Structures*, pp. 206 ff, G. Bell and Sons, Ltd., 1953.

[24] The final full-matrix refinement used a new version of the program OR FLS adapted for the IBM 360 computer by Dr. C. K. Johnson. OR FLS for the CDC 1604 computer was described by H. A. Levy, C. K. Johnson, and R. D. Ellison in *Chem. Div. Ann. Progr. Rept. May 20, 1965*, ORNL-3832, p. 129.

[25] For background see discussion in S. C. Nyburg, *X-Ray Analysis of Organic Structures*, pp. 134 ff, Academic, New York, 1961.

[26] D. H. Templeton, p. 214 in *International Tables for the Determination of Crystal Structures*, vol. 3, Kynoch Press, Birmingham, England, 1962.

[27] For definitions see G. M. Brown and R. Chidambaram, "The Structure of Copper Ammonium Sulfate Hexahydrate from Neutron-Diffraction Data," this report.

significant; they establish the absolute configuration unambiguously. After further least-squares refinement of the parameters for the correct configuration, $R(F) = 0.031$, $R(F^2) = 0.038$, and $\sigma_1 = 1.31$. In the final full-matrix cycles,[23] the following 334 parameters were optimized: one scale factor for each of the two crystal specimens; three coordinates for each of the 49 atoms; six anisotropic thermal parameters for each of the 27 atoms other than hydrogen; a single isotropic thermal parameter for each of the 22 hydrogen atoms; and the dispersion term $\Delta f''$ of bromine. The standard errors in the atomic coordinates derived in the least-squares procedure are as follows: bromide ion, ~0.0004 A; C, N, and O atoms, 0.002 to 0.005 A; H atoms, 0.03 to 0.08 A.

The molecular structure and absolute configuration are shown in the stereoscopic drawing of Fig. 8.5, which also shows the bond lengths of all the chemical bonds not involving hydrogen. As is usual in x-ray crystal-structure analysis, especially in crystals containing relatively heavy atoms such as bromine, the bond lengths involving hydrogen atoms are not determined accurately. The C–H bond lengths range from 0.86 to 1.12 A, averaging 0.99 A. The N–H and O–H lengths are 0.98 and 0.84 A.

The absolute configuration is the same as that found in the x-ray analysis of the methiodide of bulbocapnine,[28,29] a related alkaloid with the hydroxyl on C(11) rather than on C(8) and without the methoxyl group on C(9). However, the twist (see Fig. 8.5) about the C(12)–C(13) bond of the biphenyl system embedded in the molecule is only about 14°, compared with the 30° twist reported in bulbocapnine methiodide. Steric interference between the oxygen atoms attached to C(11) and C(14) in bulbocapnine causes the greater twist. The information about the twist in leucoxine may be useful in correlating twist angle with optical rotatory dispersion effects resulting from the twisted biphenyl system in aporphine alkaloids. The biphenyl ring system in leucoxine is slightly bent along the C(1)–C(13)–C(12)–C(9) axis; thus, angle C(1)–C(13)–C(12) is 3.7° and angle C(9)–C(12)–C(13) is 3.0°. Further detailed analysis of the molecular geometry is in progress.

The refinement of the dispersion term $\Delta f''$ of the bromide ion led to the value 1.2 ± 0.05 electrons. This experimental value is probably more reliable than the theoretical value 1.4 electrons.

[28] T. Ashida, R. Pepinsky, and Y. Okaya, *Acta Cryst.* **16** (Suppl.), A48 (1963).

[29] Results from authors of ref. 28, quoted by M. Shamma and W. A. Slusarchyk, *Chem. Rev.* **64**, 59 (1964).

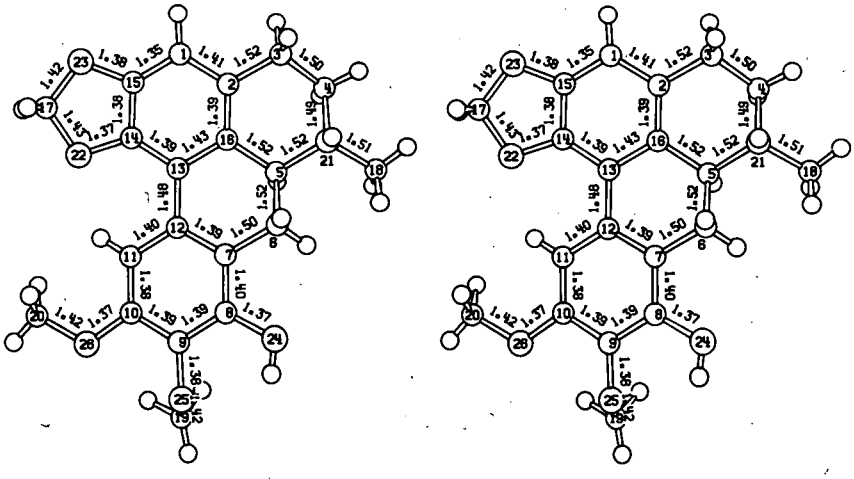

Fig. 8.5. Stereoscopic View of the Positive Ion in Leucoxine Hydrobromide. The ion is shown in correct absolute configuration. Atoms 1 to 20 are carbons; 21 is nitrogen; 22 to 26 are oxygens; unnumbered atoms are hydrogens. The numbers associated with bonds are bond lengths in angstroms.

The Structure of Copper Ammonium Sulfate Hexahydrate from Neutron-Diffraction Data

G. M. Brown R. Chidambaram[30]

Neutron-diffraction analysis[31] of the structure of copper ammonium sulfate hexahydrate, $Cu(NH_4)_2(SO_4)_2 \cdot 6H_2O$, was performed to determine precisely the coordinates of the hydrogen atoms in order to examine in detail the structural parameters of the water molecules, the ammonium ion, and the hydrogen bonds. An incidental aim was to compare the heavy-atom parameters derived from the neutron analysis with those from previous x-ray analyses.

The crystals are monoclinic ($P2_1/a$) with cell parameters[32] $a = 9.2105 \pm 0.0014$ A, $b = 12.3795 \pm 0.0017$ A, $c = 6.3016 \pm 0.0013$ A, $\beta = 106.112° \pm 0.018°$. The structure determination is based on 2032 independent structure-factor squares F_o^2 from intensity measurements of a 49.9-mg crystal on the Oak Ridge automatic single-crystal neutron diffractometer.[33] The data were recorded and processed by standard procedures.[34] An approximate, two-dimensional x-ray analysis[35] provided starting values of the atomic coordinates for refinement, including, through application of chemical sense, the coordinates of the hydrogen atoms. In full-matrix least-squares refinement, the following parameters were adjusted: the scale factor on the calculated F^2 values; the three coordinates and six anisotropic thermal parameters of each atom; and the neutron scattering factors of copper, sulfur, oxygen, and nitrogen (the scattering factor of hydrogen was held fixed at -0.378×10^{-12} cm). The final reliability indices given by the equation

$$R(F^k) \equiv \frac{\Sigma \left| |F_o^k| - |F_c^k| \right|}{\Sigma |F_o^k|}$$

are 0.085 for $k = 1$ and 0.082 for $k = 2$, when 153 reflections affected by extinction and 79 reflections of small F_o^2 value and undetermined phase sign are omitted from the refinement. The standard deviation of fit, σ_1, is 1.15, where $\sigma_1 = [\Sigma w_{F^2}(F_o^2 - F_c^2)^2/(n - p)]^{1/2}$, w_{F^2} is the weight[34] of the observation F_o^2, n is the number of observations, and p is the number of parameters fitted to the data. The standard errors of the atomic coordinates are in the range 0.0010 to 0.0023 A for the N, S, and O atoms and 0.0025 to 0.0053 A for the H atoms (the copper atom is fixed at the origin of the unit cell by symmetry).

The neutron scattering factors and standard errors derived are as follows (all relative to $f_H = -0.378 \times 10^{-12}$ cm): $f_{Cu} = 0.785 \pm 0.007$; $f_S = 0.283 \pm 0.004$; $f_O = 0.588 \pm 0.003$; $f_N = 0.957 \pm 0.006$. Except for f_{Cu} these new scattering factors appear to be significantly different from the values from Bacon's table[36] ($f_{Cu} = 0.79$; $f_S = 0.31$; $f_O = 0.577$; $f_N = 0.94$), which we used at the beginning of the refinement.

A view of the crystal structure in the direction $-c$ is shown in Fig. 8.6.

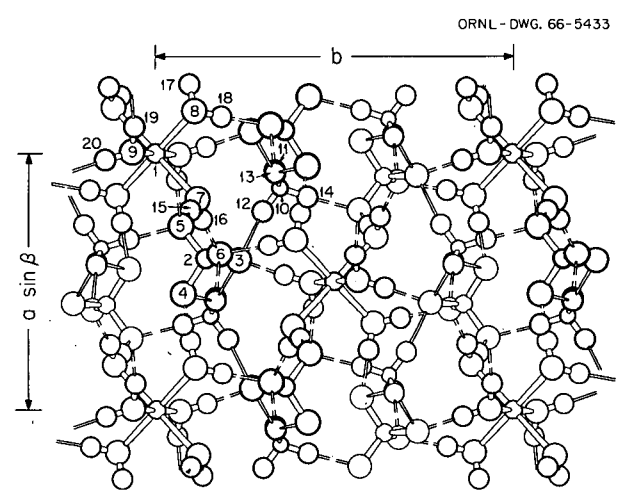

Fig. 8.6. A View of the Crystal Structure of Copper Ammonium Sulfate Hexahydrate in the Direction $-c$. The atoms are identified as follows: copper, 1; sulfur, 2; sulfate oxygens, 3 to 6; water oxygens, 7 to 9; nitrogen, 10; hydrogens of NH_4, 11 to 14; water hydrogens, 15 to 20.

[30] Guest scientist, 1964–65, from the Atomic Energy Establishment, Trombay, Bombay, India.

[31] For a preliminary report see *Chem. Div. Ann. Progr. Rept. May 20, 1965*, ORNL-3832, p. 124.

[32] E. C. Lingafelter, University of Washington, private communication.

[33] W. R. Busing, H. G. Smith, S. W. Peterson, and H. A. Levy, *J. Phys. (Paris)* 25, 495 (1964).

[34] G. M. Brown and H. A. Levy, *J. Phys. (Paris)* 25, 497 (1964).

[35] M. W. Webb, H. F. Kay, and N. W. Grimes, *Acta Cryst.* 18, 740 (1965).

[36] G. E. Bacon, *Neutron Diffraction*, p. 31, Oxford Univ. Press, 1962.

The lengths of the chemical bonds are given in Table 8.2, in which appropriate comparisons are made with the corresponding bond lengths from the x-ray work of Montgomery and Lingafelter.[37] The bond lengths in italics have been "corrected" on the assumption that the "riding" model[38] applies. Detailed analysis of the thermal parameters shows that the riding model is of uncertain validity for correction of the bonds Cu(1) – O(7) and Cu(1) – O(8) but that it probably is valid at least approximately for the other bonds in the table. The data in Table 8.2 show reasonably good, though not entirely satisfactory, agreement between the x-ray and neutron results for the bonds in the centrosymmetric $Cu(H_2O)_6^{2+}$ ion and in the SO_4^{2-} ion. The O – Cu – O angles are as follows: O(7) – Cu – O(9), 88.9°; O(8) – Cu – O(9), 90.7°; O(8) – Cu – O(9), 89.0° (all ± 0.1°). The six O – S – O angles range from 108.3 to 110.9° (all ± 0.2°). Each of the angles is within 1° of the value from the three-dimensional x-ray analysis.

The O – H bond lengths before correction are in the range 0.961 to 0.980 A, the shortest two being in the water molecule which has the weakest hydrogen bonding. The corrected bond lengths range from 0.982 to 1.003 A, averaging 0.991 A; they probably are upper limits to the true bond lengths. The three water angles are: H(15) – O(7) – H(16), 109.3°; H(17) – O(8) – H(18), 105.9°; H(19) – O(9) – H(20), 105.7° (all ± 0.3°).

The accuracy of the determination of the N – H bond lengths is impaired by the considerable thermal motion of the hydrogen atoms of the ammonium ion. The average N – H distance before correction of 1.000 A becomes 1.06 A after application of the "riding" model correction. The extreme deviations of the individual values from the average suggest that the uncertainty in the average corrected value is about 0.01 A. Previous values reported for the N – H bond lengths in ammonium salts determined by neutron analysis have been consistently lower than 1.06 A: NH_4Cl and ND_4Cl,[39] 1.03 ± 0.02 A;

Table 8.2. Lengths (A) of Chemical Bonds in the Copper Ammonium Sulfate Hexahydrate Crystal Structure

A standard error (least significant figures of bond length) is shown in parentheses for each class of chemical bond. The italic figures are the bond lengths after correction for thermal motion according to the "riding" model

Bond	This Work	Montgomery and Lingafelter
Cu(1) – O(7)	2.2300 (14)	2.209 (5)
	2.237	
Cu(1) – O(8)	2.0725	2.084
	2.078	
Cu(1) – O(9)	1.9660	1.960
	1.971	
S(2) – O(3)	1.475 (3)	1.479 (5)
	1.489	
S(2) – O(4)	1.457	1.463
	1.481	
S(2) – O(5)	1.479	1.476
	1.486	
S(2) – O(6)	1.477	1.465
	1.490	
O(7) – H(15)	0.964 (3)	
	0.982	
O(7) – H(16)	0.963	
	0.983	
O(8) – H(17)	0.978	
	0.993	
O(8) – H(18)	0.978	
	0.993	
O(9) – H(19)	0.981	
	1.002	
O(9) – H(20)	0.976	
	0.991	
N(10) – H(11)	0.998 (4)	
	1.061	
N(10) – H(12)	1.004	
	1.061	
N(10) – H(13)	0.999	
	1.070	
N(10) – H(14)	1.000	
	1.052	

[37] H. Montgomery and E. L. Lingafelter, *Acta Cryst.* **20**, (1965), in press. Table 8.2 shows the bond lengths from the coordinates in this paper recalculated with the new cell parameters of ref. 32.

[38] W. R. Busing and H. A. Levy, *Acta Cryst.* **17**, 142 (1964).

[39] H. A. Levy and S. W. Peterson, *Phys. Rev.* **86**, 766 (1952).

ND_4Br,[40] 1.026 ± 0.02 A to 1.037 ± 0.02 A (various crystal forms); ND_4I,[41] 1.03 A; $NH_4H_2PO_4$,[42] 1.00_4 A; $(NH_4)_2BeF_4$,[43] 1.03 ± 0.03; $NH_2OH \cdot HCl$,[44] 1.04 ± 0.01; $(NH_4)_2C_2O_4 \cdot H_2O$,[45] 1.02_3 A (average). However, most of the other neutron-diffraction determinations were based on a small number of intensity data, and the refinements were not so complete as the present one. The $NH_2OH \cdot HCl$ determination was the only one based on three-dimensional data. Only in the work on the ammonium halides was the effect of thermal motion on bond length taken into account, and in that work the structural parameters were obtained by trial calculation. It is not clear, therefore, that the bond length of 1.06 A for N – H is really discrepant against the background of values from the other determinations. There remains, however, the fact that N – H bond lengths of 1.03 to 1.04 A have been reported in NH_4Br and NH_4Cl from nuclear magnetic resonance.[46,47] The N – H bonds in copper ammonium sulfate hexahydrate may be longer because the hydrogen bonding is stronger than in the ammonium halides. Clearly, more data are needed from precise neutron-diffraction analyses of other ammonium salts.

The H – N – H angles vary from 106.5 to 113.9°. Every hydrogen atom in the water molecules and in the ammonium ion is involved in hydrogen bonding; the acceptor atom is in each case an oxygen atom of a sulfate group. All the hydrogen bonds from the water molecules are nearly linear, normal hydrogen bonds, with angles O – H ··· O from 168.7 to 178.1° and distances 2.68 to 2.83 A. The N – H··· O bonds are on the average bent more than the O – H··· O bonds. There is one unsymmetrically bifurcated hydrogen bond

$$N(10)-H(13) \begin{array}{l} \cdot\cdot O(3') \\ \cdot\cdot O(4') \end{array}$$

in which the distances and angles are: N(10)··· O(3′), 3.01 A; N(10)··· O(4′), 3.12 A; N(10) – H(13)··· O(3′), 158.6°; N(10) – H(13)··· O(4′), 134.9°. In the other N – H··· O bonds the distances range from 2.86 to 2.98 A and the angles range from 157.3 to 176.3°.

A Model for Torsional Oscillators in Least-Squares Refinement of Crystal Structures: Application to the Methyl Groups in $Cu_2(CH_3COO)_4 \cdot 2H_2O$

G. M. Brown R. Chidambaram[30]

In a previously reported[48] refinement of the crystal structure of hydrated copper acetate, $Cu_2(CH_3COO)_4 \cdot 2H_2O$, based on neutron-diffraction data, the six hydrogen atoms of the methyl groups were located only with difficulty and the apparent C – H bond lengths (distances between mean atomic positions) finally derived were short, averaging 1.038 A. The difficulty in finding the hydrogen atoms and the short C – H distances[49,50] were obviously consequences of large-amplitude torsional oscillation or, possibly, of restricted rotation of the methyl groups. Analysis of the anisotropic thermal parameters found for the hydrogen atoms in the least-squares refinement showed that for each hydrogen these parameters correspond to root-mean-square vibrational amplitudes near 0.17, 0.30, and 0.52 A. The axis of largest amplitude is in each case nearly parallel to the tangent to the arc which would be described by the hydrogen atom in torsional oscillation about the C – C axis of the O_2C-CH_3 group to which it belongs.

A proper model for the motion of the methyl hydrogens is necessary if reliable structural parameters for the methyl groups are to be obtained and if residual errors in other portions of the structure arising from an inadequate model for the methyl groups are to be avoided. Although the orientations of the hydrogen thermal-parameter ellipsoids

[40] H. A. Levy and S. W. Peterson, *J. Am. Chem. Soc.* **75**, 1536 (1953).

[41] H. A. Levy and S. W. Peterson, *J. Chem. Phys.* **21**, 366 (1953).

[42] L. Tenzer, B. C. Frazer, and R. Pepinsky, *Acta Cryst.* **11**, 505 (1958).

[43] M. I. Kay, J. Lajzerowicz, Y. Okaya, and R. Pepinsky, *Abstracts of American Crystallographic Association Meeting*, Ithaca, N. Y., 1959, p. 40.

[44] V. M. Padmanabhan, S. W. Peterson, and H. G. Smith, 1962. Unpublished, cited in ref. 45.

[45] V. M. Padmanabhan, S. Srikantha, and S. M. Ali, *Acta Cryst.* **18**, 567 (1965).

[46] H. S. Gutowsky, G. E. Pake, and R. Bersohn, *J. Chem. Phys.* **22**, 643 (1954).

[47] R. Bersohn and H. Gutowsky, *J. Chem. Phys.* **22**, 651 (1954).

[48] R. Chidambaram and G. M. Brown, *Chem. Div. Ann. Progr. Rept. May 20, 1965*, ORNL-3832, p. 121.

[49] D. W. J. Cruickshank, *Acta Cryst.* **9**, 757 (1956); **14**, 896 (1961).

[50] W. R. Busing and H. A. Levy, *Acta Cryst.* **17**, 142 (1964).

seem sensible, it is clear that the model on which the anisotropic temperature factor

$$\exp\left[-(h^2\beta_{11} + k^2\beta_{22} + l^2\beta_{33} + 2hk\beta_{12} + 2hl\beta_{13} + 2kl\beta_{23})\right]$$

is based is inappropriate. In the derivation[51] of this factor, the probability distribution assumed for the displacements of an atom from its mean position is the Gaussian distribution

$$P(x,y,z)\,dx\,dy\,dz = [(2\pi)^{3/2}\,u_x u_y u_z]^{-1} \times \exp\left[-x^2/2u^2_x - y^2/2u^2_y - z^2/2u^2_z\right] dx\,dy\,dz\ ,$$

where x, y, and z are the instantaneous displacements in the Cartesian coordinate system of the principal axes and u_x, u_y, and u_z are the root-mean-square component displacements. This symmetrical distribution cannot apply to a methyl hydrogen atom in large-amplitude torsional oscillation.

We propose to use for the torsional motion[52] a Gaussian probability function in the form

$$P(\phi) = \left[1/(\beta\sqrt{2\pi})\right] e^{-(\phi - \phi_0)^2/2\beta^2}$$

for the angle ϕ of a given hydrogen about its C – C axis, where ϕ_0 is the mean angle and β is the root-mean-square angular displacement of ϕ from ϕ_0. To an approximation which we believe is useful, the contribution of each hydrogen to the structure factor $F(\mathbf{h})$ may be written:

$$g = f_H T e^{2\pi i \mathbf{h}\cdot\mathbf{x}_c}\left[J_0(a) + 2\sum_{m=1}^{\infty} i^m J_m e^{-m^2\beta^2/2}\cos(m\phi_0)\right].$$

Here f_H is the atomic scattering factor, $\mathbf{x}_c$ is the vector of coordinates of the center of torsional oscillation, J_m is the Bessel function of order m, and a is $2\pi|\mathbf{h}|\,|\mathbf{r}|$, where $\mathbf{r}$ is the vector from the center to the atom. T is a three-parameter thermal factor based on a Gaussian probability function for rectilinear motion in the plane perpendicular to the arc on which the atom moves in its torsional oscillation. In deriving the expression for g, we follow closely the derivation of g for the hindered rotator by King and Lipscomb.[53] In this approximation we are neglecting any displacements of the hydrogen atoms in the tangential direction arising from motion of the methyl carbon atom, as is strictly justifiable only if such displacements are small relative to those arising from torsional oscillation.

The least-squares refinement program XFLS[54] was modified so that the rotatory oscillation of the hydrogen atom could explicitly be taken into account through the above equation for g. The parameters adjusted for each methyl hydrogen atom were the three coordinates, the torsional parameter β, and the three other thermal parameters. For the remaining atoms in the structure, the coordinates and the usual six anisotropic thermal parameters were adjusted. When the refinement converged, the usual measures of goodness of fit[55] were slightly less satisfactory than those reached in the previous refinement: $R(F^2) = 0.0968$ instead of 0.087 and $\sigma_1 = 1.32$ instead of 1.30. However, the C – H bond lengths derived show marked improvement, averaging 1.106 A, which is very close to the accepted value 1.10 A. Table 8.3 shows the individual values of the bond lengths and compares them with uncorrected and "corrected" values from the earlier refinement. The "corrected" values were obtained by using the "riding" model of Busing and Levy.[50] Judging from the orientations of the hydrogen thermal ellipsoids alone, one might consider this to be a favorable case for use of the riding model. Clearly, however, the "corrected" values are unreliable.

We believe that our results demonstrate the validity of our approach. Further work is planned to make the program embracing the model more general and more flexible. We intend also to investigate the relation of our model to others proposed for torsional oscillation[56] and for restricted rotation.[53]

---

[51] W. Cochran, *Acta Cryst.* 7, 503 (1954).

[52] We treat the motion as torsional oscillation. The effects of restricted rotation would be similar, but the mathematical treatment is more complicated (see ref. 53); and we do not believe the two types of motion can be distinguished in the present case.

[53] M. V. King and W. N. Lipscomb, *Acta Cryst.* 3, 155 (1950).

[54] H. A. Levy, C. K. Johnson, and R. D. Ellison, *Chem. Div. Ann. Progr. Rept. May 20, 1965*, ORNL-3832, p. 129.

[55] For definitions, see G. M. Brown and R. Chidambaram, "The Structure of Copper Ammonium Sulfate Hexahydrate from Neutron Diffraction Data," this report.

[56] M. I. Kay and D. R. Behrendt, *Acta Cryst.* 3, 157 (1963).

Table 8.3. Carbon-Hydrogen Bond Lengths (A) in $Cu(CH_3COO)_4 \cdot 2H_2O$

Bond	Previous Refinement		Torsional Oscillator Refinement
	Uncorrected	"Corrected"	
1	1.021	1.117	1.094
2	1.029	1.134	1.093
3	1.063	1.189	1.139
4	1.049	1.125	1.108
5	1.045	1.129	1.095
6	1.020	1.159	1.107
Average	1.038	1.143	1.106

A Neutron Diffraction Study of the Cubic Phase of Xenon Hexafluoride

P. A. Agron C. K. Johnson
H. A. Levy

A study of the monoclinic phase of xenon hexafluoride has been reported previously.[57] Here we describe a neutron diffraction study of a cubic phase of XeF_6.

A crystal of XeF_6 was seeded at 8 to 10°C in a sealed fluorothene tube and grown to several millimeters in size for the collection of neutron data. The neutron measurements disclosed this crystal to be face-centered cubic, $a = 25.34 \pm 0.05$ A, probable space group $F\bar{4}3c$ or $Fm3c$. This crystal has been observed to undergo a transformation when warmed above 22°C and to revert to the original crystal when cooled to below 14°C. At this time, a specific heat measurement of XeF_6[58] indicated a phase transition in the above-mentioned temperature range. It is plausible that the monoclinic phase[59] corresponds to XeF_6(I) and that the cubic phase may be identified with XeF_6(II) reported in the thermal study.[58]

A controlled thermoelectric cooling device was developed and successfully used during the collection of neutron diffraction data on the cubic phase of XeF_6. It is a single-stage unit which is capable of reducing the temperature of an enclosed crystal specimen to a lower limit of −40°C.

[57] P. A. Agron and H. A. Levy, *Chem. Div. Ann. Progr. Rept. June 20, 1964*, ORNL-3679, p. 108.

[58] J. G. Malm, F. Schreiner, and D. W. Osborne, *Inorg. Nucl. Chem. Letters* 1, 97 (1965).

[59] P. A. Agron, C. K. Johnson, and H. A. Levy, *Inorg. Nucl. Chem. Letters* 1, 145 (1965).

The Oak Ridge Computer-Controlled X-Ray Diffractometer

W. R. Busing S. P. King
R. D. Ellison H. A. Levy

Since July 1965 we have had in operation a Picker four-circle x-ray diffractometer which is controlled in a simple way by a Digital Equipment Corporation PDP-5 computer. During its first ten months this instrument has been used to measure intensities of a total of 22,000 reflections from seven different materials. Programs have been prepared to perform a variety of useful operations, and some typical experimental procedures are described below.

The computer, which is the main component of the system, has 4096 12-bit words of random-access core memory, a 6-μsec memory cycle, a program interrupt feature, and paper tape or typewriter input-output facilities. The interface hardware has been reduced to a minimum by requiring the computer to do as much work as possible.

Four Slo-Syn stepping motors are mounted on the diffractometer, and each shaft is equipped with a simple photoelectric detector to generate "1° reference" signals. The computer controls the shafts by sending a calculated number of pulses to the stepping motors. An external oscillator interrupts the computer 300 times each second to control the

rate at which these pulses can be generated. The program is able to start the motors gradually, so that inertia can be overcome without losing count of the steps. As a check on the accuracy of the drive, the 1° reference device signals the computer once during each motor revolution so that the program can correct small errors or take appropriate action in the case of large ones. The motors have been found to drive the diffractometer smoothly and reliably at a speed of 90°/min.

The system uses the computer itself to count pulses from the x-ray detector, so that the count input is only a single electrical line. The PDP-5 will accept pulses at a maximum rate of about 10^5 counts/sec, and an external divider circuit is provided to scale the input in cases for which higher rates are expected.

Routines simulating manual operation of the diffractometer facilitate mounting and centering of the sample. If the unit cell or orientation is unknown, it is possible to search for reflections automatically over half of a spherical shell in reciprocal space. More often, however, a preliminary photographic investigation has been made, so that the lattice parameters and orientation are known approximately. A reflection can then be located by an automatic two-dimensional scan over the region in which it is expected. Another program systematically sets the instrument to maximize the intensity and center the reflection in the counter. Instrument angles for two reflections located in this way serve to define the sample orientation. This information together with the cell parameters enables the computer to calculate angle settings for any given set of Miller indices, so that other reflections can be readily located. If desired, the measured instrument angles for several reflections can be used as observations for a least-squares program which refines the cell and orientation parameters.

A data collection program establishes the sequence of reflections to be measured either from a list of indices or from a range of Bragg angles with specified restrictions on the indices. Provision is made for measuring reference reflections periodically during the data collection. For each reflection the instrument angles are computed and set, and a θ-2θ step scan is made. The count for each step is corrected for coincidence loss, and an integrated intensity corrected for background is computed and punched on paper tape for further processing on a large computer. In typical operation 20 to 30 reflections are measured in 1 hr.

Another routine permits rotation of the sample about the scattering vector. Scans made in this way confirm that multiple-reflection effects may often cause significant errors in intensity measurements, especially for weak reflections. We have therefore prepared another data collection program which permits the azimuth to be specified, and a program has been written[60] for a large computer to aid in choosing this parameter.

Stereoscopic Drawings Showing the Symmetry Elements of the Crystallographic and Shubnikov Space Groups

C. K. Johnson S. P. King[61]

A detailed comprehension of the arrangement of symmetry elements in a particular space group is essential for most crystallographic studies. Illustrations are the most satisfactory method for obtaining this information. The International Tables for X-Ray Crystallography[62] has illustrations showing the symmetry elements of the crystallographic space groups up to cubic symmetry. The cubic space groups are not shown in the latest edition, presumably because of their complexity.

In addition to the 230 regular space groups, there are 230 gray Shubnikov groups and 1191 black-white Shubnikov groups.[63] The gray and black-white groups contain both symmetry and antisymmetry elements. The black-white Shubnikov groups are becoming increasingly popular for describing magnetic structures.[64] At present there are very few published drawings illustrating the black-white Shubnikov groups; however, a Russian publication[65] with such illustrations is scheduled for 1966.

The experience gained in utilizing computer graphics for drawing stereoscopic illustrations of

---

[60] H. L. Yakel, ORNL-TM (in preparation).

[61] Mathematics Division, ORNL.

[62] N. F. M. Henry and K. Lonsdale, eds., *International Tables for X-ray Crystallography*, vol. I, Kynoch Press, Birmingham, 1952.

[63] A. V. Shubnikov, N. V. Belov, *et al.*, *Colored Symmetry*, Pergamon, New York, 1964.

[64] M. Atoji, *Am. J. Phys.* 33, 212 (1965).

[65] V. Kopcik, Monograph on Shubnikov Groups (in Russian), Publishing House of Moscow State University, Moscow (in press).

crystal structures[66] indicated that similar techniques can be used to produce stereoscopic drawings of the crystallographic and Shubnikov space groups. A computer program which can plot any of these space groups is being developed. The input parameters are: (1) unit cell angles, (2) lattice centering translations and their coloration, (3) generators for the group and their coloration, and (4) instructions describing the type of illustration to be drawn. The stereoscopic illustrations of the cubic crystallographic groups will be considered for inclusion in a forthcoming edition of the *International Tables for X-Ray Crystallography*.

The Structure of $MnCl_2 \cdot 4H_2O$: A Neutron-Diffraction Study

Z. M. El Saffar[67] G. M. Brown

We became interested in neutron-diffraction analysis of manganese chloride tetrahydrate, $MnCl_2 \cdot 4H_2O$, because of the antiferromagnetism[68] which this substance exhibits at 1.62°K. Nuclear magnetic resonance (NMR) data are often used in the determination of magnetic space groups to eliminate all but one of the possible color groups. The use of precisely determined hydrogen positions is essential in correlating the observed local fields at the proton sites with the calculated local fields for the possible color groups.[69,70] The hydrogen positions determined in the present neutron-diffraction study have already been useful to Spence and Nagarajan in an NMR study of $MnCl_2 \cdot 4H_2O$ at low temperatures.[70]

The heavy-atom structure of $MnCl_2 \cdot 4H_2O$ (α, room-temperature form, a = 11.186 ± 0.006 A, b = 9.513 ± 0.005 A, c = 6.186 ± 0.002 A, β = 99.74 ± 0.04°, space group $P2_1/n$, four formula units per cell) was determined rather precisely and the hydrogen atoms located approximately in an x-ray analysis by Zalkin, Forrester, and Templeton.[71] Baur then proposed a detailed pattern for the hydrogen bonding by using the heavy-atom coordinates in a calculation by which the hydrogen atoms were located by finding their positions of least electrostatic energy.[72] Baur's hydrogen positions are in fair agreement with the approximate x-ray positions except for atom H(32). (For the numbering scheme of the atoms see Fig. 8.7.) An NMR study[73] at room temperature did not furnish proton-proton vectors; the spectrum was

[66] C. K. Johnson, *OR TEP: A Fortran Thermal Ellipsoid Plot Program for Crystal Structure Illustrations*, ORNL-3794 (1965).

[67] Guest Scientist from Iraq.

[68] M. A. Lasheen, J. Van Den Brock, and C. J. Gorter, *Physica* **24**, 1061 (1958).

[69] R. D. Spence, P. Middents, Z. M. El Saffar, and R. Kleinberg, *J. Appl. Phys.* **35**, 854 (1964).

[70] R. D. Spence and V. Nagarajan, *Phys. Rev.*, to be published.

[71] A. Zalkin, J. D. Forrester, and D. H. Templeton, *Inorg. Chem.* **3**, 529 (1964).

[72] W. H. Baur, *Inorg. Chem.* **4**, 1840 (1965).

[73] Z. M. El Saffar, unpublished.

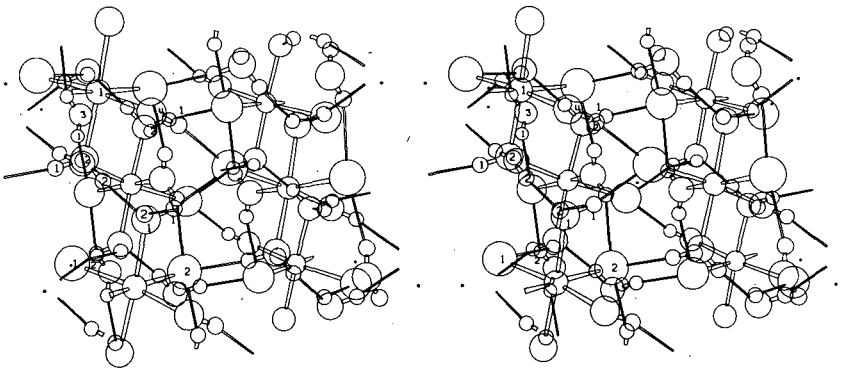

Fig. 8.7. Stereoscopic View Along −b of the Crystal Structure of $MnCl_2 \cdot 4H_2O$. Dots mark the corners and the center of the cell. Axis c is horizontal from left to right; axis *a* runs from bottom to top, 10° from the vertical. The atoms of each kind in the asymmetric unit are numbered sequentially, 1, 2, ..., *n*. In the text, the hydrogen No. 2 on the oxygen No. 1 is designated H(12), etc.

unusual, there being only a single bell-shaped peak with a width of about 12 gauss and no dipole-dipole splitting. Final results of a previous attempt by Gardner[74] at neutron analysis of $MnCl_2 \cdot 4H_2O$ were never reported. Our precise determination of hydrogen coordinates establishes that Baur's hydrogen bonding pattern is basically correct.

Intensities of some 3000 (2328 independent) reflections from a 57-mg crystal of $MnCl_2 \cdot 4H_2O$ were recorded on the Oak Ridge single-crystal neutron diffractometer and processed by the usual procedures[75] used in this laboratory to a set of structure-factor squares F_o^2 and standard errors σ_{F^2}. Full-matrix least-squares refinement was started using the atomic parameters from the x-ray analysis and neutron scattering factors from the compilation of Bacon.[76] Eventually, the following parameters were refined to convergence: the scale factor on the calculated F^2 values; three coordinates and six parameters of anisotropic thermal motion for each atom; the scattering factors of Mn, Cl, and O (the scattering factor of hydrogen was held fixed at -0.378×10^{-12} cm). The final values of the usual measures of goodness of fit[77] were: $R(F) = 0.076$, $R(F^2) = 0.076$, $\sigma_1 = 1.12$, when 224 strong reflections were omitted because of extinction error and 77 other weak reflections were omitted because their signs were not determined.

The initial and final scattering factors f are shown in Table 8.4. The final values for f_O and f_{Cl} are in good agreement with the values from the neutron-diffraction studies in this laboratory (copper ammonium sulfate hexahydrate,[77] $f_O = 0.589 \pm 0.003$; chloral hydrate,[78] $f_O = 0.590 \pm 0.003$, $f_{Cl} = 0.962 \pm 0.005$; potassium hydrogen chloromaleate,[79] $f_O = 0.603 \pm 0.003$, $f_{Cl} = 0.965 \pm 0.005$). The ratios f_O/f_H and f_{Cl}/f_H appear to be significantly different from the ratios corresponding to the initial scattering factors.

Table 8.4. Scattering Factors Derived in Neutron-Diffraction Analysis of $MnCl_2 \cdot 4H_2O$, Compared with Previous Values Tabulated by Bacon

Values are expressed in units of 10^{-12} cm and relative to the value -0.378 for hydrogen

Atom	Scattering Factors	
	This Work	Bacon
Mn	-0.379 ± 0.003	-0.36
Cl	0.975 ± 0.006	0.99
O	0.592 ± 0.003	0.577
H		-0.378

Our heavy-atom coordinates are in very good agreement with those from the x-ray analysis. However, the neutron thermal parameters imply vibration amplitudes significantly lower than those corresponding to the x-ray thermal parameters. Further analysis of the thermal parameters is in progress. Our hydrogen positions differ on the average by 0.26 A from those of Zalkin *et al.* and by 0.09 A from those of Baur.

The geometry of each of the water molecules is given in Table 8.5, and a view of the overall structure showing the hydrogen bonding appears in Fig. 8.7. Of the eight hydrogen atoms, H(11), H(21), H(31), and H(41) are hydrogen-bonded to chlorine atoms, with H···Cl distances 2.227, 2.201, 2.294, and 2.374 A and O–H···Cl angles 165.7, 174.1, 158.7, and 164.4° respectively. Hydrogen atoms H(22) and H(42) are bonded to oxygen atoms, with H···O distances 1.969 and 2.014 A and O–H···O angles 170.4 and 174.4°. Atom H(12) forms a bifurcated bond from O(1) to two Cl atoms, as proposed by Baur. The O(1) and H(12) atoms and the two chlorine atoms lie in a plane with H···Cl distance and O–H···Cl angle parameters 2.499 A and 140.4° and 2.635 A and 127.4°. Atom H(32) is in a configuration with O(3) and two chlorine atoms which may be regarded as an extremely unevenly bifurcated hydrogen bond, with H···Cl distance and O–H···Cl angle parameters 2.495 A and 148.3° and 2.948 A and 113°. The second of the two H···Cl interactions must be quite weak.

On the whole, the hydrogen-bonding interactions just described are somewhat weak, judged by the distances H···Cl and H···O. The bifurcated bonds are especially weak, as is indicated also by their

[74] W. E. Gardner, *Bull. Am. Phys. Soc.* **5**, 461 (1960).

[75] G. M. Brown and H. A. Levy, *J. Phys. (Paris)* **25**, 497 (1964).

[76] G. E. Bacon, *Neutron Diffraction*, 2d ed., p. 31, Oxford University Press, 1962.

[77] See G. M. Brown and R. Chidambaram, "The Structure of Copper Anmonium Sulfate Hexahydrate from Neutron Diffraction Data," this report.

[78] G. M. Brown and H. A. Levy, unpublished.

[79] R. D. Ellison and H. A. Levy, *Acta Cryst.* **19**, 260 (1965).

Table 8.5. Geometry of the Water Molecules in $MnCl_2 \cdot 4H_2O$

Distances have not been corrected for thermal motion

Water $H_2O(k)$	Distances (A) $O(k)$–$H(k1)$	$O(k)$–$H(k2)$	$H(k1)$–$H(k2)$	Angle (deg) $H(k1)$–$O(k)$–$H(k2)$
$H_2O(1)$	0.967 ± 0.002	0.944 ± 0.003	1.509 ± 0.004	104.3 ± 0.3
$H_2O(2)$	0.963 ± 0.002	0.971 ± 0.002	1.546 ± 0.003	106.4 ± 0.2
$H_2O(3)$	0.955 ± 0.003	0.923 ± 0.003	1.561 ± 0.004	112.4 ± 0.3
$H_2O(4)$	0.941 ± 0.002	0.953 ± 0.003	1.565 ± 0.004	111.4 ± 0.3

large vibrational amplitudes and by the evident shortening of the apparent bond lengths O(1)–H(12) and O(3)–H(32) resulting from the perturbing effects of the thermal motion. Thermal motion is probably responsible for the fact that dipole-dipole splittings of the NMR lines are not observed at room temperature, as is observed, for example, from $BaCl_2 \cdot 2H_2O$,[80] in which the hydrogen bonding is somewhat stronger.

X-Ray Reflection Data for Analysis of the Crystal Structure of Sedoheptulosan Monohydrate

G. M. Brown H. A. Levy

The chemical proof of the structure of sedoheptulosan, the anhydride of the seven-carbon sugar sedoheptulose, has led after some false turns to the conclusion that the compound is 2,7-anhydro-β-D-altroheptulopyranose[81] (see Fisher projection formula **1** below). However, the decision between the structure **1** and another possibility represented

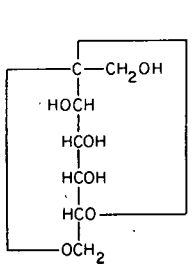

1

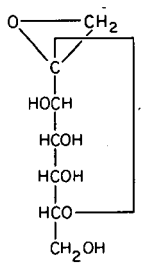

2

by formula **2** was reached by rather subtle reasoning and chemical judgment. A successful x-ray analysis would provide an independent and unambiguous determination of the chemical linkages, as well as precise metrical data for the molecule.

Crystals of the monohydrate of sedoheptulosan are tetragonal (space group $P4_1$, four molecules per cell) with $a = b = 11.0739 \pm 0.0005$ A and $c = 7.3746 \pm 0.0005$ A. Using the new Oak Ridge computer-controlled x-ray diffractometer,[82] we have collected a full three-dimensional set of reflection intensity data for the monohydrate, from which we hope to determine the crystal and molecular structure.

Citric Acid Monohydrate: A Crystal-Structure Determination by Neutron Diffraction Using Deuterium for Isomorphous Replacement

C. K. Johnson

An interesting aspect of neutron diffraction is that different isotopes of certain elements have widely different coherent-scattering amplitudes b for thermal neutrons. This suggests that neutron diffraction coupled with isomorphous replacement through the use of isotopes could be a powerful technique[83] for solving the phase problem in crystal-structure determination. The isomorphism of compounds having isotopic substitution is inherently much more nearly perfect than the isomorphism of compounds having chemical substitution. One of the most convenient isotopic pairs

[80] Z. M. El Saffar, *Acta Cryst.* **20**, 310 (1966).

[81] J. W. Pratt, N. K. Richtmeyer, and C. S. Hudson, *J. Am. Chem. Soc.* **74**, 2200 (1952).

[82] W. R. Busing, R. D. Ellison, S. P. King, and H. A. Levy, "The Oak Ridge Computer-Controlled X-Ray Diffractometer," this report.

[83] R. Pepinsky, *Science* **117**, 1 (1953).

for this method is hydrogen ($b = -0.378 \times 10^{-12}$ cm) and deuterium ($b = 0.65 \times 10^{-12}$ cm). A hydrogen-deuterium isomorphous pair can be prepared in some cases simply by growing crystals from ordinary water and from heavy water. Another method is to use enzymatic reactions to deuterate stereospecifically one particular position in a molecule.

A stereospecifically deuterated citric acid was prepared by I. A. Rose at the Institute for Cancer Research in Philadelphia, Pennsylvania. The enzyme aconitase was used to add heavy water across the double bond of *cis*-aconitic acid to form an isomer of 2-deuteriocitric acid. In this reaction two asymmetric carbon atoms are formed, so that there are four possible stereoisomers as shown in Fig. 8.8. The present study can only determine relative configuration, that is, it can determine whether the isomer belongs to pair 1 or to pair 2 of Fig. 8.8. (Pair 1 is the experimental result.) An absolute configuration assignment[84] will be performed later with neutron diffraction by utilizing the anomalous dispersion of ^{6}Li in ^{6}Li 2-deuteriocitrate. The evidence from biochemical studies[85] suggests that 2*R*,3*R* 2-deuteriocitrate is the correct isomer, and this is consistent with the present result.

Three-dimensional neutron-diffraction data were collected from crystals of citric acid monohydrate [$C_6H_8O_7 \cdot H_2O$ (I)] and two deuterated isomorphs [$C_6H_4D_4O_7 \cdot D_2O$ (II) and $C_6H_3D_5O_7 \cdot D_2O$ (III)]. Crystals of II and III were prepared by growing ordinary citric acid and enzymatically deuterated citric acid respectively from heavy water. Approximately 2000 neutron data were collected from each crystal, with 90% having a net count greater than one standard deviation. Absorption corrections were applied to the data.

The cell dimensions[86] for citric acid monohydrate are $a = 6.290$ A, $b = 9.318$ A, $c = 15.39$ A, and the space group is $P2_12_12_1$, with four molecules per unit cell.

The structure was solved with the data from compounds II and III, which differ by deuterium substitution in a single position. Two candidate positions for the substituted atom were indicated in a $\left||F_{III}| - |F_{II}|\right|^2$ synthesis map. [This $(\Delta F)^2$ synthesis technique is used by protein crystallographers to locate heavy atoms.] It later became apparent that both positions were correct because of an unusual disordering phenomenon (see below). A fourfold superposition based on the most prominent of the two candidate positions was then performed on a difference Patterson synthesis ($|F_{III}|^2 - |F_{II}|^2$). This superposition map clearly positioned an additional 10 of the 24 atoms. The remaining 13 atoms were found by the first F_o Fourier synthesis.

Refinement by the method of least squares with anisotropic temperature parameters proceeded normally for the data from compounds I and II. A reliability factor of 5.2% on F (8.2% on F^2) was achieved for I and 8.4% on F (13.1% on F^2) for form II. Form II has rather severe extinction errors which have not at present been adequately corrected.

Refinement of the data from form III did not converge readily, and it was obvious that the model on which the refinement was based was not adequate. Large thermal-motion parameters for atoms D(1) and H(3) (see Fig. 8.11 for numbering system) suggested that perhaps partial substitution had taken place at two sites rather than complete substitution at a single site. This "multiple substitution" model was refined by varying the scattering amplitudes for both D(1) and H(3). This model refined to a reliability factor of 10% on F (13% on F^2), and the results indicated 57% D in position D(1) and 38% D in position H(3). The

ORNL-DWG. 66-2029

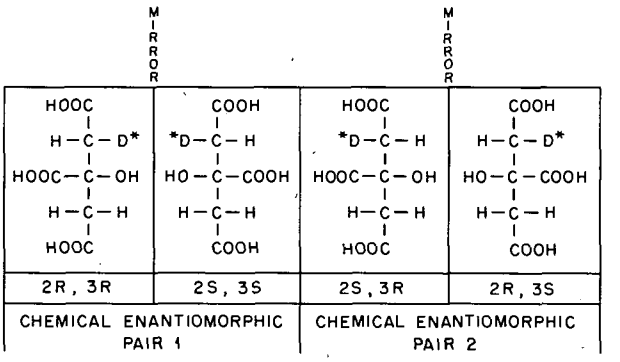

Fig. 8.8. Stereoisomers of 2-Deuteriocitric Acid Shown with Fischer Convention. Stereochemical nomenclature is that of R. S. Cahn, C. K. Ingold, and V. Prelog, *Experientia* 12, 81 (1956).

[84] C. K. Johnson, E. J. Gabe, M. R. Taylor, and I. A. Rose, *J. Am. Chem. Soc.* 87, 1802 (1965).

[85] K. R. Hanson and I. A. Rose, *Proc. Natl. Acad. Sci.* 50, 981 (1963).

[86] D. M. Burns and J. Iball, *Acta Cryst.* 7, 137 (1954).

effective scattering amplitude for position H(3) was essentially zero, and the positional and thermal parameters for that atom were meaningless.

An alternate model ("multiple-domain" model) for the disorder is possible, since (1) the space group $P2_12_12_1$ is noncentrosymmetric and (2) the asymmetric carbon atoms of 2-deuteriocitric acid are asymmetric only in the isotopic sense and not in the chemical sense. This suggests that enantiomorphous crystals might be found in any crystallization crop and that enantiomorphous coherent diffracting domains might exist in a given single-crystal specimen. Enantiomorphous conformations of 2*R*,3*R* 2-deuteriocitric acid are shown schematically in Fig. 8.9. The two enantiomorphs will give two completely different sets of neutron-diffraction intensities. The structure factor calculation procedure for this model requires that F^2 values rather than F values from the two domains be added. A least-squares calculation based on this model showed 65.5% of one domain and 34.5% of the enantiomorphic domain, with 95% deuterium substitution in the D(1) position. A reliability factor of 8.9% on F (12% on F^2) was realized, and the bond distances and angles became closer to those of forms I and II. Thus the multiple-domain model gives a better fit than the multiple-substitution model.

Figure 8.10 shows the bond distances in the three isomers. At the present state of refinement it is not possible to state that there are any differences between the three isomeric compounds.

ORNL-DWG. 66-2030

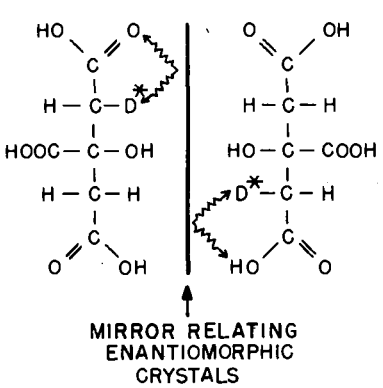

Fig. 8.9. Crystallographic Enantiomorphous Configurations of 2*R*, 3*R* 2-Deuteriocitric Acid. Arrows emphasize important differences which influence the neutron-diffraction intensities.

ORNL-DWG. 66-1770

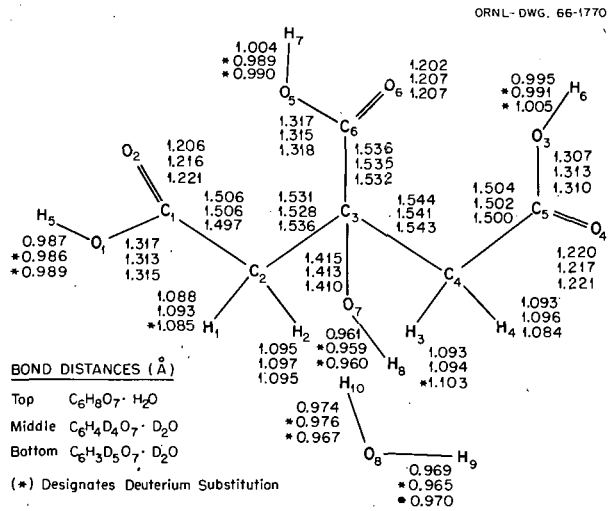

Fig. 8.10. Covalent Bond Distances in Citric Acid Monohydrate.

Furthermore, there is no indication that the hydrogen bonds O–H···O are shorter than the deuterium bonds[87] O–D···O. The five hydrogen bond lengths range from 2.624 to 2.775 A. Figure 8.11 is a stereoscopic illustration[88] showing the hydrogen bonding and molecular packing. Figure 8.12 shows the thermal-motion probability ellipsoids at the 50% level for the three compounds. If there are differences in the thermal motion of hydrogen and deuterium, they are not detectable at the present stage of refinement.

The Crystal Structure of Sodium Zirconium Fluoride, $Na_7Zr_6F_{31}$[89]

J. H. Burns[90] R. D. Ellison
H. A. Levy

The structure of $Na_7Zr_6F_{31}$ was determined from x-ray diffraction data from about 750 reflections collected by the computer-controlled diffractometer

[87] J. A. Ibers, *Ann. Rev. Phys. Chem.* **16**, 387 (1965).

[88] C. K. Johnson, *OR TEP: A Fortran Thermal-Ellipsoid Plot Program for Crystal Structure Illustrations*, ORNL-3794 (1965).

[89] For an earlier report on this study, see *Reactor Chem. Div. Ann. Progr. Rept. Dec. 31, 1965*, ORNL-3913, pp. 17–19.

[90] Reactor Chemistry Division.

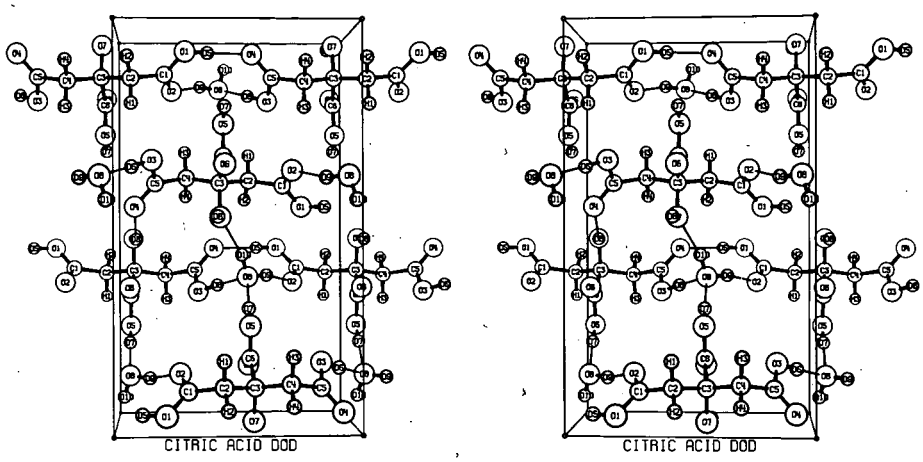

Fig. 8.11. Stereoscopic Illustration Showing Molecular Packing and Hydrogen Bonding Scheme in Citric Acid Monohydrate.

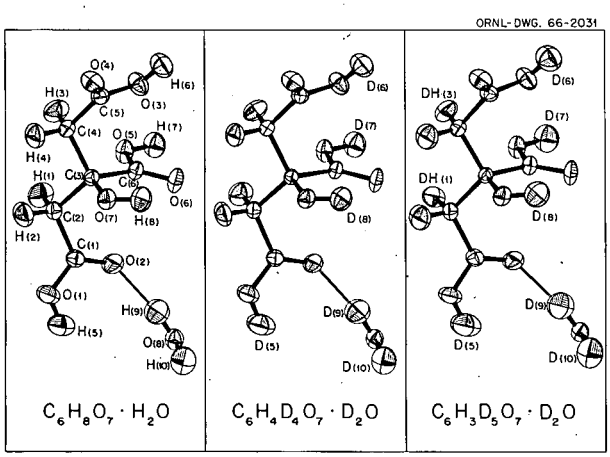

Fig. 8.12. Comparison of Thermal-Motion Probability Ellipsoids in Isomers of Citric Acid Monohydrate.

described elsewhere in this report.[91] Atomic positions were deduced from Patterson and electron-density difference maps. Refinement, including anisotropic thermal parameters, was carried out by the method of least squares.

The rhombohedral unit cell, with a = 8.5688 A, α = 107°21′, contains one formula weight of $Na_7Zr_6F_{31}$. Six Na atoms, six Zr atoms, and thirty F atoms occupy general 6(f) sites of $R\bar{3}$, while one Na atom is in 1(b) and one F atom is statistically distributed over 2(c).

Each Zr atom is bonded to eight F atoms arranged as a square antiprism with Zr-F distances ranging from 2.03 to 2.18 A (average of 2.09 A). Six antiprisms share corners to enclose a cuboctahedral cavity inside of which is one F atom randomly occupying either of the two sites 2(c). The position of this F atom, close to the intersection of the unique axes of three of the six antiprisms, suggests that it is weakly covalently bonded to three Zr atoms at the rather long distance of 2.63 A. A closer approach of this F atom to these Zr atoms would require reduction of the very short (2.25 A) contact that it makes with three other F atoms. The Na atoms are located outside the cuboctahedron and share the F atoms of each of its eight triangular faces. One edge of each antiprism is shared with an antiprism of a different octahedral group, bridging all groups together. The F–F distances within each antiprism range from 2.50 to 2.66 A (average 2.58 A) except for the shared edge, in which the F–F distance is 2.38 A.

X-Ray Diffraction Studies of Liquids

A. H. Narten H. A. Levy

Diffractometer. – The diffraction pattern from the horizontal surface of the liquid sample is obtained

[91] W. R. Busing, R. D. Ellison, S. P. King, and H. A. Levy, "The Oak Ridge Computer-Controlled X-Ray Diffractometer," this report.

with a divergent beam technique similar to the Bragg-Brentano flat sample system used for powder samples.[92] The instrument provides for simultaneous angular motion of the x-ray tube and the detector about a horizontal axis lying in the liquid surface. This method eliminates sample holder absorption and scattering. Monochromatic x radiation, essential to good work with liquids, is obtained through the use of a bent and ground crystal monochromator mounted in the diffracted beam.

Data collection with this instrument, and the various correction procedures applied to the raw data, as well as ways of obtaining meaningful information on liquid systems from these data, have now been described in detail.[93]

Water. – Work on the structure of water, started by M. D. Danford (1962), has been completed. The diffraction pattern of liquid water in equilibrium with water vapor has been analyzed at 4, 25, 50, 75, 100, 150, and 200°C. Deuterium oxide at 4°C was also studied. The radial distribution functions derived from these experiments are shown in Fig. 8.13; the curves are in agreement with most of the previously published work on water, showing, however, much higher resolution. They show deviations from a uniform distribution of distances out to 8 A at room temperature, and significant but gradual changes occur with increasing temperature.

An attempt has been made to compare the experimental radial distribution functions with curves computed from proposed models of water structure. Intensity functions were computed for a model based on an anisotropically expanded ice I structure; occupancy of the large dodecahedral cavities typical of this structure was permitted. The intensity functions for the model are in agreement with the x-ray data over the whole range of scattering angles. Radial distribution functions obtained by Fourier inversion of the model intensity functions are in agreement with those derived from experiment to distances of 10 A and beyond. The same model, with proper adjustment of nearest neighbor distances and mean-square displacements of these and longer range distances, explains the x-ray data over the whole temperature range covered by our experiments.

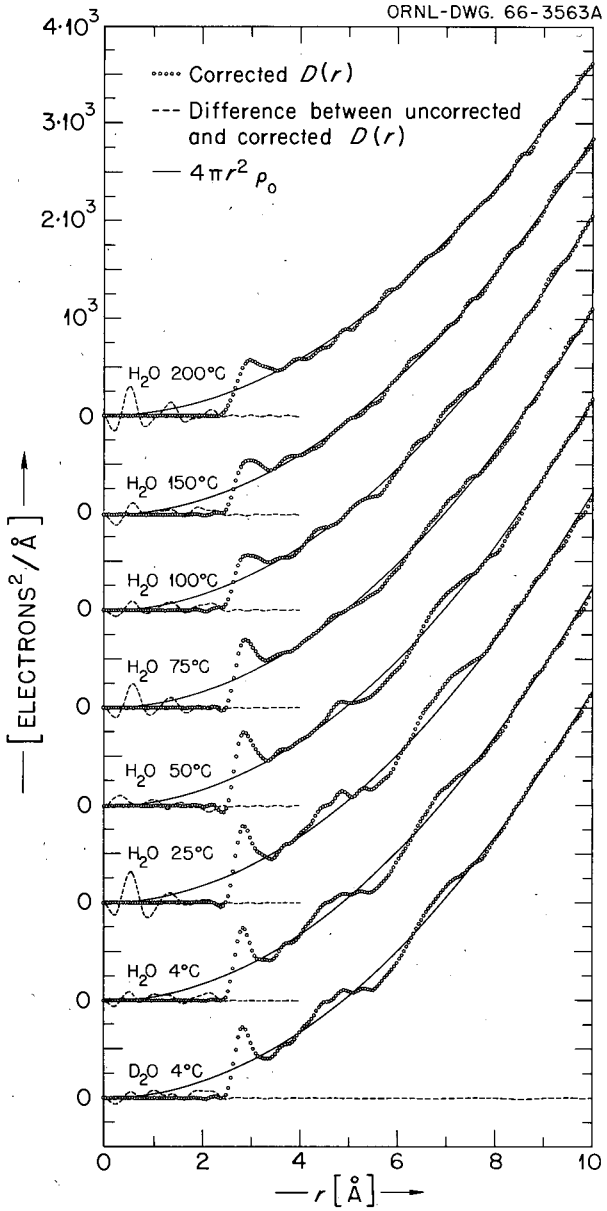

Fig. 8.13. Radial Distribution Functions Derived from X-Ray Diffraction Data.

Carbon Tetrachloride. – The diffraction pattern of liquid carbon tetrachloride at 25°C was measured by M. D. Danford (1956). A computed radial distribution function, based on a model structure, is in quantitative agreement with that derived from the diffraction data. In the model, which assumes

[92] P. S. Sharrah, H. A. Levy, P. Agron, M. D. Danford, R. D. Ellison, and M. A. Bredig, *Chem. Div. Semiann. Progr. Rept. June 20, 1955*, ORNL-1940, pp. 39–42.

[93] H. A. Levy, M. D. Danford, and A. H. Narten, *Data Collection and Evaluation with an X-Ray Diffractometer Designed for the Study of Liquid Structure*, ORNL-3960-A (May 5, 1966).

tetrahedal arrangement of chlorine atoms around the carbon in the CCl_4 molecule, the arrangement of CCl_4 molecules in the liquid is described in terms of a perturbed close packing of chlorine atoms. Intramolecular distances derived from this model are in excellent agreement with those derived from electron-diffraction data.

MOLECULAR BEAM STUDIES

Elastic Scattering in Hydrogen-Helium Systems

G. E. Moore Sheldon Datz
F. van der Valk[94]

The investigation of the total cross sections for scattering of H_2 and D_2 by ^3He and ^4He was concluded. Absolute cross sections for the H_2-^3He and D_2-^3He systems were determined simultaneously from the pressure dependence of the attenuation of mixed modulated beams of H_2 and D_2 by a fixed scattering length of ^3He at 77°K. The intensities were measured by a mass-spectrometric beam detector following the scattering cell. Beam temperatures were varied from 77 to 600°K, giving a most probable collision relative velocity range of 1.17×10^5 to 2.64×10^5 cm/sec for H_2-^3He and 0.98×10^5 to 1.92×10^5 cm/sec for D_2-^3He. Similar measurements were made on the H_2-^4He system. For the D_2-^4He system, considerable uncertainty was introduced by the interference of mass 4 background from the ^4He. The angular resolution according to the Kusch criterion[95] was 15′ of arc.

The evaluation of cross sections requires a correction for the velocity distributions in the beam and in the target gas.[96] The correction is a function of the velocity dependence of the cross section, and the appropriateness of the choice of a given velocity dependence can be evaluated from the internal consistency of the data, that is, by the determination of the slope of the corrected cross section vs the most probable relative velocity. Of the two potential models tried, "hard sphere" and "attractive sixth," the hard-sphere model gave consistent results at all except the lowest relative velocities. Since the hard-sphere-model cross sections should be independent of velocity, the mixed-beam technique permits a direct point-for-point comparison of the relative scattering cross sections of H_2-^3He and D_2-^3He. This experimental arrangement eliminates the error in relative cross-section determinations due to pressure and scattering length uncertainties. The resultant ratio of cross sections was not measurably different from unity (±5%).

The absolute cross sections so determined (to ±1 A^2) were 41.5, 42.5, and 42.5 A^2 for the H_2-^3He, D_2-^3He, and H_2-^4He systems respectively, except at the lowest beam temperature. All these values are considerably smaller than those determined by Harrison.[97]

Alkali-Atom–Halogen-Molecule Reactions

Robert E. Minturn Sheldon Datz

The theoretical mechanism which was devised to treat the data obtained from last year's experimental work on alkali–halogen-molecule reactions was extended. This model, called "spectator stripping," successfully predicts the gross features of the observed distributions and leads to a prediction of the maximum intermolecular distance at which reaction can occur. The effect of electron transfer from the alkali atom to the halogen molecule at large distances was shown to be almost equivalent to spectator stripping in the predicted cross section, if the vertical electron affinity of the halogen molecule is used. Even larger cross sections would be predicted if the adiabatic electron affinity were used; however, an evaluation of the probability of adiabatic adjustment of the halogen internuclear distances during the collision time appears to preclude this possibility.

The model predicts that, for alkali reactants with relatively high ionization potentials, such as sodium and lithium, the maximum impact parameter at which reaction can occur lies inside the distance of the potential minimum for the van der Waals complex of alkali atom and halogen molecule. This leads to the expectation of observable rainbow scattering in these systems. Experiments to test this hypothesis were done and are being evaluated.

---

[94] Visiting Scientific Staff Member from The Netherlands.

[95] P. Kusch, *J. Chem. Phys.* **40**, 1 (1964).

[96] K. Berkling *et al.*, *Z. Physik* **166**, 406 (1962).

[97] H. Harrison, *J. Chem. Phys.* **37**, 1164 (1962).

A Molecular Beam Study of the Reaction of Ozone with Atomic Hydrogen

Sheldon Datz Thomas W. Schmidt[98]

The new permanent-gas scattering apparatus was used to survey the feasibility of studying several new reaction types. In this apparatus, shown in Fig. 8.14, the source and detector are mounted external to the scattering chamber, and the detector section may be rotated through an angle of 130° without disturbing the vacuum. The detector is a four-pole mass filter with resolution $\Delta m/M = 1/100$ at mass 100. It is bakeable and is separated from the scattering region by two stages of differential pumping. As planned, modulation and particle counting techniques were introduced, which further increased the sensitivity of the instrument. The reaction of NO + O_3 was investigated, and all parts of the instrument were found to function in the expected manner. Because of the soft x-ray background in the detector, it was found that the reaction cross section ($\sim 10^{-21}$ cm^2 expected) was too small to be observed. However, it was also found that the OH^+ background attained in the mass analyzer was small enough to permit the study of the reaction of atomic hydrogen with ozone. This reaction is thought to be the cause of the observed OH radical spectra in the upper atmosphere.

For this experiment, liquid ozone is formed by a radio-frequency discharge in oxygen at 77°K. The temperature is then raised to create a pressure behind a fused glass capillary array, which acts as the primary beam source. The atomic hydrogen cross beam is formed by an in situ radio-frequency discharge in molecular hydrogen. Beam formation and detection for both components have proved satisfactory, and initial scattering experiments have been performed.

[98]ORAU Predoctoral Fellow.

Collisional Excitation of Vibrational Levels in Hydrogen

Sheldon Datz Peter F. Dittner

A new technique is being developed for the determination of cross sections for collision-induced

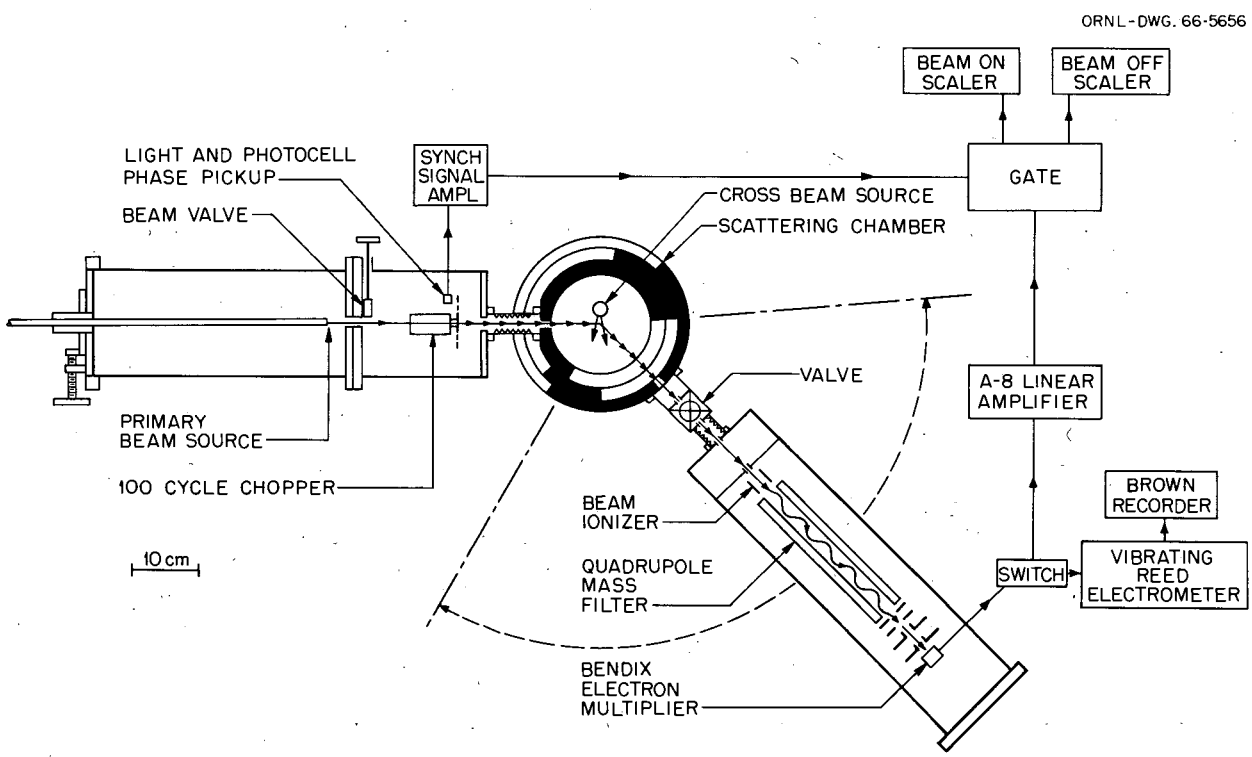

Fig. 8.14. Schematic Drawing of the Permanent-Gas Reactive Scattering Apparatus.

vibrational excitation. The method involves a time-of-flight measurement of the energy of a fast projectile atom or ion following its collision with a target molecule. The degree of excitation in the collision appears as a loss in the velocity of the projectile particle. In the first experiment, a fast (30 ev) beam of K^+ ions, formed by techniques which were developed for our ion-molecule elastic scattering studies of last year, is pulsed and passed through a scattering chamber containing hydrogen gas. In the second experiment, the ion beam first traverses a region of high-density thermal-energy potassium atoms, producing a beam of high-energy (>30 ev) neutral atoms via charge exchange. The relative collision energy is only 1.5 ev and, hence, is only able to cause transitions in the H_2 molecule from the ground vibrational state to any of the first three excited states. The time-of-flight spectrum is recorded on a multichannel analyzer, and the relative excitation cross sections so determined will hence be independent of fluctuations in beam intensity and scattering gas pressure. Information obtainable from this experiment should prove valuable in the theory of molecular relaxation and of unimolecular decomposition. The apparatus has been constructed, and initial experiments on beam formation, pulsing, timing, and detection have been completed.

The two isotopes of potassium have been clearly resolved with peak-to-valley ratios of 100 and 5 for the ^{39}K and ^{41}K peak respectively. The full width at half maximum of the ^{39}K peak is typically 0.6% of the total flight time, independent of ion energy.

A Program to Compute the Classical Deflection Function

M. H. Lietzke M. G. Menendez

A measurement of the angular distribution of elastic scattering can lead to some information about the interatomic potential. A computer program has been written which may be useful in the interpretation of experimentally measured angular distributions in terms of classical mechanics. The program, written in both ALGOL and FORTRAN II, is divided into two parts. The first part is used to adjust the minimum value of the interatomic potential, $\phi(r)$, to any desired equilibrium internuclear distance by adjusting the strength of the repulsive portion of the potential (the A parameter). The second part computes the classical deflection function, $\chi(b)$, the corresponding phase shift, $\eta(b)$, and the angular spacing between the principal rainbow and the second-order rainbow.

The application of classical mechanics to scattering events yields the following well-known relationship for the differential cross section:

$$\sigma(\chi) \sin \chi = b \left| \frac{d\chi}{db} \right|^{-1} , \qquad (1)$$

where χ is the scattering angle in the barycentric system of coordinates, $\sigma(\chi)$ is the differential cross section, and b is the impact parameter. The scattering angle expressed as a function of the impact parameter is called the classical deflection function, $\chi(b)$; $\chi(b)$ is related to the interatomic potential $\phi(r)$ by the integral equation

$$\chi(b) = \pi - 2b \int_{r_c}^{\infty} \left[1 - \frac{b^2}{r^2} - \frac{\phi(r)}{E_r} \right]^{-1/2} \frac{dr}{r^2} , \qquad (2)$$

where E_r is the relative energy of collision and r_c is the distance of closest approach given by the smallest root of

$$\frac{b}{r_c} = \left[1 - \frac{\phi(r_c)}{E_r} \right]^{1/2} . \qquad (3)$$

In order to obtain information about $\phi(r)$ from a measurement of the angular distribution, Eq. (2) must be solved for assumed representations of $\phi(r)$ until good agreement is reached with the experimental data. This procedure is especially well suited to collisions at low energies, where $\chi(b)$ is a sensitive function of $\phi(r)$, such as in rainbow scattering, orbiting collisions, and glory scattering. Furthermore, it is helpful to have a priori knowledge of the form of the potential function.

A reasonably general interatomic potential may be written as

$$\phi(r) = \frac{A}{r^m} - \frac{B}{r^n} - \frac{C}{r^p} - D(r) , \qquad (4)$$

where A, B, C, m, n, p, and $D(r)$ take on any set of values. The term $D(r)$ is included to represent attractive terms that may not have a simple dependence on r. Examples of $\phi(r)$ for ion-atom and atom-atom interactions may be written as

$$\phi(r) = \frac{A}{r^{12}} - \frac{B}{r^4} - \frac{C}{r^6} \tag{5}$$

and

$$\phi(r) = \frac{A}{r^{12}} - \frac{C}{r^6} \tag{6}$$

respectively. Mason[99] has used a potential of the type given by Eq. (5) to represent elastic scattering of ions from atoms.

It is convenient to transform Eq. (2), by making the substitution $\sin\theta = r_c/r$, to

$$\chi(b) = \pi - \frac{2b}{r_c}\int_0^{\pi/2}\left[1 - \frac{b^2\sin^2\theta}{r_c^2} - \frac{\phi(r_c/\sin\theta)}{E_r}\right]^{-1/2}\cos\theta\, d\theta\,, \tag{7}$$

which is amenable to numerical integration.

It is often useful in an analysis of this type to know the phase shift, $\eta(b)$, corresponding to $\chi(b)$, since this is the first link to a semiclassical treatment. The corresponding phase shift in the sense of the WKBJ approximation is given by

$$\eta(b) = \frac{1}{2}\left[\int_0^b \chi(b)\, db - \int_0^\infty \chi(b)\, db\right] = -\frac{1}{2}\int_b^\infty \chi(b)\, db\,. \tag{8}$$

In the present program, the functional form of $D(r)$ is taken to be

$$D(r) = \frac{2[S(r)]^2}{1 + [S(r)]^2} \times \frac{[E_I + (B\sin^4\theta)/2r_c^4 + (C\sin^6\theta)/2r_c^6]}{[I_m - E_I - (B\sin^4\theta)/r_c^4 - (C\sin^6\theta)/r_c^6]}\,. \tag{9}$$

In this equation E_I is an electron affinity, I_m is an ionization potential, and $S(r)$ is a two-center overlap integral. Values of the overlap integrals $S(r)$ must be supplied to correspond with each value of $\chi(b)$ computed. If no overlap is assumed, then the entire set of $S(r)$ may be taken as zero.

Specifically the calculational procedure is as follows:

1. For a given set of the parameters B, C, m, n, p, and the parameters which enter into the expression for $D(r)$, the value of A in the chosen representation of $\phi(r)$ is adjusted such that the minimum is made to occur at r_m, the desired equilibrium internuclear distance. This is done by using the "Search for A" program.
2. Equation (3) is then solved by successive approximations to determine the value of r_c corresponding to each value of b for a given value of E_r and the expression for $\phi(r)$ used in step 1.
3. The integration shown in Eq. (7) is then performed to produce a set of values of $\chi(b)$ for values of b from 0 to 20.0 in steps of 0.1. The integration is performed by eight-point Gaussian quadrature. Corresponding values of the phase shift $\eta(b)$ are computed by double Gaussian quadrature. In order that the Gaussian points not be distributed over too large a range of b, the calculation is broken down as follows:

Let b_0 be the minimum value of b at which $\chi(b) = 0$; this value is found by linear interpolation. Then for values of $b > b_0$:

$$\eta_1(b) = -\frac{1}{2}\left[\int_b^{b'} \chi(b)\, db + \int_{b'}^{b_\infty} \chi(b)\, db\right], \tag{10}$$

where b' and b_∞ are arbitrary input numbers.

For values of $b > b_0$:

$$\eta_2(b) = -\frac{1}{2}\int_b^{b_0} \chi(b)\, db + \eta_1(b_0)\,. \tag{11}$$

The value of $\eta(b)$ is very sensitive to the distribution of the Gaussian points in performing the integration of Eq. (10), since the area under the $\chi(b)$ curve decreases rapidly as the value of b increases. Hence it may be necessary to adjust the value of b' in Eq. (10) so that the value of $\eta(\max)$ will occur at b_0.

When the conditions for rainbow scattering are met, it is desirable to obtain some idea of the location of the second-order rainbow (supernumerary rainbow).[100] A rough estimate of the angular spacing between the principal rainbow and the

[99] E. A. Mason and J. T. Vanderslice, *J. Chem. Phys.* **31**, 594 (1959).

[100] E. A. Mason and L. T. Monchick, *J. Chem. Phys.* **41**, 7 (1964).

second-order rainbow can be obtained by using the approximation given by Ford and Wheeler.[101] Briefly the method is as follows:

1. Two parabolas are fitted about the minimum of the $\chi(b)$ vs b function, that is, on both sides of the minimum,

$$\chi(b) = Q'(M \pm 2)\, b^2 \,. \tag{12}$$

2. A transformation from b space to l space is accomplished by using the expression

$$l = 21.95(E_r)^{1/2}(\mu)^{1/2} b \,, \tag{13}$$

where l is the angular momentum quantum number, μ is the reduced mass, 21.95 is a constant, and E_r is the relative energy in electron volts.

3. The angular spacing between the principal rainbow, $\chi_r(M)$, and the second-order rainbow, $\chi_2(M \pm 2)$, is computed from

$$\chi_r(M) - \chi_2(M \pm 2) = 2.2294[Q(M \pm 2)]^{1/3} \,, \tag{14}$$

where 2.2294 is a constant determined from the spacing between maxima of the Airy function[101] and $Q(M \pm 2)$ is the analog of $Q'(M \pm 2)$ in l space. In general, the two values, $\chi_r(M) - \chi_2(M + 2)$ and $\chi_r(M) - \chi_2(M - 2)$, will not differ greatly.

Additional quantities computed and output by the program are:

1. the value of r_e(min),
2. the value of χ_e(min) and the corresponding value of b(min),
3. the slope of the classical deflection function at b_0, that is,

$$\left(\frac{d\chi(b)}{db}\right)_{b=b_0} ,$$

where b_0 corresponds to $\chi(b) = 0$.

A detailed description of the program, along with sample input and output, is given in ORNL-3881.

[101] K. W. Ford and J. A. Wheeler, *Ann. Phys.* 1, 259, 287 (1959).

MASS SPECTROMETRY AND RELATED TECHNIQUES

Mass Spectrometric Evidence for H_3O, HD_2O, and D_3O[102]

C. E. Melton P. S. Rudolph

The ions H_3O^+, HD_2O^+, and D_3O^+ have been observed in a research mass spectrometer. Evidence from a rather detailed study indicates that the progenitors are the corresponding neutral trihydrogen oxides, which are formed by a heterogeneous reaction on the walls of the ion source. The ion beam at $M/E = 19$ has, in the past, been attributed to either H_3O^+ formed by an ion-molecule reaction, or F^+ from residual background gases.

In this study, samples of either H_2O or D_2O were introduced into a research mass spectrometer with a stainless steel ion source at a pressure of (1 to 5) $\times 10^{-8}$ torr. An actual scan of the mass 20 through 22 range with D_2O in the instrument at a pressure of 1×10^{-8} torr is shown in Fig. 8.15. Qualitative appearance potential measurements showed that the ionization potential of D_3O was about 1 ev lower than that of D_2O. Wall reactions[103] of D_2O^*(g) to form D_3O^+(g) appear to be ruled out in this study because of the low concentration of D_2O^*. Furthermore, the walls were made negative with respect to the ion repeller to prevent the possible evolution of ions from the surface.[104]

A second possible origin of the ions, ion-molecule reactions with D_2O^+ or some other abundant ion from D_2O, is eliminated by the following consideration. The intensity ratios HD_2O^+/HDO^+ and D_3O^+/D_2O^+ were measured as a function of the electric field strength within the ionization chamber. No change in these ratios was observed for changes in the electric field strength from about 0 to 20 v/cm. This observation proves that HD_2O^+ and D_3O^+ were not produced by ion-molecule reactions, since the abundance of secondary ions is sensitive to changes in the electric field strength within the ionization chamber. A third possible origin of the ions, dissociative ionization of a

[102] C. E. Melton and P. S. Rudolph, *J. Catalysis* 5, 387 (1966).

[103] P. Marmet and J. D. Morrison, *J. Chem. Phys.* 36, 1238 (1962).

[104] T. W. Martin, *J. Chem. Phys.* 43, 1422 (1965).

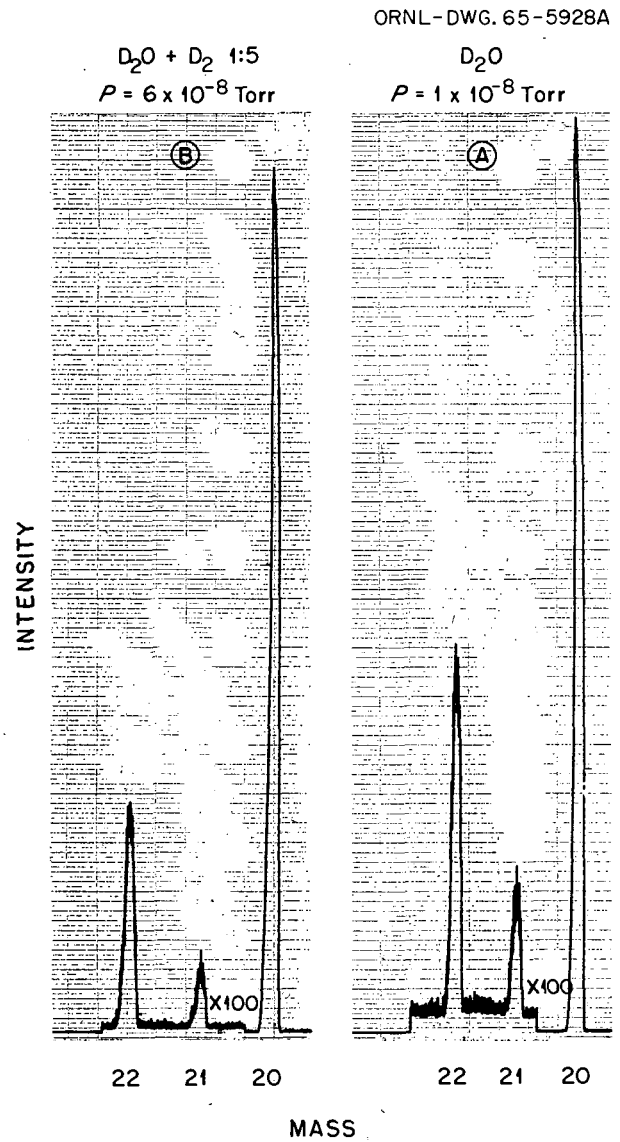

Fig. 8.15. Mass Spectra Showing Evidence for HD_2O (Mass 21) and D_3O (Mass 22). In *B*, D_2 is added to the system and the abundance of HD_2O and D_3O, relative to D_2O (mass 20), is greatly reduced, suggesting a surface reaction.

dimer evolving from the surface, although apparently unlikely, could not be ruled out in the present study.

The intensity of D_3O^+ was reduced by about a factor of 2 when D_2 or O_2 was added to the D_2O, thus suggesting that D_3O was formed on the surface. Figure 8.15 shows the effect of adding D_2.

Evidence from these experiments strongly suggests the formation of neutral H_3O by a surface reaction. The lifetime, with respect to spontaneous decomposition, of H_3O in the gas phase must be at least 10^{-6} sec (transit time from the surface to the electron beam).

Transient Species Produced by the Heterogeneous Decomposition of Acetone in a Mass Spectrometer

C. E. Melton

The heterogeneous decomposition of acetone over platinum has been studied in our research mass spectrometer for pressures ranging from 10^{-2} to 1 torr and temperatures ranging from 273 to 1673°K. Two negative ions, CH_3^- and $CH_3COCH_2^-$, and two free radicals, CH_3 and CH_3COCH_2, were observed, in high concentrations, in the gas phase during the course of the decomposition reaction. Gas-phase free radicals were identified by maintaining the energy of the ionizing electrons below that necessary to produce interfering fragment ions by dissociative ionization of either residual or reactant gases. Charged species evolving from the surface of the hot metal were identified by direct observation, that is, without an ionizing electron beam. Charged species may be produced on the surface by two different methods, (1) dissociation and ionization of adsorbed molecules followed by evaporation of the resultant ions from the surface and (2) surface ionization of gas-phase species striking the hot surface.

The abundance of all of the neutral species observed in the gas phase during the decomposition was as follows: CH_3 (28%), CO (26%), CH_4 (23%), and CH_3COCH_2 (21%). Pressure studies of CH_3 showed a first-order rate dependence, in accord with heterogeneous decomposition. These observations, together with the amount of CO observed, permit us to state with a high degree of certainty that the first step in the decomposition of acetone involves one molecule of acetone and is of the form

$$CH_3COCH_3 \xrightarrow{Pt} 2CH_3 + CO \,. \qquad \text{I}$$

Reaction I, as written, is about 80 kcal endothermic, but, if one of the methyl radicals is chemisorbed, the energetics are much more favorable. Results obtained by temperature studies indicated that

the activation energy is 34.3 kcal, clearly demonstrating a surface reaction rather than a homogeneous decomposition reaction. Results for the abundance of neutral species suggest that the second step of the decomposition leads to either CH_3COCH_2 or CH_4 or both because of their high abundance. Gas-phase radical-radical reactions are improbable under our experimental conditions because of the relatively low abundance of free radicals in the gas phase. We postulated the reaction of a methyl radical with acetone to give CH_4,

$$CH_3 + CH_3COCH_3 \longrightarrow CH_4 + CH_3COCH_2 \,, \quad \text{II}$$

though realizing that we had no way to distinguish between a surface and a gas-phase reaction. We tested the pressure dependence of the products, and the results showed that the abundance of CH_3COCH_2 is proportional to the square of the pressure. The abundance of CH_4 was also second order with respect to pressure, as required by reaction II. Thus, the postulated reaction (II) is indeed consistent with the experimental observations. Therefore reaction (II) appears to be the second step of the overall decomposition.

The existence of charged species in the gas phase during the catalytic reaction is shown by the striking results of Fig. 8.16. In this experiment the temperature of the catalyst was suddenly changed from room temperature to 1473°K and back to room temperature while monitoring the CH_3^- ion beam with no ionizing electron beam present. The CH_3^- intensity increases and decreases abruptly corresponding to abrupt changes in the catalyst temperature, thus demonstrating that the hot metal is the source of the ions.

A similar study of the $CH_3COCH_2^-$ ion beam gave identical results, showing that $CH_3COCH_2^-$ is also produced by the hot platinum. No other positive or negative ions were observed in the gas phase with the surface hot and the electron beam turned off. The measured concentrations of CH_3 and CH_3COCH_2 radicals in the gas phase were higher than that required to produce the corresponding ions by surface ionization according to the relationship

$$\frac{N^-}{N_0} = \frac{(1 - r_i)}{(1 - r_0)} \frac{\omega_i}{\omega_0} \exp \frac{(\mathrm{EA} - \phi)}{(kT)} \,. \qquad (1)$$

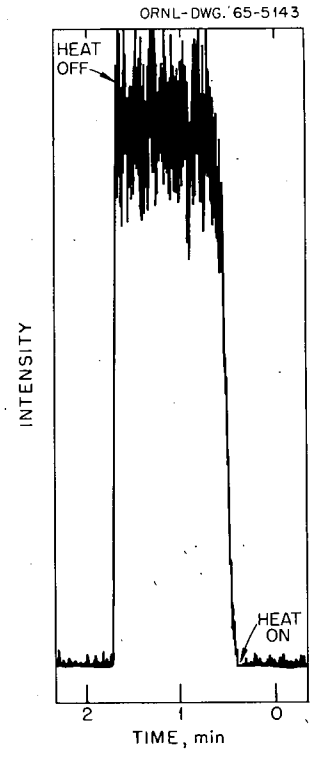

Fig. 8.16. Concentration of CH_3^- Ions as a Function of Surface Temperature in the Decomposition of Acetone over Pt. "Heat on" is 1473°K, and "heat off" is about room temperature.

The symbols are defined as:

N^-/N_0 = ratio of the charged to the neutral component leaving the surface,

r_i and r_0 = reflection coefficients of the surface for the ion and the neutral molecule,

ω_i and ω_0 = statistical weighting factors for the ion and the neutral molecule,

EA = electron affinity,

ϕ = electron work function of the metal.

Thus, one might conclude that surface ionization is actually the mechanism. Such a conclusion would not necessarily be valid, because the system is not in equilibrium and Eq. (1) was developed by assuming an equilibrium condition. Consequently, we are unable to determine from the present study whether the CH_3^- ions result from surface ionization of the CH_3 gas-phase radical or actually evolve from the surface as ions produced by the dissociation and ionization of acetone. The elementary reaction mechanism for the removal

of both the CH_3 neutral and the CH_3^- ion give CH_4 as a product, thus preventing the differentiation of the processes on the basis of the final products.

General Conditions for Ionization by Surfaces. – Evidence from the present study indicated that the ionic species $CH_3COCH_2^-$ in the gas phase were formed by surface ionization of gas-phase free radicals rather than by displacement of adsorbed ions from the surface. On the other hand, the ionic species, NH_4^+, observed in the study[105] of the decomposition of NH_3 apparently did not result from surface ionization of gas-phase free radicals, but rather evolved directly from the catalytic surface, therefore suggesting an appreciable concentration of adsorbed ions on the surface. Results from these two studies show that the observation of ions in the gas phase during a catalytic reaction does not necessarily indicate a high concentration of adsorbed ionic species on the surface. The question as to the experimental conditions under which one expects appreciable ionization on the surface was investigated by elementary thermochemical considerations in which ΔH for a given reaction was estimated. One needs as parameters (1) the ionization potential (I), (2) the electron affinity (EA), (3) the heat of adsorption of an ion (E_a), (4) the energy of chemisorption (E_c), (5) the energy of physical adsorption (E_p), (6) the work function of the catalyst (ϕ), and (7) the dissociation energy (D) of the molecule of interest. For positive ionization ΔH is given by

$$\Delta H = \eta E_p + D + I - \phi - \eta E_a - \eta E_c \qquad (2)$$

and for negative ionization

$$\Delta H = \eta E_p + D + \phi - \mathrm{EA} - \eta E_a - \eta E_c \,, \qquad (3)$$

where η refers to the number of species. All of these parameters are either available or can be estimated.

For a typical dissociation reaction such as

$$\underset{S}{AB} \rightarrow \underset{S}{A^{\pm}} + \underset{S}{B} \,,$$

where AB is any molecule, B is uncharged, and $A^{\pm}$ is either a positive or negative ion, Eqs. (2) and (3) show that ΔH is negative (the reaction is exothermic) for either $I \leqq 10$ ev or EA $\geqq 0.6$ ev for a platinum surface with $\phi = 5$ ev. Thus, molecules (or atoms) with high ionization potentials and low electron affinities, such as N and H, are unlikely to reside on the surface as ions. These conclusions are consistent with those of Emmett and Teller[106] regarding ions on catalytic surfaces.

[105] C. E. Melton and P. H. Emmett, *J. Phys. Chem.* **68**, 3318 (1964).

[106] P. H. Emmett and E. Teller, *Twelfth Report of the Committee on Catalysis*, p. 68, Wiley, New York, 1940.

Experimental and Theoretical Considerations for Ionization of Simple Hydrocarbons, H_2, D_2, O_2, H_2O, and the Rare Gases by 2.2-Mev Alpha Particles and by Electrons in a Mass Spectrometer

P. S. Rudolph C. E. Melton

Ionization cross sections and primary mass spectra produced by 2.2-Mev alpha particles have been measured for CH_4, C_2H_2, C_2H_4, C_2H_6, H_2O, H_2, D_2, O_2, N_2, He, Ne, Ar, and Kr in a research mass spectrometer. A specially designed ion source (Fig. 8.17) employing a 2.7-curie ^{210}Po alpha source as the ionizing medium was used for these measurements. The ion source had the following essential characteristics: (1) had a well-collimated alpha beam of known energy (2.2 Mev) and a reasonably high intensity (1.8×10^9 alpha particles per second), (2) operated at low pressures ($<10^{-5}$ torr), (3) was essentially free from secondary electrons, and (4) had approximately equal collection efficiencies for ions of different initial kinetic energies.

The experimental cross sections for He and H_2 are compared with detailed calculations in the Born-Bethe and in the classical approximations as shown in Table 8.6. The ionization cross sections for the removal of one electron from the outer shell conform well to the predictions, although the experimental results are systematically lower than the theoretical values. The present experimental values for He, Ar, H_2, and N_2 are in good agreement with extrapolated experimental data of D. W. Martin *et al.*[107] (cf. Table 8.6).

[107] D. W. Martin, R. A. Langley, D. S. Harmer, J. W. Hooper, and E. W. McDaniel, *Phys. Rev.* **136**, A385 (1964).

ORNL-LR-Dwg. 42950D

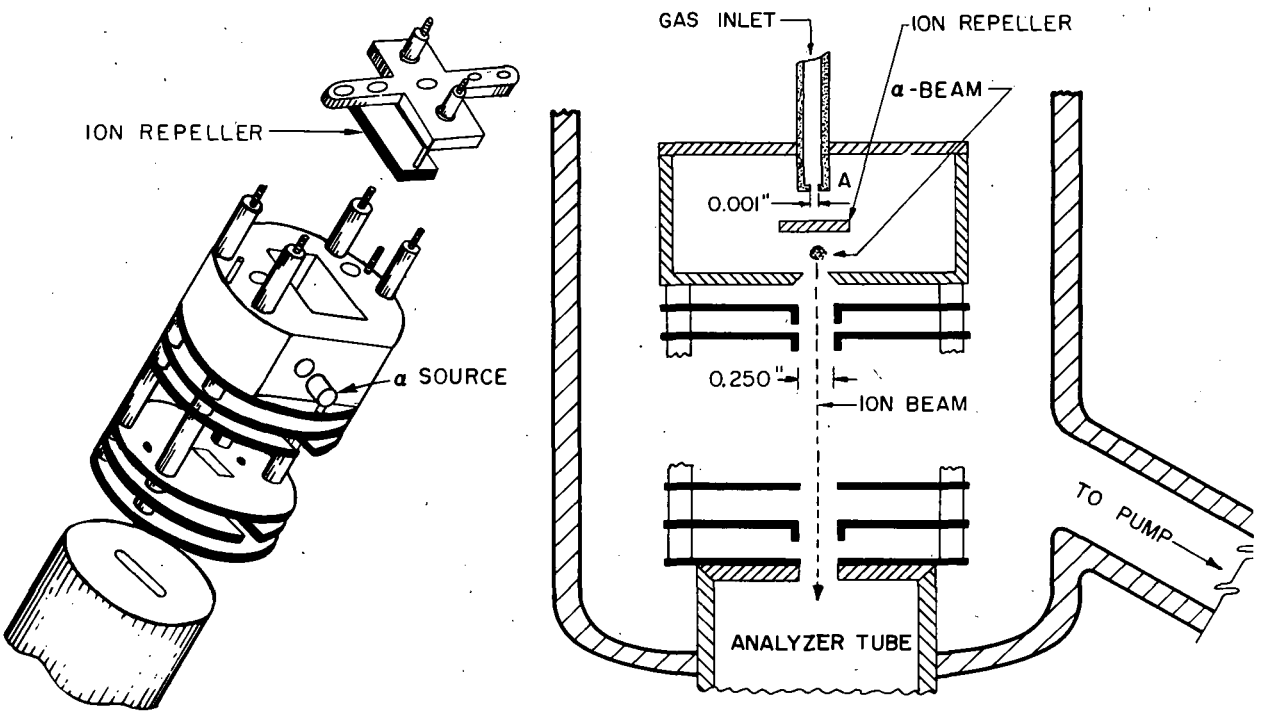

Fig. 8.17. Alpha-Particle Ion Source Designed for the Study of Primary Reactions with the Mass Spectrometer.

The mass spectrum of C_2H_2 produced by 2.2-Mev alpha particles shows the same fragments as produced by electrons of equivalent energy (296 ev, equal velocity); however, the abundance of some fragment ions is much greater for the electrons. This is shown in Table 8.7, where "relative dissociation" is the ratio of abundance by electron impact to abundance by alpha-particle impact normalized to the parent ion. These data agree very well with the results from the most recent study by Wexler,[108] who compared the fragmentation of C_2H_2 by 2.25-Mev protons to that by electrons of equivalent energy (1.225 kev). Both studies show that the mass spectrum produced by heavy ions is significantly different from that produced by electrons. Such differences are completely unexpected for high-energy collisions on the basis of the Born-Bethe approximation, since neither the nature nor charge of the exciting projectile appears in the relationship.[109]

Even in the rare gases, the Born-Bethe approximation does not hold, as evidenced by significantly more multiple ionization by electrons than by alpha particles of the same velocity. This anomaly was most pronounced in Ar. The ratios of abundances of Ar ions produced by electron impact to that produced by alpha bombardment, normalized to Ar^+, are: $Ar^{2+} = 1.9$, $Ar^{3+} = 2.2$, and $Ar^{4+} = 3.5$.

[108] S. Wexler, *J. Chem. Phys.* 41, 2781 (1964).

[109] H. Bethe, *Ann. Physik* 5, 325 (1930).

Table 8.6. Cross Section for Ionization of Simple Gases by 2.2-Mev Alpha Particles

Compound	σ, Cross Section (cm^2/molecule)		
	Experimental	Theoretical	Previous Work[a]
	$\times 10^{-16}$	$\times 10^{-16}$	$\times 10^{-16}$
He (1+)	0.8 ± 0.1	0.9,[b] 1.1[c]	1
Ne (1+)	5		
Ar (1+)	17 ± 3.0	20[c]	14
Kr (1+)	14		
H_2 (1+)	2 ± 0.3	2.3,[b] 2.0[c]	2
D_2 (1+)	2		
O_2 (total)	13		
CH_4 (total)	20		
H_2O (total)	7		
C_2H_2 (total	18		
C_2H_4 (total)	20		
C_2H_6 (total)	30		
N_2 (total)	15		14

[a]Obtained by extrapolating the experimental data in ref. 107.
[b]Obtained from the Born-Bethe approximation, ref. 109.
[c]Obtained from classical theory.

Table 8.7. Mass Spectra of C_2H_2 Produced by Alpha Particles and by Electrons of the Same Velocity

Mass	Positive Ion	Abundance (%)		Relative Dissociation $(EI/\alpha I)$[a]
		2.2-Mev Alpha Particles (αI)	296-ev Electrons (EI)	
1	H	0.25	0.68	2.9
12	C	0.49	1.76	3.9
13	CH	1.23	3.02	2.6
24	C_2	3.65	4.28	1.3
25	C_2H	13.29	15.67	1.3
26	C_2H_2	81.09	75.21	1.0

[a]Normalized to the parent ion.

High-Transmission and Dual-Electron-Beam Ion Sources for Mass Spectrometry

C. E. Melton

Two high-transmission electron-bombardment ion sources, based on a principle of electrical rather than mechanical ion collimation, have been developed and tested with a 6-in.-radius, sector-type mass spectrometer. The new ion sources had a measured transmission efficiency of 88 and 85% as measured by two different techniques. One ion source, shown in Fig. 8.18, was designed for general use for experiments in which high sensitivity is required, while the second, shown in Fig. 8.19, was designed for the study of unstable species

ORNL-LR-Dwg. 42950F

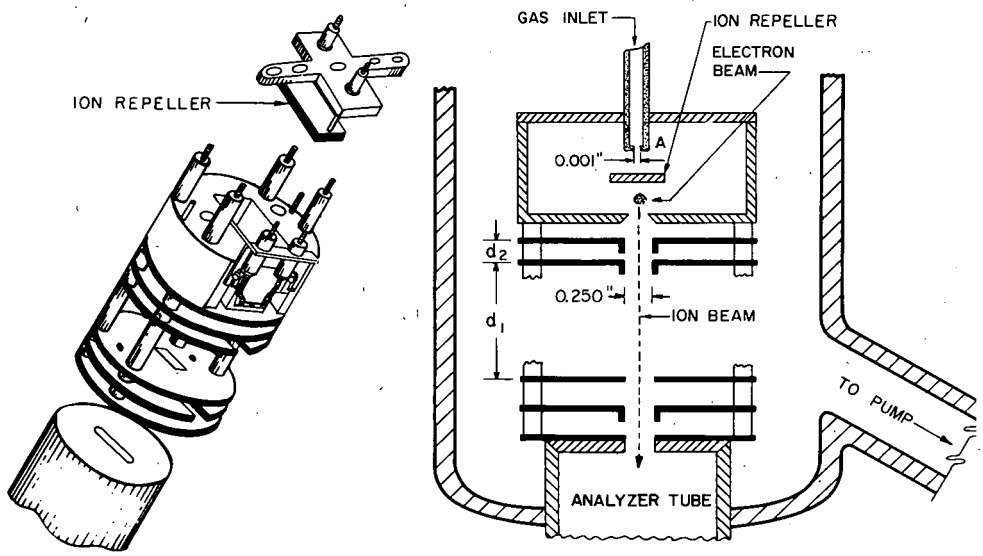

Fig. 8.18. General-Purpose High-Transmission Ion Source for Mass Spectrometry.

ORNL-LR-Dwg. 42950E

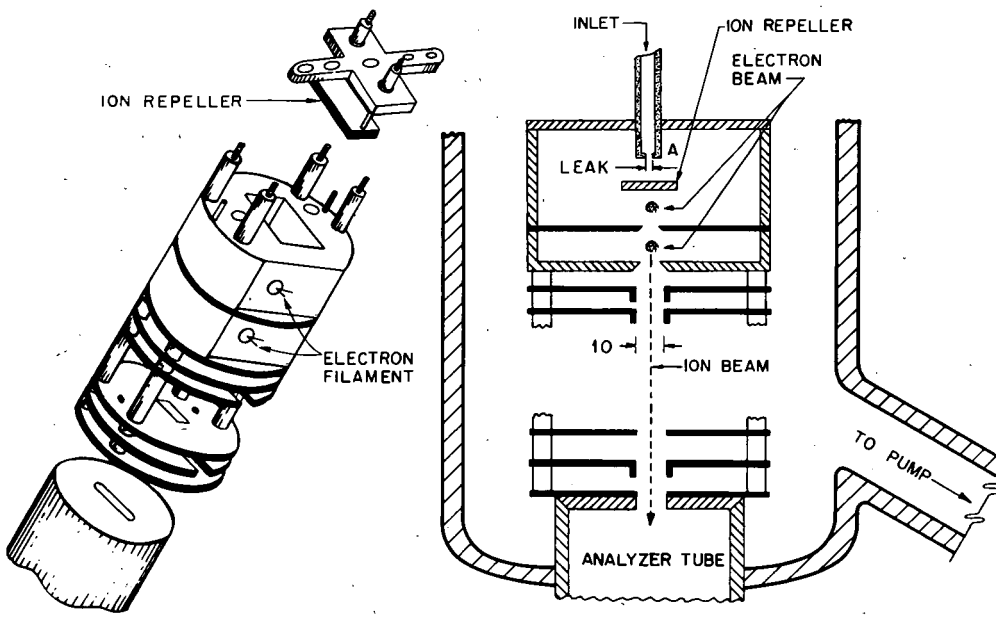

Fig. 8.19. Dual-Electron-Beam Ion Source for the Study of Transient Species.

such as excited neutral molecules, products of ion-molecule reaction, and free radicals. These sources are capable of measuring partial pressures of both unstable and stable species as low as 10^{-17} atm.

Collimating slits of 0.250 by 0.500 in. are used throughout the general-purpose ion source to give electrical rather than mechanical collimation of the ion beam. Electrical collimation increased the transmission by over two orders of magnitude with respect to mechanical collimation, whereas the resolution was only reduced by about a factor of 6, as shown in Fig. 8.20.

The "unstable species" ion source utilizes a principle of two parallel electron beams. One electron beam is used to produce a desired species, and the second electron beam ionizes the species for mass identification. An experiment in which helium was excited to the 1s2s metastable level by 23-ev electrons in the first electron beam and subsequently ionized in the second electron beam by 6-ev electrons was performed, and the results are shown in Fig. 8.21.

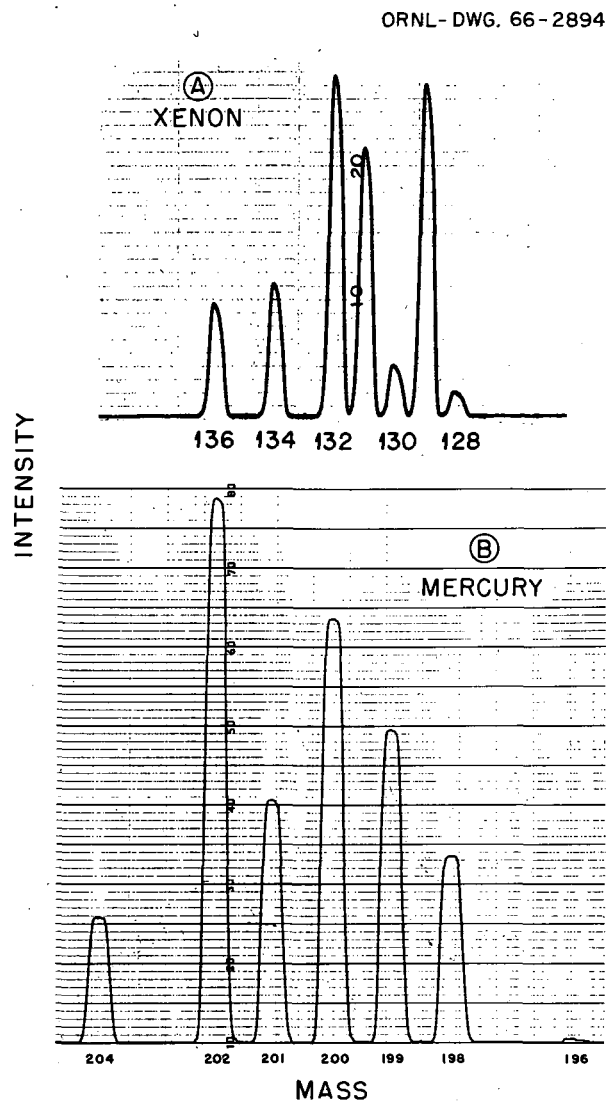

Fig. 8.20. Resolution of the High-Transmission Ion Source as Shown and Scon of the Isotopes of Xe with Wide, 0.250 × 0.500 in., Slits (*A*) and Hg with Narrow, 0.005 × 0.500 in., Slits (*B*). Wide slits increased the transmission of the source over two orders of magnitude and reduced the resolution by a factor of 6.

Two-Stage Mass Spectrometer

Russell Baldock L. E. Idom

The two-stage mass spectrometer has been in continuous operation in support of the neutron cross-section measurement program of the Chemistry Division. Much of the effort has been of an exploratory nature to establish the quality and purity of the starting materials, which often are enriched isotopes, and to monitor chemical procedures for possible introduction of contamination following irradiation. The isotope dilution technique employing enriched stable isotopes is often employed to measure the yield of newly developed procedures. A continuous effort is made to improve sample handling techniques. The electrodeposition of isotopic samples on small wires (~6 mils in diameter) has been developed and used in conjunction with properly shaped ovens previously described[110] to successfully circumvent two types of sample preparation problems. In the case of californium and certain uranium samples when the specific activity was high, samples were electrodeposited on platinum wires, and this eliminated the hazard of spreading activity while drying samples in ovens in the usual procedure. In the case of palladium, the metal was electrodeposited on a rhenium wire from the sample solution, which contained salts that interfered with ion generation. Samples electrodeposited on wires are easily handled, and small sections of wire are readily and safely secured in ovens for measuring isotopic abundances.

[110] *Advan. Mass Spectrometry, Proc. Conf., vol. III, Paris, 1964*, pp. 749–54 (1966).

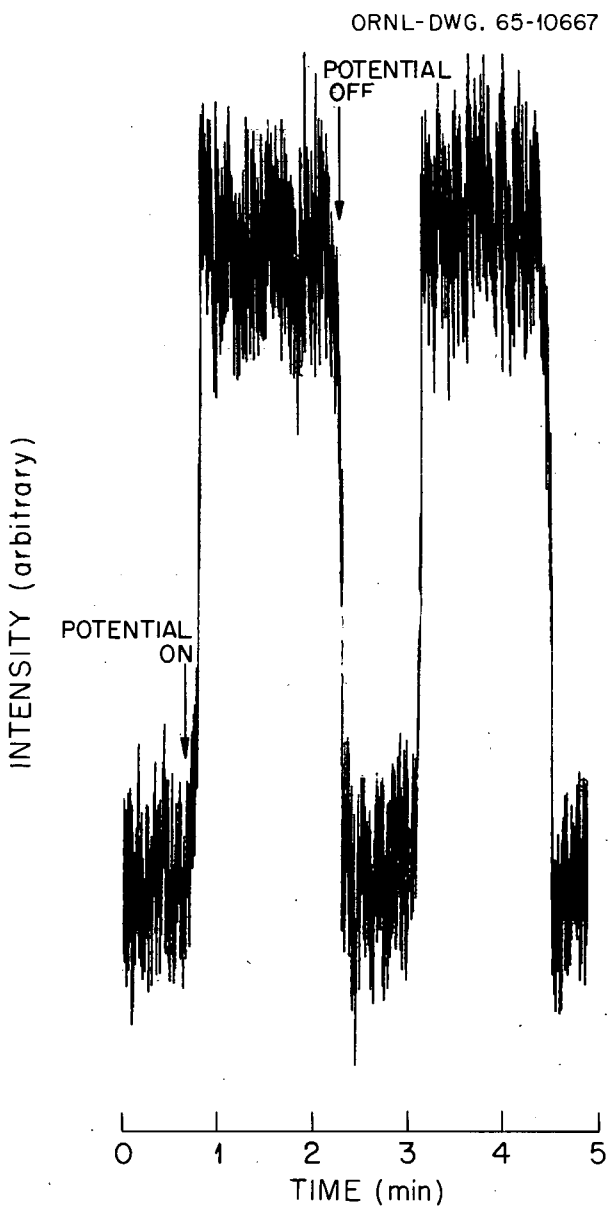

Fig. 8.21. Detection of Metastable (1s2s) Helium with the Dual-Electron-Beam Ion Source. At $t = 0$ the upper and lower filaments were emitting electrons. No potential was applied to the upper filament, and the energy of the lower electron beam was controlled at 6 ev. At $t = 1$, a potential of 23 ev [I(He) = 24.6 ev] was applied to the upper electron beam, and He^+ ions were observed, as indicated by the rapid increase in the He^+ intensity. Since each electron beam was operating at an energy lower than the ionization potential of He, He^+ ions had to be formed by impact of two electrons.

All analyses have been completed for measuring the thermal cross section and resonance integral for ^{105}Rh.[111] All analyses for measuring the neutron capture cross section of ^{237}U,[112] ^{110}Cd, ^{111}Cd, and ^{112}Cd have been completed.[113] All exploratory analyses and isotopic abundance required prior to irradiation have been made for measuring the burnup of ^{233}U.

Measurement of the Relative Abundances and Recoil Energy Spectra of Fragment Ions Produced as the Initial Consequences of X-Ray Interaction with C_2H_5I, $C_2H_3D_2I$, and $Pb(CH_3)_4$[114]

Thomas A. Carlson R. Milford White[115]

When an x ray interacts with a molecule, it generally does so by converting all of its energy to the ejection of an electron from one of the inner shells of a constituent atom. If the molecule contains a heavy atom, the probability is often high that the x ray preferentially interacts with this atom. The hole in the heavy atom will subsequently be filled by a series of radiative and nonradiative processes with a high probability for extensive multiple ionization. Electrons may then be transferred from other atoms in the molecule to the locus of electron depletion, giving rise to a collection of positively charged ions that repel one another with considerable recoil energy.

The phenomenon described above has been previously examined[116] for CH_3I, HI, and DI, based on measurements of the fragment ions and their recoil energies that result from the x irradiation of gaseous molecules in a specially designed mass spectrometer. Studies have now been extended to C_2H_5I and $Pb(CH_3)_4$.

---

[111] J. Halperin, C. R. Baldock, L. E. Idom, J. H. Oliver, and R. W. Stoughton, "Thermal Neutron Cross Section and Resonance Integral of 36-hr Rhodium-105," this report.

[112] J. Halperin, C. R. Baldock, J. J. Pinajian, J. H. Oliver, and R. W. Stoughton, "Neutron Capture Cross Section of the 6.75-day Uranium-237," this report.

[113] C. R. Baldock, J. Halperin, L. E. Idom, and J. H. Oliver, "Reactor Neutron Cross Sections for the Cadmium Isotopes 110, 111, and 112," this report.

[114] Research sponsored jointly with the ORNL Physics Division.

[115] ORINS summer research participant from Baker University, Baldwin, Kan.

[116] T. A. Carlson and R. M. White, *J. Chem. Phys.* (in press).

The study on ethyl iodide poses the interesting question of whether the methyl group, which is one carbon removed from the iodine atom, will completely decompose following a vacancy in the heavy atom or will instead retain its identity by breaking off from the molecule as CH_3^+. The study on tetramethyl lead is of interest simply because of its size (17 atoms). The larger the molecules we examine, the better we should be able to extrapolate our studies to an understanding of what happens in condensed media.

Table 8.8 shows the relative abundances and recoil energies of the fragment ions that result from the x irradiation of C_2H_5I. The average x-ray energy was about 8 kev, which will produce initial vacancies primarily in the *L* shell of iodine. Table 8.8 also shows similar data from the irradiation of $Pb(CH_3)_4$. In this study the average x-ray energy was about 15 kev, and most vacancies were initially formed in the *L* and *M* shells of lead.

In both studies we note that the observed abundances of molecular ions are very low. Essentially, only the constituent elements, carbon, hydrogen, and the heavy atoms, are found in their various charged states. The consequence of the inner-shell vacancy has been the nearly complete destruction of the molecule. It is useful to give the results in Table 8.8 in the following equations

Table 8.8. Relative Abundances and Recoil Energies of the Fragment Ions Formed in the X Irradiation of C_2H_5I[a] and $Pb(CH_3)_4$[b]

C_2H_5I			$Pb(CH_3)_4$		
Ion	Relative Abundance ($\sum I = 1.00$)	Recoil Energy[c] (ev)	Ion	Relative Abundance ($\sum Pb = 1.00$)	Recoil Energy[c] (ev)
I^+	0.19	1.1	Pb^+	0.51	<0.05
I^{2+}	0.22	3.8	Pb^{2+}	0.21	<0.1
I^{3+}	0.20	6.1	Pb^{3+}	0.10	
I^{4+}	0.18	8.4	Pb^{4+}	0.077	
I^{5+}	0.13	15.3	Pb^{5+}	0.035	
I^{6+}	0.04	24.3	Pb^{6+}	0.024	
I^{7+}	0.02		Pb^{7+}	0.022	
C^+	1.01	12.2	Pb^{8+}	0.018	
C^{2+}	0.78	31.7	Pb^{9+}	0.005	
C^{3+}	0.13	70.1	Pb^{10+}	0.005	
C^{4+}	0.01		C^+	1.95	11
H^+	5.06	30.4	C^{2+}	1.72	57
$C_2H_nI^+$	0.02		C^{3+}	0.23	
CH_nI^+	0.003		C^{4+}	0.02	
$C_2H_5^+$	<0.02		H^+	10.8	29
$C_2H_4^+$	<0.015		CH_3^+	0.02	
$C_2H_3^+$	<0.01		CH_2^+	0.07	
$C_2H_2^+$	<0.03		CH^+	0.17	
C_2H^+	<0.03		$Pb(CH_n)_4^+$	0.003	
C_2^+	0.045		$Pb(CH_n)_3^+$	<0.015	
CH_3^+	<0.005		$Pb(CH_n)_2^+$	<0.008	
CH_2^+	0.015		$Pb(CH_n)^+$	0.03	
CH^+	0.035				

[a]The x-ray source is a Macklett AEG50 tube, operated at 40 kev, tungsten target, filtered through 10 mils of beryllium. This x-ray source will produce vacancies primarily in the *L* shell of I.

[b]The x-ray source is a Macklett AEG50 tube, operated at 50 kev, molybdenum target, filtered through 40 mils of beryllium. This x-ray source will produce vacancies primarily in the *L* and *M* shells of lead.

[c]Peak of the recoil spectrum.

based on the average charge and relative abundances of the different fragment ions normalized to the heavy atom:

$$C_2H_5I + \text{x ray} \rightarrow 0.98I^{3.0+} + 0.02C_nH_mI^+ + 1.93C^{1.6+} + 5.06H^+ + 0.15C_nH_m{}^+ + 11.3 \text{ electrons},$$

$$Pb(CH_3)_4 + \text{x ray} \rightarrow 0.96Pb^{2.2+} + 0.04Pb(CH_n)_m{}^+ + 3.7C^{1.6+} + 10.4H^+ + 0.25CH_n{}^+ + 18.7 \text{ electrons}.$$

The average charges for iodine or lead, if they were present as an atomic gas, are estimated[117] to be respectively +8 and +9. Thus, the incorporation of the atoms into molecules has increased the extent of ionization (see the equations) by about 11 − 8 = 3 in the case of C_2H_5I, and about 19 − 9 = 10 in the case of $Pb(CH_3)_4$.

Calculations were made using a model of a many-body Coulombic repulsion, as computed under the code name BLAM. As with our earlier studies, the agreement between theory and experiment was generally satisfactory, although the experimental results lay somewhat lower, which suggests some separation of the charges before the ionization processes are complete.

Experiments were also carried out on $C_\beta H_3 C_\alpha D_2 I$. Of particular interest is the recoil energy of deuterium relative to hydrogen, since this ratio can be taken as an indication of the charge residing on the two carbon atoms. When this ratio, 0.88, is compared with calculations, it appears that the data fit best the conclusion that the average charge on the β carbon was as great or greater than that on the α carbon. Not only has the CH_3 group, which is once removed from the iodine, suffered complete decomposition (cf. Table 8.8), but its carbon became just as highly ionized as the one adjacent to the iodine.

Finally, it should be noted from Table 8.8 that lead has essentially zero recoil energy, demonstrating that the Coulombic explosion of the multiply charged $Pb(CH_3)_4$ was symmetrical. This observation reminds us that in condensed media, even though an atom undergoes extensive ionization, it may not receive kinetic energy if it is neutralized equally from all directions.

[117] From data taken on the charge spectra of xenon and mercury atoms with the same x-ray sources as used with C_2H_5I and $Pb(CH_3)_4$.

Publications

NUCLEAR CHEMISTRY

N. R. Johnson and W. N. Bishop,[1] "Decay of ^{194}Os," *Nucl. Phys.* **69**, 131 (1965).

J. H. Hamilton,[2] H. W. Boyd,[3] and N. R. Johnson, "Energy Levels in ^{132}Xe," *Nucl. Phys.* **72**, 625 (1965).

N. R. Johnson, K. Wilsky,[4] P. G. Hansen,[4] and H. L. Nielsen,[4] "High-Energy Transitions in the Decay of ^{132}I," *Nucl. Phys.* **72**, 615 (1965).

B. van Nooijen,[2] A. V. Ramayya,[2] J. H. Hamilton,[2] J. J. Pinajian,[5] and N. R. Johnson, "Internal Conversion Processes," pp. 193–96 in *Proceedings of International Conference on the Internal Conversion Process*, ed. by J. H. Hamilton, Academic, New York, 1966.

L. H. Niece,[6] "Independent Yields of ^{95}Zr from Thermal Neutron Fission of ^{235}U and ^{233}U," thesis, University of Missouri, Columbia; ORNL-TM-1333.

J. K. Dickens[7] and R. J. Silva, "Elastic and Inelastic Scattering of 12.0-MeV Protons from ^{62}Ni, ^{63}Cu, and ^{64}Zn," ORNL-3851 (September 1965).

J. K. Dickens,[7] F. G. Perey,[7] and R. J. Silva, "Elastic Scattering of 12.0- and 14.0-MeV Deuterons from ^{90}Zr and the Reaction ^{90}Zr$(d,p)^{91}$Zr," ORNL-3850 (September 1965).

J. K. Dickens,[7] E. Eichler, R. J. Silva, and G. Chilosi, "Elastic and Inelastic Scattering of 12.7-MeV Protons from ^{90}Zr, ^{92}Zr, and ^{94}Zr: Tabulated Differential Cross Sections," ORNL-3934 (May 1966).

R. W. Stoughton and R. L. Ferguson, review of book, *Fission Product Yields and Their Mass Distribution* by Yu. A. Zysin, A. A. Lbov, and L. I. Sel'chenkov, *Nucl. Sci. Eng.* **21**, 129 (1965).

ISOTOPE CHEMISTRY

A. H. Narten and L. Landau, "Separation of Oxygen-17 from Natural Oxygen in Thermal Diffusion Columns," *J. Chem. Phys.* **43**, 751 (1965).

L. L. Brown and J. S. Drury, "Nitrogen Isotope Effects in the Decomposition of Diazonium Salts," *J. Chem. Phys.* **43**, 1688–91 (1965).

---

[1] ORINS predoctoral fellow from the University of Florida.

[2] Vanderbilt University.

[3] ORINS summer research participant, West Georgia College.

[4] Danish Atomic Energy Commission, Risø, Denmark.

[5] Isotopes Division.

[6] ORINS predoctoral fellow, University of Missouri.

[7] Neutron Physics Division.

D. F. Smith[8] and G. M. Begun, "Infrared and Raman Spectra and Valence Force Constants of Iodine Oxide Pentafluoride (IOF_5)," *J. Chem. Phys.* **43**, 2001 (1965).

D. A. Lee and J. S. Drury, "The Enrichment of Lithium Isotopes by Ion Exchange Chromatography: The Influence of Eluent Concentration on the Separation Factor," *J. Inorg. Nucl. Chem.* **27**, 1405–7 (1965).

RADIATION CHEMISTRY

P. S. Rudolph, "Samuel Colville Lind," American Philosophical Society Year Book, 1965.

F. T. Jones[9] and T. J. Sworski, "Nitrous Oxide Dosimetry: Effects of Temperature, Pressure, and Electric Field," *J. Phys. Chem.* **70**, 1546 (1966).

G. G. Meisels[10] and T. J. Sworski, "Radiolysis of Ethylene. III. Identification of Ionic Intermediates and Formation of Excited Species by Application of Electrostatic Fields," *J. Phys. Chem.* **69**, 2867 (1965).

T. J. Sworski, "Kinetic Evidence that 'Excited Water' Is Precursor of Intraspur H_2 in the Radiolysis of Water," *Advan. Chem. Ser.* **50**, 263 (1965).

J. W. Chase and G. E. Boyd, "Radiolysis of the Crystalline Alkaline-Earth Bromates by ^{60}Co Gamma Rays," *J. Phys. Chem.* **70**, 1031 (1966).

T. G. Ward, Jr., "The Radiolysis of Lithium Nitrate," doctoral dissertation, Princeton University, March 1966.

H. W. Kohn, "Chemical Reactions of Color Centers," *J. Chem. Educ.* **42**, 356 (1965).

H. W. Kohn, "γ Radiation-Induced Exchange of Deuterium with Silica Surfaces," *J. Am. Chem. Soc.* **87**, 3521 (1965).

ORGANIC CHEMISTRY

C. J. Collins, B. M. Benjamin, and M. H. Lietzke, "Molekulare Umlagerungen, XXII. Modelle für offene Carboniumionen-Mechanismen: Reaktionen von 1.2.2-Triphenyläthyl- und 3-Phenyl-2-butyl-Derivaten," *Ann. Chem.* **687**, 150–60 (1965).

V. F. Raaen, M. H. Lietzke, and C. J. Collins, "A Method for Relating Rates of Interconversion and Destruction of Classical Carbonium Ions," *J. Am. Chem. Soc.* **88**, 369–70 (1966).

B. M. Benjamin and C. J. Collins, "Stereospecific 6,1-Migration of Deuterium During Rearrangement of 2-Phenylnorbornane-2,3-*cis-exo*-diol-5,6-d_2," *J. Am. Chem. Soc.* **88**, 1556 (1966).

B. M. Benjamin, B. W. Ponder,[11] and C. J. Collins, "Stereospecific Elimination and Migration of Deuterium During Hydrolysis of a Substituted Norbornyl Tosylate," *J. Am. Chem. Soc.* **88**, 1558 (1966).

B. Z. Egan,[12] R. A. Zingaro,[13] and B. M. Benjamin, "Extraction of Alkali Metals by 4-sec-Butyl-2-(α-methylbenzyl)-phenol (BAMBP)," *Inorg. Chem.* **4**, 1055–61 (1965).

---

[8]Oak Ridge Gaseous Diffusion Plant.

[9]ORINS summer research participant from Stevens Institute of Technology.

[10]Union Carbide Nuclear Co., Tuxedo, N.Y.

[11]ORINS summer research participant from the University of Alabama.

[12]Chemical Technology Division.

[13]Temporary employee, Chemical Technology Division.

E. Campaigne[14] and C. J. Collins, "An Investigation of Abnormal Products in the Reaction of Benzyl and 2-Thenyl Grignard Reagents with ^{14}C-Carbon Dioxide," *J. Heterocyclic Chem.* **2**, 136 (1965).

C. J. Collins and J. F. Eastham,[15] "Rearrangements Involving the Carbonyl Group," chap. 15 in "The Chemistry of the Carbonyl Group," ed. by Saul Patai, Interscience, 1966.

C. E. Higgins and W. H. Baldwin, "The Pyrolysis of *n*-Butyl Phosphate Esters and Salts," *J. Org. Chem.* **30**, 3173 (1965).

W. H. Baldwin and C. E. Higgins, "Isomerization in Residual Alkyls from Pyrolytic and Ester Interchange Reactions of Tributyl Phosphate," *J. Org. Chem.* **30**, 3230 (1965).

CHEMISTRY OF AQUEOUS SYSTEMS

M. H. Lietzke, H. B. Hupf,[16] and R. W. Stoughton, "Electromotive Force Studies in Aqueous Solutions at Elevated Temperatures. VI. The Thermodynamic Properties of HCl-NaCl Mixtures," *J. Phys. Chem.* **69**, 2395 (1965).

M. H. Lietzke and R. W. Stoughton, "Electromotive Force Studies in Aqueous Solutions at Elevated Temperatures. VII. The Thermodynamic Properties of HCl-$BaCl_2$ Mixtures," *J. Phys. Chem.* **70**, 756 (1966).

M. H. Lietzke and R. W. Stoughton, "The Solubility of Lanthanum Sulphate in Sulphuric Acid Solutions at Elevated Temperatures," *J. Inorg. Nucl. Chem.* **28**, 1063 (1966).

R. W. Stoughton, "Solutions of Electrolytes," *Ann. Rev. Phys. Chem.* **16**, 297 (1965).

W. C. Waggener, A. J. Weinberger, and R. W. Stoughton, "Spectrophotometry of Aqueous Homogeneous Reactor Fuel Solutions from 4 to 280°C and 0 to 930 psi (abs)," *Nucl. Sci. Eng.* **24**, 336 (1966).

F. Nelson, D. C. Michelson, H. O. Phillips, and K. A. Kraus, "Ion Exchange Procedures VII. Separation of Alkali Metal Ions," *J. Chromatog.* **20**, 107 (1965).

F. Nelson, "Ion Exchange Procedures VIII. Separation of Silver from a Number of Elements by Partition Chromatography," *J. Chromatog.* **20**, 378 (1965).

F. Vaslow, "Densities and Apparent Molal Volumes of the Alkali Metal Chlorides in Aqueous Solution at 25°," ORNL-TM-1438 (April 1966).

G. E. Boyd and S. Lindenbaum, "A Thermodynamic Calculation of the Ionic Strength Dependence of Ion-Exchange Reaction Selectivity Coefficients," *J. Phys. Chem.* **69**, 2378 (1965).

S. Lindenbaum and G. E. Boyd, "Thermodynamic Quantities in the Exchange of Lithium with Cesium Ion on Cross-Linked Polymethacrylate Ion Exchangers," *J. Phys. Chem.* **69**, 2374 (1965).

A. Schwarz[17] and G. E. Boyd, "Thermodynamics of the Exchange of Tetramethylammonium with Sodium Ions in Cross-Linked Polystyrene Sulfonates at 25°," *J. Phys. Chem.* **69**, 4268 (1965).

G. E. Boyd, A. Schwarz,[17] and S. Lindenbaum, "Structural Effects on the Osmotic and Activity Coefficients of the Quaternary Ammonium Halides in Aqueous Solutions at 25°," *J. Phys. Chem.* **70**, 821 (1966).

S. Lindenbaum, "Thermodynamics of Aqueous Solutions of Tetra-*n*-alkyl Ammonium Halides. Enthalpy and Entropy of Dilution," *J. Phys. Chem.* **70**, 814 (1966).

---

[14] ORINS summer research participant, Indiana University.

[15] University of Tennessee.

[16] Graduate student, University of Tennessee.

[17] Visiting scientific staff member from Israel.

Water Research Program

R. D. Lanier, "Properties of Organic-Water Mixtures III. Activity Coefficients of NaCl in Water-Organic Media by Cation-Sensitive Glass Electrodes," *J. Phys. Chem.* **69**, 3992 (1965).

R. D. Lanier, "Activity Coefficients of NaCl in Aqueous Three Component Solutions by Cation Sensitive Glass Electrodes," *J. Phys. Chem.* **69**, 2697 (1965).

A. E. Marcinkowsky, H. O. Phillips, and K. A. Kraus, "Properties of Organic-Water Mixtures V. Self-Diffusion Coefficients of Na^+ in Alcohol-Water Mixtures at 25°C," *J. Phys. Chem.* **69**, 3968 (1965).

F. Nelson, D. C. Michelson, H. O. Phillips, and K. A. Kraus, "Ion Exchange Procedures VII. Separation of Alkali Metal Ions," *J. Chromatog.* **20**, 107 (1965).

R. J. Raridon and K. A. Kraus, "Properties of Organic-Water Mixtures IV. The Effect of Various Salts on the Miscibility Gap of the Glycerol Triacetate-Water System," *J. Colloid Sci.* **20**, 1000 (1965).

R. W. Stoughton and M. H. Lietzke, "Calculation of Some Thermodynamic Properties of Sea Salt Solutions at Elevated Temperatures from Data on NaCl Solutions," *J. Chem. Eng. Data* **10**, 254 (1965).

J. S. Johnson, L. Dresner,[7] and K. A. Kraus, "Hyperfiltration (Reverse Osmosis)," p. 345 in *Principles of Desalination*, Academic, New York, 1966.

K. A. Kraus, A. E. Marcinkowsky, J. S. Johnson, and A. J. Shor, "Salt Rejection by a Porous Glass," *Science* **151**, 194 (1966).

W. H. Baldwin, D. L. Holcomb,[18] and J. S. Johnson, "Preparation and Hyperfiltration Properties of a Polyacrylate-Cellophane Membrane," *J. Polymer Sci.* **A3**, 833 (1965).

ELECTROCHEMICAL KINETICS AND ITS APPLICATION TO CORROSION

G. H. Cartledge, "Discussion of the Paper by Spitsin *et al.* on the Inhibiting Properties of the Pertechnetate Ion," *Corrosion* **21**, 216 (1965).

G. H. Cartledge, "The Passivation of Iron in the Presence of Pertechnetate and Chromate Ions," *J. Electrochem. Soc.* **113**, 328 (1966).

E. J. Kelly, "The Active Iron Electrode, I. Iron Dissolution and Hydrogen Evolution Reactions in Acidic Sulfate Solutions," reply to comments by W. J. Lorenz and G. Eichkorn, *J. Electrochem. Soc.* **112**, 1255 (1965).

F. A. Posey and T. Morozumi,[19] "Theory of Potentiostatic and Galvanostatic Charging of the Double Layer in Porous Electrodes," *J. Electrochem. Soc.* **113**, 176 (1966) (Water Research Program).

R. E. Meyer, "Rotating Disk Study of the Dissolution of Zirconium in $HF-HNO_3$," *J. Electrochem. Soc.* **112**, 684 (1965).

R. E. Meyer and S. M. Zettl,[20] "Rotating Disk Study of the Dissolution of Zirconium in $HF-H_2SO_4$," *J. Electrochem. Soc.* **112**, 1092 (1965).

M. J. Joncich,[15] L. S. Stewart,[15] and F. A. Posey, "Hydrogen Overvoltage on Rhenium and Niobium Electrodes," *J. Electrochem. Soc.* **112**, 717 (1965).

R. E. Meyer, "New Edition of 'A New System of Chemical Philosophy,' by John Dalton," book review, *Nucl. Sci. Eng.* **24**, 312 (1966).

---

[18] Plant and Equipment Division.

[19] Visiting scientific staff member from Hokkaido University, Japan.

[20] ORINS student trainee, Texas Wesleyan College.

NONAQUEOUS SYSTEMS AT HIGH TEMPERATURES

B. D. Lichter[21] and M. A. Bredig, "Solid and Liquid Phase Miscibility of Calcium Metal and Calcium Fluoride," *J. Electrochem. Soc.* **112**, 507 (1965).

H. R. Bronstein, "An All-Metal Cell Technique for the Measurement of the EMF of Molten Metal–Metal Halide Solutions Corrosive to Ceramics," *J. Electrochem. Soc.* **112**, 1032 (1965).

A. J. Shor,[22] W. T. Smith, Jr.,[15] and M. A. Bredig, "Condensed-Phase Behavior of the Aluminum Chloride–Zirconium Chloride System," *J. Phys. Chem.* **70**, 1511 (1966).

CHEMICAL PHYSICS

R. H. Busey, "The Entropy of $K_3Fe(CN)_6$ and $Fe(CN)_6^{3-}(aq)$. Free Energy of Formation of $Fe(CN)_6^{3-}(aq)$ and $Fe(CN)_6^{4-}(aq)$," *J. Phys. Chem.* **69**, 3179 (1965).

R. H. Busey, R. B. Bevan, Jr., and R. A. Gilbert, "The Heat Capacity of Potassium Hexabromorhenate(IV) from 7 to 300°K. Manifestation of Thermal History Behavior. Antiferromagnetic Anomaly near 15°K. Entropy and Free Energy Functions," *J. Phys. Chem.* **69**, 3471 (1965).

R. B. Bevan, Jr., R. A. Gilbert, and R. H. Busey, "The Heat Capacity of Rhenium Trichloride from 7 to 310°K. Entropy and Free Energy Functions," *J. Phys. Chem.* **70**, 147 (1966).

R. Livingston and H. Zeldes, "Paramagnetic Resonance Study of Liquids During Photolysis: Hydrogen Peroxide and Alcohols," *J. Chem. Phys.* **44**, 1245 (1966).

J. H. Burns[22] and W. R. Busing, "Crystal Structures of Rubidium Lithium Fluoride, $RbLiF_2$, and Cesium Lithium Fluoride, $CsLiF_2$," *Inorg. Chem.* **4**, 1510 (1965).

J. P. Glusker,[23] D. van der Helm,[23] W. E. Love,[23] M. L. Dornberg,[23] J. A. Minkin,[23] C. K. Johnson, and A. L. Patterson,[23] "X-Ray Crystal Analysis of the Substrates of Aconitase. VI. The Structures of Sodium and Lithium Dihydrogen Citrates," *Acta Cryst.* **19**, 561 (1965).

P. A. Agron, C. K. Johnson, and H. A. Levy, "Xenon Hexafluoride: Crystallographic Data and Phase Transitions," *Inorg. Nucl. Chem. Letters* **1**, 145 (1965).

G. M. Brown and L. A. Walker,[24] "Refinement of the Structure of Potassium Heptafluoroniobate, K_2NbF_7, from Neutron-Diffraction Data," *Acta Cryst.* **20**, 220 (1966).

R. D. Ellison and H. A. Levy, "A Centered Hydrogen Bond in Potassium Hydrogen Chloromaleate: A Neutron Diffraction Structure Determination," *Acta Cryst.* **19**, 260 (1965).

W. R. Busing and H. A. Levy, "Crystal and Molecular Structure of Hydrogen Peroxide: A Neutron-Diffraction Study," *J. Chem. Phys.* **42**, 3054 (1965).

C. K. Johnson, "X-Ray Crystal Analysis of the Substrates of Aconitase. V. Magnesium Citrate Decahydrate, $[Mg(H_2O)_6][MgC_6H_5O_7(H_2O)]_2 \cdot 2H_2O$," *Acta Cryst.* **18**, 1004 (1965).

H. A. Levy, M. D. Danford, and A. H. Narten, "Data Collection and Evaluation with an X-Ray Diffractometer Designed for the Study of Liquid Structure," ORNL-3960-A (May 1966).

R. E. Minturn, S. Datz, and R. L. Becker,[25] "Alkali-Atom–Halogen-Molecule Reactions in Molecular Beams: The Spectator Stripping Model," *J. Chem. Phys.* **44**, 1149 (1966).

---

[21] Metals and Ceramics Division.

[22] Reactor Chemistry Division.

[23] Institute for Cancer Research, Philadelphia, Pa.

[24] ORINS summer research participant from Marshall University.

[25] Physics Division.

F. van der Valk,[26] G. E. Moore, and S. Datz, "Elastic Scattering in Hydrogen-Helium Systems," pp. 164–67 in *Proceedings of the 4th International Conference on the Physics of Electronic and Atomic Collisions, Univ. Laval, Quebec*, Science Bookcrafters, New York, 1965.

S. Datz and R. E. Minturn, "Molecular Beam Studies of Alkali Halogen Reactions: The Spectator Stripping Model," pp. 177–80 in *Proceedings of the 4th International Conference on the Physics of Electronic and Atomic Collisions, Univ. Laval, Quebec*, Science Bookcrafters, New York, 1965.

M. G. Menendez and S. Datz, "Measurement of the Angular Distribution of Elastically Scattered Cs^+ from Ar, Kr, and N_2," pp. 264–68 in *Proceedings of the 4th International Conference on the Physics of of Electronic and Atomic Collisions, Univ. Laval, Quebec*, Science Bookcrafters, New York, 1965.

M. H. Lietzke and M. G. Menendez, "A Program to Compute the Classical Deflection Function," ORNL-3881 (February 1966).

G. E. Moore, S. Datz, and E. H. Taylor, "The Reflection and Thermal Accommodation of Helium Beams on Platinum," *J. Catalysis* **5**, 218 (1966).

S. Datz, T. S. Noggle,[27] and C. D. Moak,[25] "Anisotropic Energy Losses in a Face Centered Cubic Crystal for High Energy ^{79}Br and ^{127}I Ions," *Phys. Rev. Letters* **15**, L515 (1965).

S. Datz, T. S. Noggle,[27] and C. D. Moak,[25] "Channeling Effects on the Energy Loss of High Energy (20–80-Mev) ^{79}Br and ^{127}I in Gold," *Nucl. Instr. Methods* **38**, 221 (1965).

R. Baldock, "Some Problems Relating to the Thermal Emission of Ions in the Mass Spectrometric Determination of Isotopic Abundances of Neutron Cross Section Measurements," pp. 749–54 in *Advances in Mass Spectrometry*, vol. III. The Institute of Petroleum, London, 1966 (Proceedings of a conference held in Paris, France, September 1964).

C. E. Melton and P. S. Rudolph, "Mass Spectrometric Evidence for H_3O, HD_2O, and D_3O," *J. Catalysis* **5**, 387 (1966).

C. E. Melton, "Transient Species Produced by the Catalytic Decomposition of Acetone in a Mass Spectrometer," *J. Catalysis* **5**, 234 (1966).

T. A. Carlson and R. M. White,[28] "Explosion of Multicharged Molecular Ions: Chemical Consequences of Inner Shell Vacancies in Atoms," in *Proceedings of a Symposium in Chemical Effects in Nuclear Transformation, Austria, 1964*, vol. I, p. 23, International Atomic Energy Agency, Vienna, 1965.

T. A. Carlson and M. O. Krause, "Electron Shake-Off Resulting from *K*-Shell Ionization in Neon Measured as a Function of Photoelectron Velocity," *Phys. Rev.* **140**, A 1057 (1965).

---

[26]Visiting scientific staff member from The Netherlands.

[27]Solid State Division.

[28]ORINS summer research participant from Baker University, Baldwin, Kan.

Papers Presented at Scientific Meetings

NUCLEAR CHEMISTRY

N. K. Aras*[29] and E. Eichler, "Decay of the ^{94}Tc Isomers to Levels in ^{94}Mo," American Physical Society, Washington, D.C., Apr. 25–28, 1966 [*Bull. Am. Phys. Soc.* **11**, 394 (1966)].

E. Eichler,* N. K. Aras,[29] and G. Chilosi,[30] "Decay of the ^{95}Tc Isomers to Levels in ^{95}Mo," American Physical Society, Washington, D.C., Apr. 25–28, 1966 [*Bull. Am. Phys. Soc.* **11**, 394 (1966)].

J. H. Hamilton,*[2] L. L. Riedinger,[2] and N. R. Johnson, "Gamma-Ray Intensities in the 12.4-year ^{152}Eu Decay," American Physical Society, Washington, D.C., Apr. 25–28, 1966 [*Bull. Am. Phys. Soc.* **11**, 407 (1966)].

N. R. Johnson* and N. K. Aras,[29] "Levels in ^{184}W Populated by the Decay of ^{184}Ta," American Physical Society, New York, Jan. 26–29, 1966 [*Bull. Am. Phys. Soc.* **11**, 12 (1966)].

A. V. Ramayya,*[2] B. van Nooijen,[2] J. H. Hamilton,[2] and N. R. Johnson, "Studies of the Decay of ^{80}Br^{m}," American Physical Society, Washington, D.C., Apr. 25–28, 1966 [*Bull. Am. Phys. Soc.* **11**, 393 (1966)].

L. L. Riedinger,*[2] J. H. Hamilton,[2] and N. R. Johnson, "Gamma-Ray Intensities in the ^{154}Eu Decay," American Physical Society – Southeastern Section, Charlottesville, Va., Nov. 1–3, 1965.

N. E. Runnalls,*[31] D. E. Troutner,[31] and R. L. Ferguson, "Half-Life and Fission Yield of Ba^{144}," Symposium on Mechanics of Nuclear Fission, American Chemical Society Meeting, Pittsburgh, Pa., Mar. 22–31, 1966.

R. J. Silva,* A. Chetham-Strode, J. R. Tarrant, and I. R. Williams, "Alpha Decay of ^{251}Cf," American Physical Society, Washington, D.C., Apr. 25–28, 1966 [*Bull. Am. Phys. Soc.* **11**, 408 (1966)].

J. R. Van Hise,* B. H. Ketelle, and A. R. Brosi, "The Decay of ^{137}Pr," American Physical Society, New York, Jan. 26–29, 1966 [*Bull. Am. Phys. Soc.* **11**, 67 (1966)].

J. R. Van Hise* and C. W. Tang,[32] "Observation and Measurement of Three Excited States in ^{117}In," American Physical Society, New York, Jan. 26–29, 1966 [*Bull. Am. Phys. Soc.* **11**, 67 (1966)].

J. R. Van Hise,* G. Chilosi,[30] and Nicholas J. Stone,[33] "An Enhanced *E*-3 Transition in ^{137}La," American Physical Society, New York, Jan. 26–29, 1966 [*Bull. Am. Phys. Soc.* **11**, 133 (1966)].

---

*Speaker.

[29]Visiting scientific staff member from Turkey.

[30]Guest scientist from Italy.

[31]University of Missouri.

[32]Massachusetts Institute of Technology.

[33]University of California.

RADIATION CHEMISTRY

C. J. Hochanadel* and R. Casey,[34] "The Yield of Reducing Radicals in the Gamma Radiolysis of Water Using Carbon Monoxide and Oxygen as Scavengers," Radiation Research Society, Philadelphia, May 24–26, 1965.

J. F. Riley, "Ozone Yields from Irradiated Oxygen-Nitrogen Solutions at 77°K," Radiation Research Society, Philadelphia, May 24–26, 1965.

H. A. Mahlman, "The H Atom in N_2O Saturated Solutions," Gordon Research Conference on Radiation Chemistry, New Hampton, N.H., Aug. 4, 1965.

F. T. Jones*[9] and T. J. Sworski, "Nitrous Oxide Dosimetry: Effects of Temperature, Pressure, and Electric Field," American Chemical Society, Pittsburgh, Pa., Mar. 22–31, 1966.

H. A. Mahlman and T. J. Sworski,* "Intraspur Formation of NO_2^- in the ^{60}Co γ-Radiolysis of Concentrated NO_3^- Solutions," American Chemical Society, Atlantic City, N.J., Sept. 12–17, 1965.

T. J. Sworski, "Kinetic Evidence that 'Excited Water' Is Precursor of Intraspur H_2 in the Radiolysis of Water," American Chemical Society, Atlantic City, N.J., Sept. 12–17, 1965 (invited paper).

J. W. Chase* and G. E. Boyd, "The Radiolytic Decomposition of Crystalline Alkali Metal and Alkaline Earth Bromates," Symposium on the Chemical and Physical Effects of High-Energy Radiation on Inorganic Substances, Annual West Coast Meeting of American Society for Testing and Materials, Seattle, Wash., Nov. 2–3, 1965 (invited).

J. W. Chase* and G. E. Boyd, "Radiolysis of Alkaline Earth Bromates by ^{60}Co Gamma Rays," American Chemical Society, Atlantic City, N.J., Sept. 12–17, 1965.

CHEMISTRY OF AQUEOUS SYSTEMS

R. W. Stoughton, "Thermodynamic Properties of Some Aqueous Electrolyte Systems," Tennessee Academy of Science, Oak Ridge, Tenn., Dec. 10, 1965.

M. H. Lietzke, "The Use of a High Speed Computer in Treating EMF Data in Aqueous Electrolyte Mixtures," Tennessee Academy of Science, Oak Ridge, Tenn., Dec. 10, 1965.

F. Vaslow, "The Apparent Molal Volumes of the Alkali Metal Chlorides and Evidence for Salt-Induced Structure Transitions," American Chemical Society, Atlantic City, N.J., Sept. 12–17, 1965.

F. Nelson* and D. C. Michelson, "Cation Exchange in Concentrated HBr Solutions," American Chemical Society, Atlantic City, N.J., Sept. 12–17, 1965.

R. J. Raridon* and K. A. Kraus, "The Effect of Various Salts on the Miscibility Gap of the Glycerol Triacetate-Water System," 39th National Colloid Symposium, Clarkson College of Technology, Potsdam, N.Y., June 23, 1965.

A. E. Marcinkowsky,* H. O. Phillips, and K. A. Kraus, "Self-Diffusion Coefficients of Na^+ in Alcohol-Water Mixtures at 25°C," American Chemical Society, Atlantic City, N.J., Sept. 12–17, 1965.

H. O. Phillips,* A. E. Marcinkowsky, and K. A. Kraus, "A Rapid Radiometric Method for Measuring Diffusion Coefficients in Thin Membranes and Films," American Chemical Society, Atlantic City, N.J., Sept. 12–17, 1965.

A. Schwarz,[17] "Thermodynamics of the Exchange of me_4N^+ with Na^+ Ions in Cross-Linked Polystyrene Sulfonates," Gordon Research Conference on Ion Exchange, New London, N.H., Aug. 2–6, 1965.

---

*Speaker.

[34]ORINS student trainee, Centenary College, and summer employee, 1963 and 1964.

A. Schwarz[17] and G. E. Boyd, "Thermodynamics of the Exchange of Tetraalkyl Ammonium with Sodium Ions in Cross-Linked Polystyrene Sulfonates at 25°," American Chemical Society, Atlantic City, N.J., Sept. 12–17, 1965.

S. Lindenbaum, "Thermodynamics of Aqueous Solutions of Tetra-*n*-alkyl Ammonium Halides. Enthalpy and Entropy of Dilution," American Chemical Society, Atlantic City, N.J., Sept. 12–17, 1965.

ELECTROCHEMICALS KINETICS, CORROSION

G. H. Cartledge, "The Mechanism of the Action of Inorganic Inhibitors," Symposium on the Inhibition of Corrosion, Birmingham and Midlands Sections, Society of Chemical Industry and Royal Institute of Chemistry, Birmingham, England, Mar. 30–31, 1966 (invited plenary lecture).

E. J. Kelly, "Specific Adsorption of an Organic Inhibitor and the Effects Thereof on the Kinetics and Mechanistics of the Active Iron Electrode," Electrochemical Society, Buffalo, N.Y., Oct. 13, 1965.

E. G. Bohlmann*[22] and F. A. Posey, "Aluminum and Titanium Corrosion in Saline Waters at Elevated Temperatures," First International Symposium on Water Desalination, Washington, D.C., Oct. 3, 1966 (invited) (Water Research Program).

F. A. Posey and S. S. Misra,*[35] "Induced Polarization of Porous and Tubular Electrodes," Electrochemical Society, Cleveland, May 6, 1966 (Water Research Program).

NONAQUEOUS SYSTEMS AT HIGH TEMPERATURE

M. A. Bredig, "Premonitory Effects in Some Solid State Transitions and Melting," Tennessee Academy of Science, Oak Ridge, Tenn., Dec. 10, 1965.

CHEMICAL PHYSICS

R. A. Gilbert* and R. B. Bevan, Jr., "Molar Enthalpies of Mixing in the Liquid LiF-NaF System," 20th Annual Calorimetry Conference, Ames, Iowa, Aug. 11–13, 1965; Tennessee Academy of Science, Oak Ridge, Tenn., Dec. 10–11, 1965.

R. H. Busey* and K. H. Gayer,[36] "Enthalpy and Free Energy of Formation of the Hexachlororhenate(IV) Ion and Its Enthalpy of Hydrolysis," Tennessee Academy of Science, Oak Ridge, Tenn., Dec. 10–11, 1965.

W. R. Busing,* R. D. Ellison, and H. A. Levy, "Oak Ridge Computer-Controlled X-Ray Diffractometer," Joint Meeting of the American Crystallographic Association and Mineralogical Society of America, Gatlinburg, Tenn., June 27–July 2, 1965.

R. Chidambaram*[37] and G. M. Brown, "A Neutron Diffraction Study of the Structure of Hydrated Cupric Acetate, $Cu_2(CH_3COO)_4 \cdot 2H_2O$," Joint Meeting of the American Crystallographic Association and Mineralogical Society of America, Gatlinburg, Tenn., June 27–July 2, 1965.

C. K. Johnson, "Procedures for Automated Plotting of Stereoscopic Crystal-Structure Illustrations," Joint Meeting of the American Crystallographic Association and Mineralogical Society of America, Gatlinburg, Tenn., June 27–July 2, 1965.

---

*Speaker.

[35]Visiting scientific staff member from India.

[36]ORINS research participant from Wayne University, 1965.

[37]Alien guest from Atomic Energy Establishment, Trombay-Bombay, India.

G. M. Brown* and R. Chidambaram,[37] "Refinement of the Structure of Copper Ammonium Sulfate Hexahydrate, $Cu(NH_4)_2(SO_4)_2 \cdot 6H_2O$, from Neutron Diffraction Data," American Crystallographic Association, Austin, Tex., Feb. 28–Mar. 2, 1966.

C. K. Johnson, "Crystal Structures of Citric Acid Monohydrate and Two Deuterated Isomorphs Determined by Neutron Diffraction Isotopic Replacement," American Crystallographic Association, Austin, Tex., Feb. 28–Mar. 2, 1966.

A. H. Narten,* M. D. Danford, and H. A. Levy, "Structure of Water Between Melting and Boiling Point," Gordon Research Conference on the Chemistry and Physics of Liquids, Tilton, N.H., Aug. 2–6, 1965.

H. W. Kohn, "Role of Adsorbed Oxygen in Desorption of H Atoms from a Platinum Catalyst," Gordon Research Conference on Catalysis, New London, N.H., June 29, 1965.

S. Datz, "Molecular Beam Methods," Hot Atom Chemistry Symposium, Purdue University, Lafayette, Ind., Apr. 1, 1966 (invited).

S. Datz,* T. S. Noggle,[27] and C. D. Moak,[25] "Channeling Effects on the Energy Loss of High Energy (20–80 Mev) ^{79}Br and ^{127}I in Gold," International Conference on Electromagnetic Isotope Separations, Related Accelerators and Their Application to Physics, Aarhus, Denmark, June 1965 (invited).

S. Datz, "Channeling Effects on the Stopping of Fast (20–100 Mev) Heavy Ions," American Physical Society, Durham, N.C., Mar. 27–30, 1966.

S. Datz,* H. O. Lutz,[38] C. D. Moak,[25] T. S. Noggle,[27] L. C. Northcliffe,[39] and H. W. Schmidt,[25] "Channeling Effects in Au Single Crystals with High Energy ^{127}I Ions," American Physical Society, New York, Jan. 27–30, 1966 [*Bull. Am. Phys. Soc.* **11**, 126 (1966)].

T. S. Noggle,*[27] C. D. Moak,[25] H. O. Lutz,[38] and S. Datz, "Scattering Patterns Associated with Channeling of 40 Mev ^{127}I Ions in Au," American Physical Society, Durham, N.C., Mar. 27–30, 1966 [*Bull. Am. Phys. Soc.* **11**, 177 (1966)].

H. O. Lutz,*[38] S. Datz, T. S. Noggle,[27] and C. D. Moak,[25] "Charge State Distributions of 40 Mev ^{127}I Ions in Au Single Crystals," American Physical Society, Durham, N.C., Mar. 27–30, 1966 [*Bull. Am. Phys. Soc.* **11**, 177 (1966)].

C. E. Melton, "Investigation of Surface Processes by Mass Spectrometry," Gordon Research Conference on Catalysis, New London, N.H., June 29, 1965 (invited).

C. E. Melton, "Surface Chemistry by Mass Spectrometry," American Chemical Society Symposium, Kansas City, Kansas, Nov. 5, 1965 (invited).

M. O. Krause* and T. A. Carlson, "Two Electron Emission in Auger and Photoabsorption Processes," American Physical Society Topical Conference on Research Problems in the Physics of X-Ray Spectra, Ithaca, N.Y., June 22–29, 1965.

M. O. Krause,* T. A. Carlson, and R. K. Dismukes,[40] "Energy Spectrum of Shake Off Electrons from the *L* Shell of Neon Accompanying *K* Photoionization," American Physical Society, Washington, D.C., Apr. 25–28, 1966.

T. A. Carlson,* W. E. Hunt,[41] and M. O. Krause, "Relative Abundances of Ions Formed as the Result of Inner-Shell Vacancies in Xe and Hg," American Physical Society, Washington, D.C., Apr. 25–28, 1966.

R. M. White* and T. A. Carlson, "Chemical Consequences of Inner Shell Vacancies," Hot Atoms Symposium, Purdue University, Lafayette, Ind., Apr. 1–2, 1966.

---

*Speaker.

[38]Solid State Division; visiting scientific staff member from Germany.

[39]On leave from Texas A and M University.

[40]USAEC Health Physics Fellow from Vanderbilt University.

[41]ORINS summer research participant from David Lipscomb College.

Lectures

NUCLEAR CHEMISTRY

C. E. Bemis, "Properties of Spherical Odd-Odd Nuclei," Physics Department Seminar, Iowa State University, Mar. 14, 1966.

E. Eichler, "The Role of Nuclear Chemistry in Nuclear Structure Studies," Clark University, Mar. 23, 1966 (ORAU Traveling Lecture Program).

E. Eichler, "Two-Parameter Analysis in Level-Scheme Studies," Mar. 24, 1966; "Gamma Radiation from Nuclear Reactions," Massachusetts Institute of Technology, Mar. 25, 1966 (ORAU Traveling Lecture Program).

R. L. Ferguson, "Rapid Separations in Radiochemistry," ORINS Modern Chemistry Institute, July 26–30, 1965.

N. R. Johnson, "Level Properties of the Deformed Nucleus ^{184}W," Purdue University, Dec. 3, 1965 (ORAU Traveling Lecture Program); Physics Seminar, Vanderbilt University, May 7, 1966.

N. R. Johnson, "Special Topics in Scintillation Counting," ORAU Radioisotope Training School, Aug. 27 and Oct. 8, 1965; Jan. 21 and May 10, 1966.

G. D. O'Kelley, "Nuclear Spectroscopy Studies of ^{101}Ru," Physical Chemistry Seminar, University of Tennessee, Feb. 17, 1966.

G. D. O'Kelley, "Scientific Experiments on Returned Lunar Samples," Physics Division Seminar, Oak Ridge National Laboratory, May 13, 1966.

ISOTOPE CHEMISTRY

A. C. Rutenberg, "Demonstration on Nuclear Magnetic Resonance Spectroscopy," ORINS Summer Institute in Modern Chemistry, July 20, 1965.

A. C. Rutenberg, "Chemical Kinetics and Isotope Exchange," ORINS Advanced Isotope Technology Institute and ORINS Basic Research Course, Aug. 18, 1965.

RADIATION CHEMISTRY

J. W. Boyle, "Radiation Chemistry," ORINS, May 24, 1965.

C. J. Hochanadel, "Dosimetry," Advanced Isotope Technology Institute, ORINS, July 29, 1965.

C. J. Hochanadel, Lectures and Laboratory Experiments in Radiation Chemistry, ORINS Summer Institute in Modern Chemistry, Aug. 2–4, 1965.

C. J. Hochanadel, "Radiation Chemistry," ORINS, June 2, 1965.

H. W. Kohn, "Effects of Radiation on Catalysts," Dickinson College, Carlisle, Pa., Apr. 18, 1966.

H. W. Kohn, "Radiation Chemistry of Surfaces," Dickinson College, Carlisle, Pa., Apr. 19, 1966 (student affiliates, American Chemical Society).

J. F. Riley, "Radiation Chemistry," Basic Research Course, ORINS, Aug. 26 and Oct. 15, 1965, and Jan. 28, 1966.

J. F. Riley, "Radiation Chemistry and Isotope Applications," Basic Research Course, ORINS, May 13, 1966.

T. J. Sworski, "Current Theories in Radiation Chemistry of Water," Stevens Institute of Technology, Hoboken, N.J., Oct. 1, 1965 (ORAU Traveling Lecture Program).

T. J. Sworski, "Intraspur Reactions in the Radiolysis of Water," Chemistry Division Seminar, Argonne National Laboratory, Jan. 12, 1966.

T. J. Sworski, "Radiolysis of Water," University of Notre Dame, Notre Dame, Ind., Jan. 13, 1966 (ORAU Traveling Lecture Program).

ORGANIC CHEMISTRY

B. M. Benjamin, "Some Rearrangement Reactions of Substituted Norbornyl Systems," Memphis State University, Memphis, Tenn., Apr. 22, 1965 (ORINS Traveling Lecture Program).

C. J. Collins, "Hydride Shifts in Carbonium Ions," University of South Carolina, Columbia, May 13, 1966.

C. J. Collins, "Hydride Shifts in Carbonium Ion Processes," Princeton University, Princeton, N.J., Dec. 8, 1965, and Allied Chemical Corporation, Dec. 9, 1965.

C. J. Collins, "Isotopic Studies of Hydride Shifts," Louisiana State University, Baton Rouge, Oct. 13, 1965, and Louisiana State University, New Orleans, Oct. 14, 1965.

C. J. Collins, "Recent Isotopic Experiments for Identifying Carbonium Ions," Vanderbilt University, Nashville, Tenn., Aug. 3, 1965 (ORINS Traveling Lecture Program).

CHEMISTRY OF AQUEOUS SYSTEMS

Water Research Program

M. H. Lietzke, "Some Thermodynamic Properties of Sea Salt Solutions," ORAU lecture, Theoretical Chemistry Institute, Solar Energy Laboratory, and Civil Engineering Department of the University of Wisconsin, Madison, Wis., July 9, 1965.

A. E. Marcinkowsky, "Ionic Diffusion in Liquids and Semipermeable Membranes," Department of Chemistry, University of Tennessee, Knoxville, Nov. 4, 1965.

R. J. Raridon, "Desalination," ORAU lecture, presented at the following:

Lamar State College of Technology, Beaumont, Tex., Nov. 15, 1965;

Sam Houston State College, Huntsville, Tex., Nov. 16, 1965;

Tuskegee Institute, Ala., Feb. 8, 1966;

Auburn University, Auburn, Ala., Feb. 9, 1966;

Florida Atlantic University, Boca Raton, Fla., Feb. 10, 1966;

University of South Florida, Tampa, Feb. 11, 1966;

Eastern Illinois University, Charleston, Feb. 16, 1966;

Southern Illinois University, Carbondale, Feb. 17, 1966;

Piedmont College, Demorest, Ga., Mar. 4, 1966;

Peabody College, Nashville, Tenn., Apr. 16, 1966;

Roanoke College, Salem, Va., May 6, 1966;

Memphis State University, Memphis, Tenn., May 13, 1966;

Lambuth College, Jackson, Tenn., May 16, 1966;

ORINS Training Class for Exhibit Managers, Aug. 9, 1965.

R. W. Stoughton, "Desalination and Water Recovery," American Chemical Society Lecture Tour (invited), presented at the following:

Maryville, Tenn., Apr. 11, 1966;

Chattanooga, Tenn., Apr. 12, 1966;

Huntsville, Ala., Apr. 13, 1966;

Nashville, Tenn., Apr. 14, 1966;

Memphis, Tenn., Apr. 15, 1966.

M. H. Lietzke, "Desalination and Water Recovery," American Chemical Society Lecture Tour (invited), Wilson Dam, Ala., Birmingham, Ala., Auburn, Ala., Athens, Ga., Apr. 18–21, 1966.

K. A. Kraus, "Desalination," Oak Ridge High School, Oak Ridge, Tenn., Jan. 11, 1966.

ELECTROCHEMICAL KINETICS AND ITS APPLICATION TO CORROSION

G. H. Cartledge, "Non-Cathodic Action of XO_4^{-n} Inhibitors," seminar, Max Planck Institut für Sondermetalle, Stuttgart, Germany, Mar. 25, 1966; National Physical Laboratory, Teddington, England, Mar. 28, 1966.

G. H. Cartledge, "The Action of the XO_4^{-n} Inhibitors of the Corrosion of Iron," East Tennessee Section, American Chemical Society, Knoxville, Tenn., May 17, 1966 (invited).

CHEMICAL PHYSICS

R. A. Gilbert, "Calorimetry, a Versatile Research Tool," Frontiers in Chemistry Series, Wayne State University, Detroit, May 9, 1966

R. W. Holmberg and H. Zeldes, Lecture-Demonstration on Electron Spin Resonance in Solids, Summer Institute in Modern Chemistry, sponsored by the Oak Ridge Institute of Nuclear Studies, ORNL, Oak Ridge, Tenn., July 22, 1965.

R. Livingston, Lectures in Magnetic Resonance Spectroscopy, Summer Institute in Modern Chemistry, Oak Ridge Institute of Nuclear Studies, Oak Ridge, Tenn., July 19, 21, and 23, 1965.

W. R. Busing, "Chemical Information from Neutron Diffraction Studies," Roanoke College, Salem, Va., Apr. 15, 1966 (ORAU Traveling Lecture Program).

W. R. Busing, "The Oak Ridge Computer-Controlled Diffractometer," Argonne National Laboratory, Sept. 16, 1965.

C. K. Johnson, "Some Modern Aspects of Crystallographic Computing," University of Minnesota, Minneapolis, Sept. 2, 1965.

S. Datz, "Molecular Beam Studies in Physical Chemistry," Sigma Xi Lecture, Georgia Tech. University, Atlanta, May 28, 1965.

S. Datz, "Molecular Beam Studies in Chemical Kinetics," Physikalisches Inst., University of Bonn, Bonn, Germany; Physikalisches Inst., University of Freiburg, Freiburg, Germany, June 1965.

S. Datz, "Molecular Beam Studies of Chemically Reactive Collisions," University of Connecticut, May 16, 1966.

R. E. Minturn, ORINS Traveling Lectures, "Molecular Beam Studies in Physical Chemistry," Oklahoma State University, Stillwater, Mar. 8, 1966; Texas A and M, College Station, Tex., Mar. 9, 1966; University of Houston, Houston, Tex., Mar. 10, 1966; University of South Carolina, Columbia, Mar. 25, 1966.

T. A. Carlson, "Multiple Ionization in Atoms and Molecules," University of Virginia, Sept. 17, 1965.

T. A. Carlson, "Explosion of Multicharged Molecular Ions," Vanderbilt University, Apr. 15, 1966.

R. Baldock, "Highlights of the Paris Mass Spectrometry Conference," Auburn University, Auburn, Ala., Mar. 25, 1966.

C. E. Melton, "Catalysis by Mass Spectrometry," ORAU Travel Lectures, Chemistry Department, Pennsylvania State University, Sept. 17, 1965; Chemistry Department, North Texas State University, Denton, Nov. 17, 1965.

C. E. Melton, "Radiation Chemistry by Mass Spectrometry," ORAU Travel Lectures, Chemistry Department, Georgia Institute of Technology, Atlanta, Nov. 12, 1965; Chemistry Department, University of Arkansas, Fayetteville, Nov. 15, 1965; Chemistry Department, Texas Woman's University, Denton, Nov. 18, 1965.

C. E. Melton, "Mass Spectrometry as a Tool in Research," ORAU Travel Lectures, Sigma Xi Lecture, Texas Woman's University, Denton, Nov. 18, 1965; Southeast Missouri State College, Cape Girardeau, Feb. 23, 1966; Oklahoma State University, Stillwater, Feb. 25, 1966; Southwestern at Memphis, Memphis, Tenn., Apr. 21, 1966.

GENERAL

H. W. Kohn, "What It Is Like to Work at Oak Ridge National Laboratory," Dickinson College, Carlisle, Pa., Apr. 18, 1966.

R. J. Raridon, "The Use of Isotopes in Chemical Research," ORAU lecture, Virginia Military Institute, Lexington, May 5, 1966.

P. S. Rudolph, "Samuel Colville Lind, the Man and the Scientist," presented at the Gordon Research Conferences, New Hampton, N.H., Aug. 2, 1965 (invited).

ORNL-3994
UC-4 – Chemistry

INTERNAL DISTRIBUTION

1. Biology Library
2–4. Central Research Library
5. Laboratory Shift Supervisor
6. Reactor Division Library
7–8. ORNL – Y-12 Technical Library Document Reference Section
9–43. Laboratory Records Department
44. Laboratory Records, ORNL R.C.
45. P. A. Agron
46. C. R. Baldock
47. W. H. Baldwin
48. D. S. Billington
49. F. F. Blankenship
50. E. G. Bohlmann
51. C. J. Borkowski
52–66. G. E. Boyd
67–74. M. A. Bredig
75. R. B. Briggs
76. H. R. Bronstein
77. A. R. Brosi
78. R. H. Busey
79. G. H. Cartledge
80. C. J. Collins
81. D. R. Cuneo
82. F. L. Culler
83. M. D. Danford
84. S. Datz
85. J. S. Drury
86. A. S. Dworkin
87. E. Eichler
88. R. L. Ferguson
89. J. L. Gabbard
90. J. A. Ghormley
91. R. A. Gilbert
92. J. H. Gillette
93. W. R. Grimes
94. J. Halperin
95. C. J. Hochanadel
96. A. Hollaender
97. A. S. Householder
98. J. S. Johnson
99. N. R. Johnson
100. W. H. Jordan
101. O. L. Keller
102. M. T. Kelley
103. B. H. Ketelle
104. K. A. Kraus
105. J. A. Lane
106. E. Lamb
107. C. E. Larson
108. H. A. Levy
109. M. H. Lietzke
110. T. A. Lincoln
111. S. Lindenbaum
112. R. Livingston
113. R. S. Livingston
114. R. N. Lyon
115. H. G. MacPherson
116. H. F. McDuffie
117. J. R. McNally, Jr.
118. K. Z. Morgan
119. A. H. Narten
120. M. L. Nelson
121. G. D. O'Kelley
122. G. W. Parker
123–124. R. B. Parker
125. J. J. Pinajian
126. F. A. Posey
127. S. A. Reynolds
128. P. S. Rudolph
129. H. E. Seagren
130. C. H. Secoy
131. E. D. Shipley
132. M. J. Skinner
133. A. H. Snell
134. R. W. Stoughton
135. C. D. Susano
136. T. J. Sworski
137–151. E. H. Taylor
152. R. E. Thoma
153. P. F. Thomason
154. F. Vaslow
155. G. M. Watson
156. A. M. Weinberg
157. G. C. Williams
158. T. E. Willmarth
159. C. A. Hutchison (consultant)
160. H. M. Sisler (consultant)
161. Gerhart Friedlander (consultant)
162. P. D. Bartlett (consultant)
163. G. Scatchard (consultant)
164. J. J. Katz (consultant)
165. J. E. Mayer (consultant)

EXTERNAL DISTRIBUTION

166. H. Miller, Office of Isotope Development, AEC, Washington
167. R. H. Schuler, Radiation Research Laboratories, Mellon Institute, 4400 Fifth Ave., Pittsburgh 13, Pa.
168. Division of Research and Development, AEC, Washington
169. Research and Development Division, AEC, ORO
170. Boeing Airplane Company
171. Union Carbide Corporation, Chemicals Division (South Charleston)
172. North American Aviation, Inc.
173. Masaharu Kondo, Professor of Chemistry, Radiation Chemistry Laboratory, Tokyo Metropolitan University, 1-950, Fukasawa-cho, Setagaya-ku, Tokyo, Japan
174. M. Daniels, Department of Chemistry, University College of West Indies, Kingston 7, Jamaica
175. J. P. W. Houtman, Reactor Institute Delft, Technische Hogeschool, Delft, The Netherlands
176. Technion, Israel Institute of Technology, Department of Nuclear Science, Haifa, Israel
177. W. T. Smith, Jr., Department of Chemistry, University of Tennessee, Knoxville
178. J. H. Green, Department of Nuclear and Radiation Chemistry, The University of New South Wales, P.O. Box 1, Kensington, N.S.W., Australia
179. Ingmar Bergstrom, Nobel Institute of Physics, Stockholm 50, Sweden
180. Riki Kobayashi, William Marsh Rice University, Houston, Texas
181. J. A. Swartout, 270 Park Avenue, New York 17, New York
182. W. W. Grigorieff, Assistant to the Executive Director, Oak Ridge Associated Universities

183–496. Given distribution as shown in TID-4500 under Chemistry category (75 copies – CFSTI)